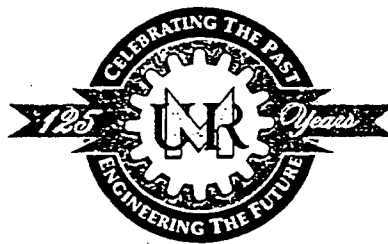PB97121362

HYSTERESIS RULES AND DESIGN PARAMETER ASSESSMENT OF RC LOW-RISE SHEAR WALLS AND BUILDINGS WITH OPENINGS

by

Franklin Y. Cheng
Curators' Professor

J.S. Yang
Former Ph.D. Student

Department of Civil Engineering
University of Missouri-Rolla
Rolla, MO 65409-0030

REPORT DOCUMENTATION PAGE

Form Approved
OMB No. 0704-0188

1. PB97-121362	2. REPORT DATE August 1996	3. REPORT TYPE AND DATES COVERED Final

4. TITLE AND SUBTITLE
Hysteresis Rules and Design Parameter Assessment of RC Low-Rise Shear Walls and Buildings with Openings

5. FUNDING NUMBERS
(G)
NSF BCS 9001494

6. AUTHOR(S)
Franklin Y. Cheng
and J.S. Yang

7. PERFORMING ORGANIZATION NAME(S) AND ADDRESS(ES)
Department of Civil Engineering
University of Missouri-Rolla
Rolla, MO 65409-0030

8. PERFORMING ORGANIZATION REPORT NUMBER
96-1

9. SPONSORING/MONITORING AGENCY NAME(S) AND ADDRESS(ES)
National Science Foundation
4201 Wilson Blvd.
Arlington, VA 22230

10. SPONSORING/MONITORING AGENCY REPORT NUMBER

11. SUPPLEMENTARY NOTES

12a. DISTRIBUTION/AVAILABILITY STATEMENT

12b. DISTRIBUTION CODE

13. ABSTRACT (Maximum 200 words)

The objective of this research project is to investigate the inelastic behavior and hysteresis rules of low-rise RC perforated shear walls through experimental and analytical studies based on various types of monotonic and earthquake loads. Results derived are then applied to seismic response analysis of typical low-rise shear wall buildings. The studies also involve development of backbone curves and equivalent viscous damping of walls as well as sensitivity analysis of design parameters for building systems. Comparison between experimental and calculated results is favorable. Hysteresis rules are based on dissipated energy envelopes calculated from experimental data for different loading states. Analytical formulation is developed by using three springs: one nonlinear equivalent shear spring; two nonlinear axial springs. Total lateral displacement of a shear wall is a result of both flexure and shear. A four-story industrial building of box type without boundary columns and a three-story commercial building consisting of isolated columns as well as walls with boundary columns are analyzed to evaluate various design parameters in building code. The three-story building is also studied on the basis of dynamic analysis with Loma Prieta earthquake (1989) and six simulated earthquakes. The sensitivity study of design parameters includes ductility reduction factor, force reduction factor, overstrength factor, and ratio of displacement amplification to force reduction factor. Results are recommended for future building code development.

14. SUBJECT TERMS

Hysteresis rules	Dynamic forces	Loma Prieta earthquake
Design	Multicomponent earthquake	Ductility
Low-rise walls	Box-type structures	Nonlinear analysis
Perforated walls	Backbone curve	

15. NUMBER OF PAGES
344

16. PRICE CODE

17. SECURITY CLASSIFICATION OF REPORT Unclassified	18. SECURITY CLASSIFICATION OF THIS PAGE Unclassified	19. SECURITY CLASSIFICATION OF ABSTRACT Unclassified	20. LIMITATION OF ABSTRACT
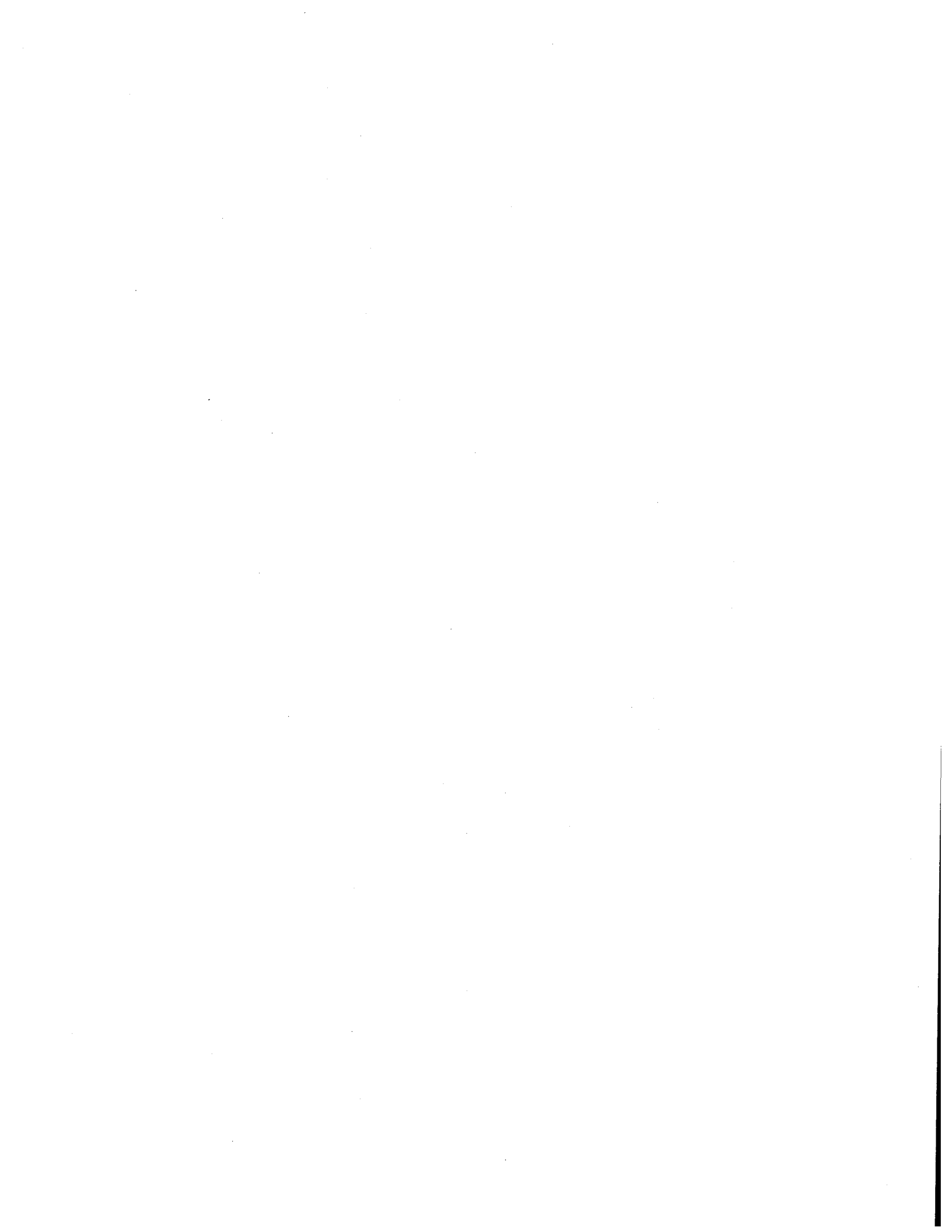
ABSTRACT

The objective of this research project is to investigate the inelastic behavior and hysteresis rules of low-rise RC perforated shear walls through a series of experimental and analytical studies based on various types of monotonic and earthquake loads. The results derived are then applied to seismic response analysis of box type structures as well as typical low-rise shear wall buildings. The studies also involve development of backbone curves of load-displacement relationship of individual walls, equivalent viscous damping of the walls, and sensitivity analysis of design parameters for building systems.

By observing the failure of cracked shear wall experimentally, a set of semi-empirical equations for backbone curve of perforated shear wall is obtained. Comparison between experimental results and calculated curves is favorable. Concept of energy dissipation is used to establish hysteresis rules which are based on dissipated energy envelopes calculated from experimental data for different loading states.

Analytical formulation for a perforated shear wall element model is developed by using three springs: one nonlinear equivalent shear spring; two nonlinear axial springs. Total lateral displacement of a shear wall is a result of both flexure and shear.

A four-story industrial building of box type consisting of solid shear walls without boundary columns and a three-story commercial building consisting of isolated columns as well as walls with boundary columns are studied for evaluating various design parameters in building code by using monotonic static analysis. The three-story building is also studied on the basis of dynamic analysis with Loma Prieta earthquake (1989) and six simulated earthquakes.

The sensitivity study of design parameters includes ductility reduction factor, force reduction factor, overstrength factor, and ratio of displacement amplification to force reduction factor. Results are recommended for future building code development.

ACKNOWLEDGMENTS

TABLE OF CONTENTS

LIST OF ILLUSTRATIONS

LIST OF TABLES

NOMENCLATURE

$[A]$, $[A_1]$, $[A_2]$, $[A_3]$, $[A_4]$, $[A_5]$	transformation matrix
A	cross-sectional area of shear wall
A_d	cross-sectional area of diagonal steel bar
A_g	transformed cross-sectional area of solid shear wall
A_h	cross-sectional area of horizontal steel bar
A_{og}	transformed cross-sectional area of section with opening
A_v	cross-sectional area of steel bar
A_1, A_{i+1}, A_n, A_{n+1}	cross-sectional area of steel bar
a	acceleration
C	cracking point on backbone curve of shear wall; function of both sites coefficient and structure's fundamental period
C'	cracking point on backbone curve of shear wall
C_d	NEHRP-defined displacement amplification factor
C_{eq}	equivalent damping coefficient
C_f	failure (collapse) base shear ratio
c	damping coefficient
D	width of wall; displacement
DAF	displacement amplification factor
D_{co}, D_c, DC	cracking displacement of backbone curve
DM	maximum displacement
D_{max}	current maximum displacement
D_{yo}, D_y, DY	yielding displacement of backbone curve
D_{uo}, D_u, DU	ultimate displacement of backbone curve

$D_{uo}(i)$	maximum force where unloading process starts
D_f, DF	failure displacement of shear wall
DPP	maximum displacement where unloading process starts
E_c	elasticity modulus of concrete
ECS	element coordinate system
EDBH	effect of diagonal bar in horizontal direction
EDBV	effect of diagonal bar in vertical direction
EHB	effect of horizontal bar
EVB	effect of vertical bar
E_s	elasticity modulus of steel
$\sum E_d$	total energy dissipation
$[F_e]$	element force matrix
F_{co}, FC	cracking load on backbone curve
F_{yo}, FY	yielding load on backbone curve
F_{uo}, FU	ultimate load on backbone curve
$F_{uo}(i)$	maximum force where unloading process starts
F_{c1}, F_{y1},	
F_{u1}	coefficient caused by opening
F_{c2}, F_{y2},	
F_{u2}	coefficient caused by vertical steel bar
F_{c3}, F_{y3},	
F_{u3}	coefficient caused by horizontal steel bar
F_I	initial force
F_D	damping force
F_S	spring force
F_t	concentrated force
F_x	applied force at x level

FPP	maximum force where unloading process starts
f_{adh}	cross section area reduction factor of diagonal bars in relation to horizontal projection
f_{adv}	cross section area reduction factor of diagonal bars in relation to vertical projection
fc'	compressive strength of concrete
f_{eu}	base shear ratio
f_{ldh}	length reduction factor for diagonal steel bars in horizontal direction
f_{ldv}	length reduction factor for diagonal steel bars in vertical direction
f_{lhh}	length reduction factor of horizontal bars
FRF	force reduction factor
f_r	end-joint reduction factor
f_y	yielding stress of steel bar
G	shear modulus
H	height of the wall
HL_{DB}	length in horizontal projection of diagonal steel bar
I	importance factor
JCS	joint coordinate system
J1, J2, J3, J4	joints defined in shear wall element model
$[K_{eg}]$	stiffness matrix
K_a	stiffness during unloading after reversal loading; axial spring stiffness used in axial hysteresis model
K_a^*	axial spring stiffness
K_b, K_c	stiffness during unloading
K_d	stiffness during unloading after reversal loading
K_e	stiffness during reloading after unloading
K_f	stiffness during unloading after reversal loading

K_s	shear spring's stiffness of shear wall element
KL	controlling factor in defining hysteresis rules
k	spring constant
k_1, k_2, k_f	spring constant
L	height of the wall
L_h	distance between outmost steel bars on both sides
L_o	height of opening
L_{c1}, L_{c2}	crack length of development
L_1, L_2, L_3	coupling influence line; moment/shear ratio
ΔL	difference in vertical deformation at each side of the wall
L'	distance from bottom of wall to top of opening
LWP	vertical location factor of opening
M, M_1, M_2	moment
M/V	moment/shear ratio
MQD	shear span length ratio
m	mass
NVB	number of vertical steel bars
n_i	ratio of steel elasticity modulus to concrete elasticity modulus
ODC	cracking displacement on backbone curve
ODY	yielding displacement on backbone curve
ODU	ultimate displacement on backbone curve
OFC	cracking load on backbone curve
OFY	yielding load on backbone curve
OFU	ultimate load on backbone curve
$OSOC$	original (initial) stiffness between origin and cracking point
$OSCY$	stiffness between cracking point and yielding point
$OSYU$	stiffness between yielding point and ultimate point

OSUF	stiffness between ultimate point and failure point
[P]	force matrix
P	external load
P_a, P_b	axial spring force
P_c	cracking load of shear wall; axial spring force
P_d	axial spring force
P_y	yielding load of shear wall
P_u	ultimate load of shear wall
P_{uo}	ultimate load on original backbone curve
P_f	failure load of shear wall
P_1, P_2, P_5	external force
p_o	maximum applied load
Q	external load
R	NEHRP-defined response modification factor
R_g	force reduction factor
Rw	UBC-defined force reduction factor
R_μ	ductility reduction factor
R_1, R_2, R_3	points where tangent lines on experimental curve intersect
R_4	presumed failure point
SCY	stiffness between cracking point and yielding point
SDP	distance between reversal point and origin
[SI]	stiffness matrix
SLEDRS	smoothed linear elastic design response spectrum
SOB	stiffness during unloading
SR	reversal stiffness
SX_oC', SOC'	stiffness during reversal loading
SX_3Y'	stiffness during unloading

SUF	stiffness between ultimate point and failure point
T	fundamental period of structure
t	thickness of shear wall; time
U	ultimate point on backbone curve of shear wall; arbitrary displacement
U'	ultimate point on backbone curve of shear wall
u_K	amplitude
u_o	maximum amplitude
u	displacement
$\dot{u}$	velocity
$\ddot{u}$	acceleration
$u_1{}^*, u_2{}^*$	amplitude
V	base shear
V_a, V_b	shear spring force
V_{eu}	maximum elastic base shear
$(V_i)_a$	allowable base shear
$(V_i)_f$	failure (collapse) base shear
$(V_i)_s$	base shear based on NEHRP provisions
VL_{DB}	length in vertical projection of diagonal steel bar
W	width of the wall; active weight of the system
W_o	width of opening
W_{D1}, W_{D2}	area bounded by damping force and amplitude
W_D	area bounded by damping force and amplitude
W_{S1}, W_{S2}	area bounded by inertia force and amplitude
W_S, W_{S4}	area bounded by inertia force and amplitude
W_1	distance from the side of the wall to the opening
[X]	displacement matrix
X_s, X_R	critical points defining reloading after unloading

X_{RO}	reversal point during unloading after reversal loading
X_1, X_2, X_3	critical points defining unloading process
x	distance starts from the top of the wall and increases downwards
Y, Y'	yielding point on backbone curve of shear wall
Z	seismic zone factor
ϕ	curvature
Φ	phase angle
Ω	frequency of motion; overstrength factor
$[\Delta_e]$	element displacement matrix
Δ_b	rotational spring's displacement of solid shear wall
Δ_s	shear spring's displacement of solid shear wall
$\Delta_{story,max}$	maximum story drift
$\Delta_{story,yield}$	yielding story drift
Δ_t	total lateral displacement of shear wall
Δ_1, Δ_2	lateral displacement caused by diagonal crack
θ	angle from horizontal line to coupling influence line
θ_1, θ_2	arc angle
α	shape factor; height of upper rigid body of shear wall element
α_0	height ratio of opening
β	height of lower rigid body of shear wall element
β_0	width ratio of opening
β_1	horizontal location factor of opening
ρ_i	steel ratio
ρ_{wh}	steel ratio of horizontal bars in the wall
ρ_{wv}	steel ratio of vertical bars in the wall
ε_{sy}	yielding strain of steel bar
σ_u	stress at ultimate point of shear wall

τ_h, PWH	horizontal shear stress
τ_v, PWV	vertical shear stress
ω_n	undamped natural frequency of structure
ξ	damping ratio
ξ_{eq}	equivalent damping ratio
η, η_1, η_2	constant
δ	story drift
δ_a	allowable story drift
δ_{max}	maximum story drift
δ_s	story drift based on NEHRP provisions
δ_y	yield story drift
μ_s	system ductility factor

I. INTRODUCTION

A. OBJECTIVES

Reinforced concrete shear walls are effective in seismic resistance for civil engineering buildings and industrial structures, such as hospital and nuclear power plants. For shear walls with openings of doors and windows, strong ground motion can significantly affect load capacity and displacement [1-10].

Current building codes use the design parameters such as force reduction factor and displacement amplification factor in modifying elastic response to inelastic response. These parameters vary for different types of buildings, but not in terms of whether the walls are solid or perforated.

This report is to show analytical and experimental studies of solid and perforated low-rise shear walls as well as elastic and inelastic response behavior of building systems. Design parameters of force reduction factor and displacement amplification factor as well as equivalent viscous damping are evaluated and assessed.

B. OVERVIEW

Sections of this report are outlined here. Section II illustrates some observations from test results. A comparison of load and displacement for solid shear walls and perforated shear walls is made. Total lateral displacement is a combination of shear displacement and flexural displacement. The role of flexure in lateral displacement is then depicted from the relationship between bending displacement and shear displacement. Finally, failure ductility is calculated for all the perforated shear walls.

Section III develops semi-empirical equations of backbone curves for perforated shear walls. Equations for load and displacement at four loading stages of cracking, yielding, ultimate, and failure are established. Curves for predicted and experimental results are then compared.

Section IV observes hysteresis response based on experimental results under seismic loading and develops a possible energy envelope for the loading process when shear walls enter the inelastic range. This dissipated envelope is called a reference curve which provides the shear wall's potential loading path. The hysteresis loop defines loading, unloading, reversal loading, reloading after unloading, and unloading after reversal loading. Calculated and experimental results are compared.

Hysteresis response for perforated shear walls clearly shows the existence of hysteretic damping. By modeling damping effect with hysteresis energy loss, characteristics of the damping coefficient are explored based on the concept of viscous damping. Formulation of equivalent viscous damping for perforated shear wall is established in Section V.

Design parameters used in building codes are in terms of force reduction factor and displacement amplification factor. Section VI discusses the aforementioned factors and their physical aspects, relationships between ductility reduction factor and overstrength factor, and maximum base shear ratio and overstrength factor as well as displacement amplification factor/force reduction factor ratio and overstrength factor.

Section VII derives analytical formulations for perforated shear walls. Element stiffness matrix is introduced. Also, the free-body diagram concept is applied to perforated shear walls.

Section VIII studies the response of a four-story industrial building. Monotonic static analysis is applied on the basis of UBC design code. Response analysis uses load-displacement relationships of shear walls with ductility range from 4.0 to 8.0. Failure story drift and failure story base shear are considered for cases of different ductilities. Cases where the building fails in (1) flexural mode, and (2) both shear and flexural mode are investigated.

2

Sensitivity of design parameters based on ductility is discussed. A comparison of design parameters includes ductility reduction factor, overstrength factor, system ductility factor, force reduction factor, and displacement amplification factor.

Section IX studies the response of three-story buildings, including an existing three-story commercial building with solid shear walls in California and other modified three-story buildings with some perforated shear walls. These structures are subjected to monotonic static loading. There are eighty-four columns in the existing building, twenty eight for each floor. The load-displacement relationships of RC columns are examined; load-displacement relationship for solid and perforated shear walls are calculated as well.

Monotonic static load is applied to the building. Effects of shear and rotational springs of shear walls along the force direction are discussed. Total displacement response at different stories in the buildings is demonstrated. An explanation of base shear vs. critical story drift relationship is given. A comparison of failure base shear and failure displacement is made.

Ductility reduction factor, overstrength factor, system ductility factor, force reduction factor, displacement amplification factor, and the ratio of displacement amplification factor to force reduction factor are discussed with respect to the sensitivity of design parameters.

Section X studies the response of three-story buildings under dynamic loading, one an existing three-story commercial building in California, the other a modified three-story building. The 1989 Loma Prieta Earthquake and six simulated earthquakes are imposed on the former and six simulated earthquakes on the latter. Responses of shear and rotational springs of shear walls at the critical story are studied. Details of shear ratio and displacement ratio by shear springs of shear walls at the critical story are illustrated. Ductility reduction factor, system ductility factor, overstrength factor, force reduction factor, and displacement amplification factor/force reduction factor ratio are also discussed. Section XI includes summary, conclusions, and recommendations.

3

C. LITERATURE REVIEW

This research is focused on the study of isolated low-rise perforated RC shear walls without boundary columns. Main work involves the development of 1) load-displacement relationship, 2) hysteresis rules, and 3) assessment of building code design parameters for both monotonic loading and earthquake excitations. The literature review presented herein pertains to this research work.

Recent work in Japan by Watabe et al. [11], among others, has focused on quantitative evaluation of load-deflection characteristics on heavily reinforced RC low-rise shear walls normally used in nuclear power plant structures. These specimens have boundary columns which are mainly subjected to monotonically increasing loading.

Recent work on RC squat shear walls in France has been carried out at the Centre Experimental de Recherches et d'Etudes du Bâtiment et des Travous Pulic. The primary objective is to determine stiffness degrading behavior for walls having different reinforcement ratios, varying from almost zero to 0.5%, in both horizontal and vertical directions. Results show that the stiffness is constant until cracking, and declines severely after cracking. Stiffness begins to slowly decrease before the first diagonal shear crack appears [12].

The French Commissariat a l'Energie Atomique-Centre d'Etudes Nucleaires also has a strong research interest in the seismic behavior of RC low-rise shear walls [13]. Results indicate that the dynamic behavior of shear walls depends strongly on the nonlinearity and time-history of the input force; the inelastic spectrum method underestimates the margin given by ductility for narrow band excitation centered on a wall's natural frequency. No experimental work was carried out, and the time-history analyses were performed with the modified Takeda model which has mainly bending deformation.

In the U.S., recent work on RC low-rise shear walls has been undertaken at the Los Alamos National Laboratory (LANL). Bennett, Anderson, Endebrock et al. [14-19]

tested a series of small scale shear walls and box-type structures subjected to both static and earthquake loadings. The purpose of these tests was to find the stiffness reduction and its effect on the natural frequency. They studied walls with height-to-width ratios varying from 1 to 0.25 and steel ratios from 0.25% to 0.6%. Tests showed a 75% stiffness reduction during a 0.75g peak acceleration earthquake signal; fundamental natural frequencies were reduced by factors of 2 or more over those calculated based on an uncracked cross-section strength-of-materials approach. This stiffness reduction caused the natural frequency to shift into the frequency range for which the earthquake's energy content is significant. It is apparent that this shift may lead to increased amplification in floor response spectra at lower frequencies, and will have significant impact on the equipment and piping design response spectra and their margins of safety. More experimental work must be undertaken to verify the early results [20].

As shown by the above literature review, low-rise shear walls have been the subject of extensive research. However, the thrust of the work has been to determine the ultimate capacity of walls, stiffness reduction, and behavior under cyclic loading. This work, including the latest information from Japan, France, and LANL (U.S.) does not provide adequate information with which to develop hysteresis rules for isolated low-rise walls because: 1) most of the walls subjected to either monotonic loading or cyclic loading had boundary elements; 2) shear and bending deformations were not separated; and 3) cyclic loading patterns used in the tests did not provide sufficient information with which to develop large and small amplitude loops for earthquake response studies.

Low-rise buildings actually constitute a large percentage of total construction. Many of these buildings are braced by shear walls without boundary columns. Therefore ongoing research is urgently needed here. Results will have a significant impact on structural design by improving safety and reducing seismic damage.

Under a joint research project between the National Cheng Kung University (NCKU) and the University of Missouri-Rolla (UMR), low-rise buildings were studied.

5

Sheu [21] at NCKU tested a series of isolated low-rise shear walls subjected to various static monotonic, cyclic, and earthquake-type loadings while Cheng at UMR incorporated experimental data from NCKU and LANL to develop hysteresis rules and to investigate inelastic response behavior of individual walls as well as systems. Note that these load-deflection relationships and hysteresis rules, as developed by Cheng, have two important features: 1) bending and shear deformations are separated; and 2) the deformations due to bending, shear, and bond slip are coupled. The importance of these two features in low-rise shear walls has long been recognized. This is because (1) shear deformation can dominate total deflections, and (2) the Takeda model, commonly used in RC shear wall analysis, is based only on bending deformation which cannot accurately predict the seismic response of low-rise shear wall structures.

In actual engineering practice, walls have openings, such as doors and windows, and low-rise buildings have walls with or without boundary columns. For instance, nuclear auxiliary buildings are built mainly of walls without boundary columns and civil structures are built of walls with or without boundary columns. Yamada et al. (1974) performed lateral monotonic load tests for low-rise RC shear walls with boundary columns and beams at the top and bottom of shear walls. Walls with openings are included in the study. Main focus of the research was to establish an RC load-displacement relationship at the elastic as well as the plastic stage [22]. Chita et al. tested low-rise heavily reinforced concrete shear walls with openings [23-25]. Walls having girders on top as well as boundary columns on both sides were tested under lateral and axial loads. The maximum shear strength of shear walls was then established.

Sotomura et al. (1985) studied ultimate shear strength of low-rise shear walls with numerous small openings for a nuclear power plant. Horizontal cyclic loads were applied to a beam mounted on top of walls which have boundary columns [26].

For design, ACI code [27] has special provisions for shear walls in Section 11.10. Shear strength of a wall must satisfy governing equations (11-32) or (11-33) in the code.

For a wall with height-to-width ratio less than 0.5, equation (11-32) may be used but does not reflect the influence of height-to-width ratio on shear strength. Opening in a shear wall, although it can significantly affect a wall's shear strength and deformation, is not addressed by the code. Consequently, ACI code has limited application to low-rise perforated shear walls.

For seismic structural design, design parameters are empirical, such as force reduction factor and displacement amplification factor. Recently, Uang (1993) studied both factors and proposed a ratio of displacement amplification factor vs. force reduction factor (DAF/FRF) on the basis of different definitions of DAF and FRF. His studies are mainly for frame structures, not for low-rise shear wall buildings [28].

In summary, some research work has been done on low-rise shear walls with boundary columns. Cheng and Mertz [29] and Cheng and Volger [30] studied seismic response behavior of low-rise shear walls without boundary columns, and shear wall systems without openings. Cheng and associates developed bending and shear load-displacement relationships as well as bending and shear hysteresis rules for such solid walls. To continue their work, Cheng at UMR and Sheu at NCKU have focused on development of load-displacement relationship, hysteresis rules, inelastic response, and design parameter assessment of low-rise RC perforated shear walls and systems as presented in this report.

II. INVESTIGATION OF TEST RESULTS

A. TEST SCHEDULE

This project joined National Cheng Kung University (NCKU) in Taiwan and University of Missouri-Rolla (UMR) in cooperative research. Experimental work was conducted by M. S. Sheu at NCKU and theoretical research was developed under F. Y. Cheng at UMR. The investigation herein of RC shear walls involves shear walls with openings, or perforated shear walls. Types of openings in the experimental program include single windows, double windows, doors and single slits. Also some solid shear walls were tested in order to distinguish the differences between them.

Test apparatus is shown in Figure 1. A large frame is fixed at ground level to provide a stable test environment. Specimens are imbedded in the steel beam on the ground. A steel beam attached to the top of a shear wall is used to transfer lateral force to the specimen. Two jacks on both sides of the specimen constitute the force system. The top of the specimen is not fixed. A test program is scheduled for both solid and perforated shear walls, with single cyclic loading and earthquake type loading applied to each specimen. There are two groups of shear walls studied in this program. One group has a height/width ratio of 0.5. The other has a height/width ratio of 0.75. Two kinds of steel bars are used, which have yielding strengths of 4617 and 5005 Kg/cm^2, respectively. Steel bars arranged in a diagonal direction within specimens are only employed for perforated shear walls. It should be noted that the opening rate for shear walls in Group I is 16.35%, but 21.8% in Group II. Compressive strength of concrete is between 254 and 345 Kg/cm^2. A summary of the test schedule is shown in Table I.

As shown in Figure 2(c), all specimens go through four stages under either a cyclic loading or a earthquake type loading. These four stages are distinguished as elastic, cracking, yielding and failure stages. Note the case of a single cyclic loading test in Figure 2(a). When loading is applied at a load increment of 0.5~1 tons up to yielding stage, the

8

①: Jack
②: Load cell
③: Steel beam to transfer load
④: Specimen

(Unit: mm)
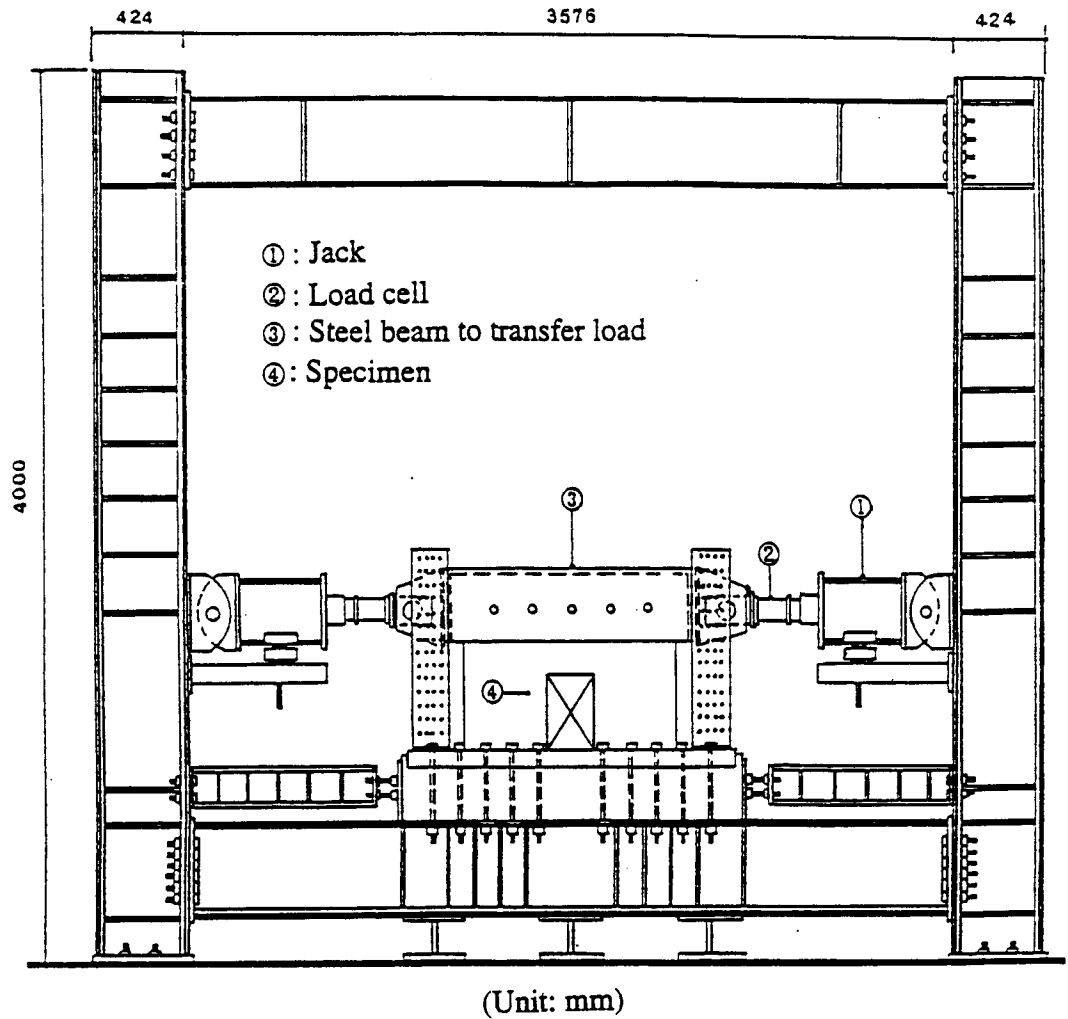
Figure 1 Experimental apparatus for NCKU shear walls

rigidity of specimens decreases and causes more displacement at the same load increment. Thus, to prevent extensive cracks in a specimen, displacement control (at an increment of 0.5~1.0 mm) dominates the rest of the test. Earthquake type loading follows the same procedure as the single cyclic loading case. The first three cycles are controlled by load increment and subsequent cycles by displacement increment (see Figure 2(b)).

Diagonal steel bars are commonly used in RC walls with openings. Among these specimens, shear walls with single windows or with double windows have more diagonal steel bars around the openings. Solid shear walls contain no diagonal steel bars. Figure 3

Table I Summary of test specimens and schedule

Group ($\frac{L}{W}$)	Type	Specimen No.	Specimen sketch	Wall size WxLxt (cm)	Opening size N×L_o×W_o	(Steel bar) Vertical Horizontal Diagonal	f_y ($\frac{kg}{cm^2}$)	f'_c ($\frac{kg}{cm^2}$)	f'_t ($\frac{kg}{cm^2}$)	Loading history
Group I	W/o opening	SW‒0E				10‒D10		254	25.0	
		SW‒1E				5‒D10		345	24.7	
		SW‒2E		100 × 50 × 10		‒‒‒		268	25.7	
	Single door	SWO‒3E			1 × 21.8 × ** 37.5 (16.35%)	10‒D10 5‒D10		299	22.6	
		SWO‒4E				D*‒D13	5005	316	17.0	
	Double window	SWO‒5E			2 × 21.8 × 18.75 (16.35%)	10‒D10 5‒D10		329	31.1	
		SWO‒6E				D‒D13		329	31.0	
	Single window	SWO‒7E			1 × 65.4 × 12.5 (16.35%)	10‒D10 5‒D10		328	24.0	
($\frac{1}{2}$)		SWO‒8E				D‒D13		328	24.0	
Group II	W/o opening	SW‒9E				10‒D13 7‒D13		294	25.7	
		SW‒10E				‒‒‒		312	25.7	
	Single slit	SWO‒11E		100 × 75 × 10	1 × 21.8 × 75.0 (21.8%)	8‒D13 7‒D13		297	22.5	
		SWO‒12E				D‒D13		297	22.5	
	Double window	SWO‒13E			2 × 21.8 × 37.5 (21.8%)	10‒D13 7‒D13	4617	321	23.2	
		SWO‒14E				D‒D13		325	23.6	
	Single window	SWO‒15E			1 × 65.4 × 25.0 (21.8%)	10‒D13 7‒D13		279	20.7	
($\frac{3}{4}$)		SWO‒16E				D‒D13		283	19.8	

* Diagonal bars   ** Opening rate
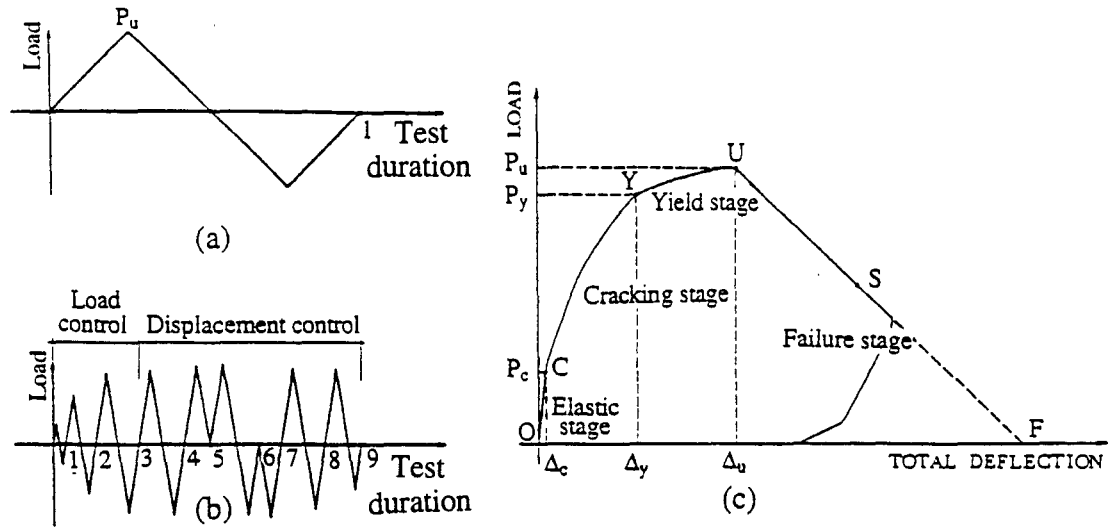
Figure 2 Loading types and stages: (a) One cyclic loading (b) Earthquake loading
(c) Schematic diagram of different loading stages for NCKU shear walls

shows the arrangement of steel bars. Three types of measurements are used for displacement during loading process. Clip-on gauges are applied in the vertical direction to measure vertical deformation while potential meters and dial gauges are used to detect displacement in the horizontal direction. Figure 4 shows the detailed setup. Properties of steel bars D10 and D13 are shown in Figure 5.

B. LOAD AND DISPLACEMENT COMPARISON BETWEEN SOLID AND PERFORATED SHEAR WALLS

Table II shows experimental load and displacement at cracking, yielding and ultimate stages for NCKU shear walls. This table demonstrates that the cracking load, which has a range of 4-6 tons or so, is stable for either solid or perforated shear walls. The key factor in the cracking load is compressive strength of the concrete. In the test program, concrete has a compressive strength of 254 to 345 tons/mm^2. Concrete strength among test specimens is close for the most part, around 300~330 tons/mm^2.

Solid shear walls have a higher yielding load than perforated shear walls. The former range from 27 to 28 tons while the latter range from 12 to 22 tons with

W/o opening (SW–0 E、1 E、2 E) Single door (SWO–3 E、4 E)

W/o opening (SW– 9 E、10 E) Single door (SWO– 11 E、12 E)
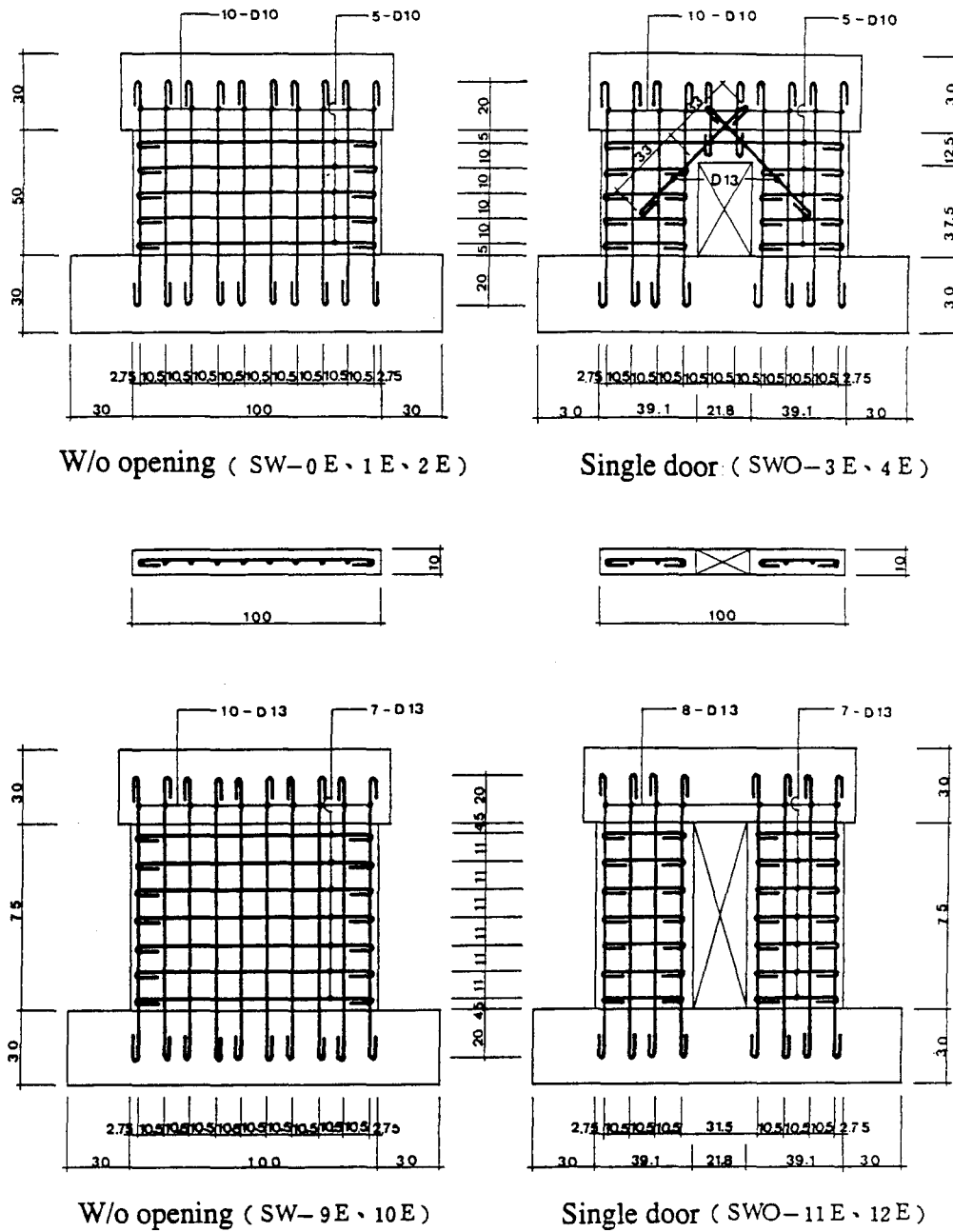
Figure 3 Configuration of steel bars for NCKU shear walls

height/width ratio of 0.5 and from 7 to 18 tons with height/width ratio of 0.75. Average

yielding load for all perforated shear walls is 15.43 tons, about 56% of that for solid shear

walls. Yielding loads for solid shear walls are stable with an average of 27.64 tons.
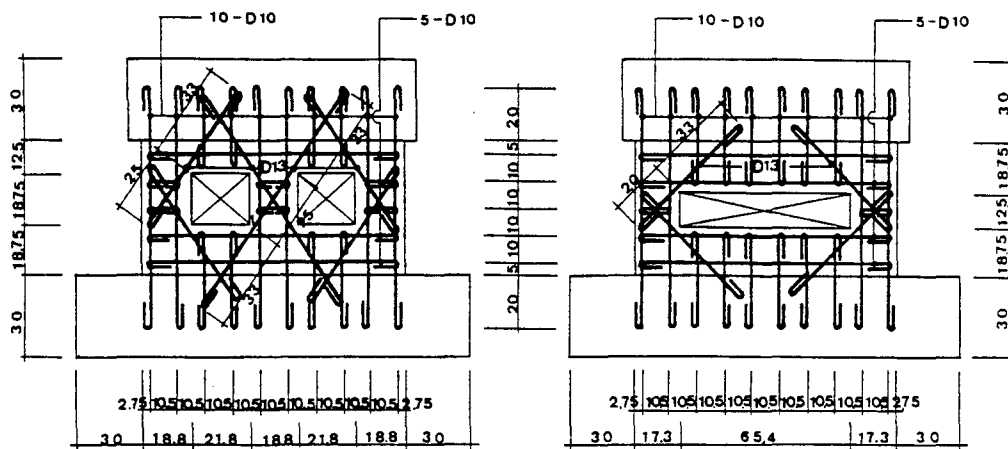
Double window (SWO−5 E、6 E) Single window (SWO−7 E、8 E)
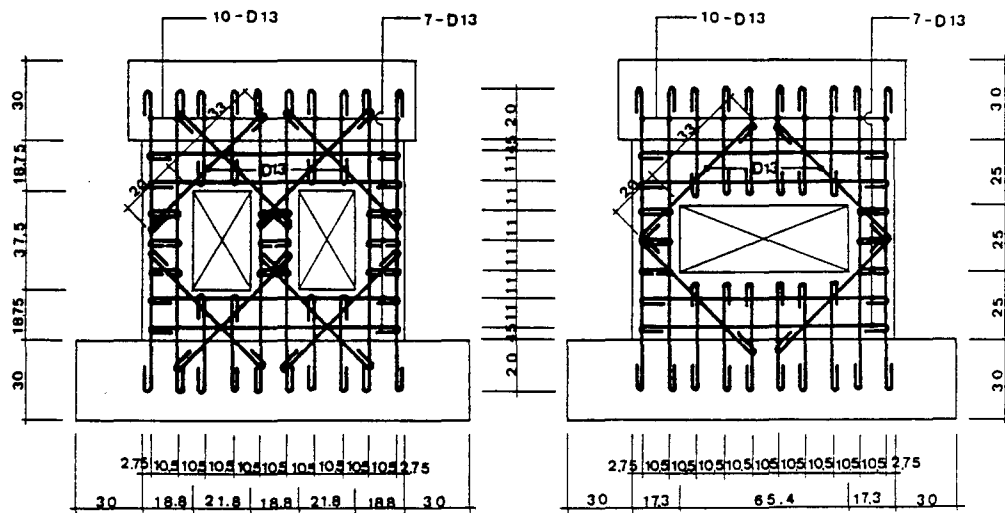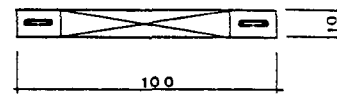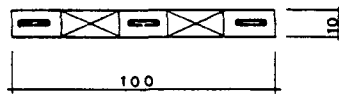
Double window (SWO−13 E、14 E) Single window (SWO−15 E、16 E)

Figure 3 (continued) Configuration of steel bars for NCKU shear walls

Ultimate loads for solid shear walls are likewise stable, from 32 to 34 tons, and higher than those for perforated shear walls. The latter have ultimate loads of 16 to 25

W/o opening (SW-0 E、1 E、2 E)

Single door (SWO-3 E、4 E)

W/o opening (SW-9 E、10 E)

Single slit (SWO-11 E、12 E)
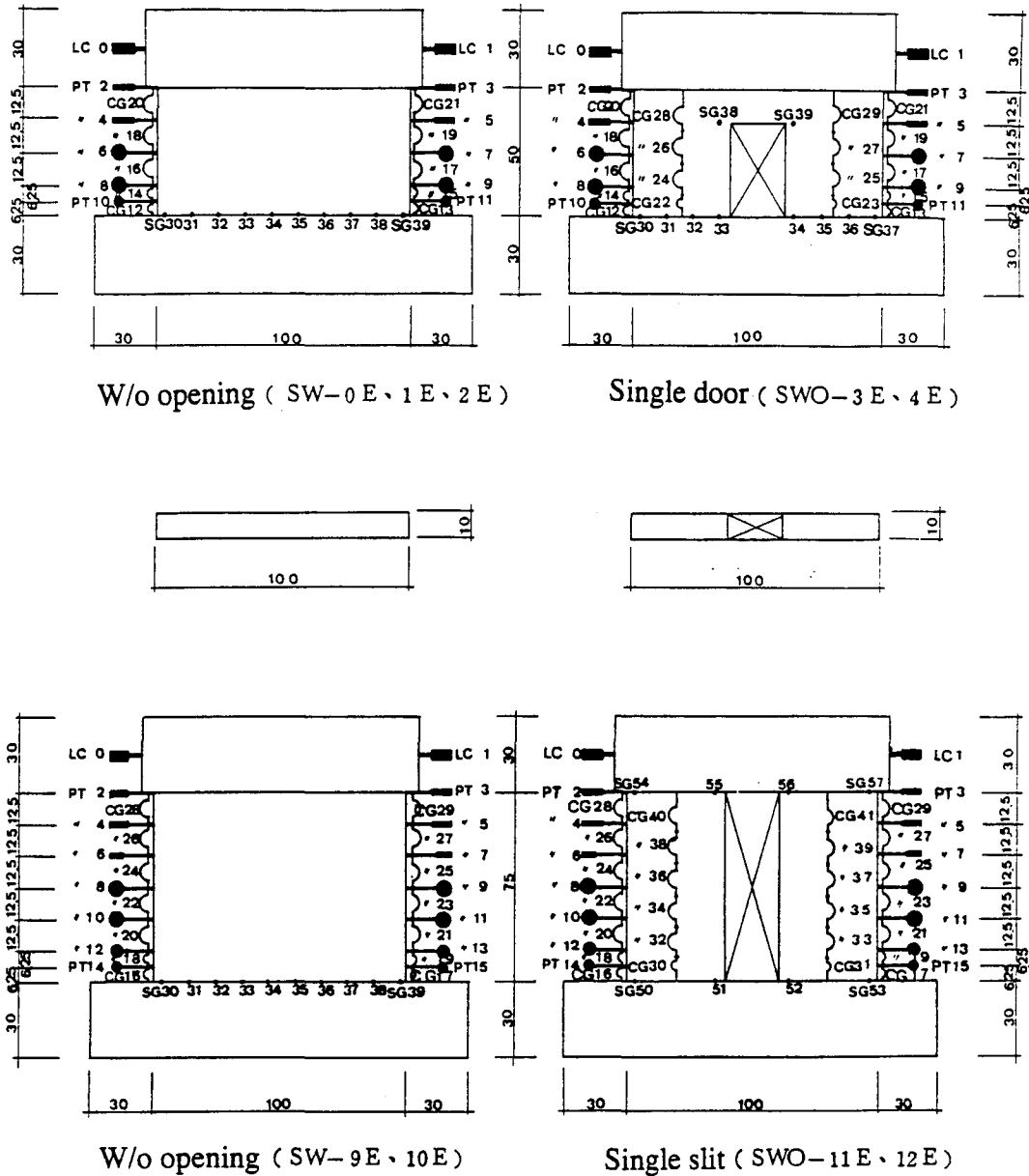
Figure 4 Locations of load cell and strain gauge for NCKU shear walls

tons, an average of 21.22 tons with a height/width ratio of 0.5, and 9 to 20 tons, an average of 14.87 tons, with height/width ratio of 0.75. Overall average of ultimate loads for perforated shear walls is 18.04 tons, less than that for solid shear walls. The ratio of

14

Double window (SWO−5 E、6 E) Single window (SWO−7 E、8 E)

Double window (SWO−13 E、14 E) Single window (SWO−15 E、16 E)
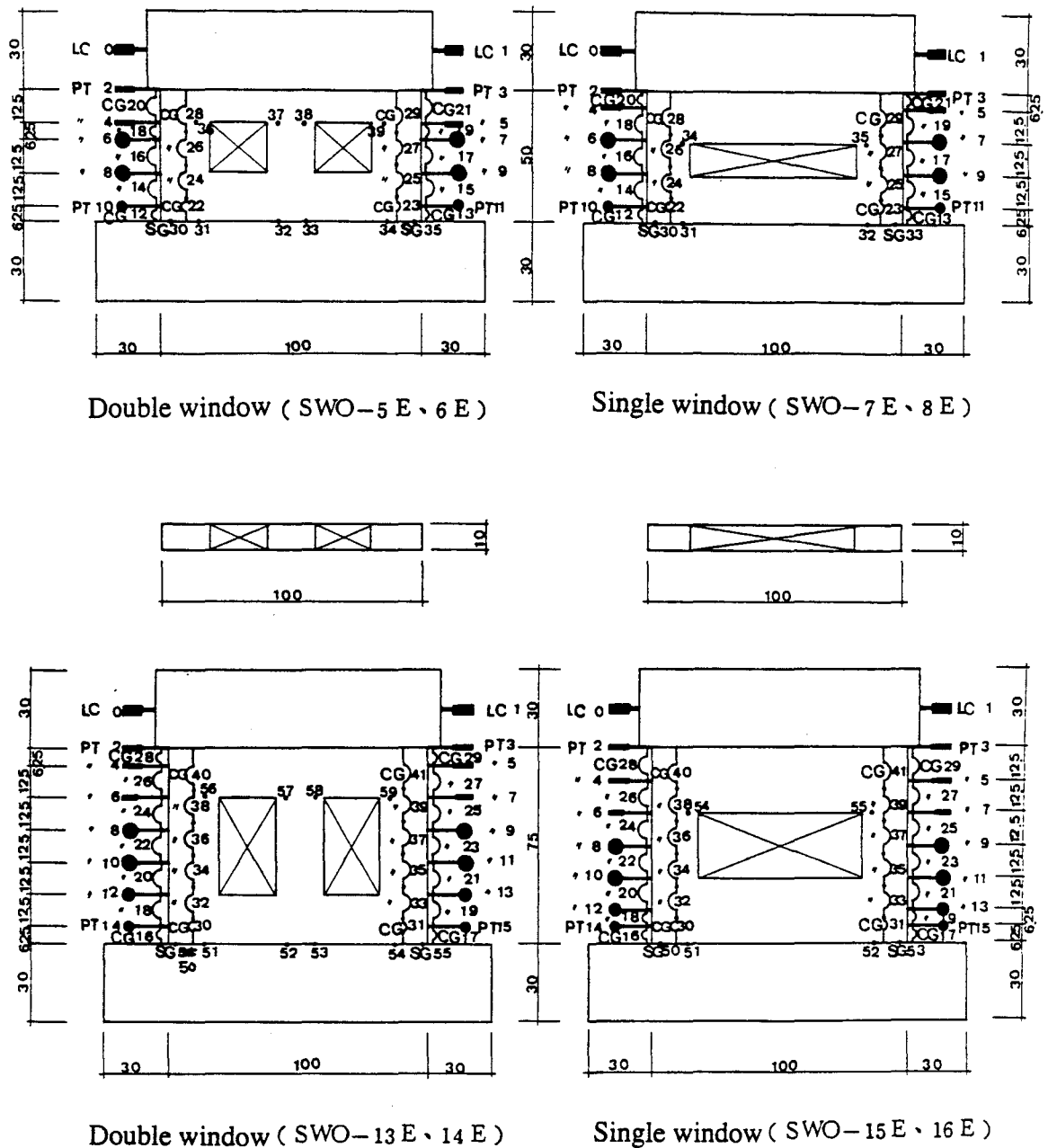
Figure 4 (continued) Locations of load cell and strain gauge for NCKU shear walls

average ultimate load between perforated (18.04 tons) and solid (33.13 tons) is 0.54, about the same ratio as average yielding load.

Displacement at the cracking stage has a wide range for either solid or perforated shear walls,0.2-0.7 mm. Cracking displacement is not as stable as cracking load. The

15
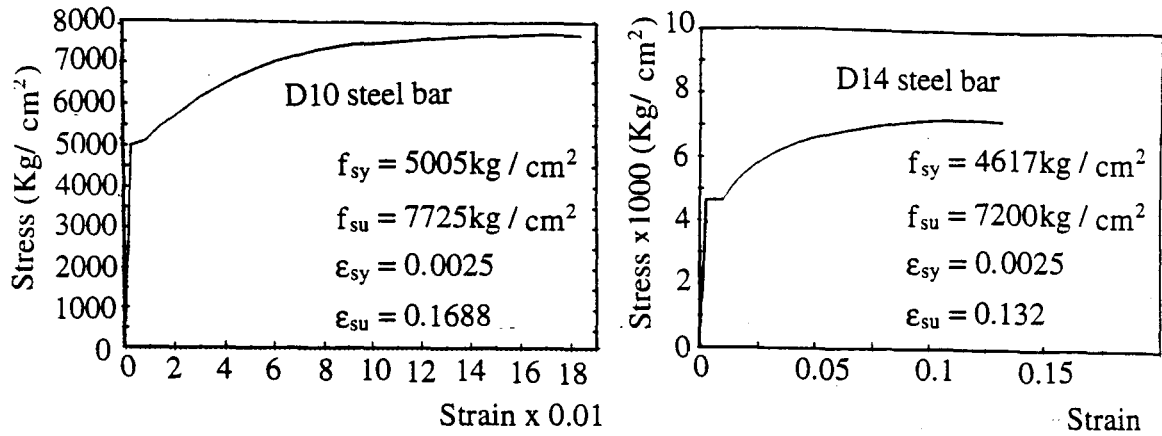
Figure 5 Stress-strain relationship for D10 and D14 steel bars

Table II Experimental load and displacement at cracking, yielding and ultimate stage for NCKU shear walls

Group	Type	Pc (ton)	Py (ton)	Pu (ton)	Δ_c (mm)	Δ_y (mm)	Δ_u (mm)
Group I	SW-0E	5.31	26.68	32.09	0.40	3.68	9.16
	SW-1E	6.21	27.87	33.00	0.31	2.57	8.45
	SWO-3E	4.94	20.91	22.62	0.134	2.48	4.69
	SWO-5E	4.47	21.50	24.65	0.37	2.43	3.92
	SWO-7E	3.63	12.17	16.39	0.23	1.40	3.14
Group II	SW-9E	4.55	28.37	34.31	0.24	3.81	11.26
	SWO-11E	5.01	18.46	20.23	0.267	5.75	10.13
	SWO-13E	4.94	12.47	14.99	0.67	2.80	3.90
	SWO-15E	4.54	7.06	9.38	0.62	1.60	3.31

reason for this difference may be the manufacturing process and nonuniformity of concrete. Displacement of solid shear walls is stable at the yielding stage, with a range of 2.6-3.7 mm, an average of 3.35 mm. For perforated shear walls, except SWO-11E, yielding displacements average 2.10 and 2.20 mm for Groups I and II, respectively. Generally, these displacements for perforated shear walls are stable except for those walls with a single slit (SWO-11E). Yielding displacement of perforated shear walls is about two-thirds that of solid shear walls. Displacement is also stable at the ultimate stage, with an average of 9.62 mm for solid shear walls, and 3.79 mm for perforated shear walls. Thus ultimate displacement of the latter is about two-fifths that of the former. Note that yielding and ultimate displacements for perforated shear walls in Groups I and II have almost the same range.

It can be concluded that openings in shear walls play an important role in load capacity and maximum displacement of those walls. Generally, cracking loads for both solid and perforated shear walls are stable and remain in a narrow range of 4 to 6 tons. But cracking displacement for both types of walls has a wide range of 0.1 to 0.7 mm. Compared to yielding and ultimate displacement, cracking displacement is small. Yielding and ultimate loads for perforated shear walls are slightly more than half those for solid shear walls. Yielding and ultimate displacement for perforated shear walls are two-thirds and two-fifths, respectively, of those for solid shear walls. Thus openings in a shear wall reduce load capacity by an average of 0.5 times decay, and decrease maximum displacement by 33% up to 60%.

C. CURVATURE DISTRIBUTION

Analytic study indicates that curvature starts from zero at the top of the wall and increases proportionally in relation to square of depth. Finally, curvature reaches its highest value at the bottom of the wall. This progression can be expressed as

$$\phi = \int_0^x \frac{\Delta L}{W} x \, dx$$

(1)

Here x starts from the top of the wall and increases downwards; W is the wall's width, and ΔL is the difference in vertical deformation at each side of the wall. In Figure 6, solid shear wall SW-0E has curves 1, 2, 3 and 4, which represent locations from top to bottom of the shear wall. Curves 1, 2, 3, 4, 5 and 6 do likewise in solid shear wall SW-9E. These locations indicate curvature is small at the top and large at the bottom of the wall, which matches the theoretical derivation very well. Perforated shear walls, except SWO-11E (with single slit), SWO-3E (with single door) and SWO-15E (with single window) respond in a manner like solid shear walls here. Note that SWO-5E and SWO-11E (with double window) and SWO-7E (with single window) have a different curvature distribution throughout the height of these walls. For shear walls SWO-5E, SWO-7E and SWO-11E, the relationship between curvature in the middle part (the section with opening) and curvature at the lower part of shear wall is similar. Thus the middle part of shear walls may occupy a crucial position in the failure mechanism of shear walls, vis-a-vis load capacity and maximum displacement.

It is interesting to note that the top portion of perforated shear walls has negative curvature, quite different from curvature response at the top of solid shear walls. Negative curvature means that the top portion rotates opposite to the normal direction, as shown by the lower portion of shear wall. This phenomenon indicates that different mechanics may prevail at the top of shear wall.

Compare curvature response between perforated and solid shear walls more closely. It can be seen that solid shear walls have a larger curvature capacity than perforated shear walls. Physically, curvature implies the effect of flexural behavior on shear walls. If curvature capacity is larger, then more bending response will occur in a shear wall. Larger curvature capacity also allows more lateral external load to act on a shear wall. Shear walls may then hold a larger load capacity. Due to their bending action,
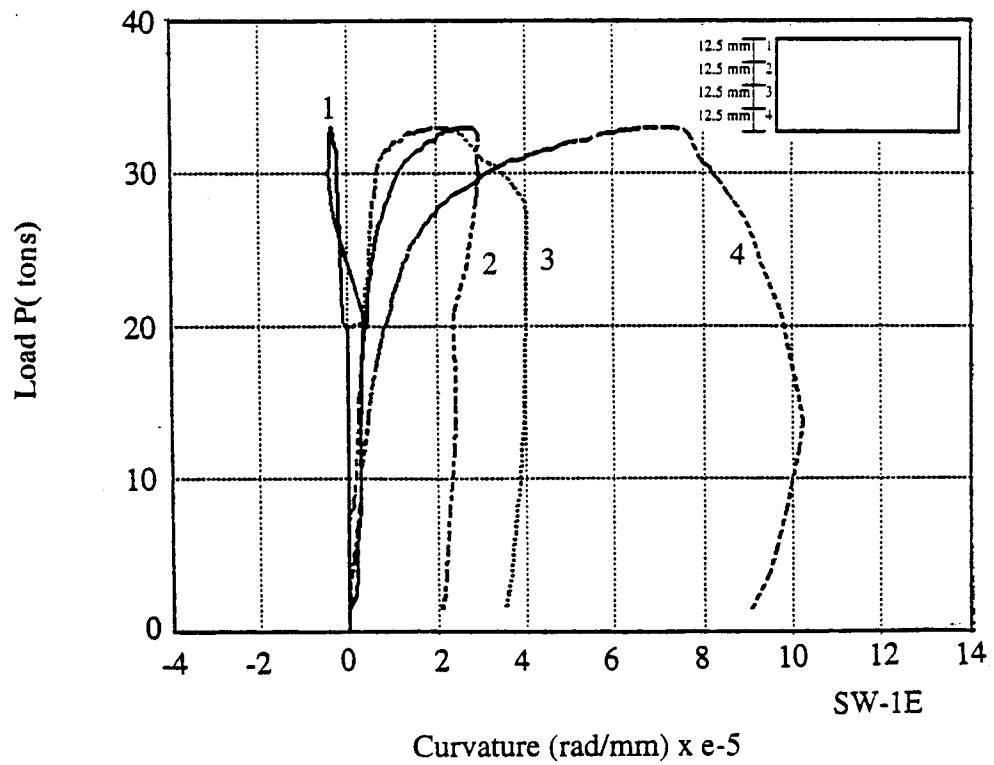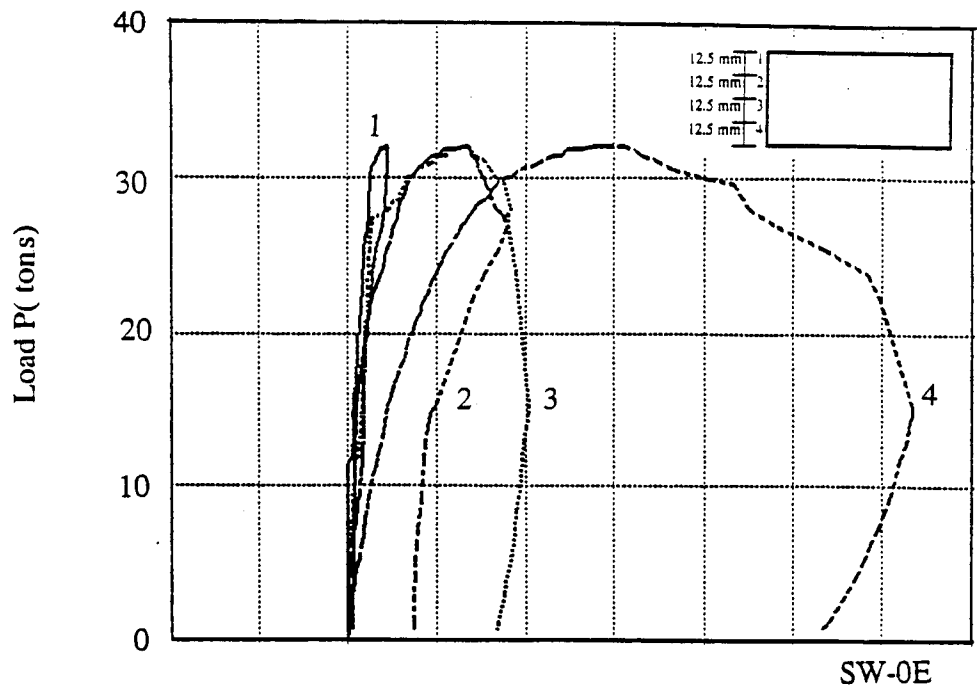
Figure 6   Relationship of load vs. curvature for NCKU shear walls
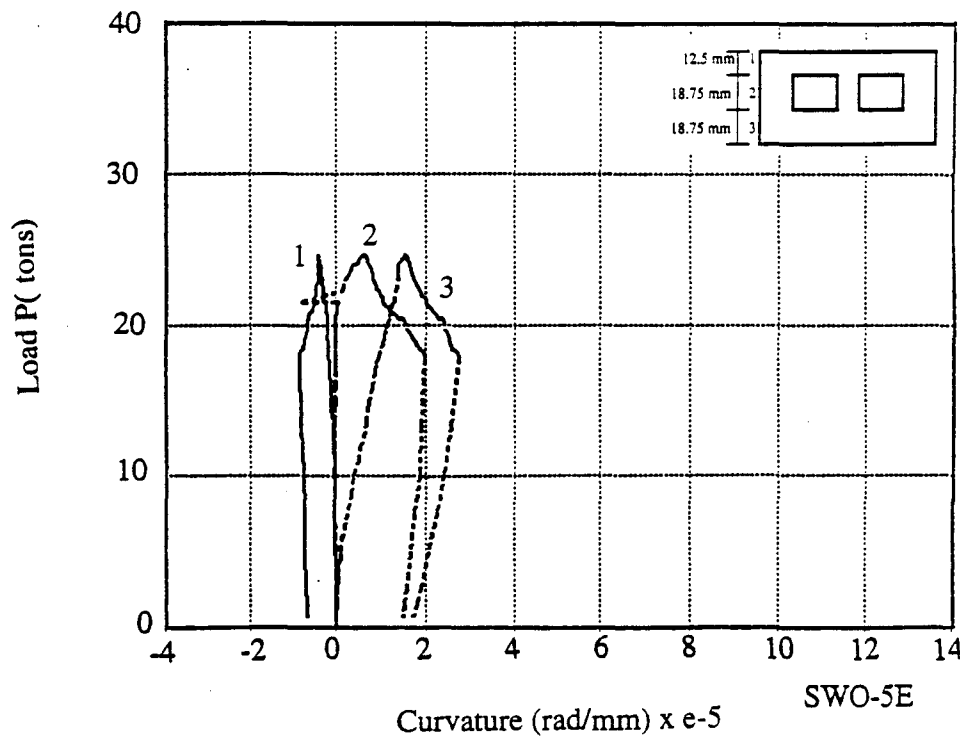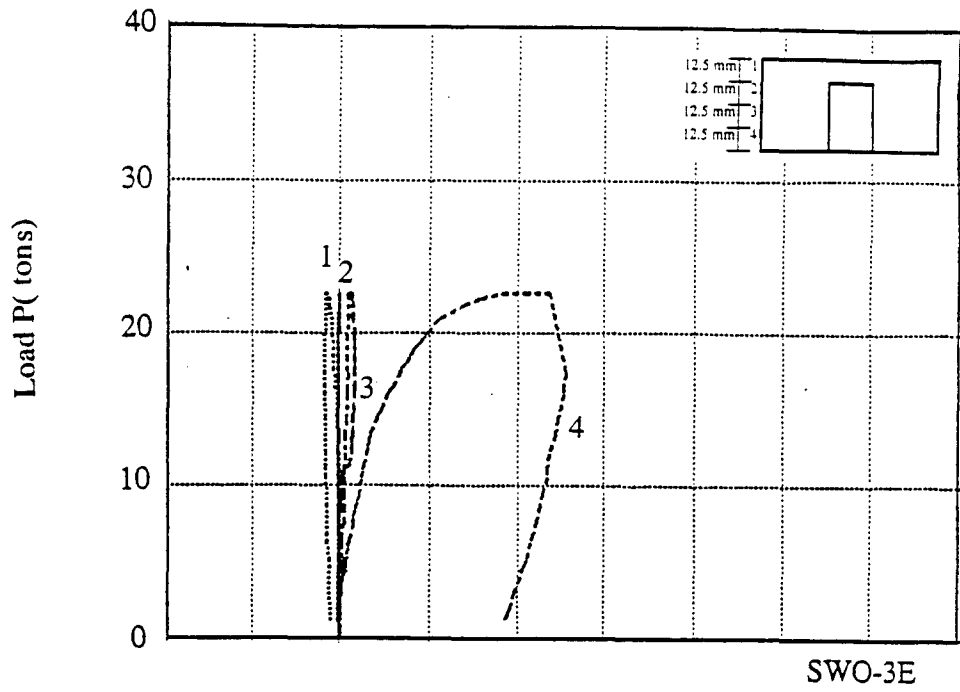
Figure 6 (continued) Relationship of load vs. curvature for NCKU shear walls

20
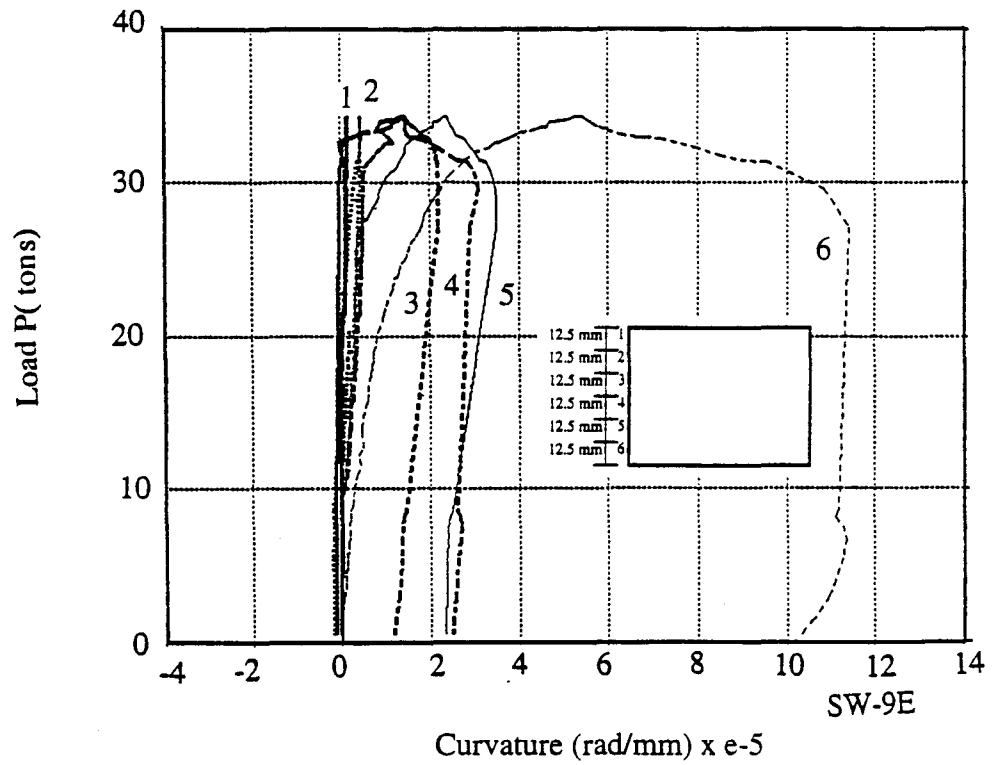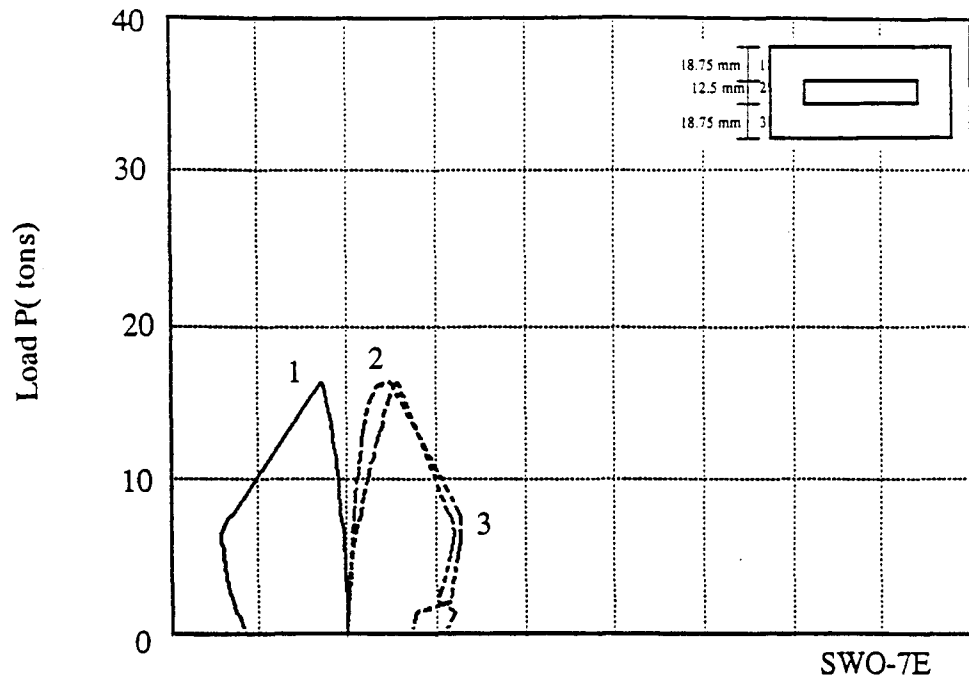
Figure 6 (continued) Relationship of load vs. curvature for NCKU shear walls
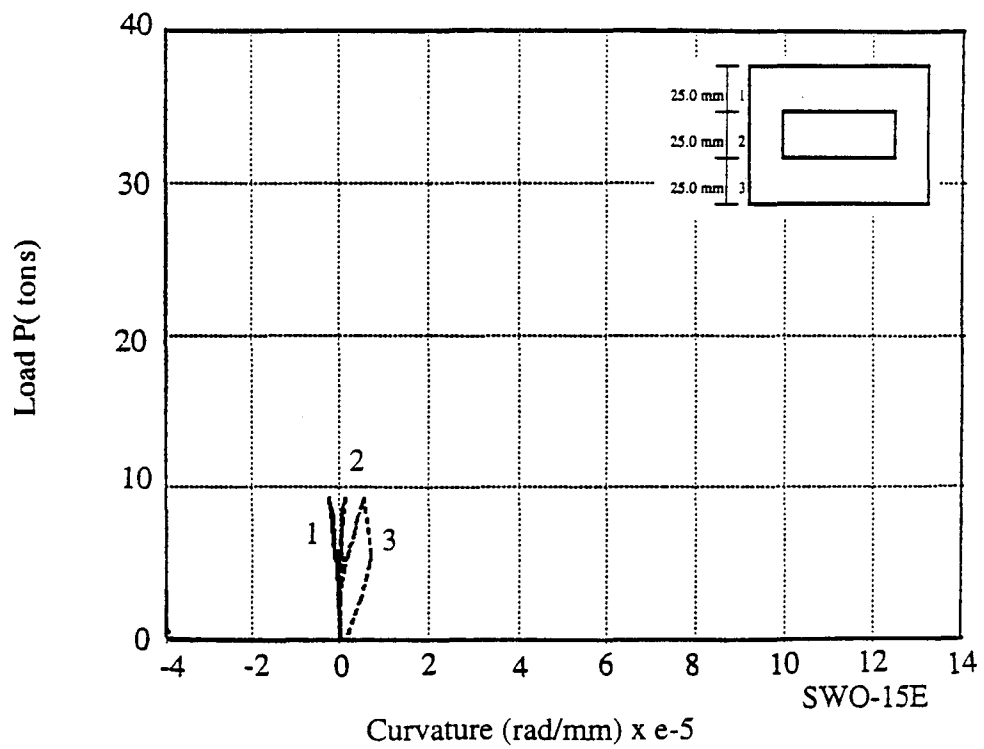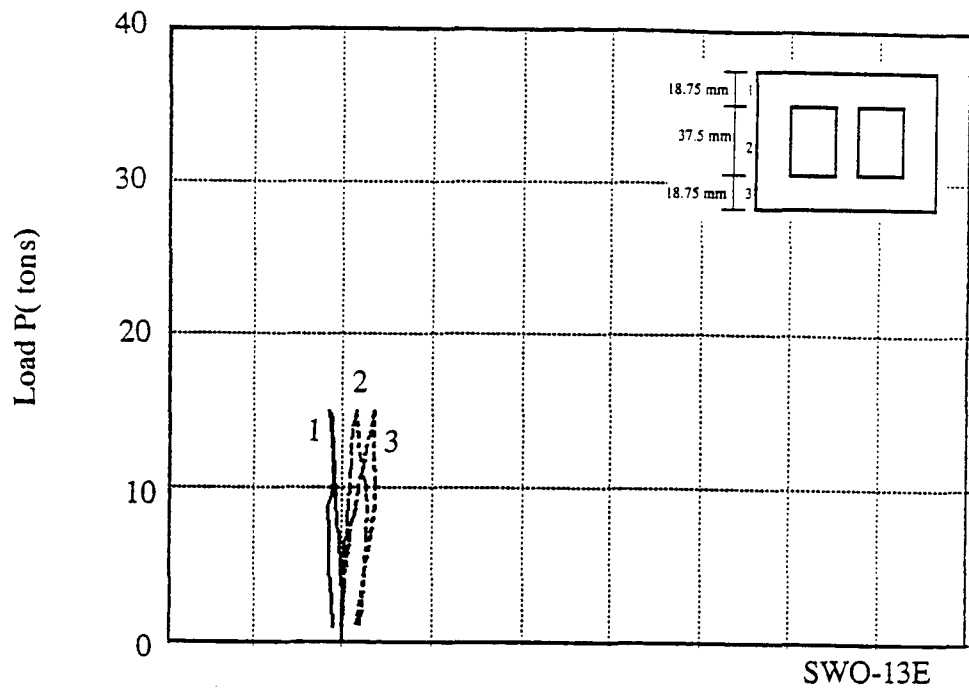
Figure 6 (continued) Relationship of load vs. curvature for NCKU shear walls

solid shear walls have a larger load capacity and maximum displacement than perforated shear walls.

D. BENDING, SHEAR AND TOTAL LATERAL DISPLACEMENT

Figure 7 shows three load-displacement curves for each NCKU shear wall. The curve for total displacement is the combination of bending and shear load-displacement curves. Bending load-displacement curve reflects the flexural characteristics of a shear wall, which are caused mainly by deformation of vertical steel bars in the shear wall. Shear load-displacement curve is likewise related to horizontal steel bars. Concrete is also important in the behavior of shear walls in either vertical or horizontal direction. For solid shear walls SW-0E, SW-1E and SW-9E, bending displacement is about 13%~40% of total lateral displacement. For perforated shear walls in Group 1, approximately 10% of total displacement is induced by flexure (i.e., bending effect). Bending (or flexural) lateral displacement of perforated shear walls in Group II accounts for 10%~45% of the total, slightly more than in Group I. Here the calculation of bending and shear displacements follows Cheng and Mertz [29].

In general, bending displacement ranges from 10%~40% of the total at ultimate state. Based on Cheng and Mertz's study, the bending displacement/total displacement ratio is about 40 to 60%, an average of 50%, at ultimate state. But shear displacement comprises a larger percentage of the total than bending displacement. If more shear capacity for shear walls is designed by increasing the ratio of horizontal steel bars, then stiffness in relation to horizontal shear also increases. Less shear displacement and more bending displacement could result. Optimal design with consideration of bending and shear thus has great importance.

E. FAILURE DUCTILITY

Failure ductility is another important factor in controlling the behavior of shear walls and, consequently, the entire structure. For solid shear walls, Cheng and Mertz
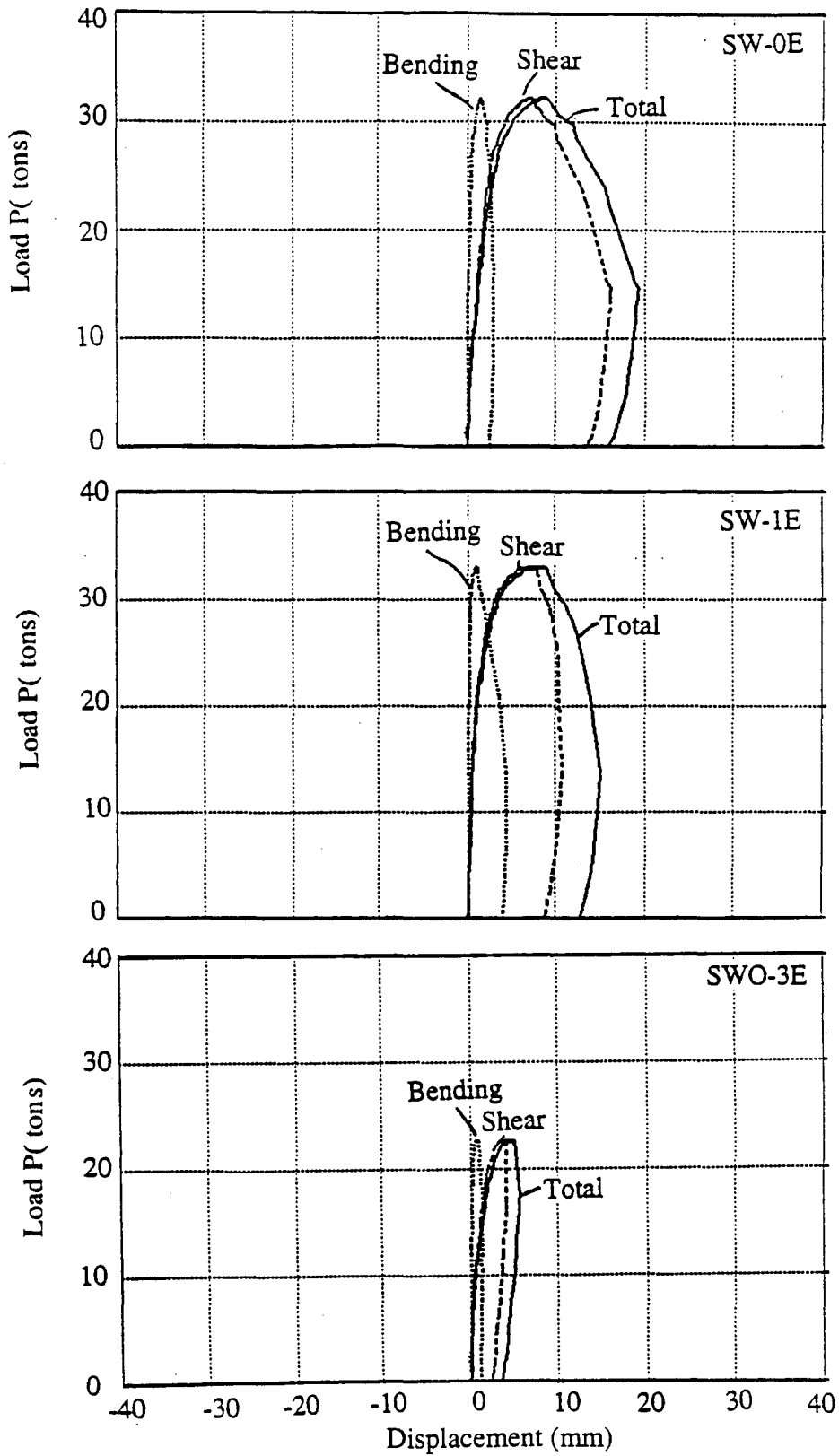
Figure 7 Relationship of load vs. bending, shear and total lateral displacement for NCKU shear walls
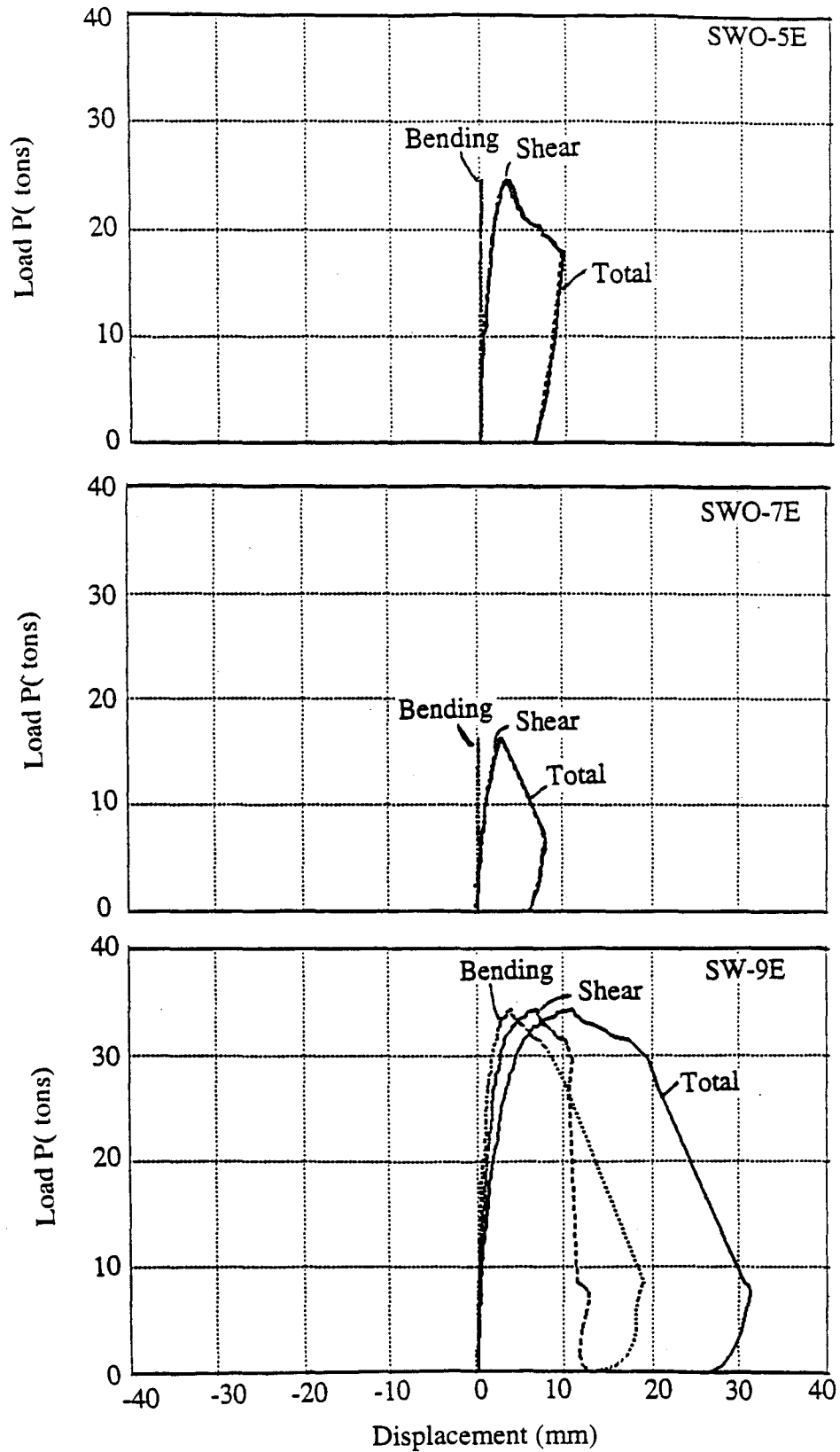
Figure 7 (continued) Relationship of load vs. bending, shear and total lateral displacement for NCKU shear walls
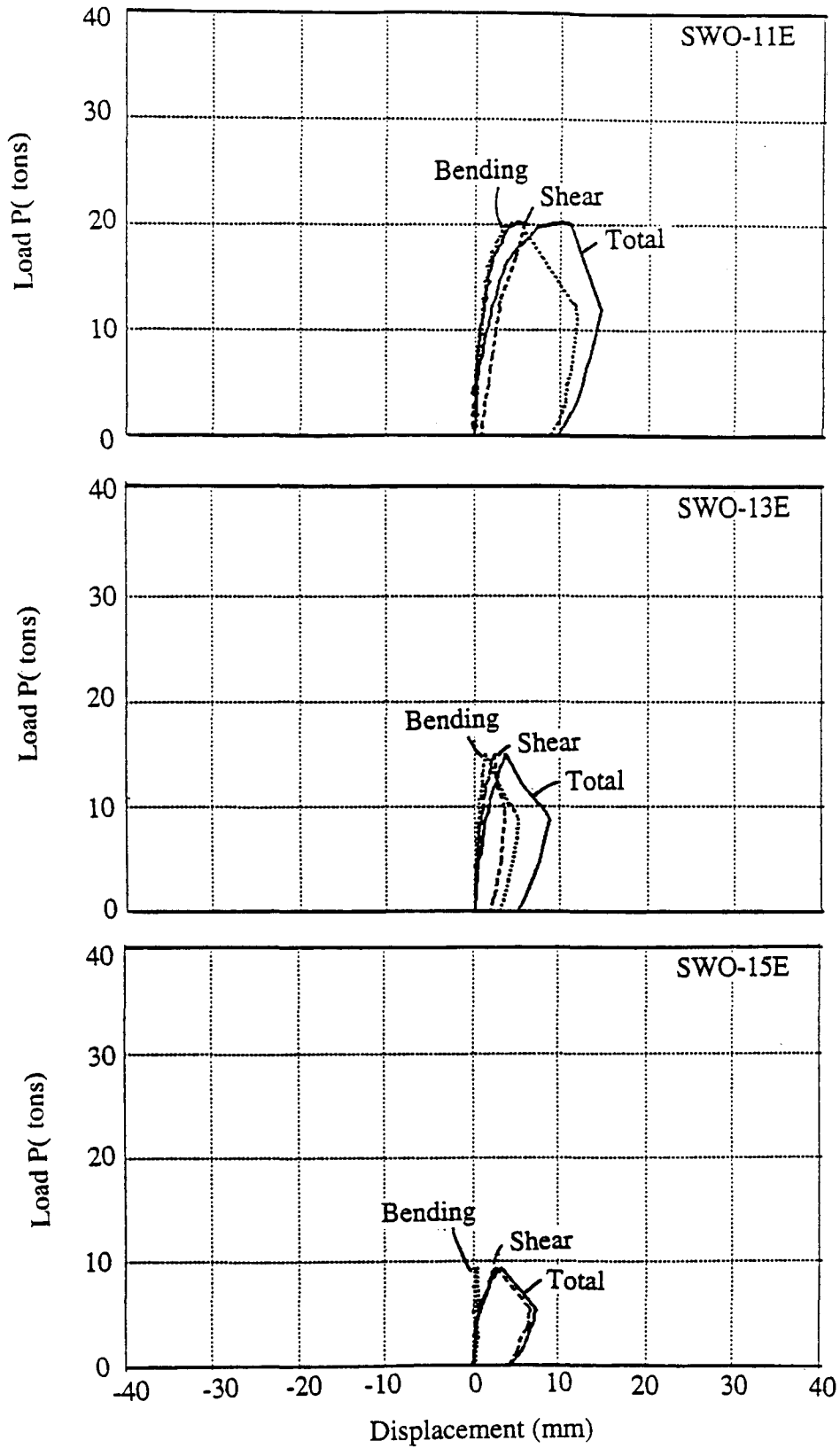
Figure 7 · (continued) Relationship of load vs. bending, shear and total lateral displacement for NCKU shear walls

observed that 4.0 is the failure ductility. Table III outlines yielding and failure displacement for perforated shear walls. Failure ductility equals the ratio of failure displacement, D_f, to yielding displacement, D_y. This table shows that perforated shear walls in both cases have a similar range of failure ductility. Ranging from 2.12 to 5.75, the average is 3.75. Thus 4.0 is recommended as the failure ductility of perforated shear walls.

Table III Summary of failure ductility
for NCKU shear walls

Wall	Dy (mm)	Df (mm)	μ_f
SWO-3E	2.480	5.259	2.12
SWO-5E	2.430	10.083	4.15
SWO-7E	1.400	8.053	5.75
SWO-11E	5.750	15.071	2.62
SWO-13E	2.800	8.944	3.19
SWO-15E	1.600	7.485	4.68

III. SEMI-EMPIRICAL EQUATIONS OF BACKBONE CURVE FOR SHEAR WALLS

A. DEVELOPMENT OF CRACKS

When RC walls undergo external loads, cracks in the concrete are a sign of more strength decay in the wall. As cracks develop further, the wall exhibits more complicated behavior due to coupled flexure and shear. If the applied load continues, the wall approaches its failure mechanism. As shown in Figure 8, many apparent diagonal cracks and broad crush of concrete on the compression side occur overall in solid shear walls such as SW-0E, SW-1E and SW-9E. Also shown in Figure 8, perforated shear walls display major diagonal cracks and crushing area (concrete crush) on both sides of and between openings. Size and frequency of cracks for perforated shear walls are generally smaller than for solid shear walls.

Again comparing perforated and solid shear walls, the length and width of major diagonal cracks is smaller in the former. As discussed later, the role of diagonal cracks is important in controlling the behavior of shear walls.

1. Initial Cracks These cracks begin at the earliest stage of the loading period. They may thus have enough duration to develop extensive width and length. Initial cracks can significantly affect steel bars. In a shear wall, decrease of strength capacity and increase of lateral displacement are strongly influenced by these cracks. Walls remain in the elastic range without these cracks.

Figure 9(a) shows a possible configuration of initial cracks in the shear wall, three on the tension side and two on the compression side. Those on the tension side usually occur first since cracks are initiated by concrete which has less tensile strength than steel bars. Also, compressive strength is greater than tensile strength in the concrete itself. Thus, cracks on the tension side happen sooner than crushing of concrete. Initial cracks can be in the diagonal or horizontal direction. Diagonal cracks may start at the corners of openings either on the tension or the compression side.
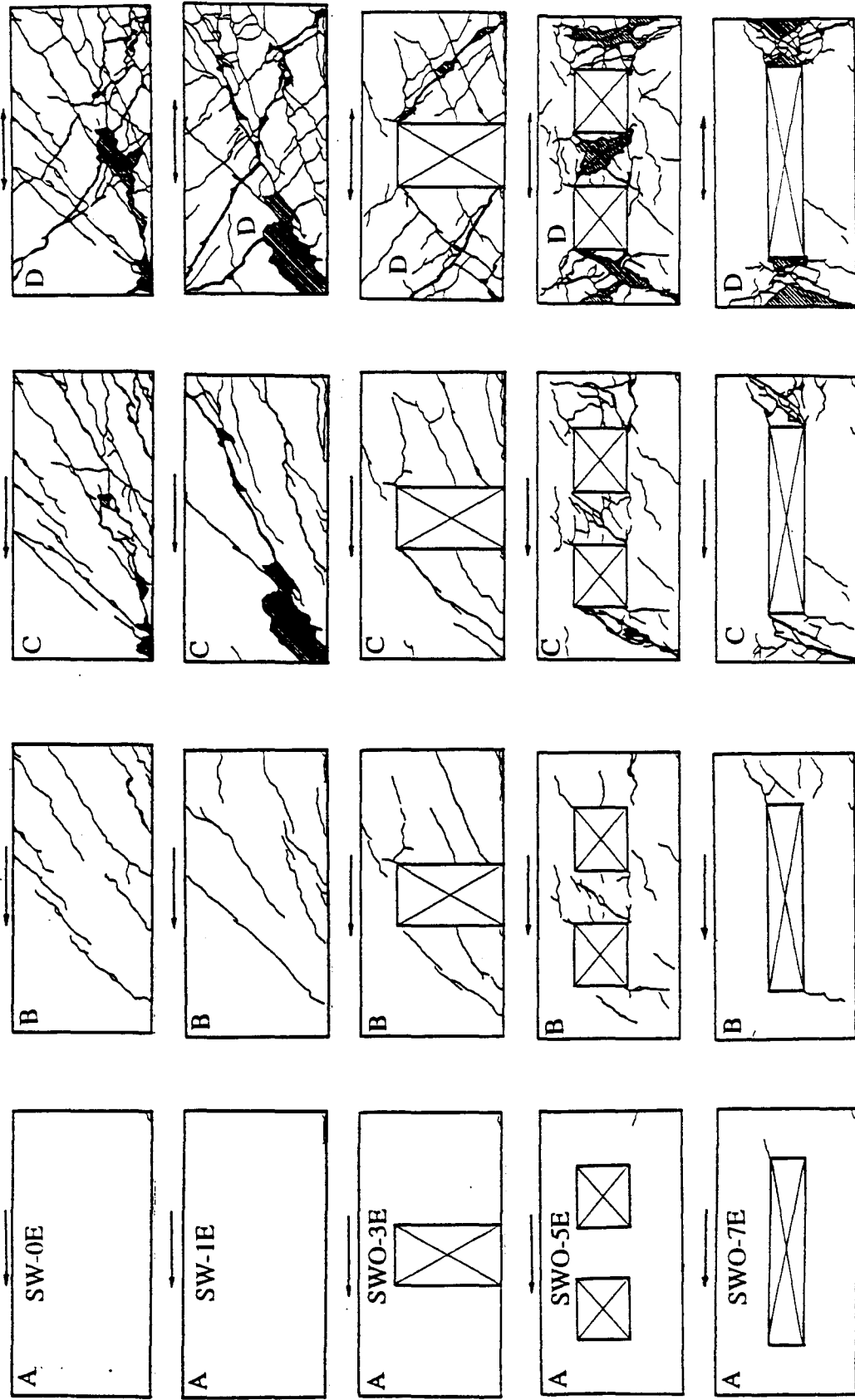
Figure 8 Development of crack (a) Elastic stage (A); (b) Cracking stage (B); (c) Yielding stage (C); (d) Failure stage (D) for NCKU shear walls

29
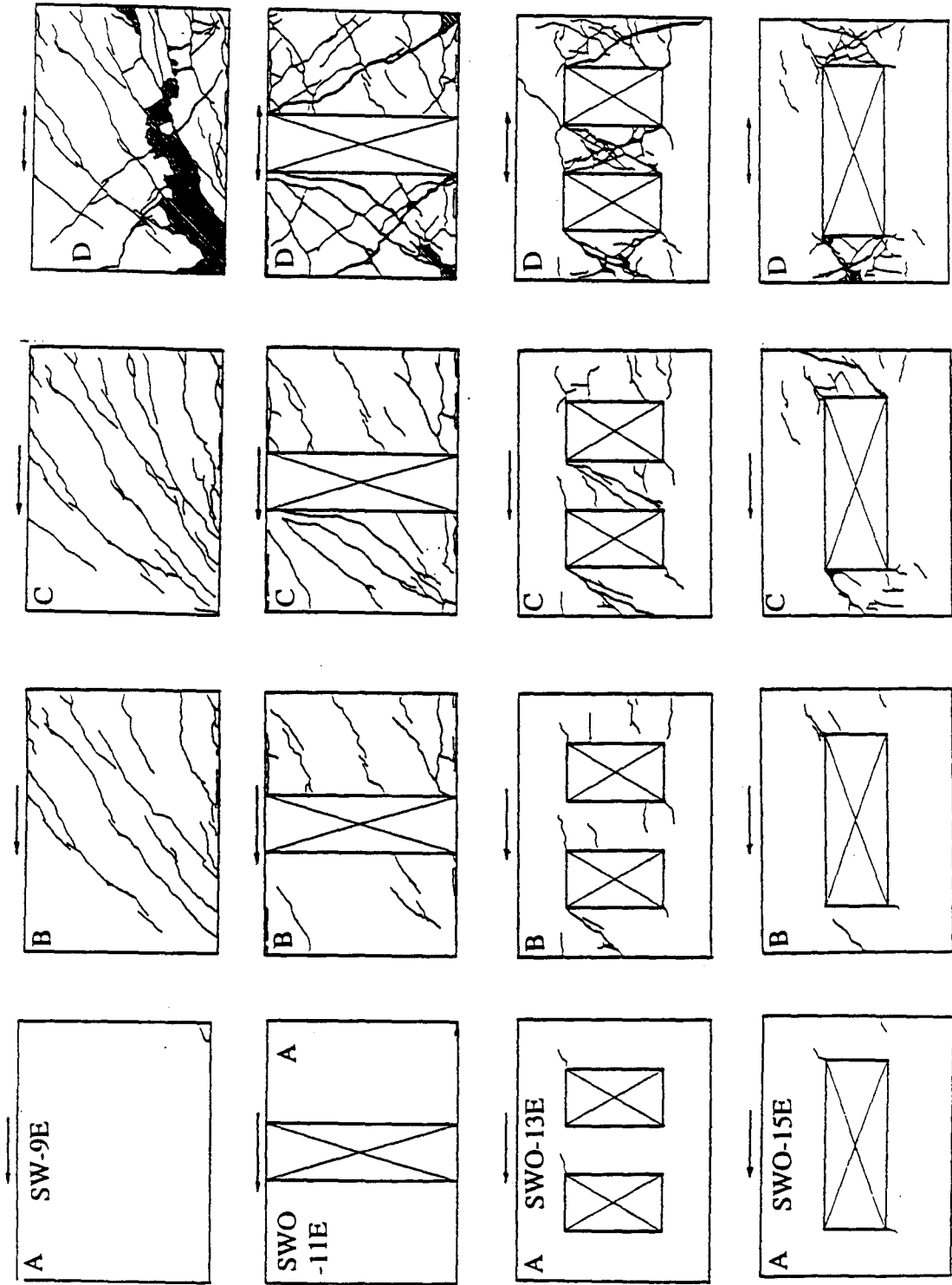
Figure 8 (continued) Development of crack (a) Elastic stage (A); (b) Cracking stage (B); (c) Yielding stage (C); (d) Failure stage (D) for NCKU shear walls
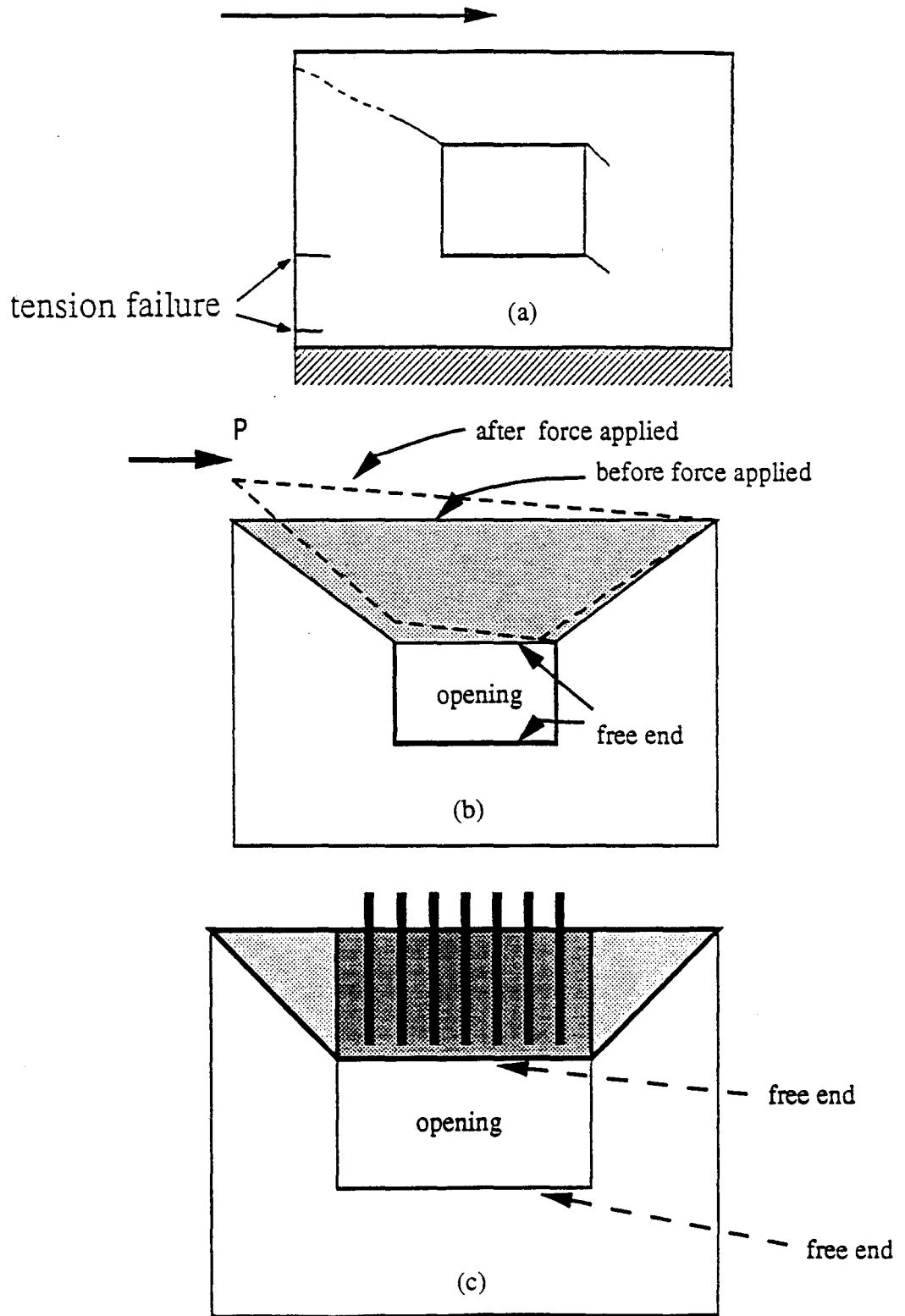
Figure 9 Possible initial cracks of perforated shear wall and cracking mechanism in top block of perforated shear wall

Three kinds of initial cracks are most likely to exist in shear walls at the early stage of loading history. Location, size and shape of openings determine which crack is first. Mechanical characteristics differ among the three kinds as follows. Diagonal cracks usually occur at the corners of openings due to stress concentration. They show the combined action of normal and shear stresses, i.e., coupling effect of bending and shear. Second, horizontal cracks beside an opening are caused by the shear mechanism. Shear failure within concete in the horizontal direction induces this kind of initial crack. Third, another horizontal crack comes from the bending effect. Flexural behavior on the tension side of a shear wall makes tensile stress of this wall more dominant than tensile strength of the concrete. Tensile cracks occur in the concrete, unlike the previous horizontal crack which is the crack-shift type. Other initial cracks on the compression side come from compression failure. Here the mechanism is that the wall's compressive stress is larger than the concrete's compressive strength. Another mechanism begins at the corner due to stress concentration.

Concerning the whole shear wall, the initial cracks will separate the integrated shear wall into several small wall elements. These cracks decrease workability of the whole shear wall. The development of subsequent cracks is then limited, and the region and scale of subsequent cracks is restricted under the initial cracks. Thus, failure mechanism occurs in one of the small wall blocks (elements). As shown in Figure 8, the critical failure block will most likely happen in the regions between openings and at both sides of openings.

As observed in many NCKU shear walls, an initial diagonal crack on the tension side induces another crack going upward on the compression side. A wedge-shaped block is then formed (see Figure 9(b)). This wedge-shaped region acts like a transition zone to transfer force from the tension to the compression side. Since no major cracks exist in this region, its integrity is assured. Both concrete and steel have the same deflection in either vertical or horizontal direction. Figure 9(c) shows that the top and bottom of openings are

free ends which do not take any load and stress. For this reason, the effect of vertical steel bars is neglected here. In general, initial diagonal cracks separate a block on top from the rest of the shear wall. This top block, or wedge-shaped region, is elastic and force-free.

Lateral displacement caused by this region thus equals summation of both elastic deformation and rotation at a given point on the shear wall's compression side. It can also be observed that subsequent cracks occur below this region and extend downward. Then the shear wall reaches the failure state. Figure 10 shows the failure region of a perforated shear wall. With rotation of the wedge-shaped region, vertical bars can yield along the crack underneath both sides of this region. Vertical bars are therefore examined on both sides of the opening along the overall height of the shear wall.

2. <u>Diagonal Cracks</u> These cracks influence a shear wall's resistance to external load, particularly initial diagonal cracks. Corresponding lateral displacement results. Figure 11(a) shows that when diagonal cracks occur in a shear wall, relative lateral displacement Δ_1 develops, with a pseudo rotating center at PRCC1. Lateral displacement Δ_1 at this point equals the product of arc angle θ_1 and crack length of development L_{c1} (see Figure 11(c)). As the external lateral load increases, this crack extends further to rotating center PRCC2 with corresponding lateral displacement Δ_2, expressed as $\Delta_2 \approx L_{c2}\theta$ (see Figure 11(b) and (c)). Since the crack length L_{c2} is larger than L_{c1}, displacement Δ_2 is larger than Δ_1. These initial diagonal cracks form the major cracks which significantly control the behavior of any shear wall. As they extend, these cracks become larger and wider. Figure 8 shows this phenomenon. Yielding and failure stages of these shear walls exhibit many large diagonal cracks in failure regions. Comparing perforated and solid shear walls, it can be seen that the latter has larger diagonal cracks than the former. As noted above, lateral displacement may result from diagonal cracks. Thus solid shear walls potentially have larger maximum displacement than perforated shear walls when subjected to external load.
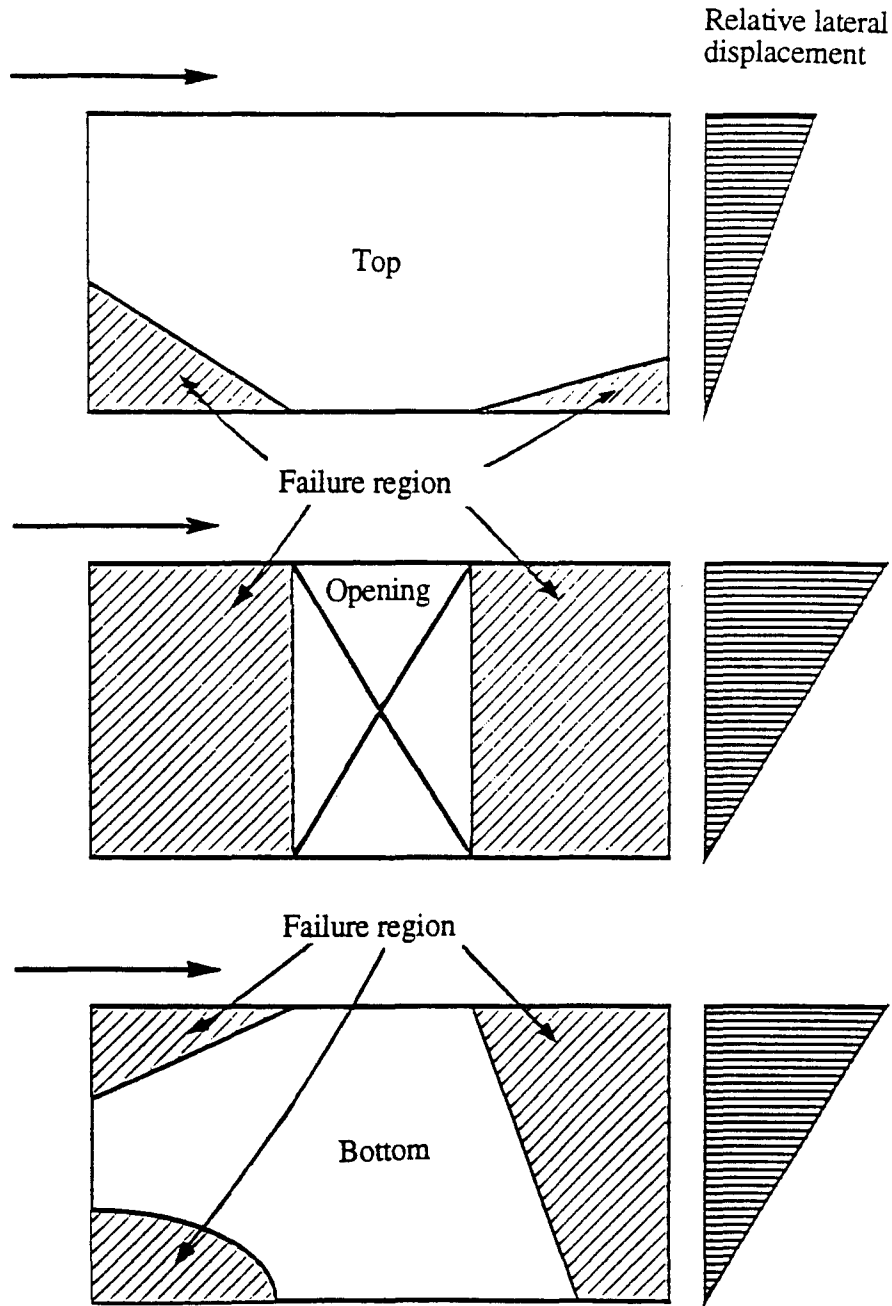
Figure 10 Failure regions in perforated shear wall

3. <u>Hinging Region</u> In the study of solid shear walls, Cheng and Mertz state that the hinging region is the solid shear wall itself [29]. This region exists where the effect of bending and shear are coupled. A solid shear wall displays this coupling behavior across
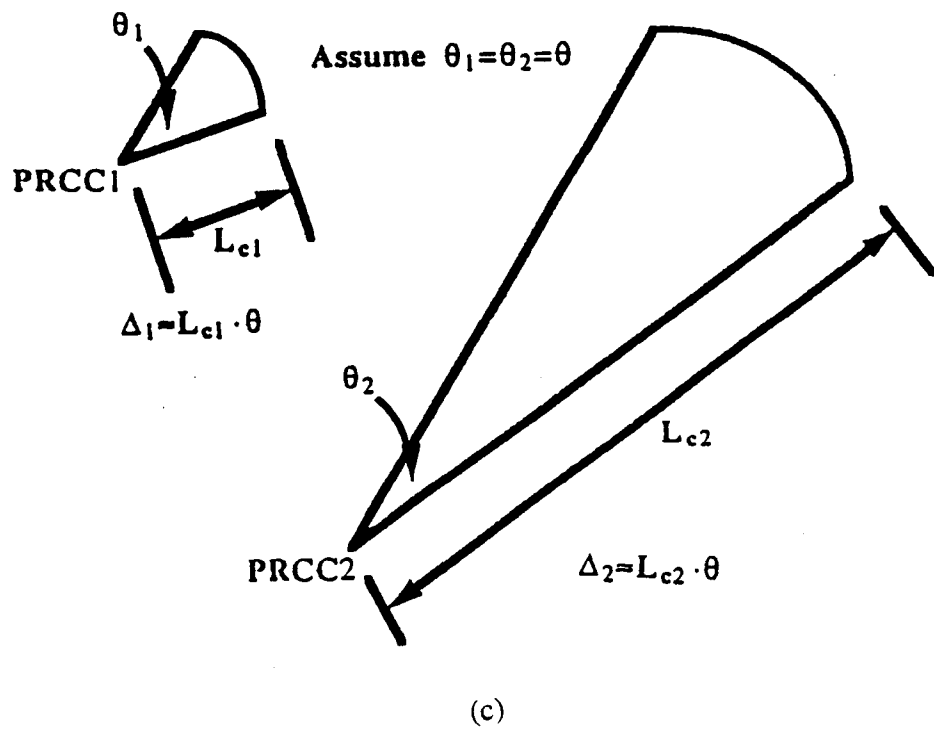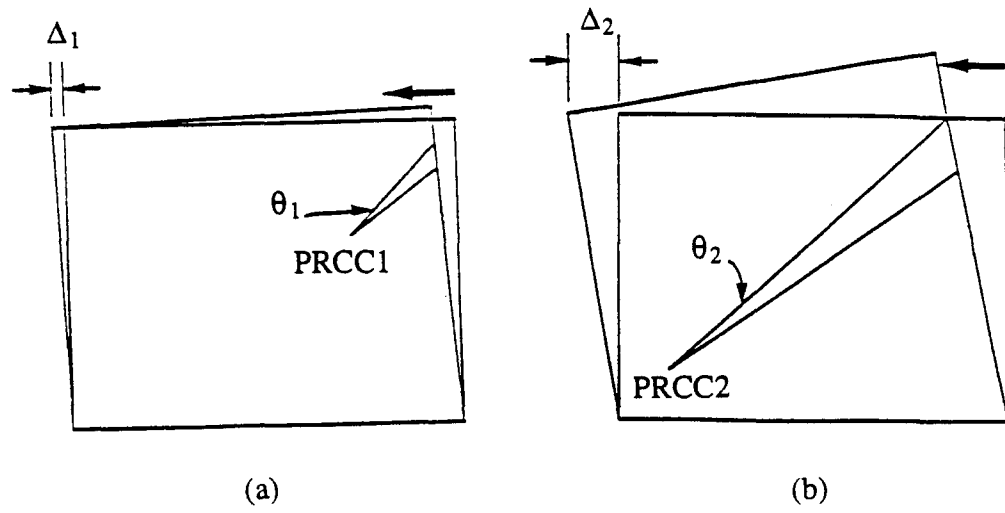
Figure 11 Pseudo rotating center of crack in relation to diagonal crack

its height. Prior to the failure mechanism, all cracks in the concrete and possible yielding of steel have developed. Figure 8 shows that the hinging region for solid shear walls SW-0E, SW-1E and SW-9E encompasses all the wall elements. In perforated shear walls, hinging regions are located at both sides of and between openings, sometimes extending slightly downward.

For simplicity, a major coupling influence line is introduced here to explore how combined bending and shear works within the shear wall. Figure 12(a) shows that a major coupling influence line covers all the wall elements. This influence line shows the area affected by diagonal cracks. In general, connecting the diagonal corners of the solid shear wall constitutes the major coupling influence line and forms the square or rectangle wherein this influence line is diagonal. This square or rectangle is the hinging region. As shown in Figure 12(b), a value of $\theta = 45°$ is used for the angle between the major coupling influence line and the horizontal line. Also shown is that the hinging regions, as determined by major coupling influence lines for perforated shear walls, meet the experimental results in Figure 8. Comparing Figure 12(a) and (b), it can be seen that the hinging region is smaller for a perforated than a solid shear wall. Load capacity and maximum displacement of perforated shear walls is therefore less.

Next to be investigated is the effect of horizontal steel bars on perforated shear walls. Stress distribution in different sections of perforated shear walls is shown in Figure 13. Section A-A's normal stress is small, caused by bending effect. Its shear stress distribution shape is somewhat uniform, due to shear effect. Section B-B displays stress redistribution on normal and shear stress. Because this section is narrower, its normal and shear stress is larger than section A-A's. Section C-C's moment is larger but its shear is the same as both A-A's and B-B's. Normal stress in this region is very high, but shear stress is less than section B-B's. For a perforated shear wall, sections B-B and C-C generally have a potentially large crack region due to high normal stress or shear stress

36

P

Major coupling influence line

L_l

$\theta = \tan^{-1}\left(\dfrac{L}{W}\right)$ or $\tan^{-1}\left(\dfrac{L}{D}\right)$

(a)

L_2 θ

major coupling influence line

OPENING

$\theta = 45°$ assumed to define critical(major) coupling influence lines

θ

L_3

(b)
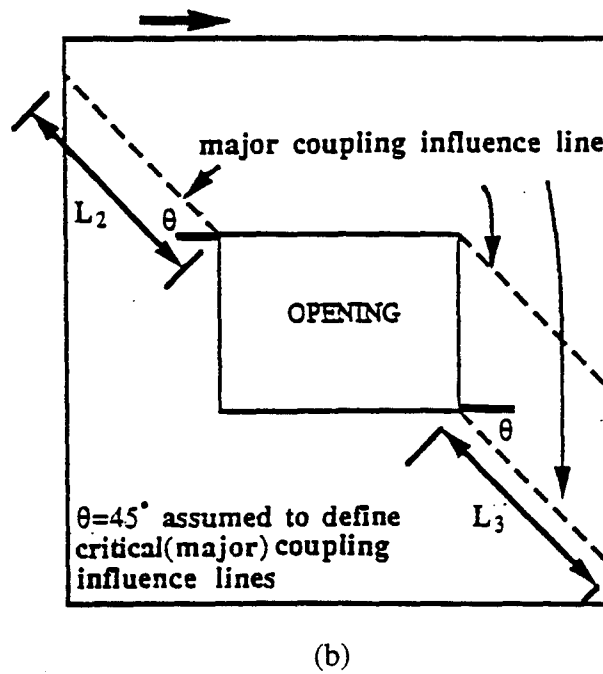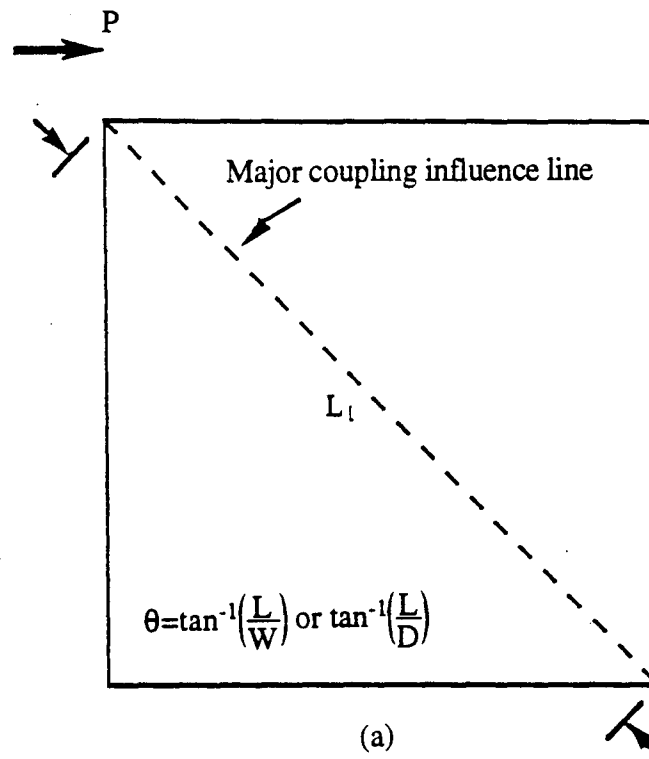
Figure 12 Major coupling influence line in both solid and perforated shear walls

37

Section A-A

Section B-B
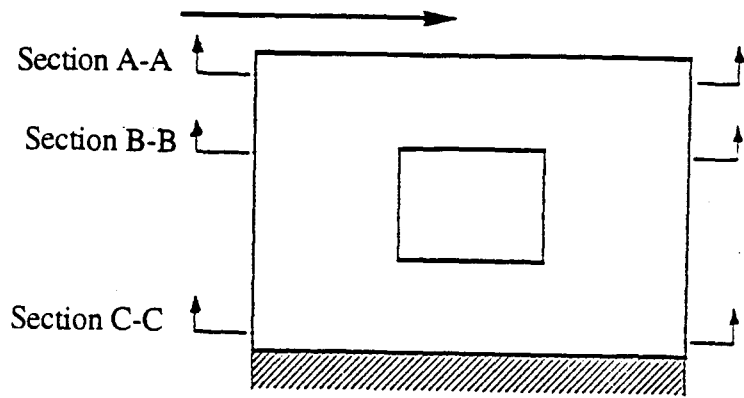
Section C-C

Normal stress distribution
(caused by bending)

Shear stress distribution
(caused by shear)

Section A-A

Section B-B
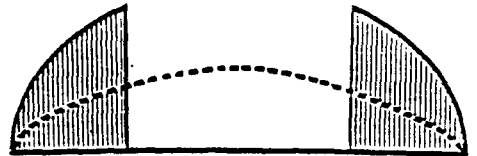
(Potentially high crack region)

Section C-C
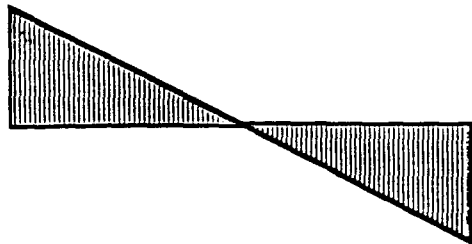
(Potentially high crack region)

Figure 13 Stress distribution in perforated shear wall

38

throughout these sections. Regions containing section B-B and C-C are critical in terms of failure. Horizontal steel bars below the level of openings are thus considered in the computation of critical loads and displacements of backbone curve.

B. BEHAVIOR OF DIAGONAL BARS

Compare displacement from different strain gauges on vertical and diagonal bars in Figure 14(a). It can be seen that strain gauge SG34 for a diagonal bar has a large elongation (7.136 mm) while the strain gauge reading SG35 on the other side of the opening is 0.000 mm. Hence the latter diagonal bar has little compression or tension; the same phenomenon can be observed in other tests.

Due to this pattern of displacement, only diagonal bars on the tension side are considered. Lower diagonal bars on that side are also considered because they are kept in a state of tension. Lower diagonal bars on the other side of opening are neglected due to compression. As shown in Figure 14(b), -0.723 mm for this bar means that the bar has been compressed that amount.

C. DEFINITION OF BACKBONE CURVE

By using analytical derivation coupled with a curve-fitting approach from experimental results, a set of equations is presented to caculate forces and displacements at different loading stages. Figure 15 shows the force-displacement relationship or backbone curve. In this figure, four critical loading points describe the characteristics of a shear wall. Cracking point indicates the loading point when concrete reaches the moment of cracking, and initial cracks first appear. Yielding point represents the stage when the outermost steel bars attain yielding stress. When the external load cannot be increased, it is called the ultimate point. After this point, the curve degrades. This demonstrates that the shear wall cannot reach the previous ultimate state again. If the load continues to increase, the curve goes downward proportionally until the failure reference point.
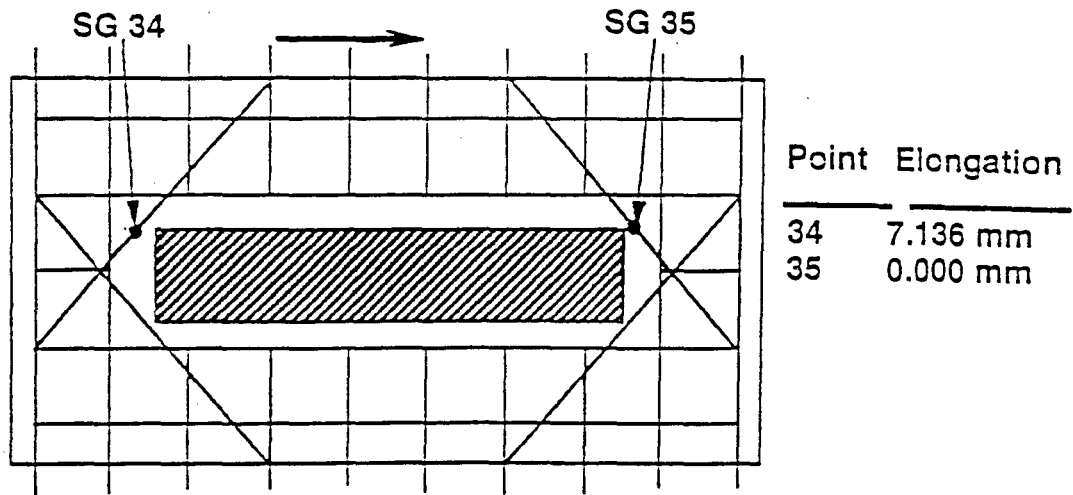
(a)
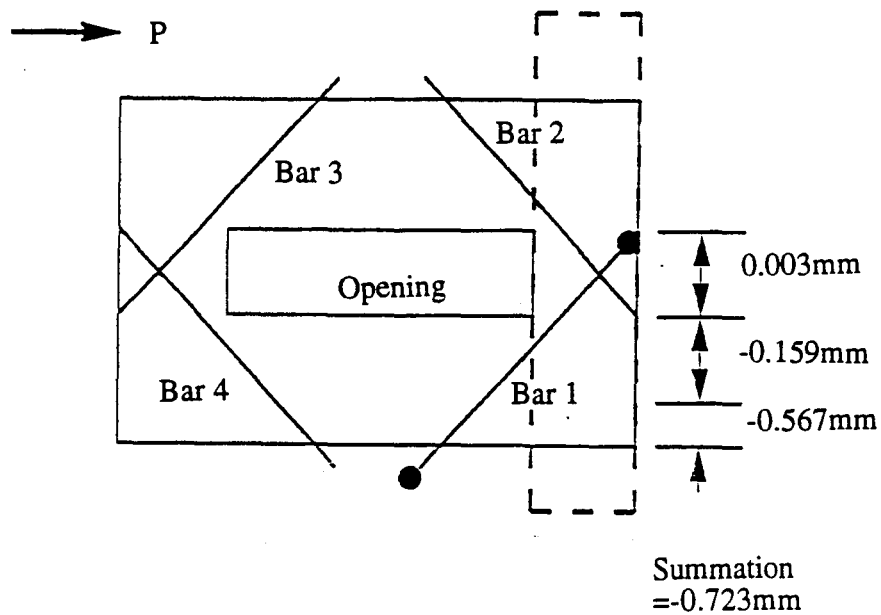
(b)

Figure 14   Elongation of diagonal steel bars for perforated shear wall SWO-3E
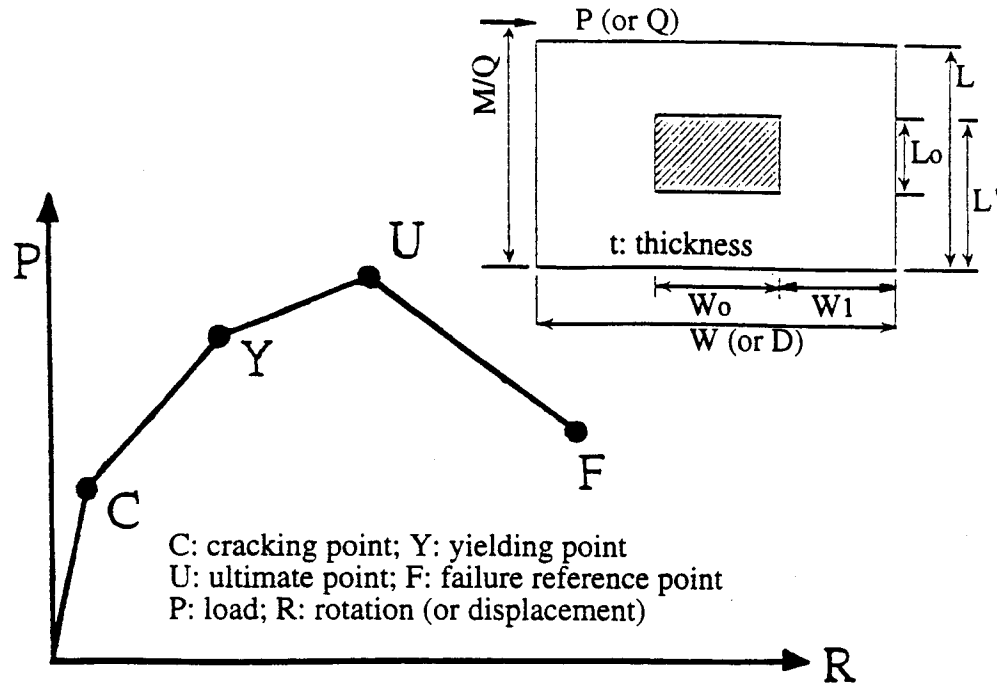
Figure 15   Critical points of defined backbone curve for perforated shear wall

1. <u>Force at Four Loading Stages</u>   Various effects are expressed here. They include

shear span length ratio MQD (= M/QD where M is the moment at the bottom of the wall, Q

is external load, D is width of whole wall), height ratio of opening α_0 (= Lo/L), width ratio

of opening β_0 $\left(=\frac{W_0}{W}\right)$, horizontal location factor of opening β_1 $\left(=\frac{W_1}{W}\right)$, and vertical location

factor of opening LWP(=L'/W1).   Units employed here are cm, Kg and Kg/cm^2.

Let

$$PWH=(\Sigma(\rho_{wh}f_y))(L/W) \tag{2}$$

$$PWH1=(\Sigma(\rho_{wh}f_y/5000))(L/W) \tag{3}$$

$$PWV=(\Sigma(\rho_{wv}f_y))(W/L)^{a_1} \tag{4}$$

$$PWV1 = (\Sigma(\rho_{wv}f_y/5000))(W/L)^{a_2} \tag{5}$$

where $a_1 = 4.7663$; ρ_{wh} and ρ_{wv} represent the steel ratios of horizontal and vertical bars, respectively. Derivation of PWH and PWV is discussed later. Equations of loading capacities at four critical stages are

Cracking point

$$P_c = \left[A_1 + A_2\left(\frac{L'}{L}\right)(\alpha_0 \cdot \beta_1)\right]\sqrt{f_c'}\, W \cdot t \tag{6}$$

or

$$\frac{P_c}{\sqrt{f_c'}\, W \cdot t} = A_1 + A_2\left(\frac{L'}{L}\right)(\alpha_0 \cdot \beta_1) \tag{7}$$

in which

$$A_1 = 0.0212 + 0.2762\,(MQD) \tag{8}$$

$$A_2 = 1.1531 - 1.2215\,(MQD) \tag{9}$$

Figure 16 shows the relationship with P_c.

Yielding point

$$P_y = \left[A_3 + A_4 \cdot \log_{10}\left[\left(\frac{L'}{L}\right)(\alpha_0 \cdot \beta_1)\right]\right]P_u \tag{10}$$
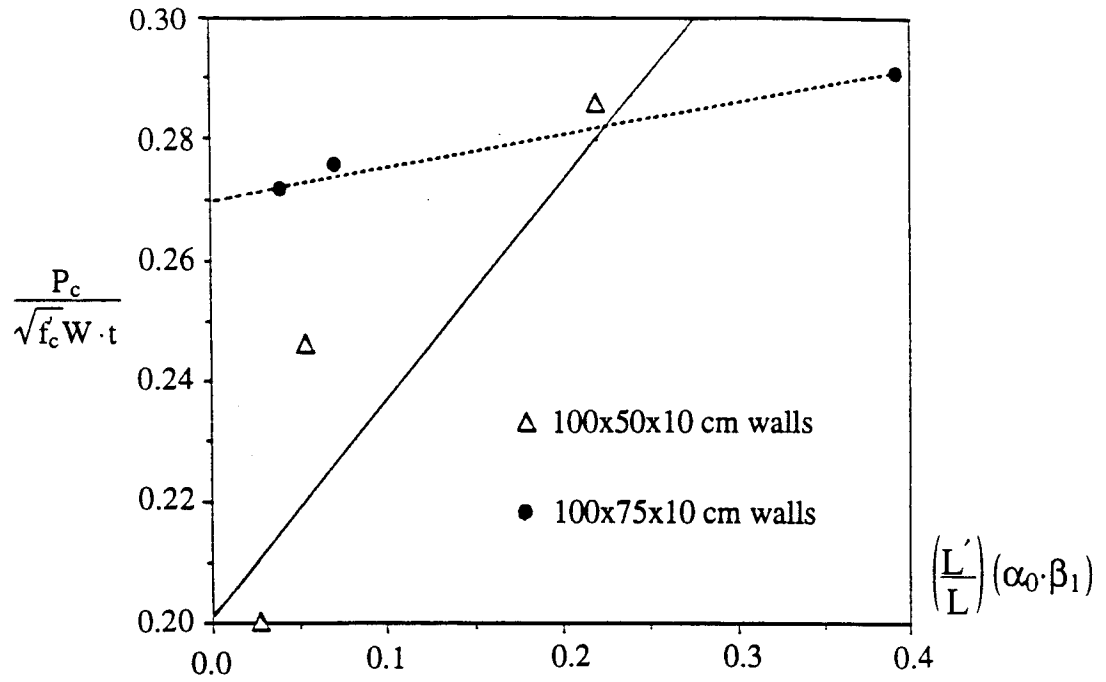
Figure 16 Relationship between cracking load and opening factors of perforated shear wall

$$\frac{P_y}{P_u} = A_3 + A_4 \cdot \log_{10}\left[\left(\frac{L'}{L}\right)(\alpha_0 \cdot \beta_1)\right]$$ (11)

in which

$A_3 = 1.2657 - 0.3188 \ (MQD)$ (12)

$A_4 = 0.2702 - 0.1362 \ (MQD)$ (13)

This is also shown in Figure 17.
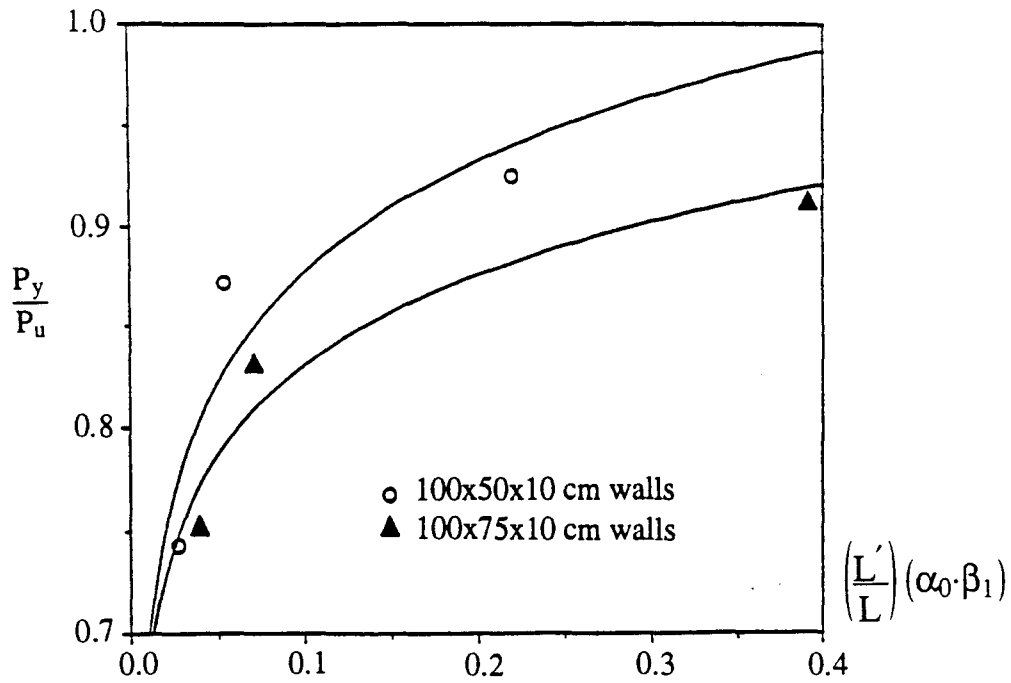
Figure 17 Relationship between ratio of yielding load/ultimate load and opening factors of perforated shear wall

Ultimate point

$$P_u = \tau_u \cdot W \cdot t \tag{14}$$

$$\tau_u = \left[U_1 + U_2 \left(\frac{L'}{L} \right) (\alpha_0 \cdot \beta_1) \right] \sqrt{f_c'} + U_3 \cdot PWH + U_4 \cdot PWV \tag{15}$$

where

$$U_1 = 0.9320 - 1.1690 \, (MQD) \tag{16}$$

$$U_2 = -1.1741 + 1.5588 \, (MQD) \tag{17}$$

44
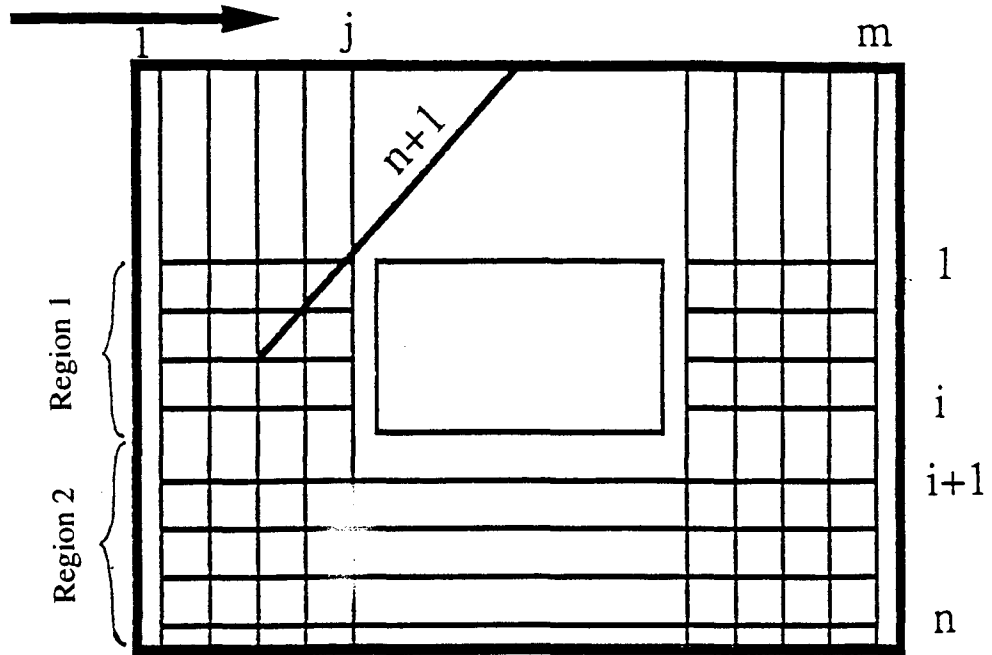
Figure 18 General configuration of vertical and horizontal steel bars in
perforated shear wall

$$U_3 = 0.3128 - 0.3249 \text{ (MQD)} \tag{18}$$

$$U_4 = 0.1759 + 0.3079 \text{ (MQD)} \tag{19}$$

Here a_1 in PWV is 4.7663.

Failure reference point

P_f is assumed to be half the sum of cracking load and yielding load, which is expressed as

$$P_f = \frac{1}{2}(P_c + P_y) \tag{20}$$

Now return to the derivations of PWH and PWV. As shown in Figure 18, a general
rotation system is used. Region 1 represents both sides of the opening and region 2 the

area below the level of opening. The load taken by vertical steel bars, horizontal steel bars and diagonal bars is denoted as P_h in the horizontal direction and P_v in the vertical direction.

Before deriving P_h and P_v, three factors need to be defined: length reduction, sectional-area reduction and modification of diagonal bars. They are expressed as follows.

From Figure 19, length reduction factor of horizontal bars is

$$f_{lhh}=(LHB_{11}+LHB_{12})/L_h \tag{21}$$

Length reduction factor of horizontal bars in region 2 is

$$f_{lhh}=L_h/L_h=1 \tag{22}$$
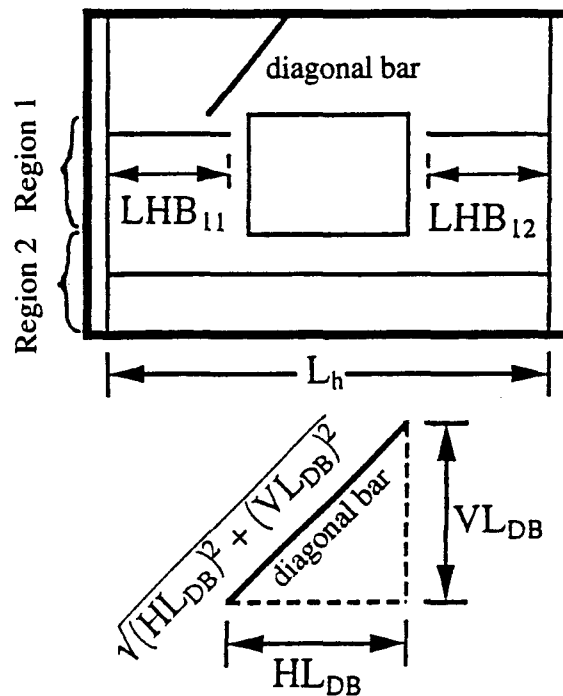
Figure 19 Length reduction factor for steel bars of perforated shear wall

Length reduction factor for diagonal steel bars in horizontal direction is

$$f_{ldh} = HL_{DB}/L_h \tag{23}$$

and in the vertical direction is

$$f_{ldv} = VL_{DB}/L \tag{24}$$

Cross section area reduction factor is demonstrated in Figure 20. Here the projection of a steel bar's normal force in the horizontal and vertical directions is $P \cdot COS\theta$ and $P \cdot SIN\theta$ formulated as

$$P \cdot COS\theta = f_y \cdot (A_s \cdot COS\theta) = f_y \cdot A_s \cdot \frac{HL_{DB}}{\sqrt{(HL_{DB})^2 + (VL_{DB})^2}} \tag{25}$$
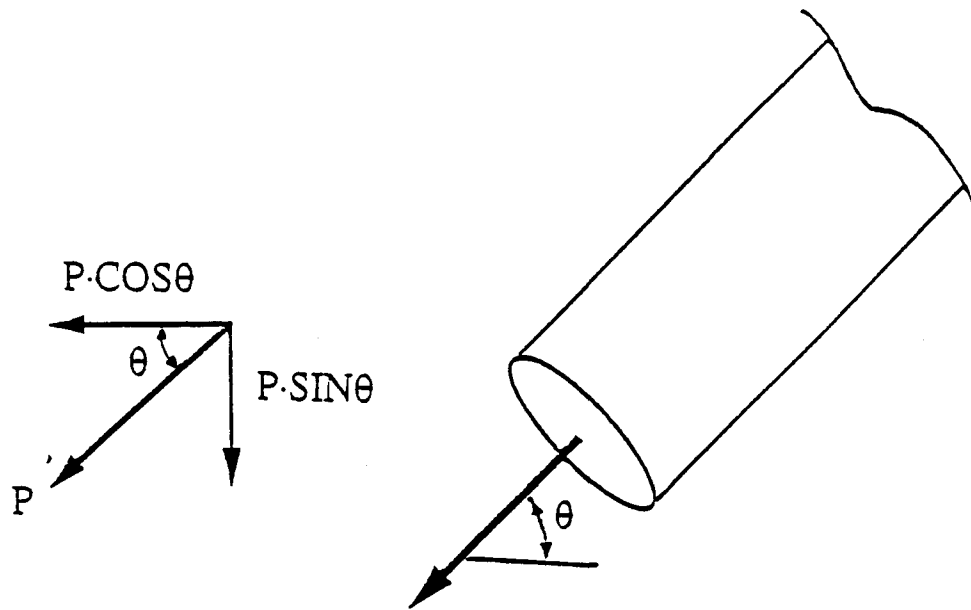
Figure 20 Projection of cross section of diagonal steel bar

$$P \cdot SIN\theta = f_y \cdot \left(A_s \cdot SIN\theta\right) = f_y \cdot A_s \cdot \frac{VL_{DB}}{\sqrt{(HL_{DB})^2 + (VL_{DB})^2}} \qquad (26)$$

where

$$\frac{HL_{DB}}{\sqrt{(HL_{DB})^2 + (VL_{DB})^2}} = f_{adh} \quad \text{(i.e., cross section area reduction factor of diagonal bars}$$

in relation to horizontal projection) $\qquad (27)$

$$\frac{VL_{DB}}{\sqrt{(HL_{DB})^2 + (VL_{DB})^2}} = f_{adv} \quad \text{(i.e., cross section area reduction factor of diagonal bars}$$

in relation to vertical projection) $\qquad (28)$

Figure 21 shows two cases of NCKU shear walls. Bar 1 indicates the lower end is not fixed which is called a semi-rigid joint. Bar 2 has a fixed joint at the lower end which is called a rigid point. Bar 3 is the same as Bar 2 but it is in a state of tension due to stretching of the wall's tension side. Since it is difficult to calculate modification factors for basic development length of diagonal bars, it is assumed as 0.5 (denoted as f_r) for the semi-rigid point (Bar 1); fr=1.0 is assigned to the rigid points (Bars 2 and 3). A summary of f_r is shown in Table IV where numbers for effective diagonal steel bars NDB are also given. From Figure 18, P_h and P_v are

$$P_h = A_1 \cdot (f_y)_1 \cdot \frac{LHB}{L_h} + \cdots + A_i \cdot (f_y)_i \cdot \frac{LHB}{L_h} + A_{i+1} \cdot (f_y)_{i+1} + \cdots + A_n \cdot (f_y)_n$$

$$+ A_{n+1} \cdot (f_y)_{n+1} \cdot \frac{HL_{DB}}{\sqrt{(HL_{DB})^2 + (VL_{DB})^2}} \cdot \frac{HL_{DB}}{L_h} \cdot (f_r)$$

$$= L \cdot t \cdot \left(\sum_{i=1}^{n} \left(\rho_i \cdot (f_y)_i \cdot (f_{lhh})_i \right) \right) + L \cdot t \cdot \left(\sum_{i=n+1}^{n+1} \left(\rho_i \cdot (f_y)_i \cdot (f_{adh})_i \cdot (f_{1dh})_i \cdot (f_r)_i \right) \right) \qquad (29)$$

Figure 21 Modification factor for diagonal bars of perforated shear wall

$$P_v=$$

$$\left\{ A_1 \cdot (f_y)_1 + \cdots + A_m \cdot (f_y)_m + A_{n+1} \cdot (f_y)_{n+1} \cdot \frac{VL_{DB}}{\sqrt{(HL_{DB})^2 + (VL_{DB})^2}} \cdot \frac{VL_{DB}}{L} \cdot (f_r) \right\} \left(\frac{W}{L}\right)^a$$

$$= \left\{ W \cdot t \cdot \left(\sum_{i=1}^{n} \left(\rho_i \cdot (f_y)_i \right) \right) + W \cdot t \cdot \left(\sum_{i=n+1}^{n+1} \left(\rho_i \cdot (f_y)_i \cdot (f_{adv})_i \cdot (f_{ldv})_i \cdot (f_r)_i \right) \right) \right\} \left(\frac{W}{L}\right)^a$$

$$(30)$$

in which a is constant.

Figure 22 shows horizontal and vertical cross sections of a shear wall. Horizontal shear stress τ_h on the horizontal cross section can be easily defined as $\tau_h = \frac{P_h}{W \cdot t}$. Vertical shear stress τ_v can likewise be defined as $\tau_v = \frac{P_h}{L \cdot t}$. Therefore

$$\tau_h = \frac{P_h}{W \cdot t} = \frac{L}{W} \left(\sum_{i=1}^{n} \left(\rho_i \cdot (f_y)_i \cdot (f_{lhh})_i \right) \right) + \frac{L}{W} \left(\sum_{i=n+1}^{n+1} \left(\rho_i \cdot (f_y)_i \cdot (f_{adh})_i \cdot (f_{ldh})_i \cdot (f_r)_i \right) \right)$$
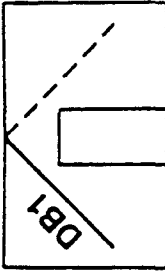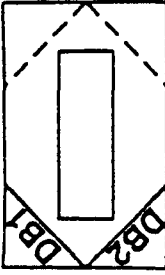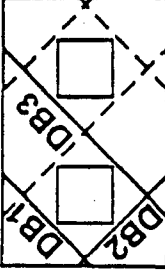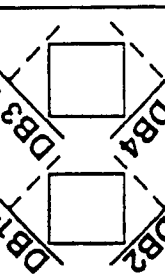
$$= \left(\Sigma \left(\rho_{wh} \cdot f_y \right) \right) \left(\frac{L}{W} \right) = PWH$$

$$(31)$$

$$\tau_v = \frac{P_v}{L \cdot t} = \frac{L}{W} \left(\sum_{i=1}^{n} \left(\rho_i \cdot (f_y)_i \cdot (f_{lhh})_i \right) \right) + \frac{L}{W} \left(\sum_{i=n+1}^{n+1} \left(\rho_i \cdot (f_y)_i \cdot (f_{adv})_i \cdot (f_{ldv})_i \cdot (f_r)_i \right) \right)$$

$$= \left(\Sigma \left(\rho_{wv} \cdot f_y \right) \right) \left(\frac{W}{L} \right)^{a1} = PWV$$

$$(32)$$

Here a1 in PWV is 4.7663. Effects of horizontal steel bars $\Sigma \left(\rho_{wh} \cdot f_y \right)$ on PWH (or PWH1) and vertical steel bars $\Sigma(\rho_{wv} f_y)$ on PWV (or PWV1) are discussed later.

Table IV Summary of coefficients NDB and fr

WALL TYPE / COEFF.	1	2		3			4			
NDB	DB1	DB1	DB2	DB1	DB2	DB3	DB1	DB2	DB3	DB4
fr	0.5	0.5	1.00	0.5	1.00	1.00	0.5	1.00	0.5	1.00
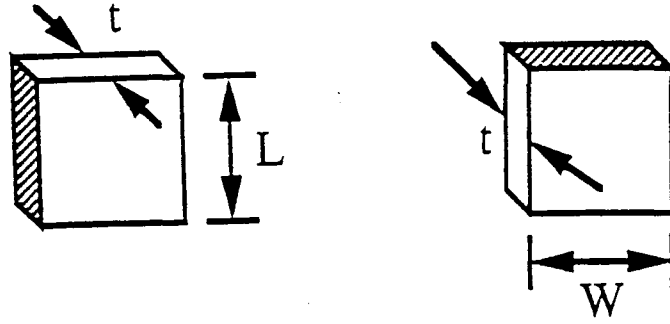
Figure 22 Schematic diagram of vertical and horizontal cross sections
in perforated shear wall

In Eqs. (2) to (5), $\Sigma(\rho_{wh}f_y)$ and $\Sigma(\rho_{wv}f_y)$ are defined as

$$\Sigma(\rho_{wh}f_y) = \frac{1}{L \cdot t}(EHB) + \frac{1}{L \cdot t}(EDBH) \tag{33}$$

$$\Sigma(\rho_{wv}f_y) = \frac{1}{W \cdot t}(EVB) + \frac{1}{W \cdot t}(EDBV) \tag{34}$$

where effect of horizontal bar is

$$EHB = \sum_{i=1}^{NHB} \left((A_h)_i \cdot (f_y)_i \cdot \left(\frac{(LHB)_i}{L_h} \right) \right) = \sum_{i=1}^{NHB} \left((A_h)_i \cdot (f_y)_i \cdot (f_{lhh})_i \right) \tag{35}$$

Effect of diagonal bar in horizontal direction is

$$EDBH = \sum_{i=1}^{NDB} \left((A_d)_i \cdot (f_y)_i \cdot \left(\frac{(HL_{DB})_i}{\sqrt{(HL_{DB})_i^2 + (VL_{DB})_i^2}} \right) \cdot \left(\frac{(HL_{DB})_i}{L_h} \right) f_r \right)$$

$$= \sum_{i=1}^{NDB} \left((A_d)_i \cdot (f_y)_i \cdot (f_{adb})_i \cdot (f_{ldh})_i \cdot f_r \right) \tag{36}$$

Effect of vertical bar is

$$EVB = \sum_{I=1}^{NVB} \left((A_v)_i \cdot (f_y)_i \right) \tag{37}$$

Effect of diagonal direction is

$$EDBV = \sum_{I=1}^{NDB} \left((A_d)_i \cdot (f_y)_i \cdot (f_{adv})_i \cdot (f_{ldv})_i \cdot (f_r)_i \right) \tag{38}$$

2. Displacement at Four Loading Stages Corresponding displacement at four critical points are now formulated. From Figure 23(a), shear deformation based on theoretical derivation is

$$D = \alpha \frac{PL}{GA} \tag{39}$$

or

$$\frac{D}{\left(\frac{PL}{GA}\right)} = \alpha \quad ; \quad \alpha = constant \tag{40}$$

where G is shear modulus.

Equations of displacement at critical points are similarly formulated. Some modifications are considered, such as compressive strength of concrete fc', effect of opening F_{c1} (and F_{y1}, F_{u1}), effect of vertical steel bars and diagonal steel bars on vertical projection F_{c2} (and F_{y2}, F_{u2}), and effect of horizontal steel bars and diagonal steel bars on

53

(a)

(b)
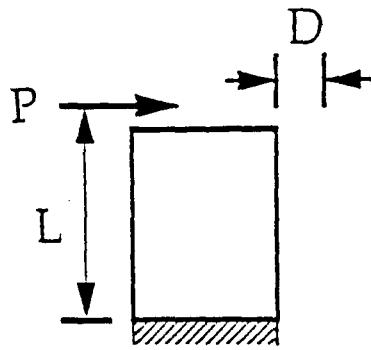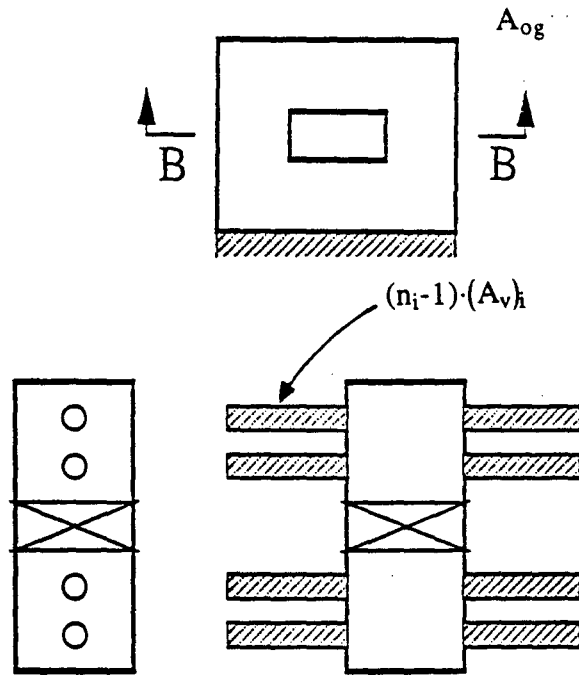
Section B - B

Figure 23 Definition of load and displacement as well as transformed cross section of perforated shear wall

54

horizontal projection F_{c3} (and F_{y3}, F_{u3}). Shear span length ratio MQD arising from the factor $C1, Y1$ and $U1$ is also involved. All these factors are constants. Thus the form of critical displacements is

cracking displacement
$$\frac{D_c \sqrt{\dfrac{f'_c}{280}}}{\left(\dfrac{P_c \cdot L}{G \cdot A_{og}}\right)} = C_1(F_{c1} + F_{c2} + F_{c3}) \qquad (41)$$

yielding displacement
$$\frac{D_y \cdot \sqrt{\dfrac{f'_c}{280}}}{\left(\dfrac{P_y \cdot L}{G \cdot A_{og}}\right)} = Y_1(F_{y1} + F_{y2} + F_{y3}) \qquad (42)$$

ultimate displacement
$$\frac{D_u \cdot \sqrt{\dfrac{f'_c}{280}}}{\left(\dfrac{P_u \cdot L}{G \cdot A_{og}}\right)} = U_1(F_{u1} + F_{u2} + F_{u3}) \qquad (43)$$

where Aog is the transformed cross sectional area in the section with an opening. Aog is described later in this section.

Displacements corresponding to the four loading stages are formulated as follows.

Cracking point

$$D_c = C_1(F_{c1} + F_{c2} + F_{c3})(P_c L/GA_{og})/\sqrt{f'_c/280} \qquad (44)$$

in which

$$C_1 = 5.007 - 3.941 MQD \qquad (45)$$

55

$$F_{c1}=0.1775-9.61\left(L'/L\right)\left(W_1/W\right)\left(\alpha_0\beta_0\right) \tag{46}$$

$$F_{c2}=1903(PWV1) \tag{47}$$

$$F_{c3}=-1092(PWH1) \tag{48}$$

and

$$\left|F_{c1}+F_{c2}\right|\geq\left|F_{c3}\right| \tag{49}$$

$$A_{og}=\left(W-W_0\right)t+\sum_{i=1}^{NVB}\left(n_i-1\right)\left(A_v\right)_i \tag{50}$$

A_v is the cross sectional area of the vertical steel bar (A_{og} in Figure 23(b))

and

$$n_i=\frac{E_s}{E_c}=\frac{\sigma_y/\varepsilon_{sy}}{15000\sqrt{f_c'}}=\frac{\sigma_y}{37.5\sqrt{f_c'}} \tag{51}$$

where ε_{sy} is assumed to be 0.0025.

Yielding point

$$D_y=Y_1\left(F_{y1}+F_{y2}+F_{y3}\right)\left(P_yL/GA_{og}\right)\sqrt{f_c'/280} \tag{52}$$

in which

$$Y_1=-1.878+3.773MQD \tag{53}$$

$$F_{y1} = 7.697 + 229.2 (L'/L)(W_1/W)(\alpha_0\beta_0) \tag{54}$$

$$F_{y2} = 2622(PWV1) \tag{55}$$

$$F_{y3} = -6691(PWH1) \tag{56}$$

and

$$|F_{y1} + F_{y2}| \geq |F_{y3}| \tag{57}$$

Here a_2 in PWV1 is 0.6751.

<u>Ultimate point</u>

$$D_u = U_1(F_{u1} + F_{u2} + F_{u3})(P_uL/GA_{og})/\sqrt{f_c'/280} \tag{58}$$

in which

$$U_1 = -0.7435 + 2.4MQD \tag{59}$$

$$F_{u1} = 13.05 + 488.6(L'/L)(W_1/W)(\alpha_0\beta_0) \tag{60}$$

$$F_{u2} = 2214(PWV1) \tag{61}$$

$$F_{u3} = -7685(PWH1) \tag{62}$$

57

and

$$|F_{u1}+F_{u2}|\geq|F_{u3}| \tag{63}$$

Here a_2 in PWV1 is 0.2997.

Failure reference point

$$D_f=(C_{f1}+C_{f2}(LWP))D_u \tag{64}$$

in which

$$C_{f1}=2.2349-3.4173MQD \tag{65}$$

$$C_{f2}=1.5608-0.4736MQD \tag{66}$$

$$LWP=L'/W_1 \tag{67}$$

D. COMPARISON OF CALCULATED AND EXPERIMENTAL RESULTS

Figure 24 shows that caculated and experimental curves compare favorably. Perforated shear wall SW-11E has a slightly larger deviation at yielding and ultimate stage, but this error (8%) is acceptable.
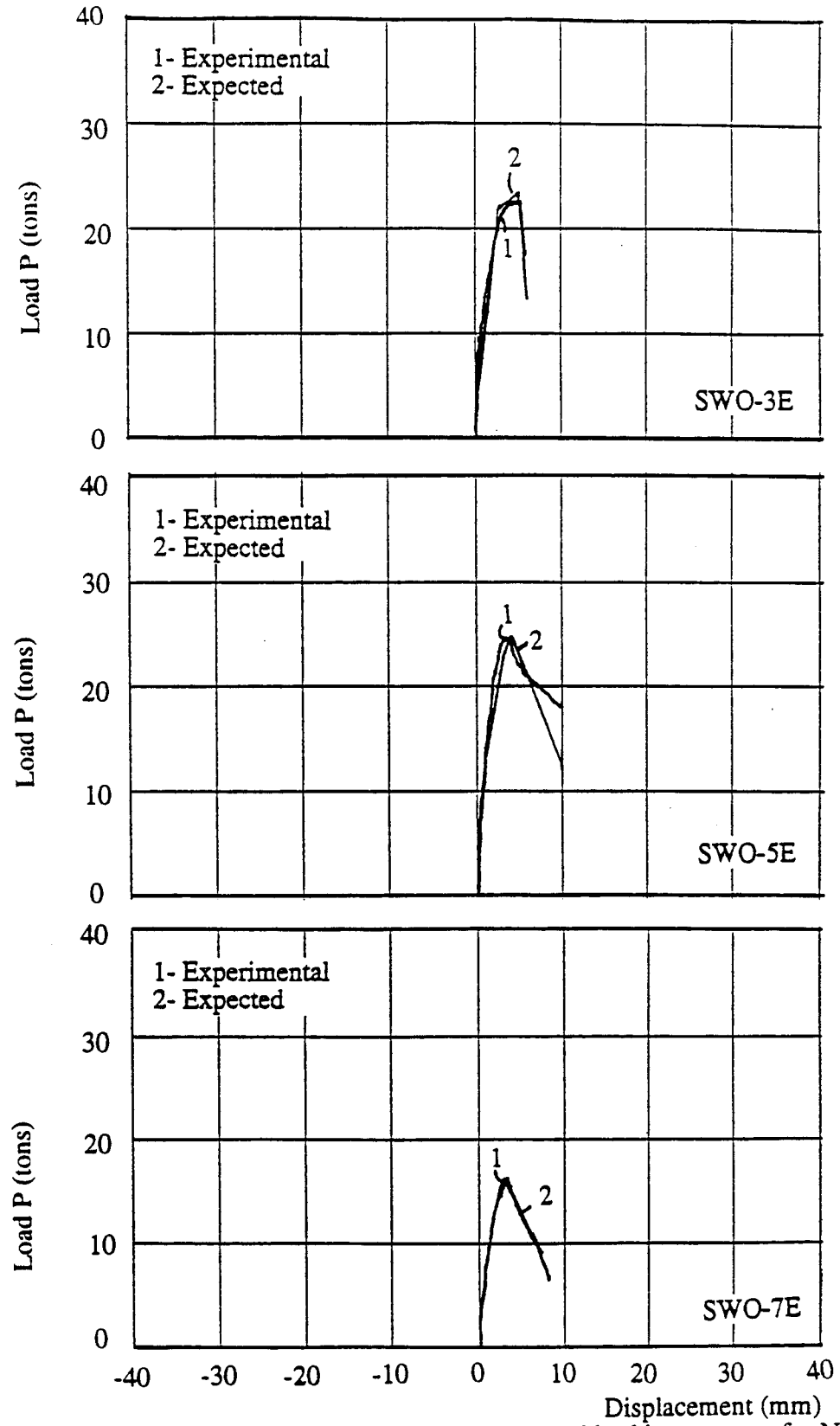
Figure 24 Comparison between expected and experimental backbone curves for NCKU shear walls
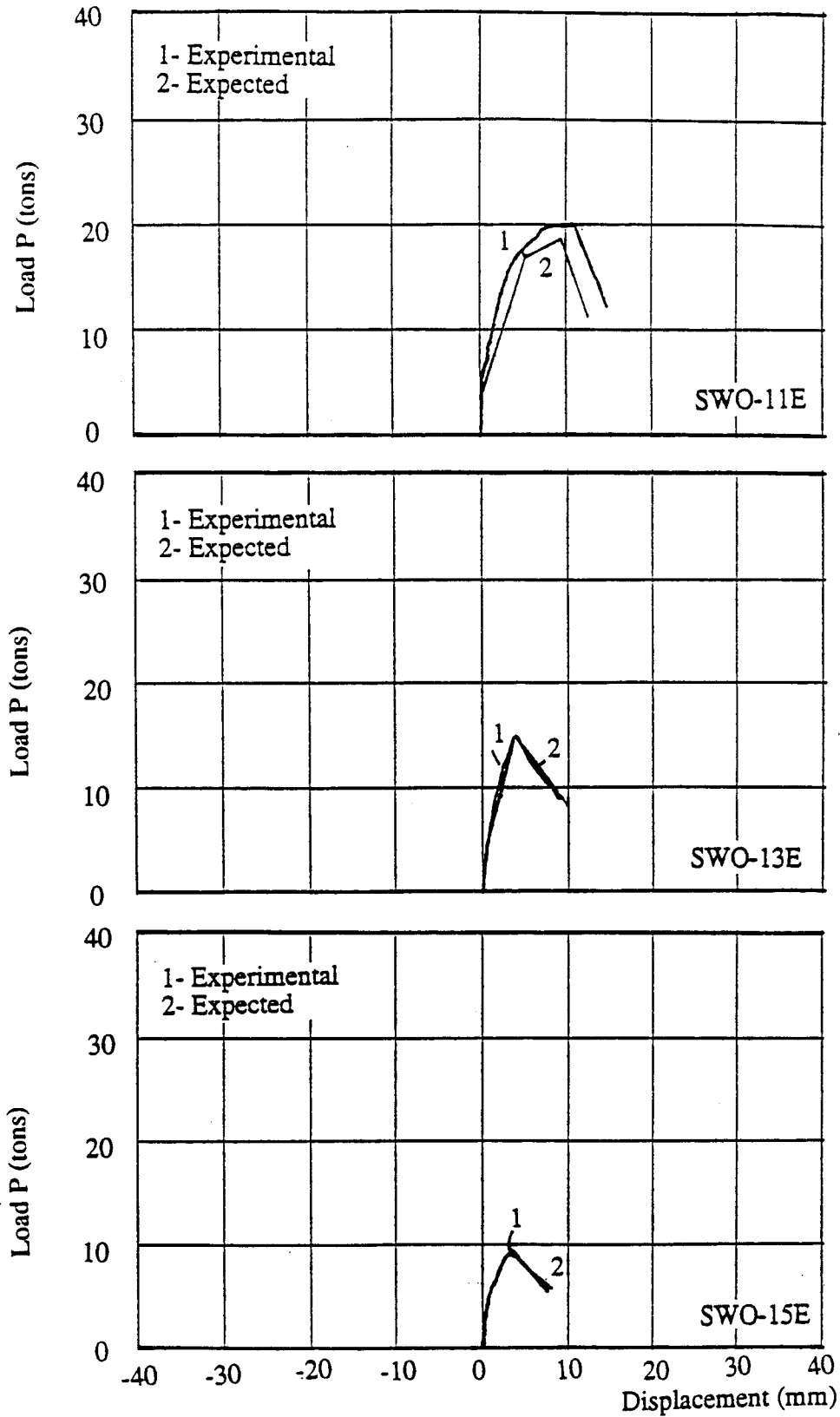
Figure 24 (continued) Comparison between expected and experimental backbone curves for NCKU shear walls

IV. HYSTERESIS RULES FOR PERFORATED SHEAR WALLS

Seismic response due to such external excitation as earthquakes, machine vibration and unexpected explosion may put structures at risk, particularly in the seismic zone. Buildings subjected to seismic oscillation deform from elastic to inelastic stages and possibly collapse through various hysteresis loops at members and structural joints. Structures absorb energy to some extent associated with hysteretic behavior. Ductile buildings are more likely to behave hysteretically. This section focuses on the development of hysteresis loops for shear walls and comparison between analytical and experimental results.

A. DEFINITION OF DISSIPATED ENVELOPE

For developing hysteresis loops of perforated shear walls, two kinds of curve exist as shown in Figure 25. One is the backbone curve; the other is the reference curve. The latter is a type of "dissipated envelope" relating to the most likely response of a wall after some degree of energy dissipation. This reference curve is set up in a manner similar to the backbone curve consisting of segments representing four distinct loading stages. In Figure 25, the shaded area enclosed by the backbone and reference curves is due to cracking or yielding of the shear wall.

B. ESTABLISHMENT OF REFERENCE CURVE

The process of curve development is based on three empirical equations concerning the effect of energy dissipation. Figure 26 shows behavior of perforated shear wall from point A, which is located at zero loading. Here the path will not pass through the origin. This is due to energy dissipation from nonlinear behavior of the shear wall. Some near-linear segments are identified in Figure 26. A tangent line is drawn for each segment and some intersection points are decided, R_1, R_2 and R_3. Note that the reference curve has
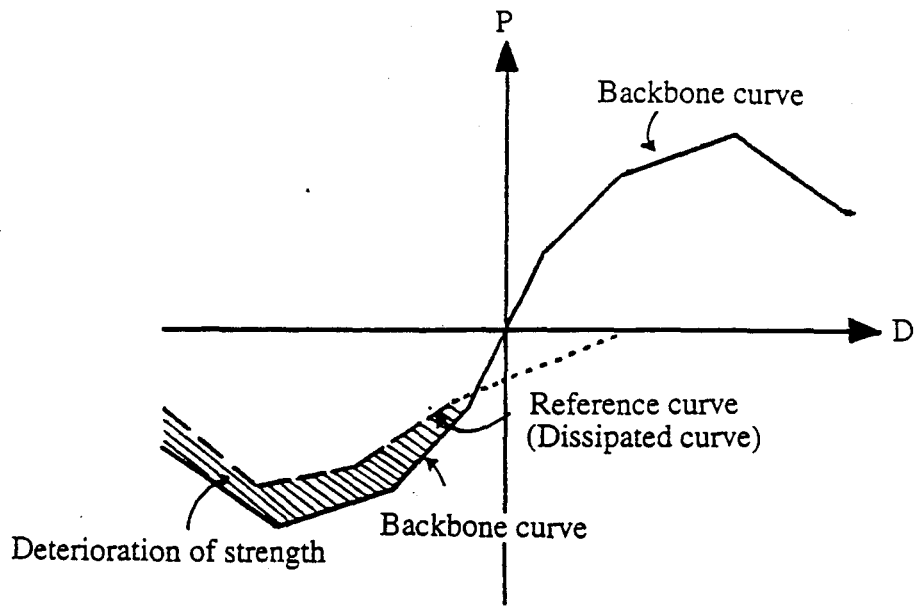
Figure 25 Comparison of backbone curve and reference curve
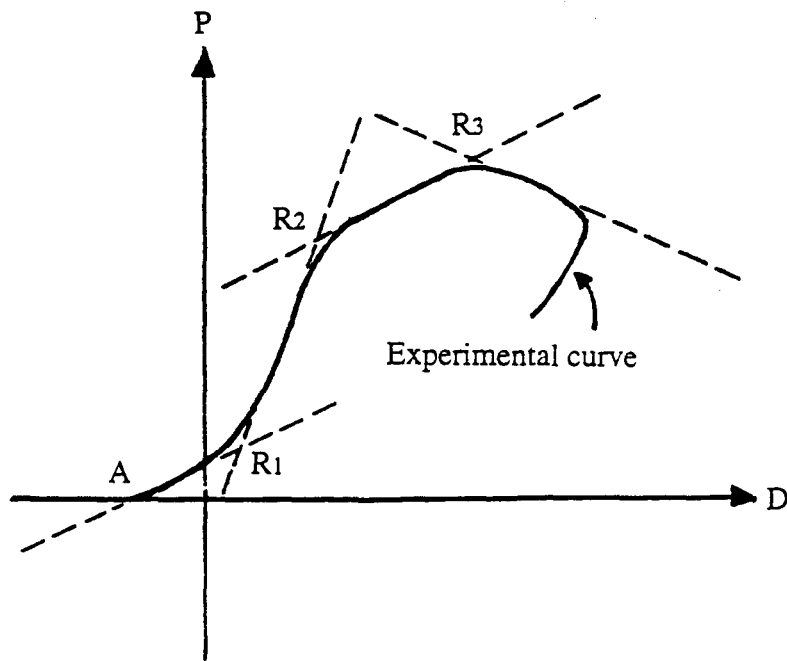
Figure 26 Possible reference curve along experimental curve

three critical points to be detected and that it resembles the corresponding three points in the backbone curve. These straight lines are connected to form a reference curve which provides three critical points called equivalent cracking, yielding and ultimate points.

Recall that the backbone curve of a perforated shear wall developed earlier. This curve's critical points are not on the tangent line, as shown in Figure 27. The backbone curve is based on experimental results under monotonic static loading while the reference curve is based on the experimental results under earthquake type loading. The latter's critical points lie on the tangent line of experimental response. For convenience, reference curve and backbone curve use the same notation: "C" represents cracking point, "Y" yielding point, and "U" ultimate point.

An additional critical point R4, representing the failure point, remains to be defined. The formula for locating point R4's load in the reference curve is assumed to be the same as in the backbone curve.

1. <u>Equivalent Cracking Point</u> Of primary concern in the reference curve is establishment of a reversal slope, if available. This slope is used to locate the equivalent cracking point, as shown in Figure 28. The relationship between reversal slope ratio (SR/OSOC) and energy dissipation ratio ($\Sigma E_d/P_{uo}D_{uo}$) is illustrated in Figure 29 while Figure 30 shows the notation of a perforated shear wall's backbone curve. Reversal slope ratio is the ratio of reversal stiffness to original (initial) stiffness (from origin to cracking point on the backbone curve), expressed by SR/OSOC. Stiffness OSOC is constant in the case of a shear wall. The energy dissipation ratio is defined as $\Sigma E_d/P_{uo}D_{uo}$ (see Figure 31). As that ratio decreases so does the SR ratio (see Figure 29). Reversal slope near the equivalent cracking point demonstrates the pinching phenomenon, a characteristic of shear behavior. Procedures to determine the equivalent cracking point are

1. When $0 \leq \Sigma E_d/P_{uo}D_{uo} \leq 0.3$,
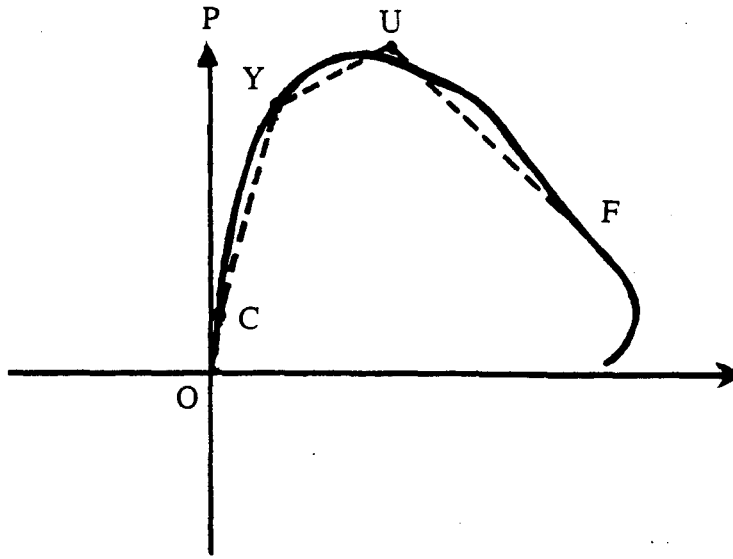
Figure 27 Expected critical points of backbone curve on monotonically experimental
curve
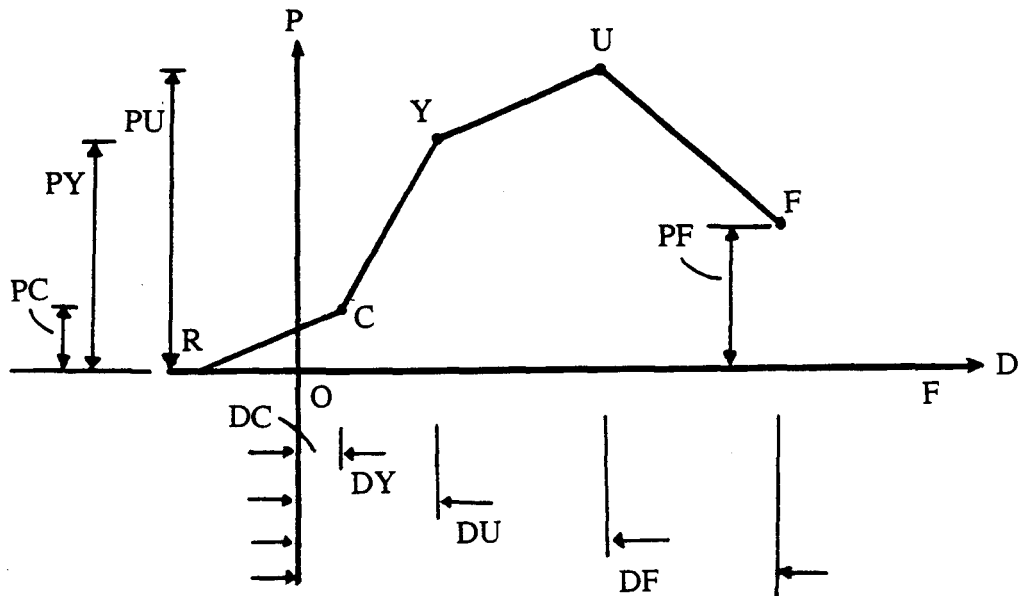
Figure 28 Schematic diagram of equivalent critical points of reference curve
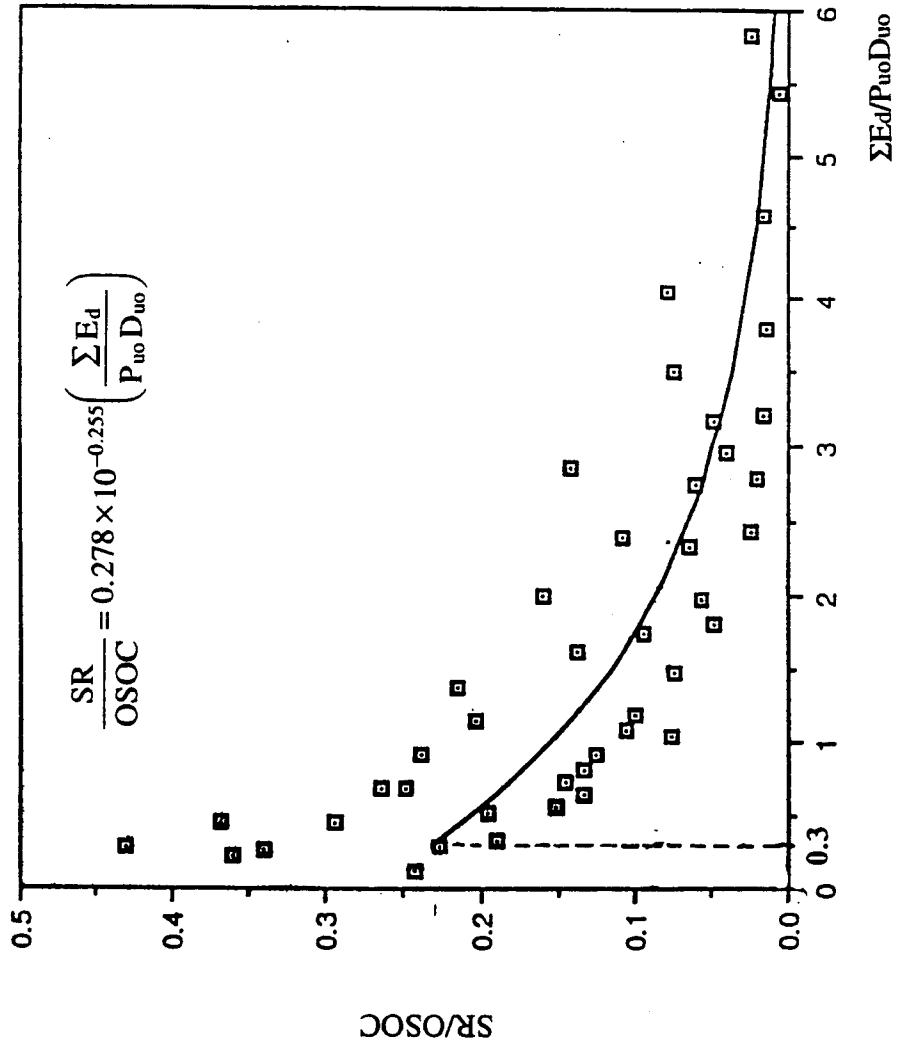
Figure 29   Relationship between reversal slope ratio and energy dissipation ratio

$$\frac{SR}{OSOC} = 0.278 \times 10^{-0.255} \left(\frac{\sum E_d}{P_{uo} D_{uo}} \right)$$

65
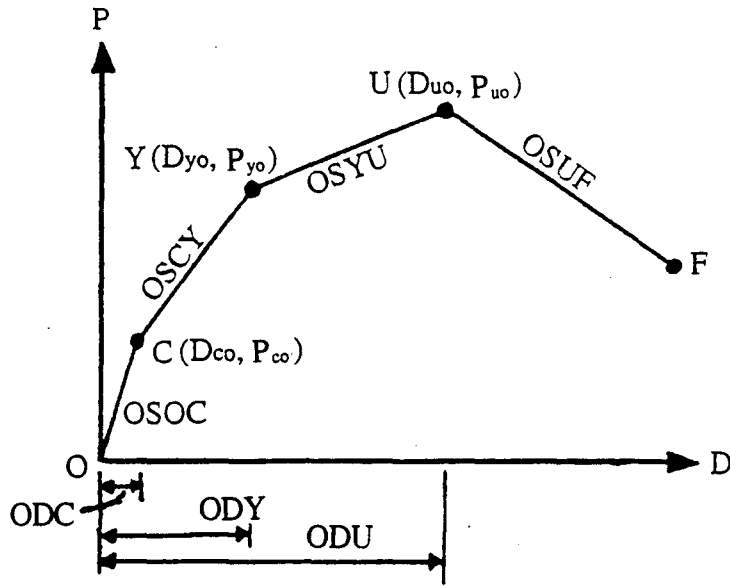
Figure 30 Notation of backbone curve of perforated shear wall

equivalent cracking displacement $DC = D_{co}$ (68)

equivalent cracking load $P_c = P_{co}$ (69)

2. When $0.3 \leq \Sigma E_d / P_{uo} D_{uo}$,

reversal slope $SR = \left[0.2780 \times 10^{-0.2547 \left(\frac{\Sigma E_d}{P_{uo} D_{uo}} \right)} \right]$ (OSOC)   (70)

and

equivalent cracking displacement $DC = |SDP| / 4 \geq ODC$ (71)

equivalent cracking load $PC = (SR)[\,|SDP| + DC] = \frac{5}{4}|SDP|(SR)$ (72)

66
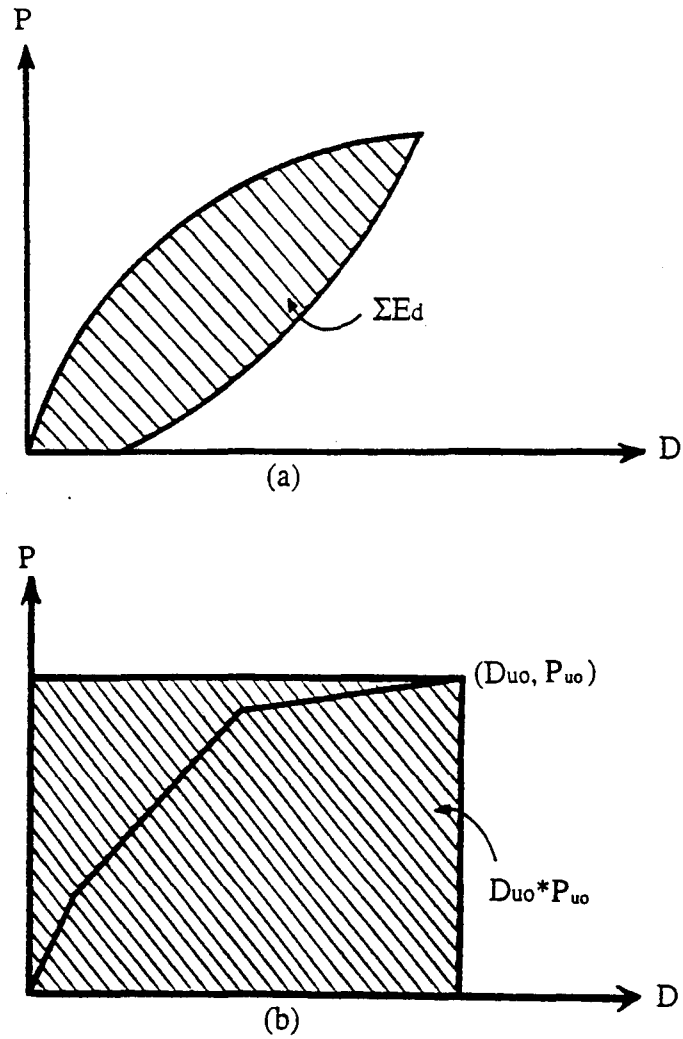
Figure 31 Definition of energy dissipation and energy dissipation ratio

where SDP (see Figure 32) is the deviation between point A (at loading = 0) and origin. It shows the current degree of inelasticity.

Data in the region of the equivalent cracking point are scant and sensitive. Thus it is difficult to decide the appropriate location for this point. At various times this point is close to the original cracking point (as it was with the backbone curve), particularly when energy dissipation is slight. Due to this, option (1) $\left(0 \leq \sum E_d/P_{uo}D_{uo} \leq 0.3\right)$ assumes the original cracking point (the first critical point on backbone curve) as the equivalent cracking point.
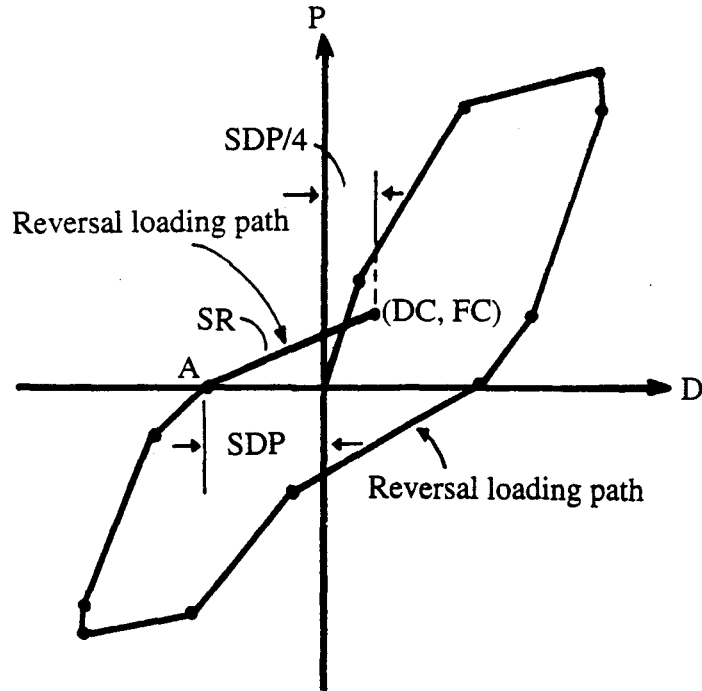
Figure 32   Schematic diagram of reversal loading path

Fortunately, when energy dissipation is slight, this assumption is accurate enough. The effect of this assumption on determination of subsequent critical points can be neglected.

Figure 33 compares calculated and experimental hysteretic responses. The response of perforated shear wall SWO-14E is shown in Figure 33(a) while that of perforated shear wall SWO-6E is shown in Figure 33(b). $(SR)_e$ and $(SR)_c$ stand for the reversal slope in experimental and calculated cases, respectively. Generally, the slope comparisons for these two figures are good. Corresponding equivalent cracking point R_1 ends the reversal slope. Experimental and calculated cracking points are represented by $(R_1)_e$ and $(R_1)_c$, respectively. Upper critical points $(R_1)_e$ and $(R_1)_c$ are close together in Figure 33(a) where displacement is slight (i.e., smaller than 1 mm). Critical points on the upper portion in Figure 33(b) are also in close proximity. In terms of equivalent critical point R_1, the above cases are in good agreement. But equivalent critical points
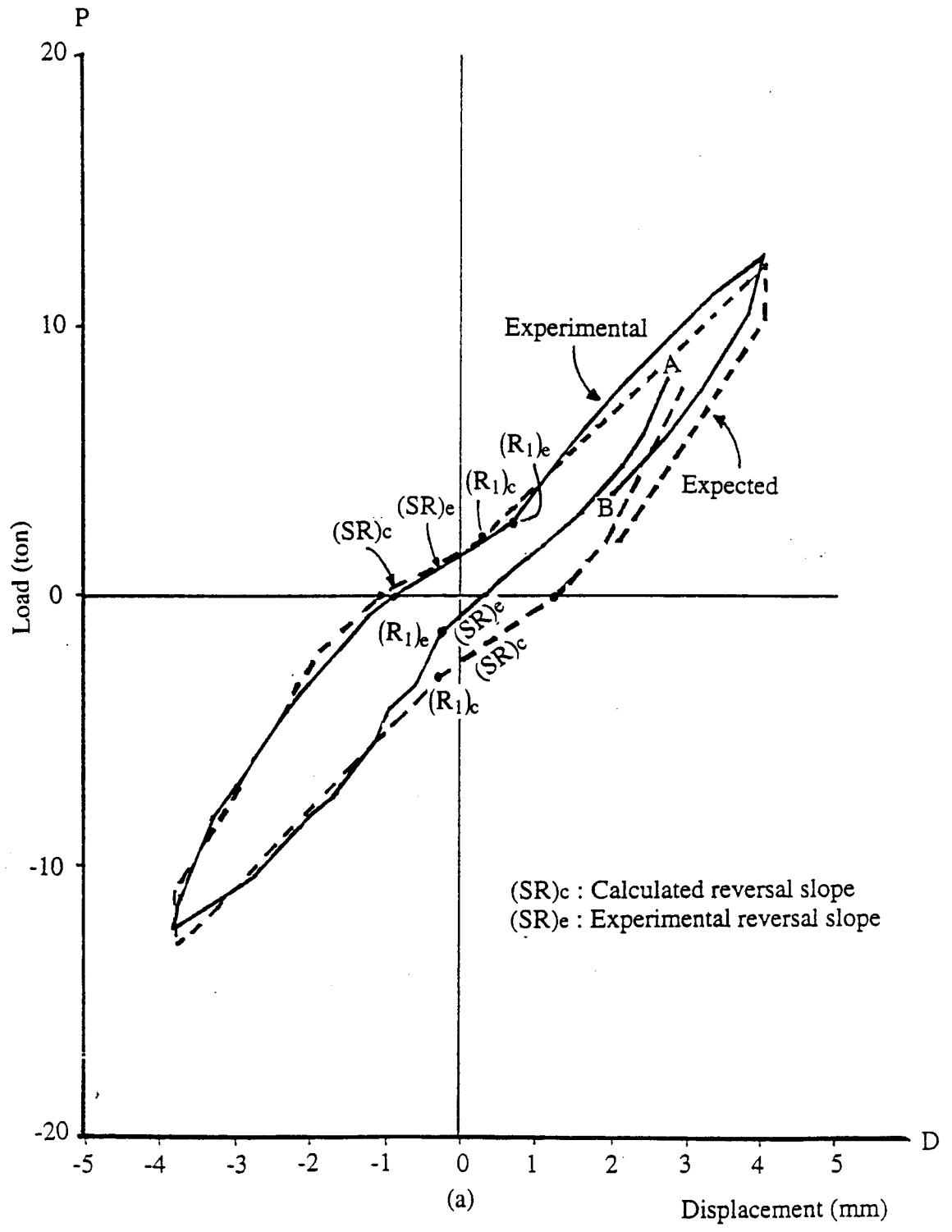
Figure 33 Comparison between expected and experimental hysteresis loop with respect to reversal slope for perforated shear wall (a) SWO-14E (b) SWO-6E
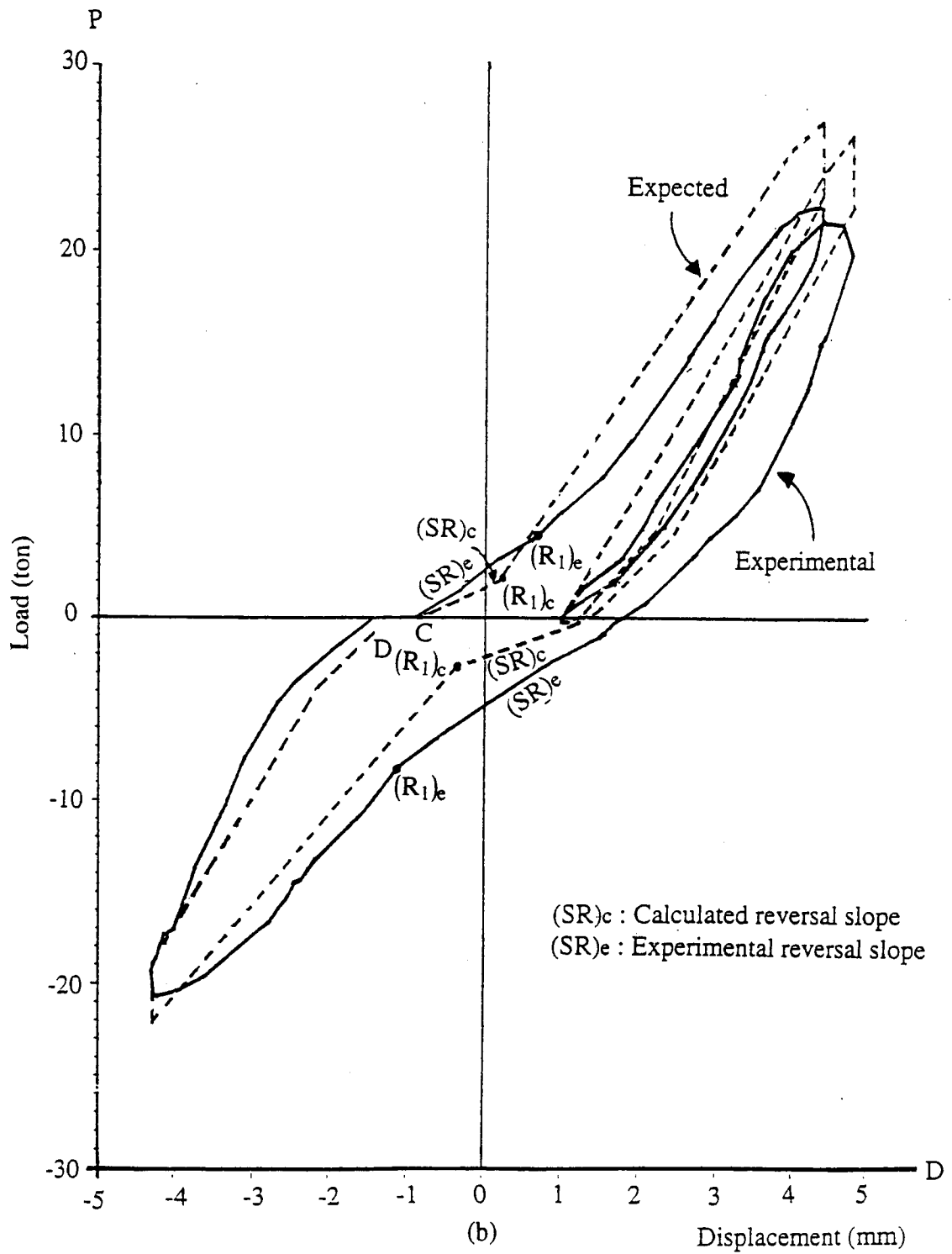
Figure 33 (continued) Comparison between expected and experimental hysteresis loop with respect to reversal slope for perforated shear wall (a) SWO-14E .(b) SWO-6E

70

$(R_1)_e$ and $(R_1)_c$ on the lower part are not close, particularly for shear wall SWO-6E (see Figure 33(b)).

2. <u>Equivalent Yielding Point</u>   As shown in Figure 28, this point is determined after the equivalent cracking point. Either of two approaches may be used to decide equivalent yielding point. Load and corresponding displacement may be determined directly by empirical equations, or the slope between the equivalent cracking point and equivalent yielding point may be found and displacement (or load) obtained. The second approach is adopted here because it is more stable in searching for the slope.

Figure 34 represents slope ratio (SCY/OSCY) with respect to energy dissipation ratio $\left(\Sigma E_d/P_{uo}D_{uo}\right)$. SCY is the slope subsequent to the cracking point, shown in Figure 28. OSCY is the slope of the second segment in the backbone curve of perforated shear wall, shown in Figure 30. The slope ratio declines to a stabilized level as energy dissipation accumulates. Note that in Figure 34 slope SCY already exists when energy dissipation occurs. Slope SCY is defined as the stiffness of the second segment on the dissipated envelope. This stiffness cannot exceed the stiffness in the same segment of the backbone curve because energy dissipated in the shear wall decreases the wall's load capacity and stiffness. In Figure 34 when energy dissipation ratio is smaller than 0.319, the corresponding second segment slope ratio is assumed to be 1.0. The equation for this slope is expressed as

$$SCY = BB \cdot OSCY \tag{73}$$

where the coefficient BB is in terms of

$$BB = (1.1578) \cdot 10^{-0.201\left(\frac{\Sigma E_d}{P_{uo}D_{uo}}\right)} \leq 1 \tag{74}$$
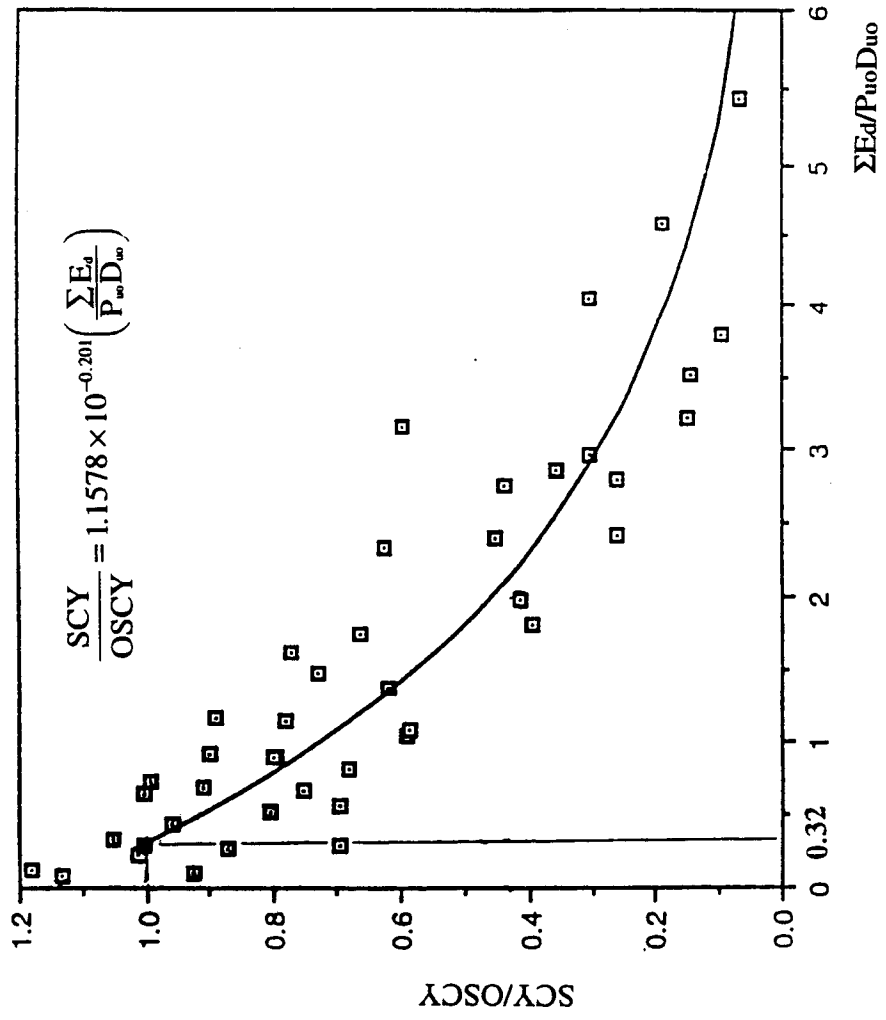
Figure 34 Relationship between SCY ratio and energy dissipation ratio

$$\frac{SCY}{OSCY} = 1.1578 \times 10^{-0.201\left(\frac{\Sigma E_d}{P_{uo} D_{uo}}\right)}$$

72

As shown in Figure 35(a) and (b), the prediction for the second segment slope is good for all the half cycles in these figures. $(SCY)_e$ and $(SCY)_c$ are almost parallel, quite close for this dissipated envelope reflected by the perforated shear wall. Even though an actual shear wall cracks or yields, it displays stability in decay of stiffness at this stage, identical to the cracking-to-yielding stage on the backbone curve of the perforated shear wall. Similar to determining the second segment slope, equivalent yielding displacement DY follows empirical equations and tends to increase in many experimental hysteresis loops (see Figure 36). Equivalent yielding displacement ratio is the ratio of equivalent yielding displacement (DY) to original yielding displacement (ODY); DY and ODY are shown in Figure 28 and 30. Lack of data and instability when energy dissipation is small limit results. When energy dissipation ratio equals 0.13, it reveals less yielding displacement on the plot, generally 60% of the original yielding displacement assumed. As shown in Figure 36, when energy dissipation ratio is smaller than 0.3, equivalent yielding displacement will be smaller than original yielding displacement. Thus the equivalent yielding displacement ratio is less than 1.0. When the energy dissipation ratio increases, equivalent yielding displacement quickly does likewise. Until energy dissipation approaches 2 and more, the equivalent yielding displacement ratio gradually reaches a more stable level and stays above 2. Equations for prediction of equivalent yielding displacement are written as follows

1. When $\dfrac{\Sigma E_d}{P_{uo}D_{uo}} = 0$,

$$DY = ODY \tag{75}$$

2. When $0 < \dfrac{\Sigma E_d}{P_{uo}D_{uo}} \leq 0.13$,

$$DY = ODY \tag{76}$$

73
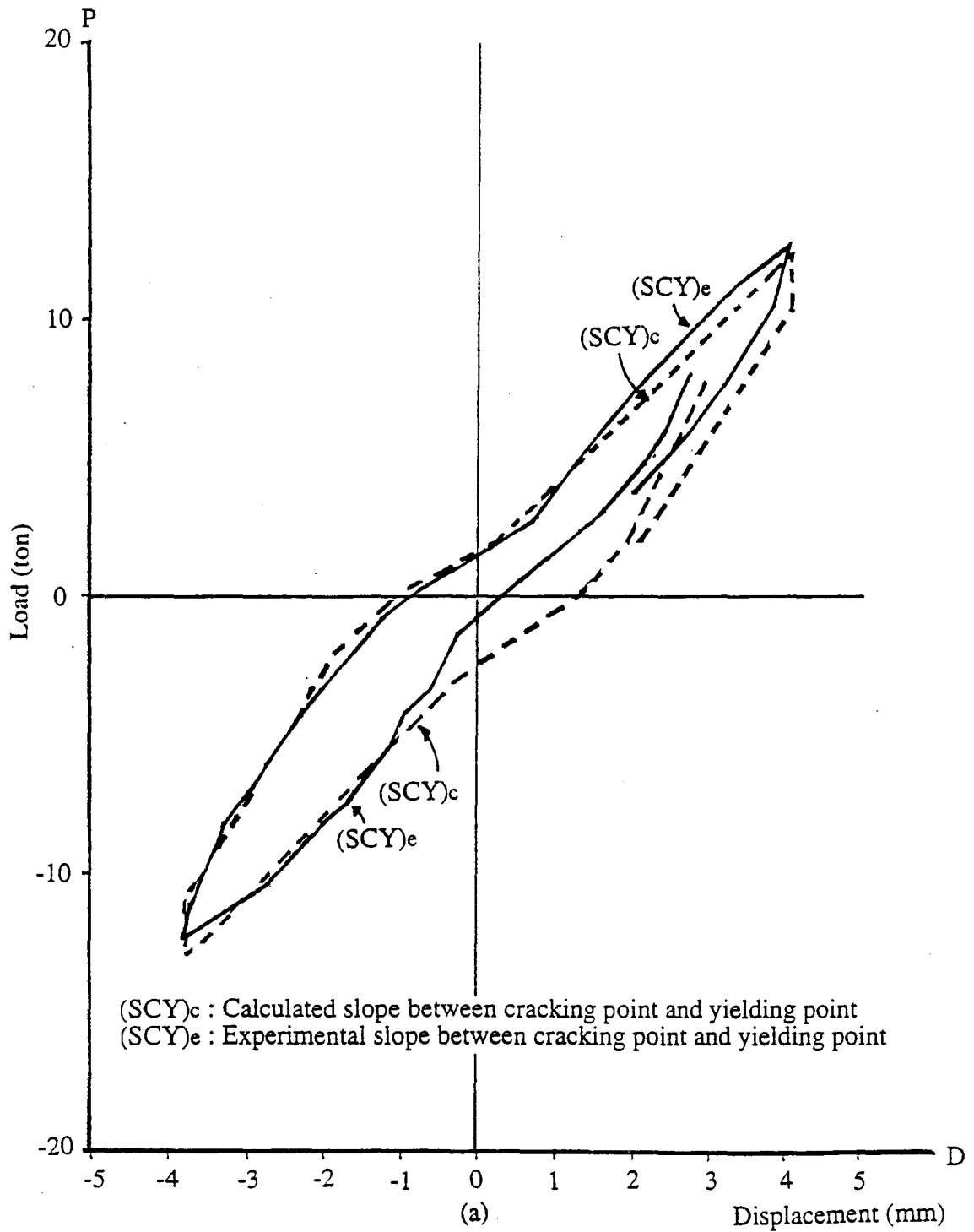
Figure 35 Comparison between expected and experimental hysteresis loop with respect
to slope from cracking point to yielding point for perforated shear wall
(a) SWO-14E (b) SWO-6E
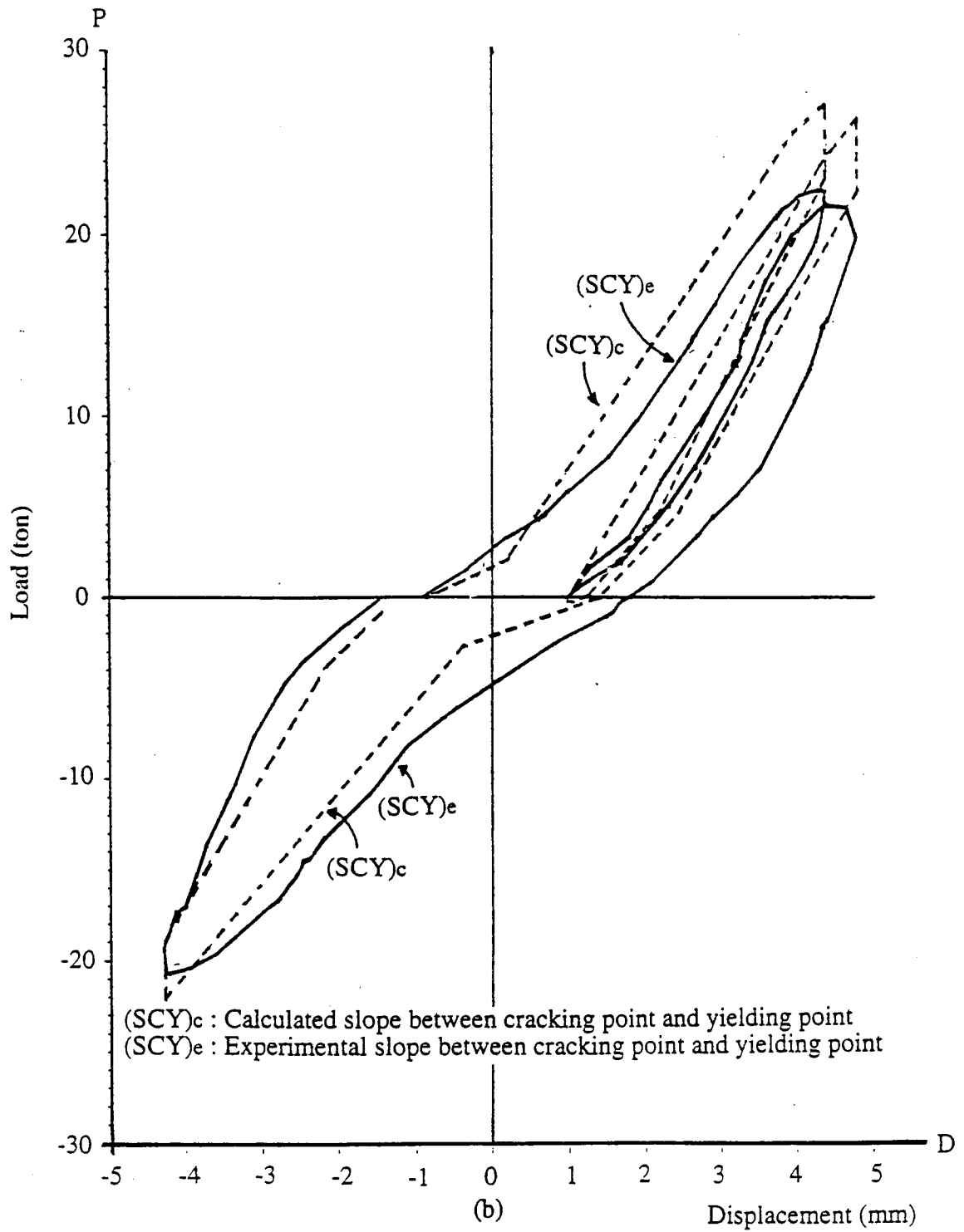
Figure 35 (continued) Comparison between expected and experimental hysteresis loop with respect to slope from cracking point to yielding point for perforated shear wall (a) SWO-14E (b) SWO-6E
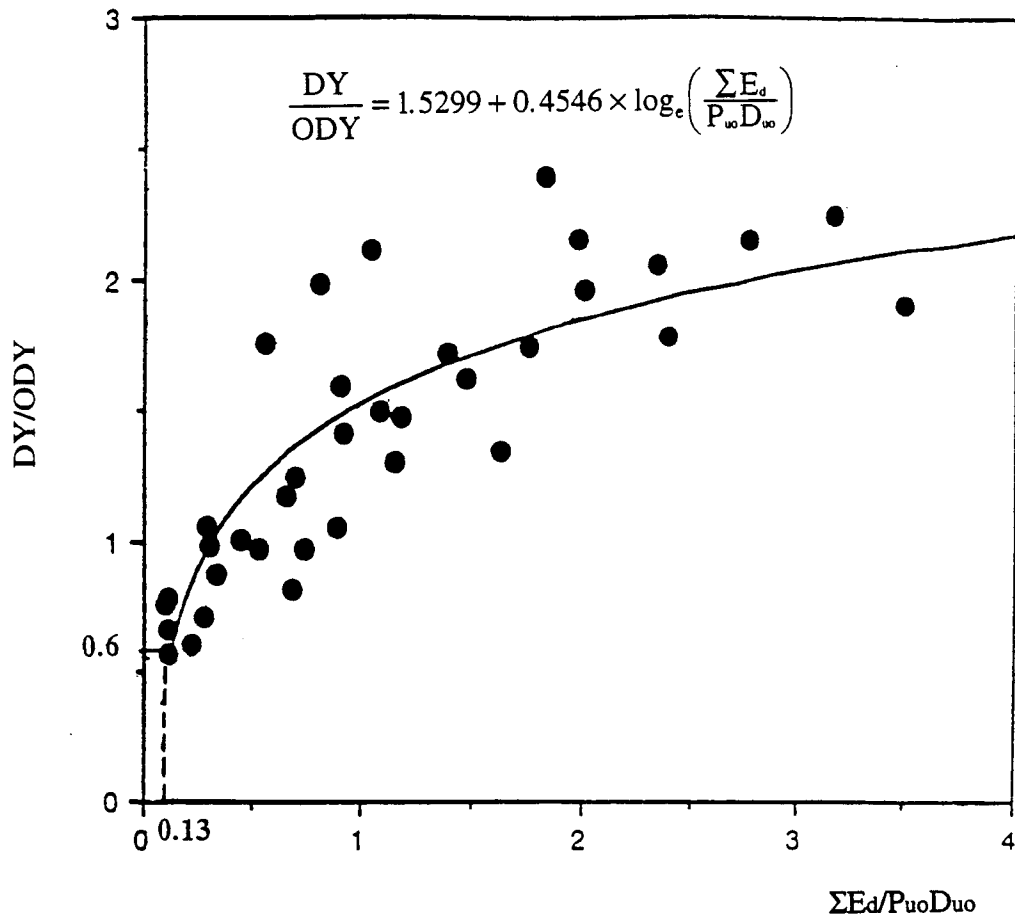
Figure 36 Relationship between yielding displacement ratio and energy dissipation ratio

3. When $0.13 < \dfrac{\Sigma E_d}{P_{uo}D_{uo}}$,

$$DY = \left[1.5299 + 0.4546 \times Ln\left(\dfrac{\Sigma E_d}{P_{uo}D_{uo}}\right) \right](ODY) \qquad (77)$$

3. **Equivalent Ultimate Point** Data for deciding the slope between equivalent yielding point and equivalent ultimate point are insufficient but some data can be compared at this stage. Assume that the ratio of SYU (slope between equivalent yielding point and equivalent ultimate point for reference curve) vs. OSYU (original slope between yielding

76

point and ultimate point for backbone curve) is equal to the ratio of SCY (slope between equivalent cracking point and equivalent yielding point for reference curve) vs. OSCY (slope between cracking point and yielding point for backbone curve). This relationship is expressed as

$$\frac{SYU}{OSYU} = \frac{SCY}{OSCY}$$
(78)

Since

$$OSYU = \frac{(P_{uo} - P_{yo})}{(D_{uo} - D_{yo})}$$
(79)

and

$$OSCY = \frac{(P_{yo} - P_{co})}{(D_{yo} - D_{co})}$$
(80)

Thus the slope between equivalent yielding point and equivalent ultimate point SYU can be written as

$$SYU = \left(\frac{P_{uo} - P_{yo}}{D_{uo} - D_{yo}}\right)\left(\frac{P_{yo} - P_{co}}{D_{yo} - D_{co}}\right)(SCY)$$
(81)

In the same manner, the determination of equivalent ultimate displacement DU can be summarized as follows

(1) when $\frac{\Sigma E_d}{P_{uo} D_{uo}} = 0$, i.e., stays in the elastic range, then

$$DU = DU$$
(82)

77

(2) When energy dissipation exists in a shear wall, then

$$\frac{DU}{ODU} = \frac{DY}{ODY} \qquad (83)$$

or

$$DU = \frac{DY}{ODY}(ODU) \qquad (84)$$

where DY is equivalent yielding displacement for reference curve; ODY is yielding displacement for backbone curve; ODU is ultimate displacement for backbone curve (see Figure 30).

4. Equivalent Reference Failure Point To determine this point, a procedure similar to determination of the reference failure point for the backbone curve in Section II is used. After the ultimate point in the backbone curve, the slope declines to the reference failure point. After the equivalent ultimate point, the slope also declines. Experimental data, which show a stable situation, yield the degrading straight line. Generally, the degrading slope is close to some constant and is expressed as

$$SUF = -0.5(SCY) \qquad (85)$$

in which SUF and SCY are the degrading slope between equivalent ultimate point and equivalent reference failure point and the slope between equivalent cracking point and equivalent yielding point on the reference curve, respectively. The load at equivalent reference failure point is assumed to be half of summation of equivalent cracking and equivalent yielding loads, as shown in Figure 37.

(a) Backbone curve
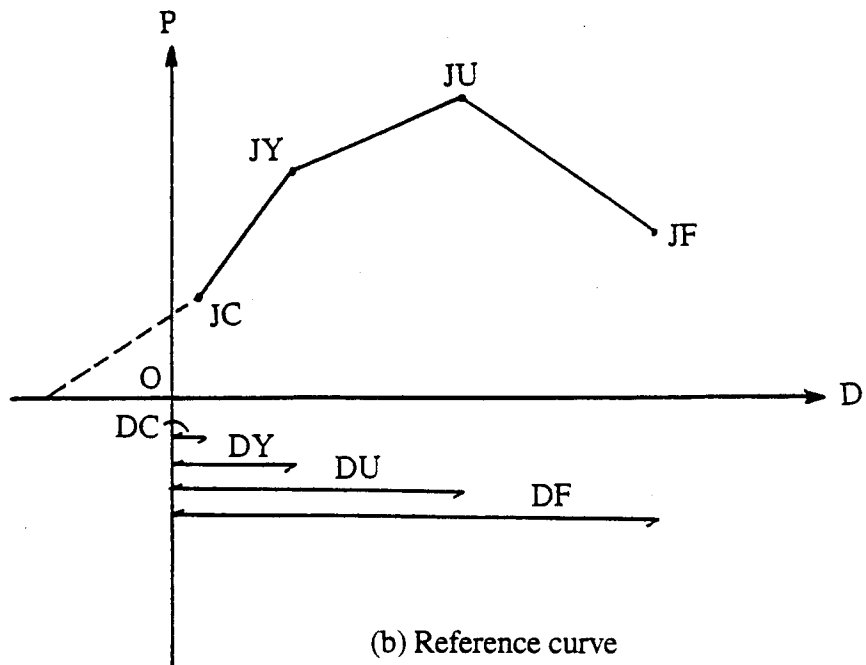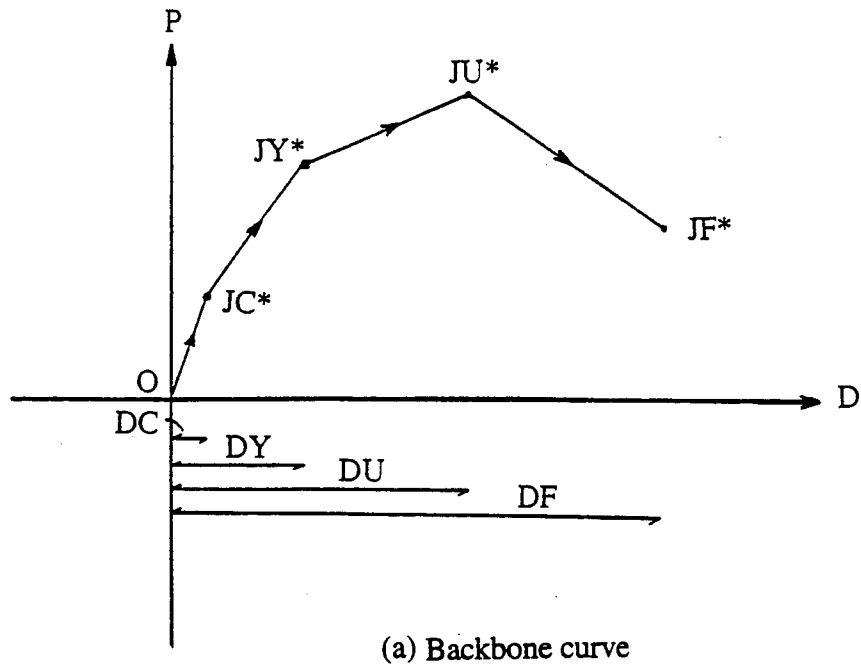
(b) Reference curve

Figure 37 Schematic diagram of loading process on (a) backbone curve (b) reference curve

So far, all critical points on the reference curve are established. Then the load at different stages on this curve can be determined as follows.

(i) Force at equivalent cracking point, PC, is described in Eqs. (69) and (72).

(ii) Force at equivalent yielding point, PY, is expressed as

$$PY = PC + (DY-DC) \cdot SCY \qquad (86)$$

(iii) Force at equivalent ultimate point, FU, is expressed as

$$PU = PY + (DU-DY) \cdot SYU \qquad (87)$$

(iv) Force at equivalent reference failure point, PF, is assumed to be $(PC + PY)/2$, as stated above.

Furthermore, the displacement at equivalent reference failure point, DF, reduces to

$$DF = DU + (PF-PU)/SUF \qquad (88)$$

C. COMPARISON OF REFERENCE CURVE AND BACKBONE CURVE

A major focus of this section is that hysteresis loops starting from zero force must follow either backbone curve or reference curve (see Figure 37). If the entire shear wall is integrated, or has no cracks, this shear wall follows a path defined by the backbone curve. If any cracks occur in the shear wall, then this wall has initiated a hysteresis response. Hysteresis response involves constant energy dissipation. In this situation the reference curve, established with regard to energy dissipation, is used.

Figure 37(a) illustrates the loading process (via the path arrow) on the backbone curve. Here the curve is shown on the positive force side; its path is identical on the

negative force side. The backbone curve, as stated in Section II, consists of four segments, each having distinct behavior. This is depicted in Figure 37(a). Likewise the reference curve consists of four segments, each having distinct behavior. This is depicted in Figure 37(b). These two curves differ in that the reference curve does not pass through the origin. This is because the reference curve is based on the curve set up for shear wall with some energy dissipation.

The symbol D_{max} is used to determine the current path and its hysteresis rules. D_{max} is taken as an absolute value even though the current path is located on the side of negative force. Positive or negative force refers to force in one direction or the opposite direction. Three stages thus occur with respect to current maximum displacement, D_{max}, as follows

(i) Elastic stage: $|D_{max}| > |DC|$ (89)

(ii) Cracking stage: $|DC| \leq |D_{max}| < |DY|$ (90)

(iii) Yielding and failure stage: $|DY| \leq |D_{max}| \leq |DF|$ (91)

In Figure 37(a), loading process is considered and current point JP has maximum displacement D_{max} on its half cycle. If

(i) current point JP is between origin and cracking point JC^*, then

$|D_{max}| < |DC|$ (elastic stage)   (92)

(ii) current point JP is between yielding point JC^* and yielding point JY^*, then

$$|DC| \leq |D_{max}| < |DY| \quad \text{(cracking stage)} \tag{93}$$

(iii) current point JP is between yielding point JY^* and failure point JF^*, then

$$|DY| \leq |D_{max}| \leq |DF| \quad \text{(yielding and failure stage)} \tag{94}$$

Similar to Figure 37(a), current point JP in the reference curve (see Figure 37(b)) has maximum displacement D_{max} on its half cycle. If

(i) current point JP is between reversal loading point A and equivalent cracking point JC, then JP is in reversal loading stage.

(ii) current point JP is between equivalent cracking point JC and equivalent yielding point JY, then

$$|DC| \leq |D_{max}| < |DY| \quad \text{(equivalent cracking stage)} \tag{95}$$

(iii) current point JP is between equivalent yielding point JY and equivalent failure point JF, then

$$|DY| \leq |D_{max}| \leq |DF| \quad \text{(equivalent yielding and failure stage)} \tag{96}$$

From the above discussion of loading process, differences between backbone curve and reference curve are highlighted:

• Backbone curve involves load vs. displacement in which the mechanical characteristics of RC shear walls are shown before any lateral load is applied. This curve is unique for a given shear wall.

- Reference curve involves load vs. displacement in which a wall element has energy dissipation. This curve is determined every half cycle. Thus the reference curve is highly related to energy dissipation and is formed when the path crosses zero force.

- Backbone curve exists for the shear wall regardless of external lateral load, but reference curve may change since energy dissipation changes with external excitation.

- Backbone curve of RC shear wall defines four loading stages as stated in Section III which are related to material properties, such as compressive strength of concrete, yielding strength of vertical and horizontal steel bars as well as location and dimension of openings, dimension and thickness of wall element. Each loading stage has its distinct behavior.

- Reference curve has four equivalent loading stages which are based on experimental observation and defined in a manner similar to backbone curve of perforated shear wall. These equivalent loading stages reflect hysteresis behavior rather than distinct physical phenomena caused by the material itself.

- If the wall follows the backbone curve, then the concrete in the RC shear wall does not crack and the wall remains in the elastic range. If the shear wall follows the reference curve, then cracks have already begun and the wall manifests nonlinear response.

- In cases of reference curve, shear walls cannot develop a path through the origin. Since energy dissipation has occurred, a hysteresis loop is developed instead of backbone curve. Shear walls do not have stiffness from origin to first critical point (cracking point) JC. These walls must follow the route from reversal loading point A to first equivalent critical point JC, which has reversal stiffness SR (see Figure 37).

D. HYSTERESIS MODEL

Overall hysteresis response reflects such aspects as loading process, unloading process, reversal loading process, reloading after unloading process and unloading after reversal loading process. First, the path related to these processes must be defined. Figure

38 presents a diagram of hysteresis rules for load vs. lateral displacement relationship in a perforated shear wall. This figure includes loading, unloading, reversal loading, reloading after unloading and unloading after reversal loading. Table V contains a summary of hysteresis rules and descriptions. Hysteresis rules in Figure 38 are the summation of combined bending and shear lateral displacement, which is so-called total lateral displacement. Figure 38(b) shows rules on the hysteretic diagram.

Before discussing the above processes, one controlling factor, as shown in Figure 39 should be introduced. This controlling factor is expressed as KL and numerically represents each individual process. From the value of KL, the program can reveal the current loading situation and the applicable hysteresis rule.

KL of 1 shows the current path is involved in the loading process if the applied force is positive. If the applied force is negative, KL is 3 for this process. As the unloading process begins, external force decreases. KL is 2 for the unloading process on the positive force side, and 4 for the unloading process on the negative force side. KL equals 5 and 6 for reversal loading process. KL of 5 indicates the reversal loading point (zero force point) on the positive force side and a shift from positive to negative. KL of 6 indicates the point on the negative force side and a shift from negative to positive. KL of 8 denotes reloading after unloading on the positive force side while KL of 7 denotes the same process on the negative force side. KL of 10 and 9 express conditions of reloading after reversal process,10 for the positive force side after KL of 5, and 9 is for negative force side after KL of 6. Numerals from 1 to 10 for controlling factor KL designate all the individual processes.

Table V shows the five groups of rules for five hysteresis paths: loading, unloading, reversal loading, reloading after unloading and unloading after reversal loading. In the first group only one rule can be applied to the loading process on the backbone curve or reference curve. Corresponding controlling factors KL are 1 and 3. In the second group rules SB 2.1, SB 2.2, SB 2.3, SB 2.4, SB 2.5 and SB 2.6 represent unloading at

Table V Summary of hysteresis rules and descriptions for perforated shear wall

Rule	Stiffness	Description	KL
SB 1.0	*1	Loading on backbone curve or reference curve	1, 3
SB 2.1	SOC	Unloading	2, 4
SB 2.2	SOC	Unloading	2, 4
SB 2.3	K_b	Unloading	2, 4
SB 2.4	K_c	Unloading	2, 4
SB 2.5	SOB	Unloading	2, 4
SB 2.6	SX_3Y' *2	Unloading	2, 4
SB 3.1	SOC' *3	Reversal loading	5, 6
SB 3.2	SR	Reversal loading	5, 6
SB 4.1	SOC *4	Reloading after unloading	7, 8
SB 4.2	K_e	Reloading after unloading	7, 8
SB 5.1	*5	Unloading after reversal loading	9, 10
SB 5.2	K_d	Unloading after reversal loading	9, 10
SB 5.3	SCY *6	Unloading after reversal loading	9, 10
SB 5.4	K_a	Unloading after reversal loading	9, 10

*1 depending on current stage

*2 or SX_3C'

*3 or SX_oC'

*4 or K_d

*5 idealized vertical line

*6 or K_f

85
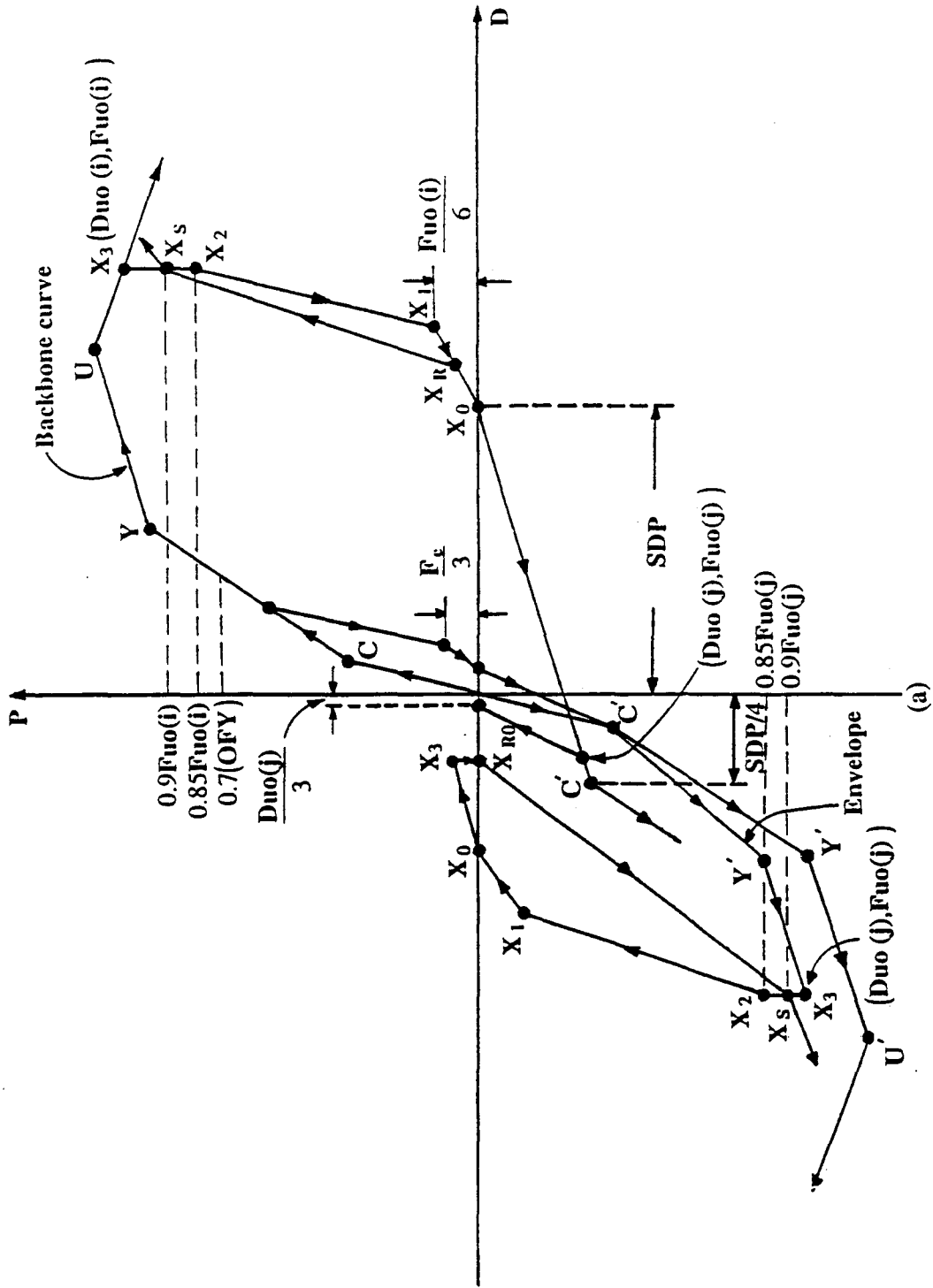
Figure 38: Diagram of hysteresis rules for load vs. displacement relationship of perforated shear wall
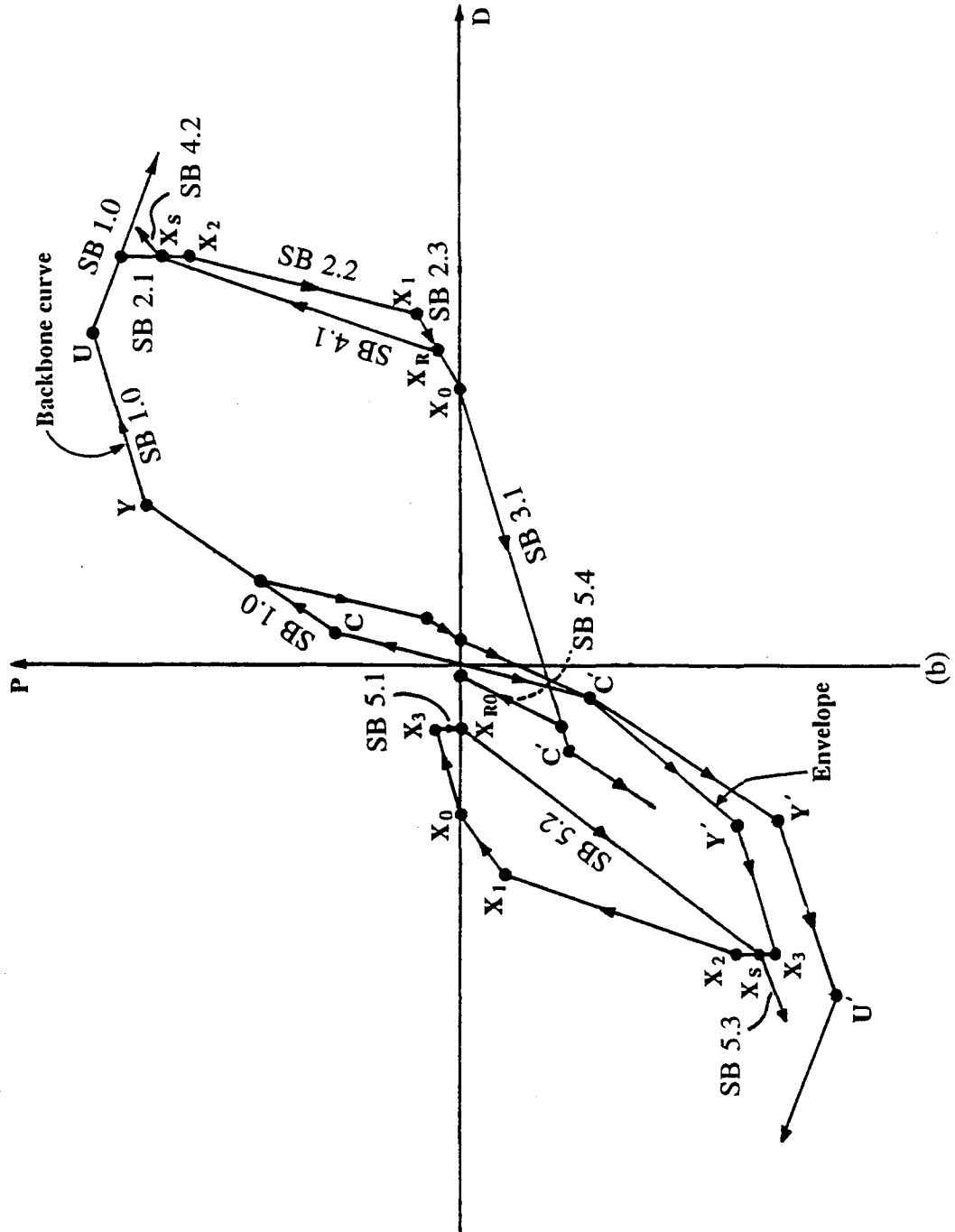
Figure 38 (continued) Diagram of hysteresis rules for load vs. displacement relationship of perforated shear wall
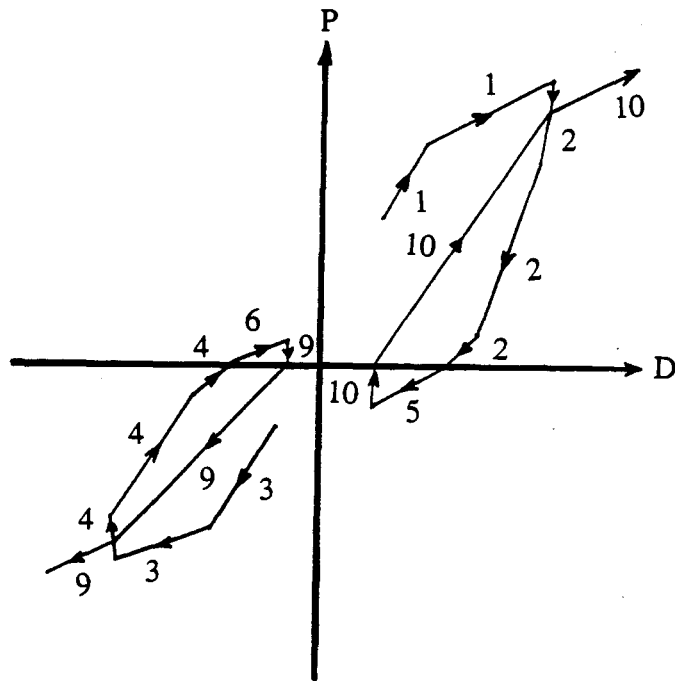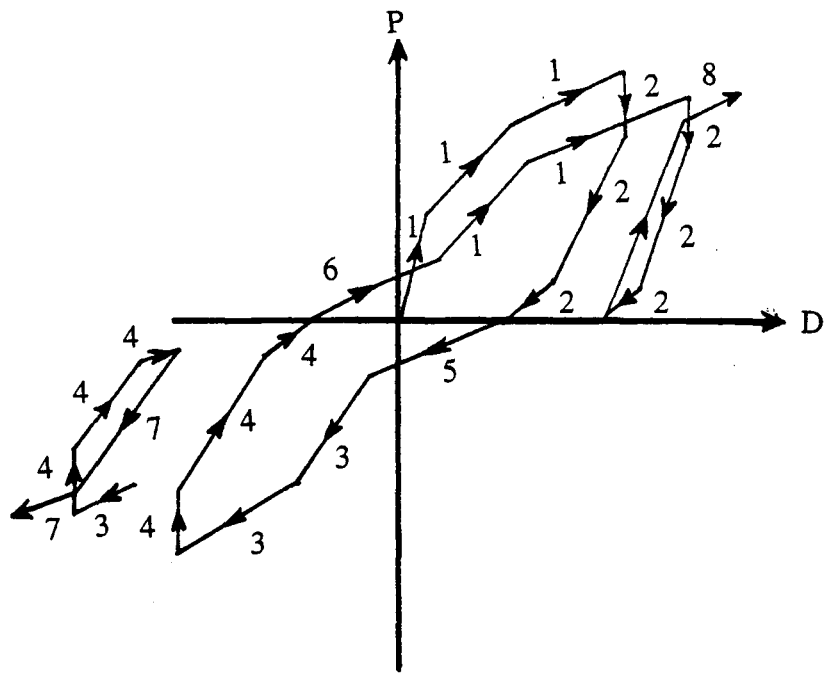
Figure 39 Definition of controlling factor used in hysteresis rules of perforated shear wall

different stages. Corresponding controlling factors KL are 2 and 4. In the third group two rules indicate reversal loading process. Corresponding controlling factors KL are 5 and 6. In the fourth group of rules two segments constitute the complete reloading process, the first with more slope than the second. Corresponding controlling factors KL are 7 and 8. In the fifth group four rules express the unloading after reversal loading process. Corresponding controlling factors KL are 9 and 10.

1. <u>Loading Process</u> During this process the external load increases. In Figure 40 an arrow shows the direction of this path. If the shear wall has no cracks, then it conforms to the path on the backbone curve. When the external load increases, the current path follows the backbone curve through cracking point, yielding point and ultimate point. As the current point approaches ultimate state, the shear wall's load capacity is reached. External force cannot exceed the load capacity of the shear wall. Thus external force decreases after ultimate point and more displacement occurs. Then on the backbone curve, the shear wall goes from ultimate point to reference failure point. As shown in Figure 40(b), the current hysteresis path on the negative force side has the same response. Similar to the loading process on the backbone curve, the reference curve has its equivalent ultimate state at the third critical point. Before reaching equivalent ultimate load, the external load acting on the shear wall goes from the equivalent cracking point through the yielding point. After the equivalent ultimate point, external load decreases until the shear wall fails (under loading process only). As shown in Figure 40(c) and (d), the path develops in the direction of the arrow.

As the current path follows the backbone curve or reference curve, the stiffness changes according to the slope of the curve. Here, the controlling factor KL is 1 (see Figure 40(a) and (c)) or 3 (see Figure 40(b) and (d)). A summary of loading processes and mathematical expressions for stiffness is shown in Table VI.
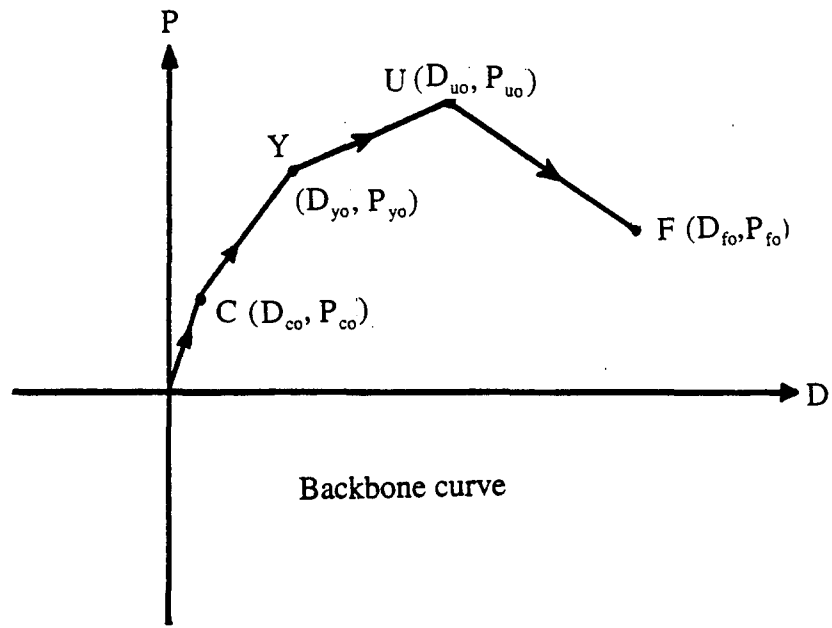
(a)
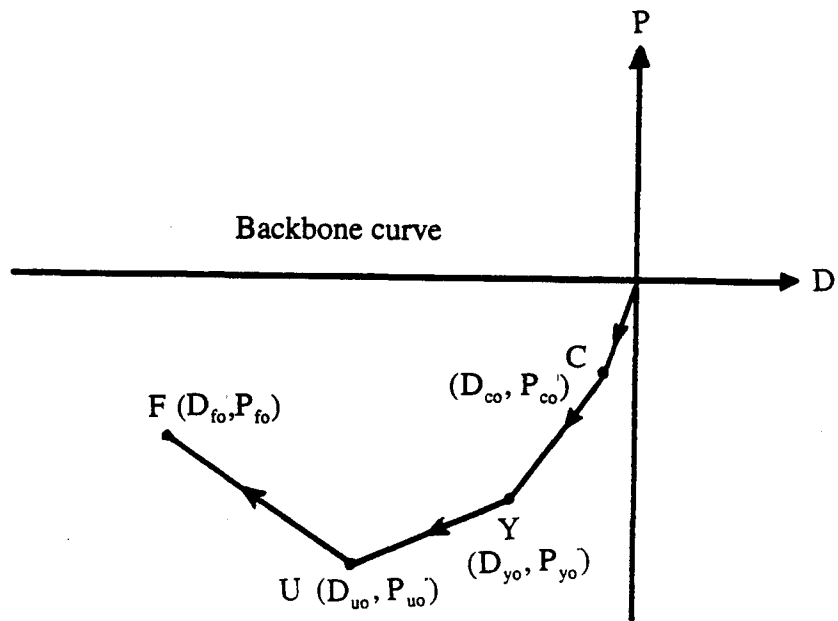
(b)

Figure 40 Diagram of loading process
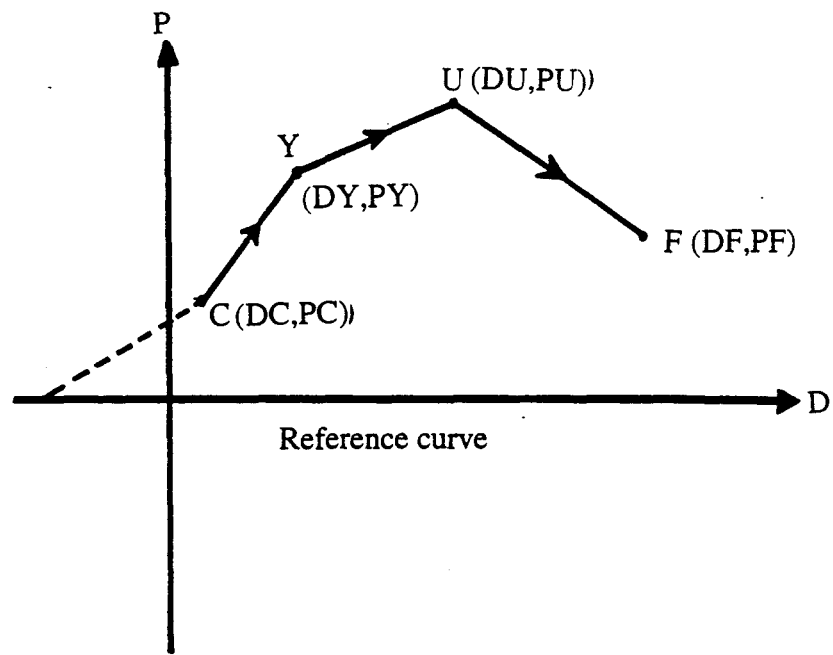
(c)
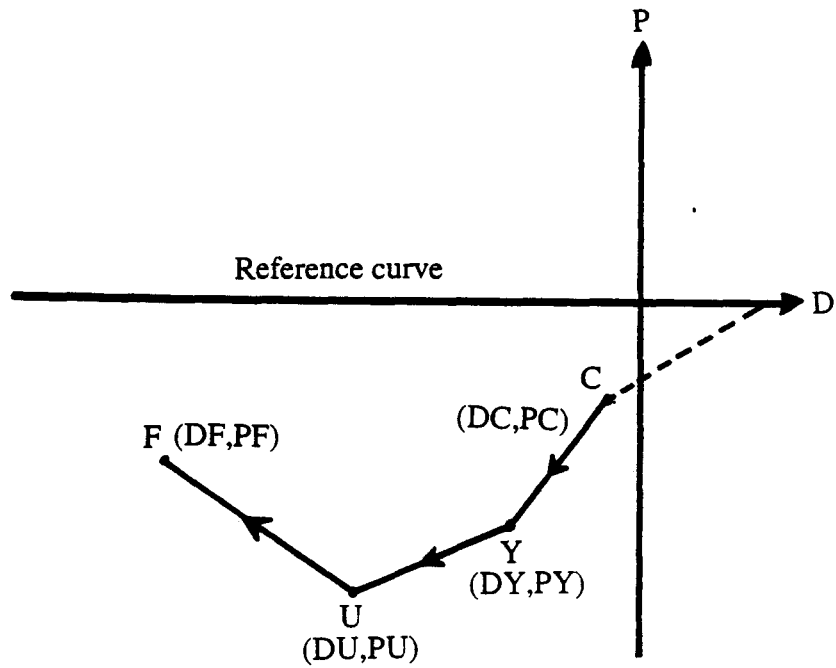
(d)

Figure 40 (continued) Diagram of loading process

Table VI Summary of loading process

Loading process

Rule SB 1.0

(1) KL = 1 (on positive force side)

KL = 2 (on negative force side)

(2) stiffness K = [P(i+1)-P(i)] / [D(i+1)-D(i)]

For example, DP represents the shear wall's current displacement. If DC<DP<DY, the current loading point is between cracking point and yielding point. The expressions of D(i+1), D(i), P(i+1), P(i) are

$$D(i+1) = DY \qquad (97)$$

$$D(i) = DC \qquad (98)$$

$$P(i+1) = PY \qquad (99)$$

$$P(i) = PC \qquad (100)$$

Therefore

$$\text{stiffness } K = \frac{PY-PC}{DY-DC} \qquad (101)$$

Note the presence of the elastic response on the first segment of backbone curve, as shown in Figure 40(a) or (b). This indicates the absence of shear wall cracks between origin and cracking point on the backbone curve.

2. <u>Unloading Process</u> During the unloading process, the applied load is released from shear wall in stages. Two main responses exist for the unloading process, one within the elastic range, the other beyond the elastic range. The latter illustrates the phenomenon of energy dissipation. An unloading path is illustrated in the following cases.

(i) Figure 41 shows the unloading process under elastic response. Maximum displacement is smaller than cracking displacement. Another factor DM is now considered as maximum displacement from the beginning of force history. It is different from D_{max}, as noted earlier, which refers to maximum displacement during current half hysteresis cycle. Since force history is still in the elastic range, maximum displacement DM or D_{max} is less than original cracking displacement (on the backbone curve) and maximum force $P_{uo}(i)$ is smaller than original cracking force (on the backbone curve). $P_{uo}(i)$ refers to the point where the unloading process starts. Maximum force $P_{uo}(i)$ is thus the maximum value during the current loading process in which corresponding maximum displacement is $D_{uo}(i)$. Stiffness for this case is the same as initial elastic stiffness on the backbone curve. The applicable hysteresis rule is SB 2.1.

(ii) Two cases here show the unloading process under energy dissipation within the wall.

(a) When maximum force $P_{uo}(i)$ (at the turning point where unloading starts) is smaller than equivalent cracking load, the unloading path is shown in Figure 42. This figure applies to positive force side or negative force side. Stiffness for this case is

$$K = \frac{-FPP}{\frac{DPP}{3} - DPP} = K_a \tag{102}$$

where (DPP, FPP) is the turning point which is the same as $(D_{uo}(i), P_{uo}(i))$.

93

$$(D_{uo}(i), P_{uo}(i))$$

(a)

$$(D_{uo}(i), P_{uo}(i))$$

(b)
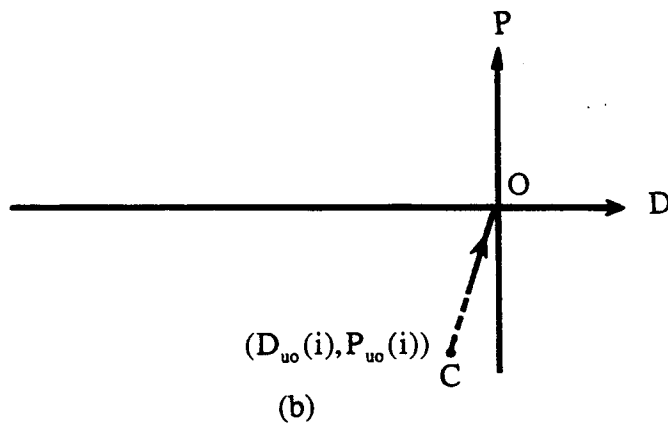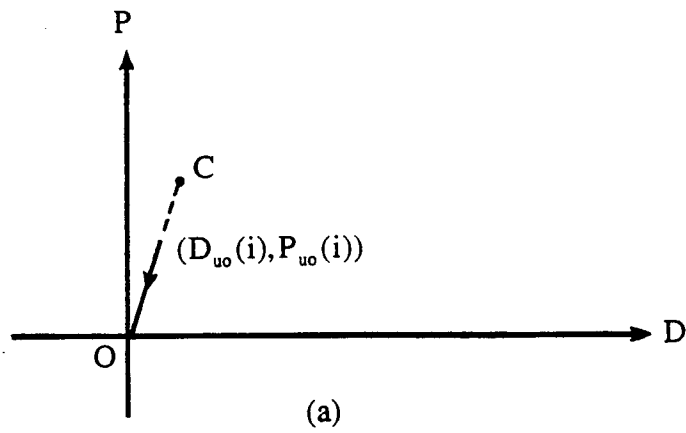
Figure 41 Unloading process within elastic range

$$(DPP, FPP) = (D_{uo}(i), P_{uo}(i))$$

$$\frac{DPP}{3} = \frac{D_{uo}(i)}{3}$$
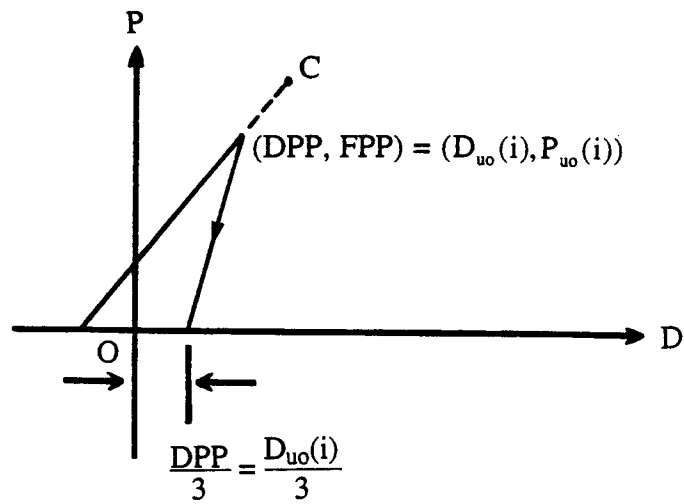
Figure 42 Unloading process below cracking point for cracked shear wall

94

When unloading extends to the horizontal axis where external force equals zero, the shear wall returns to a presumed distance of DPP/3. The shear wall exhibits energy dissipation and deviates from the origin by a displacement of DPP/3. The applicable hysteresis rule is SB 5.4, same rule for the case of unloading after reversal loading.

(b) In the other unloading case with some shear wall energy dissipation, the current loading point goes beyond equivalent cracking point but remains below the yielding point. Thus two segments exist during the unloading process. The first goes from the turning point (at the end of the loading process) to the unloading force and equals a load one-third of equivalent cracking load, i.e., $F_c/3$. The applicable hysteresis rule is SB 2.2. The second is more flat and points to the opposite equivalent cracking point (C') but stops at zero force. The applicable rule is SB 2.3. To elaborate, the first segment moves downward from turning point X_4 to break point X_5 where the load equals $F_c/3$ and the second segment moves downward from break point X_5 to zero force point X_6. The area enclosed by points O, C, X_4, X_5 and X_6 contains energy dissipation for the current half cycle. This half cycle constitutes part of the hysteresis loops and is shown in Figure 43.

Stiffness for the first segment is the same as initial elastic stiffness of the original backbone curve

$$K = OSOC \tag{103}$$

where OSOC (see Figure 30) is initial elastic stiffness of the backbone curve. Stiffness for the second segment is calculated as the slope between break point and equivalent cracking point on the opposite side

$$K = \frac{FCP-FPP}{DCP-DPP} = K_b \tag{104}$$

in which DCP = SIGN (DC, -DPP) \hfill (105)

(a)

(b)
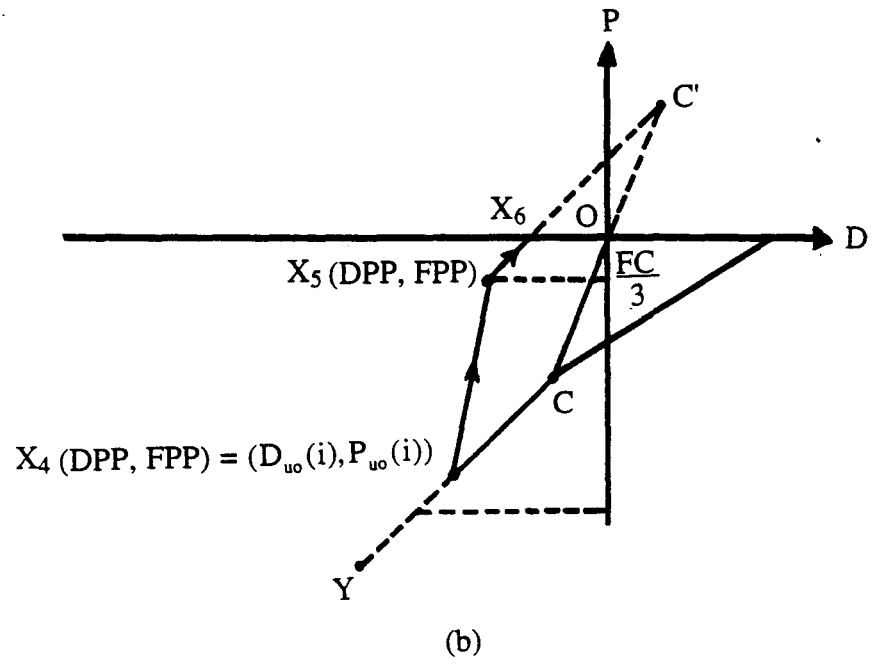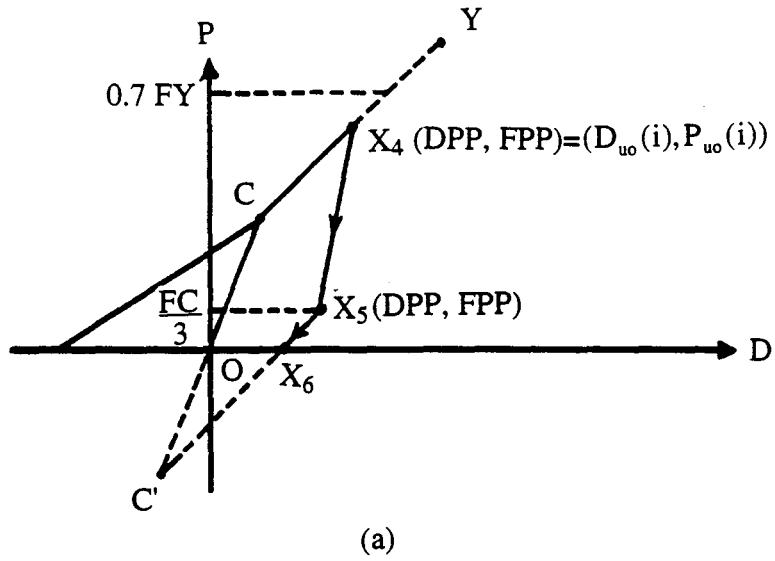
Figure 43. Unloading process as current path between cracking point and yielding point

$$FCP = SIGN\ (FC,\ DCP) \tag{106}$$

(c) When the current loading point exceeds 70 percents of equivalent yielding point (Y) but remains below equivalent ultimate point (U), this unloading case occurs. It is shown as path $\boxed{1}$ or $\boxed{2}$ in Figure 44(a) and (b). Three segments exist for the entire process. Path $\boxed{2}$ is illustrated for this case.

i) Assume the stiffness of the first segment goes downward vertically until the load decreases to 0.85 of maximum load $P_{uo}(i)$. Stiffness is expressed as

$$K = SX_3X_2 = K_C\ (\text{idealized vertical line}) \tag{107}$$

where SX_3X_2 is the slope of line segment from X_3 to X_2. The applicable rule is SB 2.4.

ii) When the force moves downward from break point X_2 to X_1, the force is assumed to be one-sixth of maximum load $P_{uo}(i)$, i.e., $P_{uo}(i)/6$. Stiffness for this segment is written as

$$K = SOB \tag{108}$$

where SOB is the slope of segment $\overline{OB}$, which is from the origin O to point B. Point B is midway between points A and Y. Points A, B and Y are in line horizontally. As shown in Figure 44(c) and (d), point A is on the initial slope's extended line from origin O to cracking point C (or equivalent cracking point). The applicable hysteresis rule is SB 2.5.

iii) In the third segment of the unloading process, the path slope connects break point X_1 and the opposite critical point. If maximum displacement D_{max} for the current half cycle is less than 1.6 times original ultimate displacement (on the backbone curve), the opposite critical point is assumed to be the yielding point. Unloading stiffness for the third segment can thus be written as
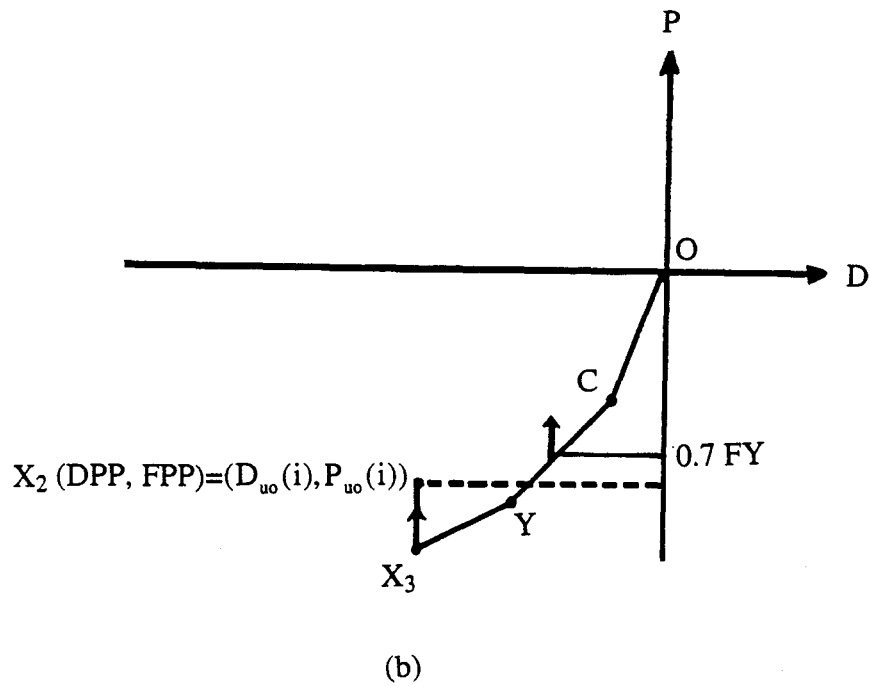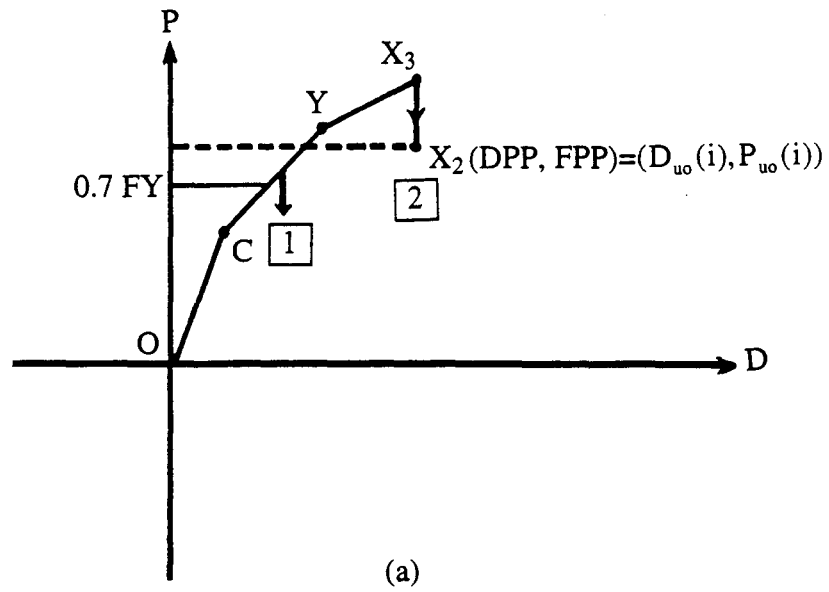
Figure 44 Unloading process as current path between yielding point and ultimate point

(c)

Y' (DYP, FYP) = (-DY, -FY)

(DCP, FCP) = (-DC, -FC)

(d)
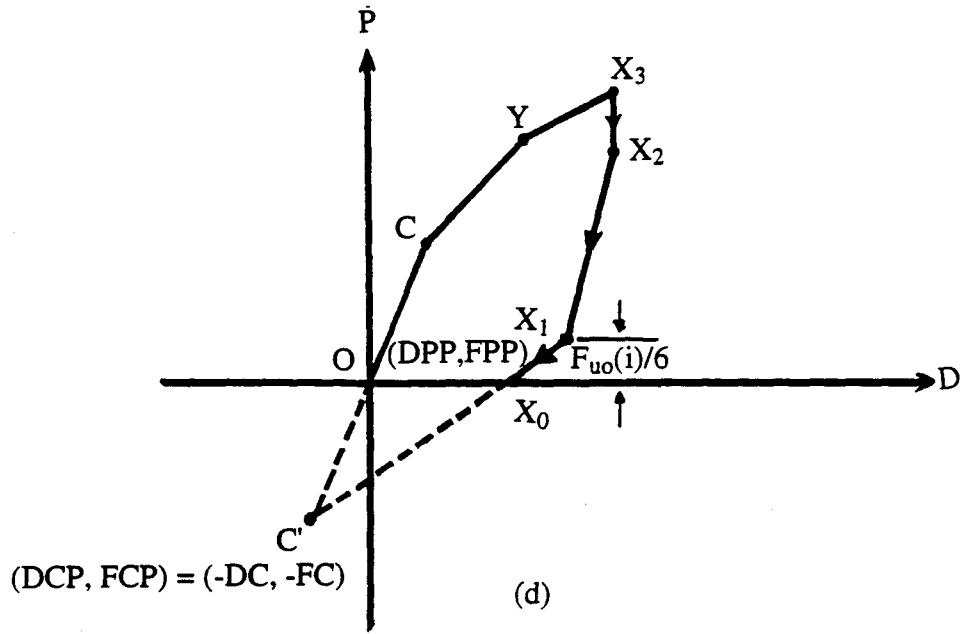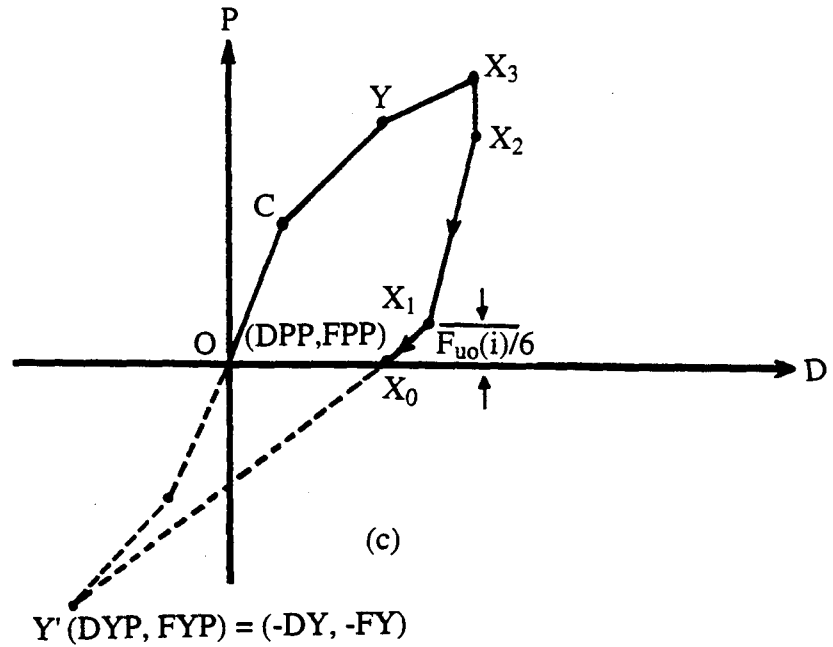
Figure 44 (continued) Unloading process as current path between yielding point and ultimate point

$$K = SX_1Y' = \frac{FYP\text{-}FPP}{DYP\text{-}DPP} \tag{109}$$

in which FYP = SIGN(FY, -FPP) and DYP = SIGN(DY, FYP).

If maximum displacement D_{max} is more than 1.6 times original ultimate displacement (on the backbone curve), the opposite critical point is set to the cracking point. Unloading then becomes

$$K = SX_1C' = \frac{FCP\text{-}FPP}{DCP\text{-}DPP} \tag{110}$$

in which FCP = SIGN (FC, -FPP) and DCP = SIGN (DC, FCP). This process is shown in Figure 44(c) and (d). The applicable hysteresis rule is SB 2.6. A summary of these unloading cases appears in Table VII.

3. Reversal Loading Process This process is associated with loading from positive force side to negative force side and vice versa. When the shear wall experiences unloading until force equals zero and continues vibrating to the other side, the behavior of shear wall is known as reversal loading stage. Cheng and Mertz [29] observed that this loading range for shear has a highly pinching effect. The corresponding energy dissipation for shear is much less than that for flexure.

(i) When displacement for the entire history (DM) is less than original cracking displacement (ODC), as shown in Figure 45, the shear wall remains in the elastic range. This wall's reversal stiffness is the same as the backbone curve's initial elastic stiffness and is written as

$$K = SOC' \ (= OSOC') \tag{111}$$

The applicable rule is SB 3.1.

Table VII   Summary of unloading process

Unloading process: (KL = 2 or 4)

(1) If DM < ODC and $P_{uo}(i) < DC$,

rule SB 2.1

stiffness K = SOC

(2)

(A) $P_{uo}(i) < DC$,

rule SB 5.4

$K = -FPP / [DPP/3 - DPP] = K_a$

(B) $FC \leq P_{uo}(i) < 0.7 FY$,

(i) If $|FP| \geq FC/3$,

rule SB 2.2

stiffness K = SOC

(ii) If $|FP| < FC/3$,

rule SB 2.3

stiffness K = [FCP-FPP] / [DCP-DPP]

$= K_b$

in which DCP = SIGN(DC,-DPP)

FCP = SIGN(FC,DCP)

(C) $P_{uo}(i) \geq 0.7 FY$,

(i) If $|0.85 P_{uo}(i)| \leq |FP| < |P_{uo}(i)|$,

rule SB 2.4

$K = SX_3X_2 = K_c$ (idealized vertically line)

(ii) If $|P_{uo}(i)/6| \leq |FP| < |0.85 P_{uo}(i)|$,

101

Table VII (continued) Summary of unloading process

---

in which FYP = SIGN(FY,-FPP)

$$DYP = SIGN(DY,FYP)$$

K = SOB

(iii) If $|FP| < |P_{uo}(i)/6|$,

   (a) If $|Dmax| \le 1.6(ODU)$,

     rule SB 2.6

     K = SX₁Y' = [FYP-FPP] / [DYP-DPP]

   (b) If $|Dmax| > 1.6(ODU)$,

     rule SB 2.6

     K = SX₁C' =[FCP-FPP] / [DCP-DPP]

     in which FCP = SIGN(FC,-FPP)

         DCP = SIGN(DC,FCP)

(ii) When maximum displacement for the entire history (DM) is more than or equal to original cracking displacement (ODC), there are two options for reversal loading process (see Figure 46). If the energy dissipation ratio $\left(=\Sigma E_d/P_{uo}D_{uo}\right)$ is less than 0.3 or maximum force at turning point X_3 is less than 70 percent of original yielding load, then the stiffness of the reversal loading path is along the segment between zero force point X_0 and opposite equivalent cracking point C'. This is formulated as

$$K = SX_0C' \qquad\qquad (112)$$

The applicable hysteresis rule is SB 3.1. By this rule, the opposite equivalent cracking point C' is symmetric at its origin to cracking point C of the backbone curve.
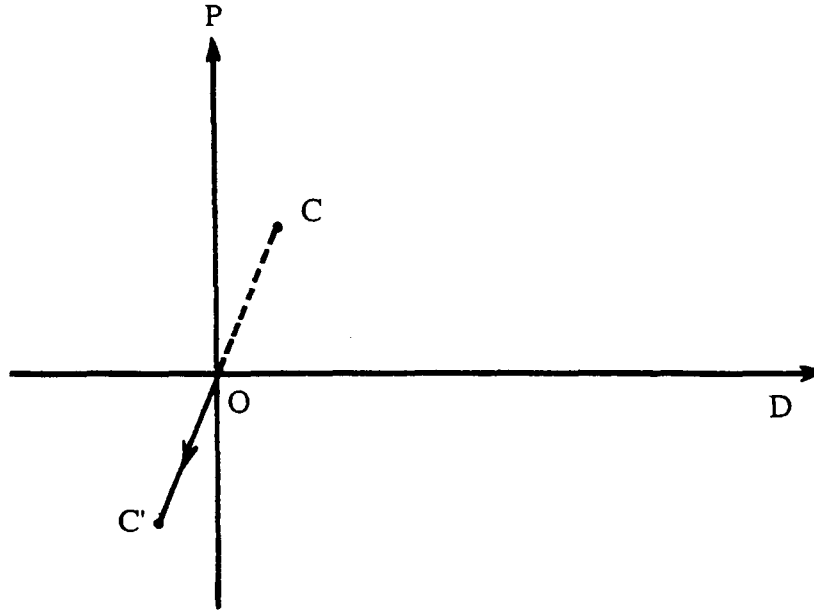
Figure 45 Reversal loading within elastic range

If the energy dissipation ratio $\left(=\Sigma E_d/P_{uo}D_{uo}\right)$ is greater than or equal to 0.3, the reversal stiffness is assumed to be SR which is obtained from an empirical equation (see Figure 29). When displacement of the shear wall at zero force point X_0 is defined as DPP (see Figure 46), the opposite cracking point C' can be determined by using one-fourth of DPP from the above case of SB 3.1. The applicable rule is SB 3.2. Reversal stiffness is expressed as

$$K = SR \qquad\qquad\qquad (113)$$

Table VIII summarizes all cases for the reversal loading process.

4. <u>Reloading after Unloading Process</u> When the shear wall is subjected to a seismic load with small amplitude, its response remains in the elastic range (shown in Figure 47). If maximum displacement for the entire response (DM) is less than original cracking displacement (ODC), reloading stiffness is the same as initial elastic stiffness and becomes
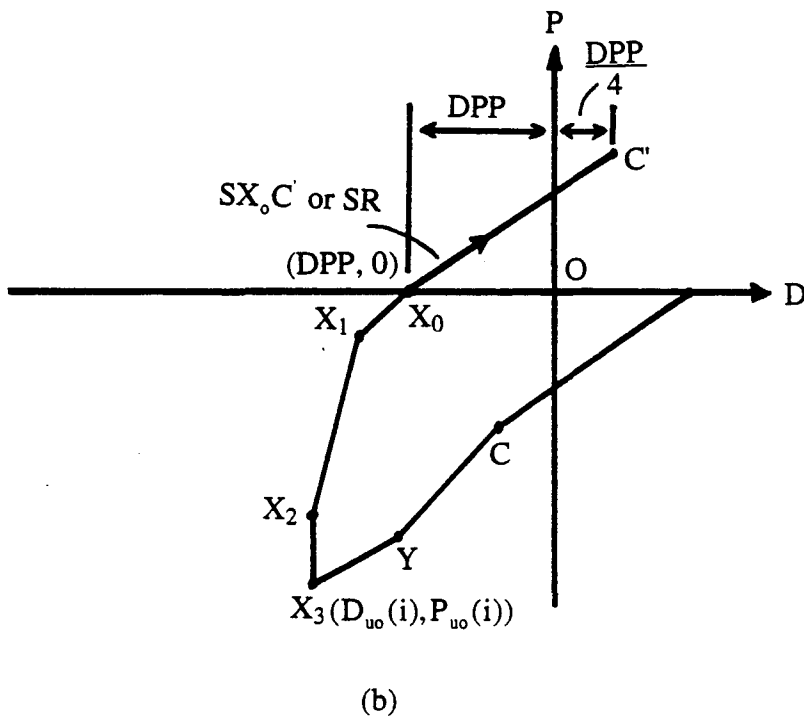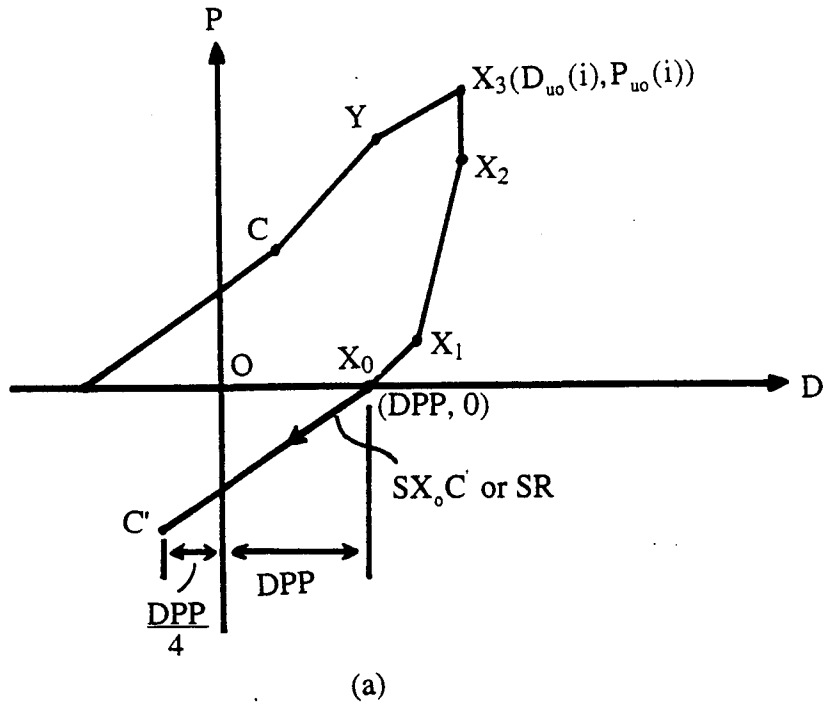
Figure 46 Reversal loading for cracked shear wall

Table VIII Summary of reversal process

Reversal process (KL = 5 or 6)

(1) If DM < ODC,

rule SB 3.1

stiffness K = SOC' (= OSOC')

(2) DM ≥ ODC,

(A) If $\Sigma E_d / P_{uo} D_{uo} < 0.3$ or $|FP| < 0.7$ FY,

rule SB 3.1

stiffness K = $SX_o C'$ (C' =C)

(B) If $\Sigma E_d / P_{uo} D_{uo} \geq 0.3$,

rule SB 3.2

stiffness K = SR

$$K = SOC(=OSOC) \tag{114}$$

The applicable hysteresis rule is SB 1.0. Both cases exhibit the same loading process in that they have the same stiffness formulation.

If maximum displacement for the entire response (DM) is greater than or equals original cracking displacement (ODC), then two segments exist for the reloading process.

(i) Turning point X_R and point X_S mark the beginning and end of the first segment (see Figure 48). Its load is 90 percent of maximum force $P_{uo}(i)$, and stiffness of reloading is defined as
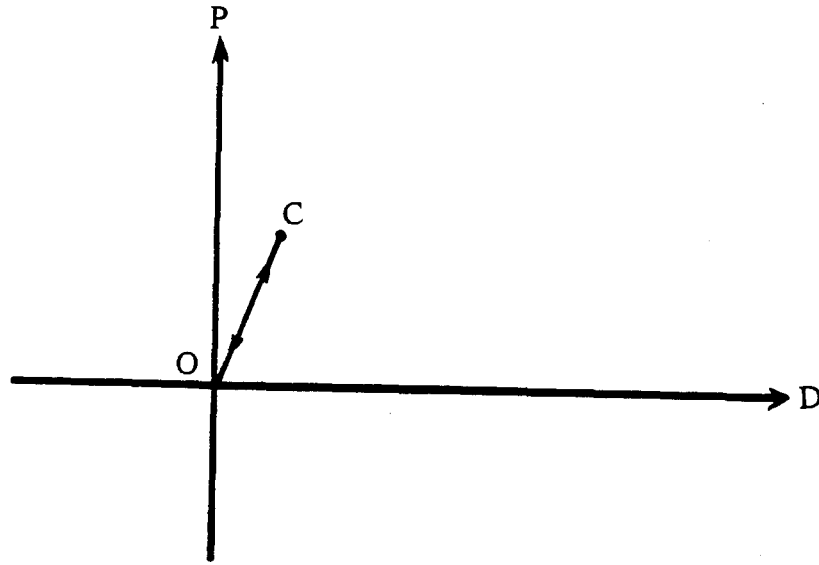
Figure 47 Reloading after unloading within elastic range

$$K = SX_RX_S = \frac{0.9P_{uo}(i)\text{-}FPP}{D_{uo}(i)\text{-}DPP} = K_d \qquad (115)$$

where $X_S = (D_{uo}(i), P_{uo}(i)*0.9)$.

(ii) This segment satisfies $|DP \geq |D_{uo}(i)||$. Point X_S, which is same as unloading maximum displacement $D_{uo}(i)$, marks the beginning of the second segment and the backbone curve or reference curve marks its end (see Figure 48). The applicable hysteresis rule is SB 4.2. Its stiffness is expressed as

$$K = 0.5(SX_RX_S) = K_e = (0.5K_d) \qquad (116)$$

Table IX summarizes the reloading after unloading process.

5. Unloading after Reversal Loading Process Here unloading is followed by loading in the opposite direction. In this process, a small loop is often formed during

106
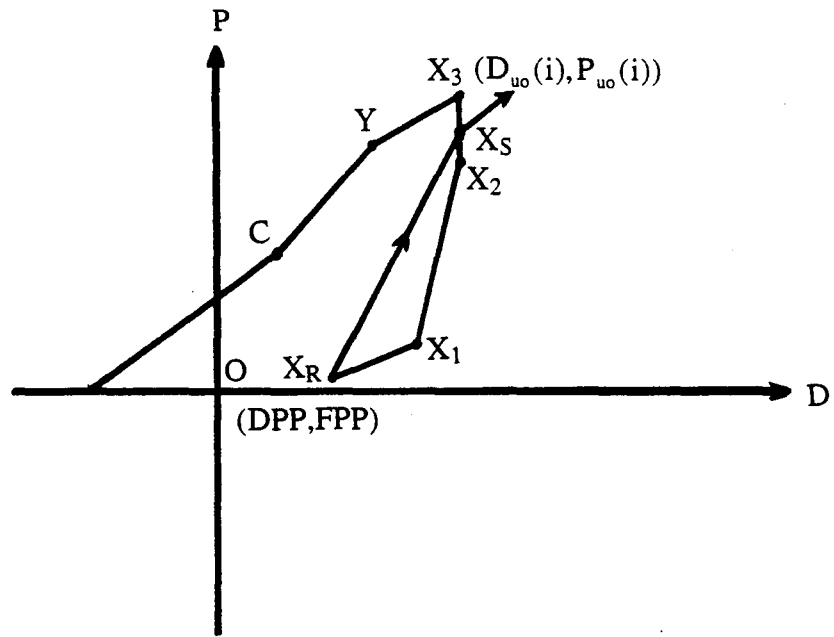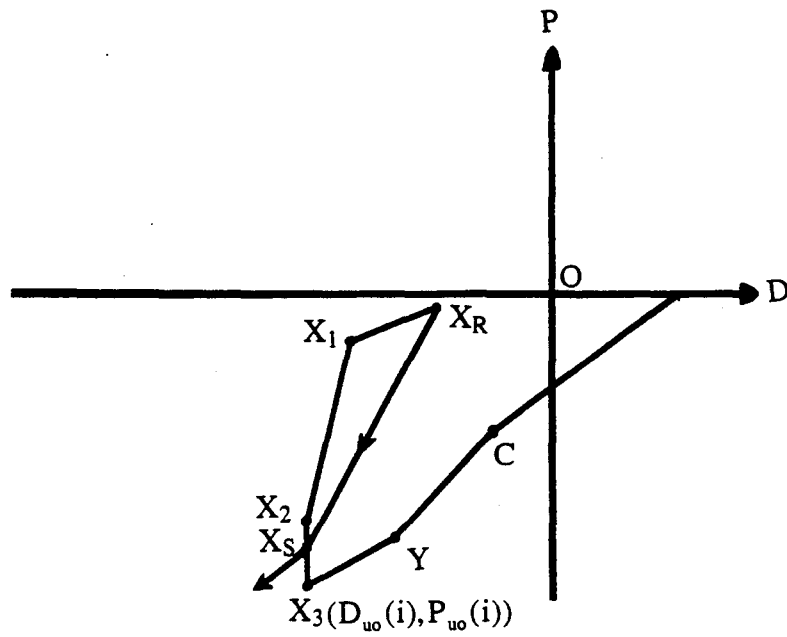
Figure 48 Reloading after unloading for cracked shear wall

seismic motion. **The following discusses two situations:** (i) elastic response (ii) inelastic response.

(i) When maximum displacement for the entire response (DM) is less than original cracking displacement (ODC), the shear wall behaves elastically. Figure 49 illustrates this. Stiffness is the same as initial elastic stiffness of the backbone curve, which can be expressed as

$$K = SOC(=OSOC) \tag{117}$$

Also stiffness is the same as the loading process within the elastic range. The applicable hysteresis rule is SB 1.0. **It can be seen in Figure 49.**

(ii) When maximum displacement for the entire response (DM) is more than original cracking displacement (ODC), the shear wall enters into inelastic response. After reversal loading, the path in a hysteresis loop is composed of three segments. The first segment meets the requirements that (1) current load P is negative and the corresponding current displacement is positive and (2) current load P is positive and the corresponding current displacement is negative. The applicable hysteresis rule is SB 5.1. For simplicity, the slope for this segment is assumed to be an idealized vertical line.

The second and third segments are similar to reloading after unloading process as shown in Figure 50. If the current path goes only from break point X_{RO} to X_S where load is 90 percent of maximum load $P_{uo}(i)$, stiffness is

$$K = SX_{RO}X_S = \frac{0.9P_{uo}(j)\text{-}FPP}{D_{uo}(j)\text{-}DPP} = K_d \tag{118}$$

The applicable hysteresis rule is SB 5.2.

After break point X_3, if energy dissipation ratio $\left(=\Sigma E_d/P_{uo}D_{uo}\right)$ is less than 0.3, stiffness is defined as

108

Table IX Summary of reloading after unloading process

Reloading after unloading process (KL = 7 or 8)

(1) If DM < ODC,

   Rule SB 1.0

   stiffness K = SOC

(2) If DM ≥ ODC,

    (A) If $|DP| \leq |D_{uo}(i)|$,

       rule SB 4.1

       stiffness K = SXRXs

       = [0.9 $F_{uo}(i)$-FPP] / [$D_{uo}(i)$-DPP] = K_d

       in which Xs = ($D_{uo}(i)$, $F_{uo}(i)$ * 0.9)

    (B) If $|DP| > |D_{uo}(i)|$,

       rule SB 4.2

       K = 0.5(SXRXs) = K_e (= 0.5 K_d)

Figure 49 Unloading after reversal loading within elastic range

$$K = SCY \tag{119}$$

If energy dissipation ratio $\left(=\Sigma E_d / P_{uo} D_{uo}\right)$ is greater than or equal to 0.3, stiffness becomes

$$K = 0.4 \left(SX_{RO}X_S\right) = K_f \tag{120}$$

Both cases are shown in Figure 50. The applicable hysteresis rule is SB 5.3.

Unloading after reversal loading also occurs when the path of reversal loading proceeds to the opposite displacement side and does not reach the first critical point (i.e., cracking point or equivalent cracking point). This case is shown in Figure 51. The applicable hysteresis rule is SB 5.4. Note that controlling factor KL is 2 on the positive force side or 4 on the negative force side. Associated stiffness K has the form of

$$K = SX_3X_0 = \frac{-FPP}{DPP/3 - DPP} = K_a \tag{121}$$

Unloading after reversal loading is summarized in Table X.

E. COMPARISON BETWEEN CALCULATED AND EXPERIMENTAL RESULTS

In Figures 52 through 57, calculated and experimental results for NCKU wall tests under earthquake type loading are compared. Some findings are discussed below.

As shown in Figure 52, calculated stiffness matches experimental initial stiffness quite well. The former is provided by the slope of the first segment on the backbone curve. Experimental maximum load for the second cycle is larger than calculated load. For the third cycle, calculated maximum load is less than experimental maximum load but the slope of the calculated path (i.e., between equivalent cracking point and equivalent yielding point) is close to the experimental slope on the same segment. Slopes for the loading process in
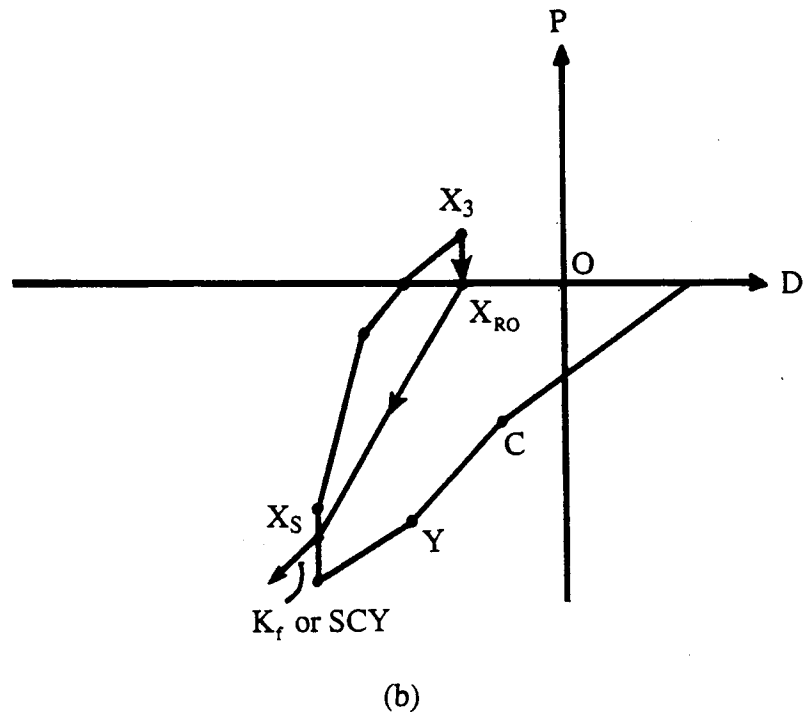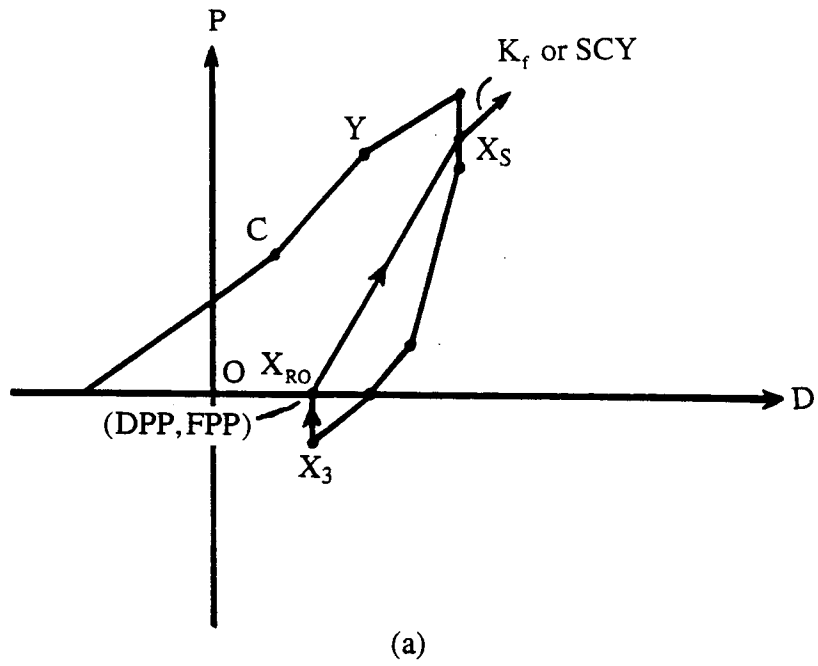
Figure 50 Unloading after reversal loading for cracked shear wall

$$\frac{DPP}{3} = \frac{D_{uo}(i)}{3}$$

$$(DPP, FPP) = (D_{uo}(i), P_{uo}(i))$$
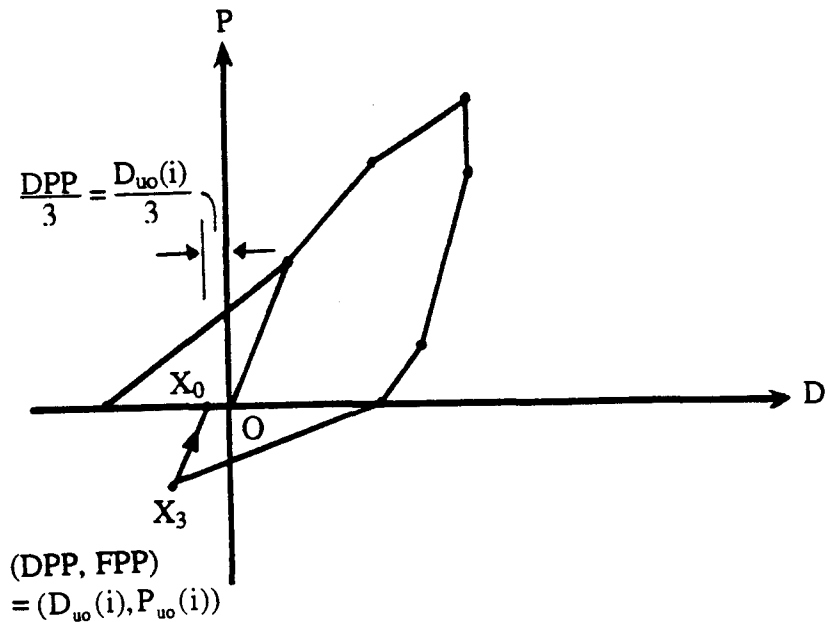
Figure 51 Unloading after reversal loading process as current path below cracking point

the fourth and fifth cycles are compatible vis-a-vis calculated and experimental loops. Deviation of the path in these two comes from uncertainty of the equivalent cracking point. In this regard, cycle 6 is similar to the fourth and fifth cycles. Cycles 4, 5, 6 and A have good agreement for the unloading process in terms of calculated path and experimental path. Cycle A is a small loop with some deviation in the reloading after unloading path between calculated and experimental results. In cycle 7 calculated and experimental curves match well. On the negative force side, B and C show large displacement. Deviation in this range is more than for previous loops, but the comparison is still good. As shown in Figure 53, shear wall SWO-6E yields a similar comparison. Maximum load for cycles 3, 4, 5 and 6 of calculated and experimental loops in the loading and unloading process matches well. Cycle 7 is in the range of high energy dissipation, which involves large displacement. For this cycle, calculated maximum load is below that of the experimental

Table X Summary of unloading after reversal process

Unloading after reversal process (KL = 9 or 10)

(1) If DM < ODC,

    rule SB 1.1

    stiffness K = SOC (= OSOC)

(2) If DM ≥ ODC,

    (A) If DPP * FPP < 0,

        Previous KL = 5 or 6

        rule SB 5.1

        $K = SX3XRO = Kc$ (idealized vertical line)

    (B) If $|DP| < |D_{uo}(i)|$,

        stiffness K = SXROXS

        $= [0.9 P_{uo}(i) - FPP] / [D_{uo}(i) - DPP] = Kd$

    (C) If $|DP| > |Duo(i)|$,

        rule SB 5.3

        If $\Sigma Ed/PuoDuo < 0.3$, K = SCY

        If $\Sigma Ed/PuoDuo > 0.3$, K = 0.4(SXROXS) = Kf

    (D) If $|Duo(i)| \leq DC$,

        KL = 2 or 4

        rule SB 5.4

        $K = SX3Xo = -FPP / [DPP/3 - DPP] = Ka$

path. On the reversal loading path, shear walls SWO-1E, SWO-6E and SWO-8E exhibit good comparison between experimental and calculated results.

For shear walls with a height/width ratio of 0.65, such as SWO-12, SWO-14E and SWO-16E, the slopes of loading, unloading, reloading and reversal loading compare well between calculated and experimental response. The calculated load capacities are generally smaller than experimental load capacities for some cycles, as shown in Figure 55 through 57.

In summary, calculated hysteresis output and experimental hysteresis results indicate good agreement when compared. All the shear walls herein display a pinching effect when force vibrates from one side to the other side. Hysteresis response of RC perforated shear wall is thus strongly controlled by shear.
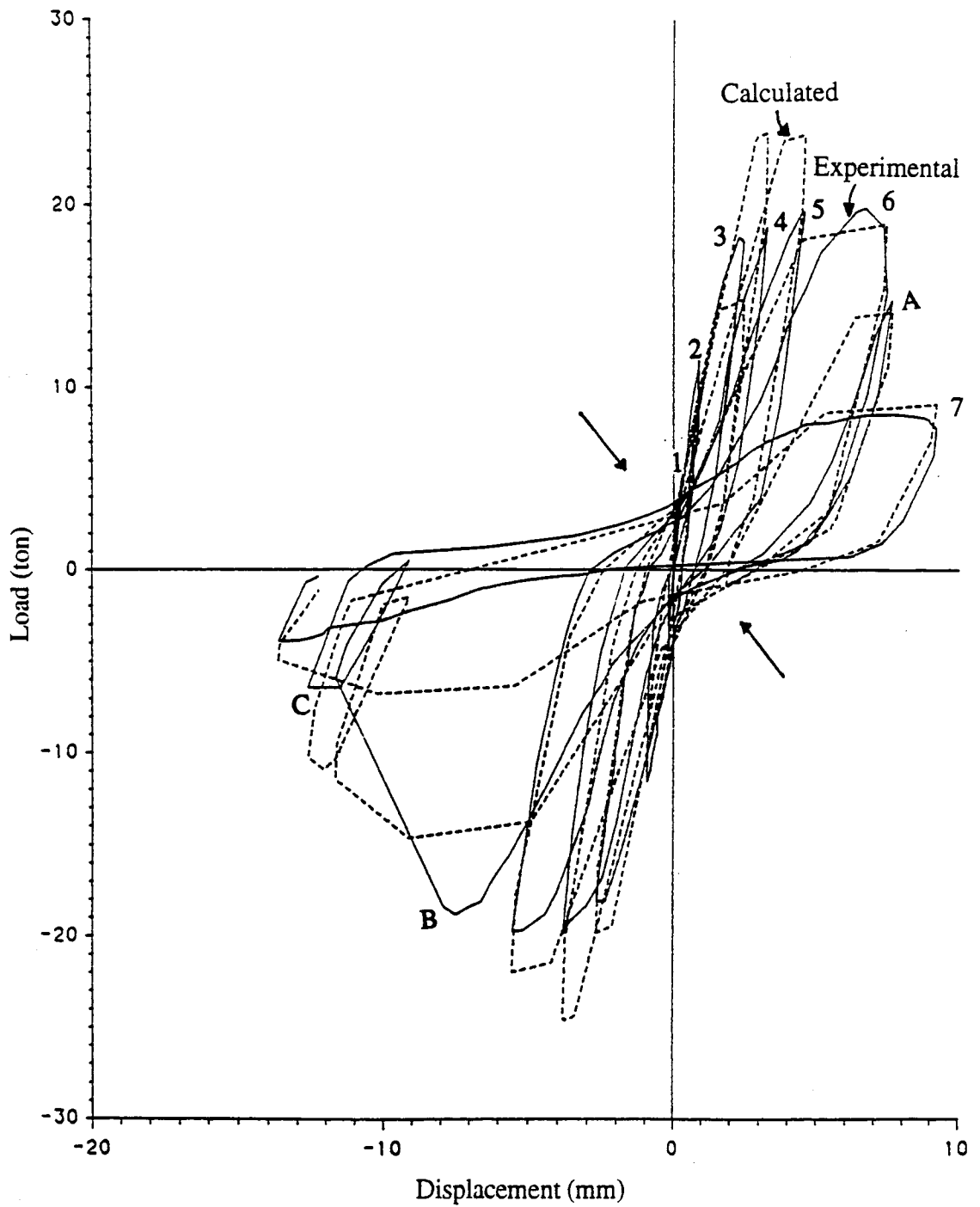
Figure 52 Comparison between calculated and experimental hysteresis response for perforated shear wall SWO-4E
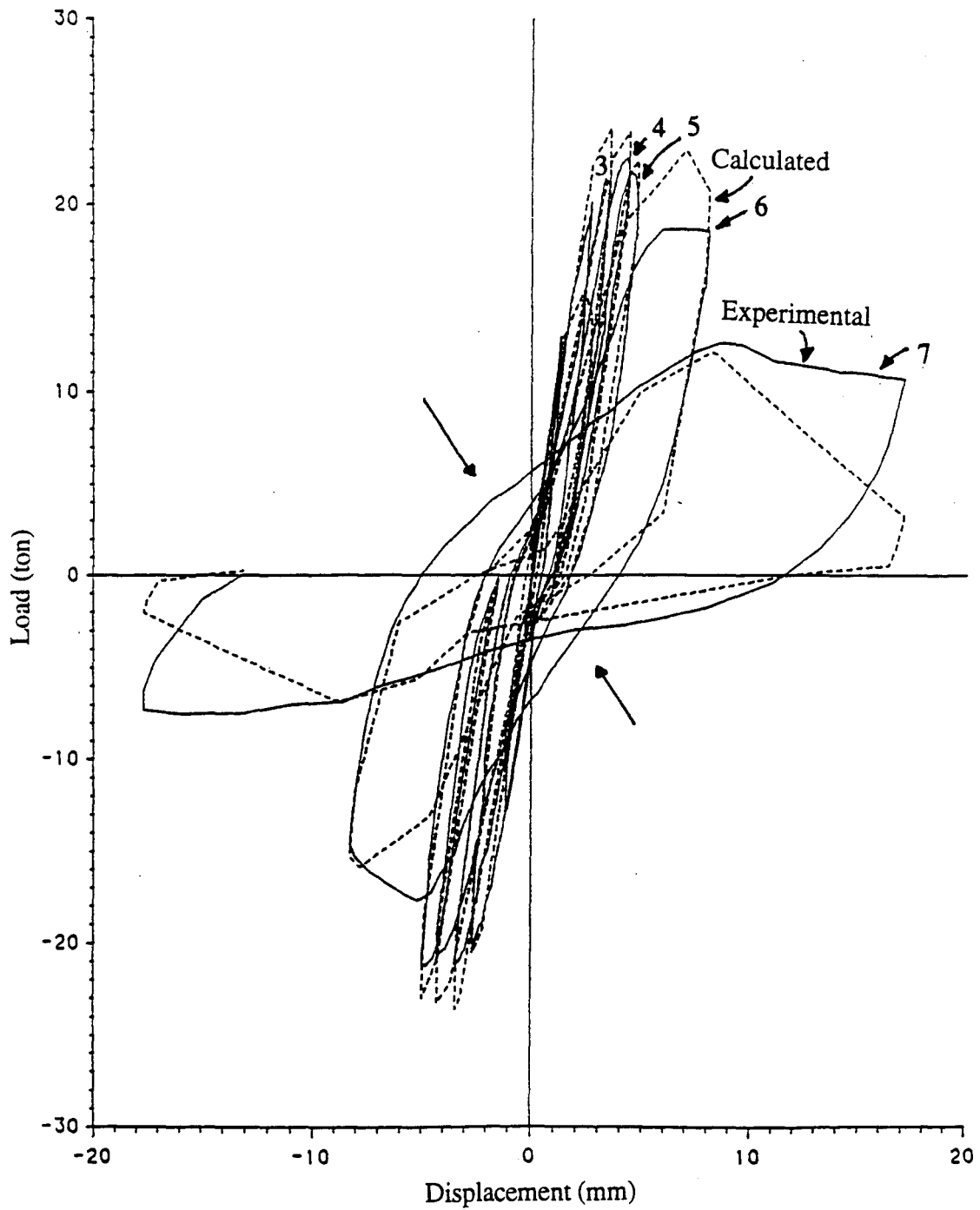
Figure 53 Comparison between calculated and experimental hysteresis response for perforated shear wall SWO-6E
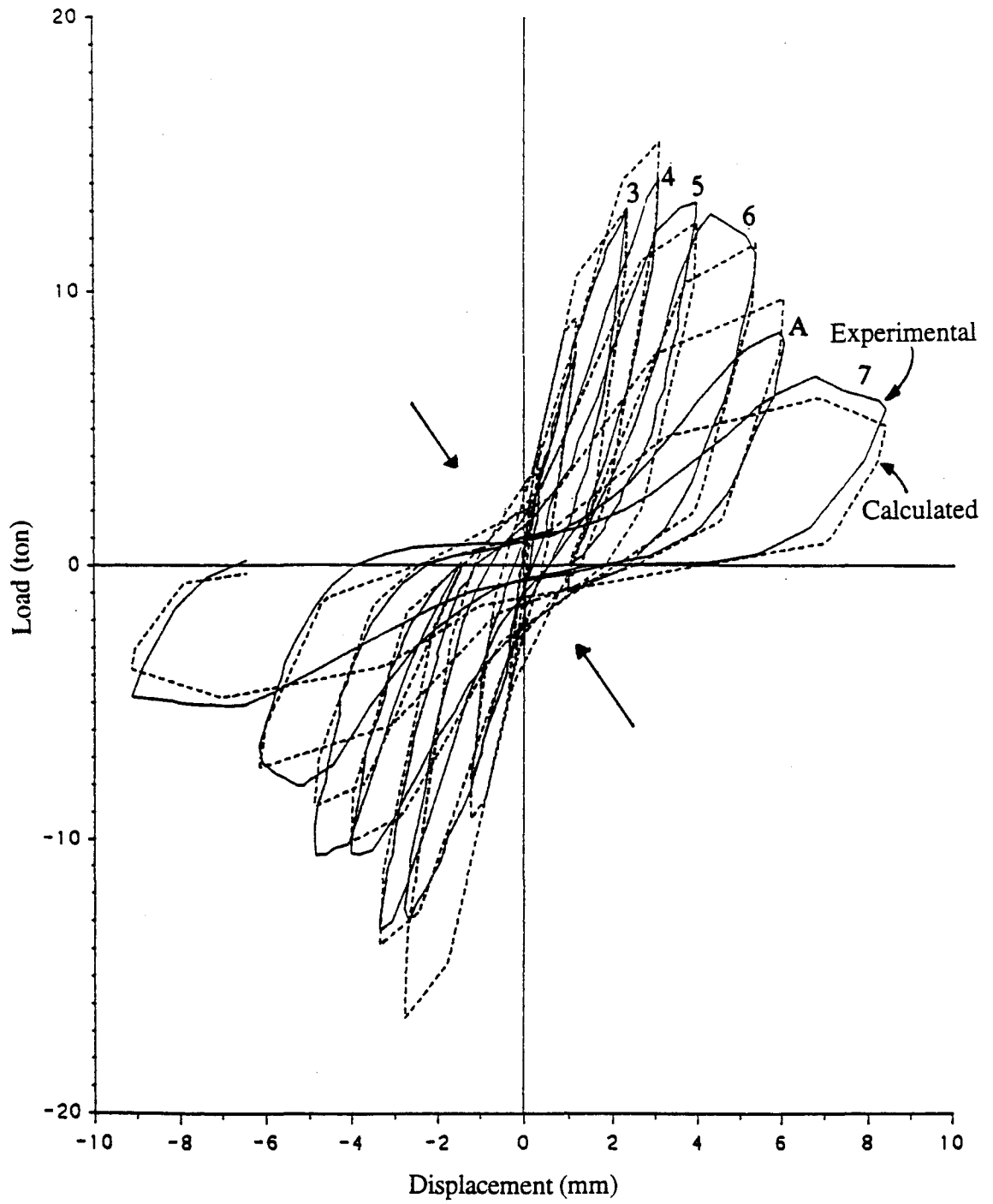
Figure 54 Comparison between calculated and experimental hysteresis response for perforated shear wall SWO-8E
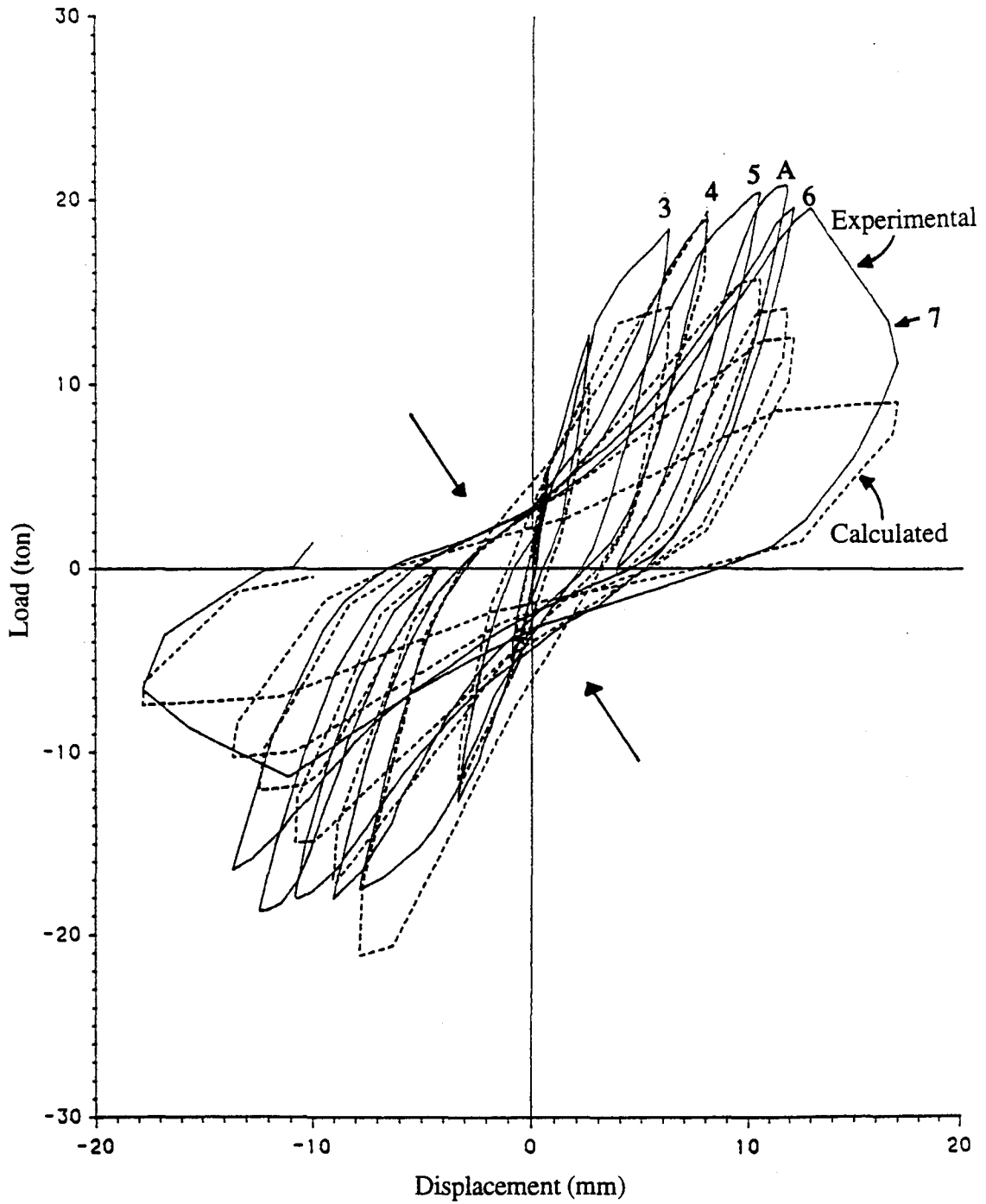
Figure 55 Comparison between calculated and experimental hysteresis response for perforated shear wall SWO-12E
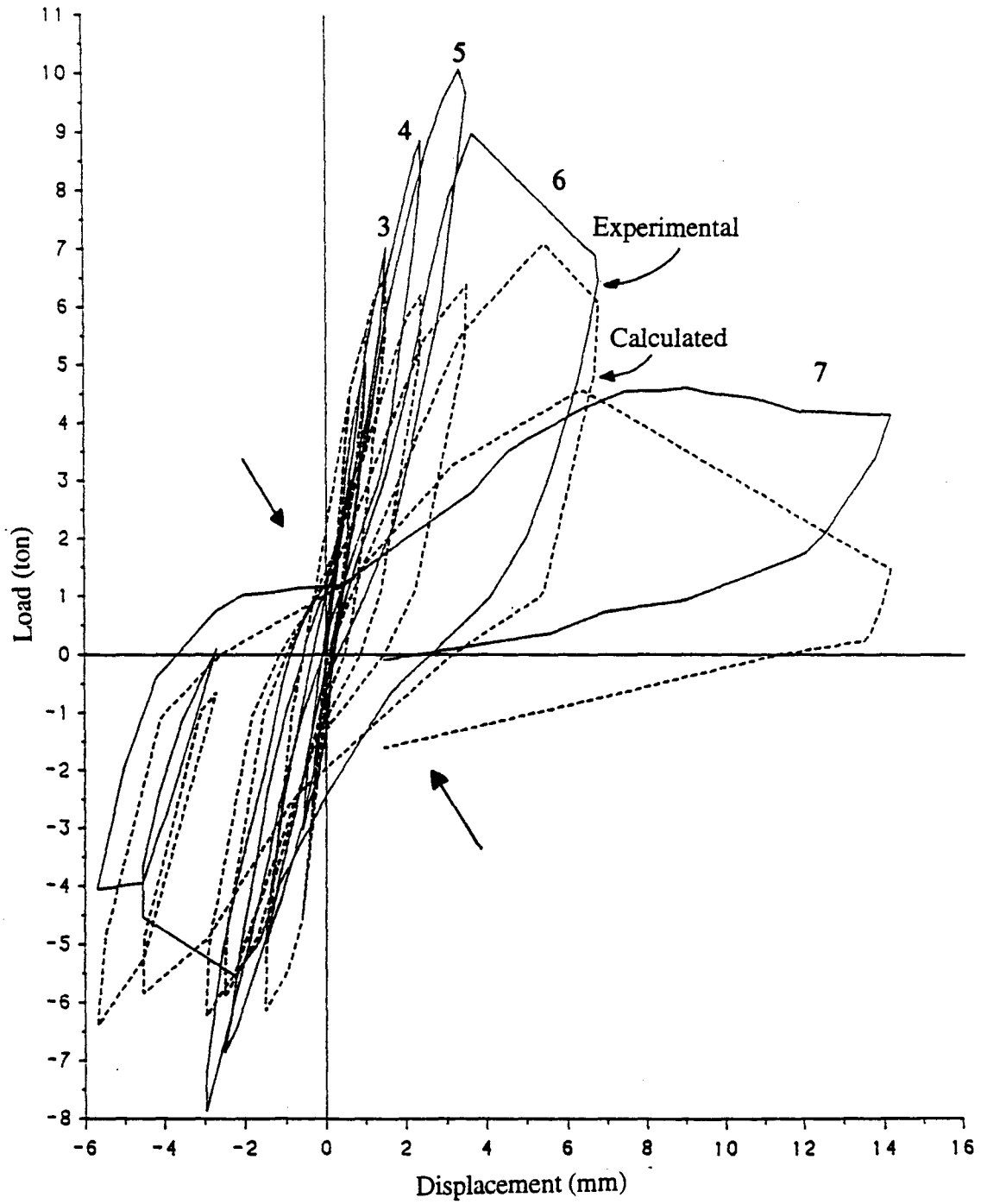
Figure 56 Comparison between calculated and experimental hysteresis response for perforated shear wall SWO-14E
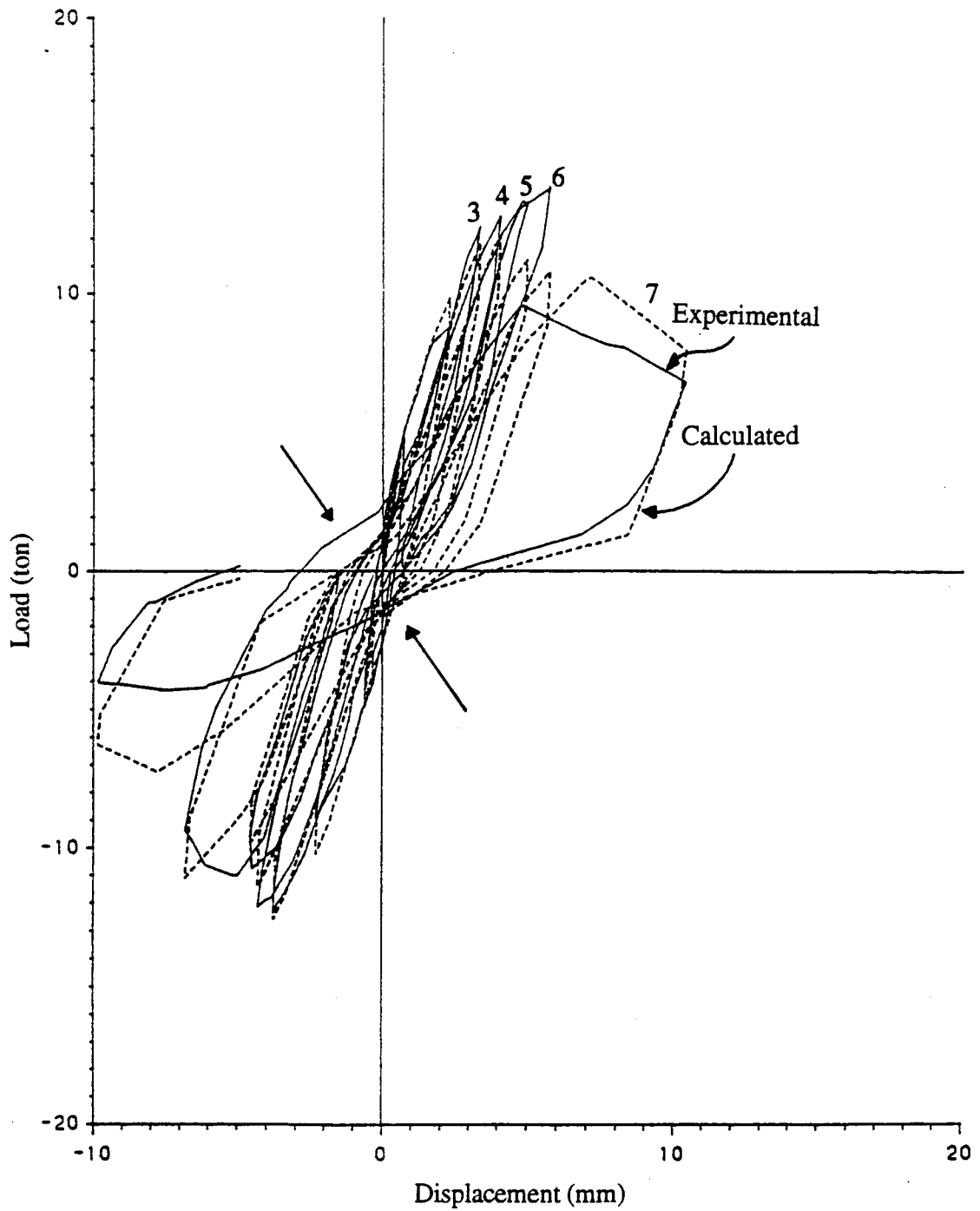
Figure 57 Comparison between calculated and experimental hysteresis response for perforated shear wall SWO-16E

V. EQUIVALENT VISCOUS DAMPING OF RC SHEAR WALL

Damping is the action of energy removal from a system subjected to excitation. Energy loss occurs in the vibration system by dissipation or transmission to protect the structure itself from failure. Researchers have established many types of damping models [31-39]. As far back as 1927, Kimball and Lovell found that many engineering materials, unlike behavior of viscous damping, exhibit energy dissipation with respect to square of displacement but independent of frequency of motion. Later this phenomenon was named hysteretic damping by Bishop and Johnson [39]. In fact, hysteresis loops are produced not only by hysteretic damping but also by a variety of damping mechanisms in a real structural system. Bishop [40] also noted that if a simple oscillator undergoes steady forced vibration, it experiences damping effects which are neither truly viscous nor truly hysteretic in character. Theories based on viscous or hysteretic damping give an approximate solution for actual behavior. These two are close to each other when damping is light; hysteretic damping becomes more evident when damping is heavier. Lancaster derived an equation of motion by combining viscous and hysteretic damping [41].

Strictly speaking, hysteretic damping is defined only for harmonic motion. In this respect, Crandall [42] emphasized that the non-physical phenomenon of this model still exists. To solve certain problems, it is often necessary to sacrifice accuracy in representing physical behavior [39], particularly for applications such as instability in steady state oscillation or stationary random vibration.

In this section the concept of viscous damping is applied to hysteretic damping. Characteristics of hysteretic damping of RC shear walls are explored in the context of NCKU experiments which involved quasi-static excitation.

A. FORMULATION

1. Harmonic Motion   When a steady harmonic excitation is imposed, a system will oscillate with some degree of energy absorption. By means of viscous damping action, this process of absorption serves to dissipate the input energy. An equation of motion reveals that applied force P consists of three forces: inertia force F_I, spring force F_S and viscous damping force F_D. Equilibrium of force is shown in Figure 58 and expressed in the following equation

$$P = F_I + F_S + F_D \tag{122}$$

Also, steady harmonic excitation provides

$$\text{applied force } P = p_o \cdot \sin\Omega t \tag{123}$$

$$\text{arbitrary displacement } u = u_o \cdot \sin(\Omega t - \Phi) \tag{124}$$

where Φ is phase angle; u_o is maximum amplitude; p_o is maximum applied load and Ω is frequency of motion.

Thus.

$$\text{inertial force } F_I = ma = m\ddot{u} \; ; \; a \text{ is acceleration , m is mass} \tag{125}$$

$$\text{spring force } F_S = ku \; ; \; k \text{ is spring constant} \tag{126}$$

$$\text{damping force } F_D = c\dot{u} \; ; \; c \text{ is damping coefficient, } \dot{u} \text{ is velocity} \tag{127}$$

Rewrite the above as
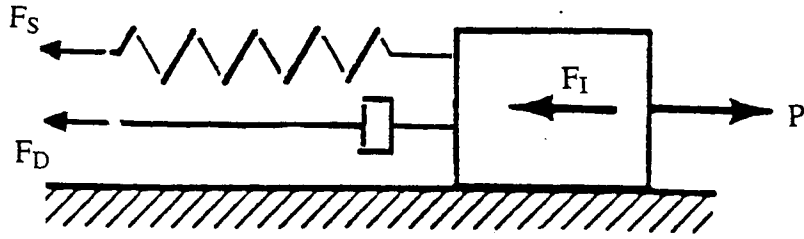
Figure 58   Schematic diagram of forces for a body subjected to external force

$$F_I = m\ddot{u} = - mu_o\Omega^2\sin(\Omega t\text{-}\Phi) \tag{128}$$

$$F_S = ku = k\,u_o\sin(\Omega t\text{-}\Phi) \tag{129}$$

$$F_D = c\dot{u} = c\,u_o\Omega\cos(\Omega t\text{-}\Phi) \tag{130}$$

Combining Eq. (124) and (130) yields

$$\left(\frac{F_D}{c\Omega u_o}\right)^2 + \left(\frac{u}{u_o}\right)^2 = 1 \tag{131}$$

Figure 59 demonstrates Eq. (131).

Equations (128) and (129) are illustrated in Figures 60 and 61. All the effects of $P = F_I + F_S + F_D$ can be seen in Figure 62.

The area bounded by inertia force-amplitude in Figure 61 is denoted by $(W_S)_1$ and $(W_S)_2$ which can be expressed as

$$W_{S1} = W_{S2} = \frac{1}{2}ku_o{}^2 \tag{132}$$

123
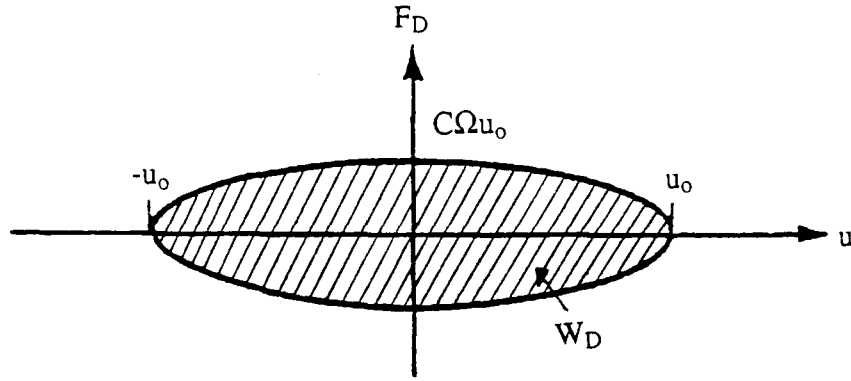
Figure 59   Damping force vs. amplitude relationship under harmonic motion
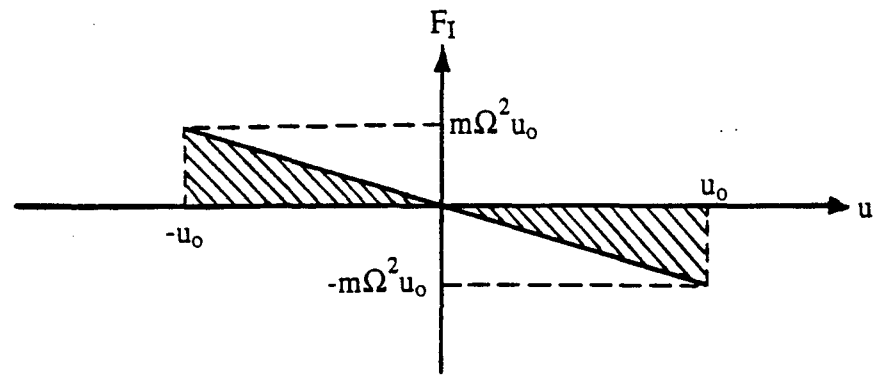
Figure 60   Inertia force vs. amplitude relationship under harmonic motion
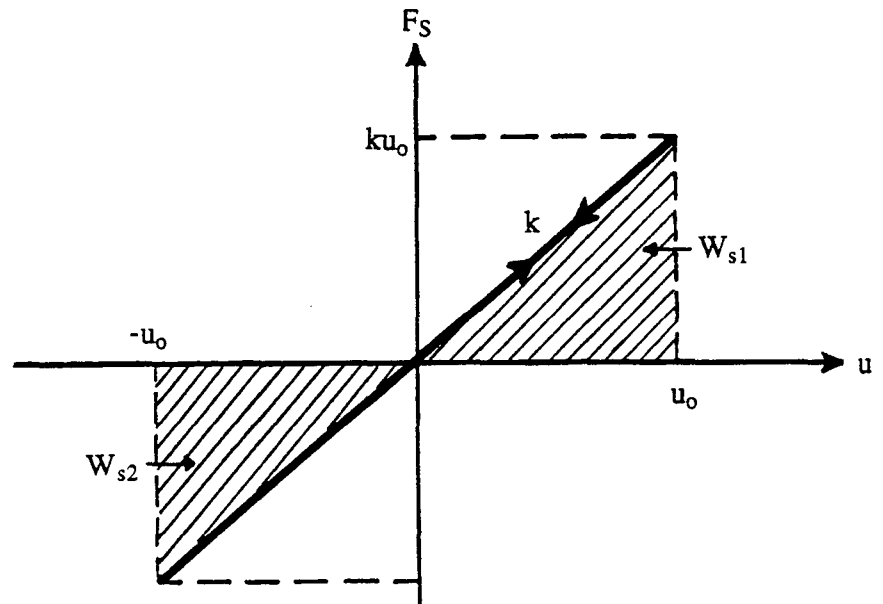
Figure 61   Spring force vs. amplitude relationship under harmonic motion

124
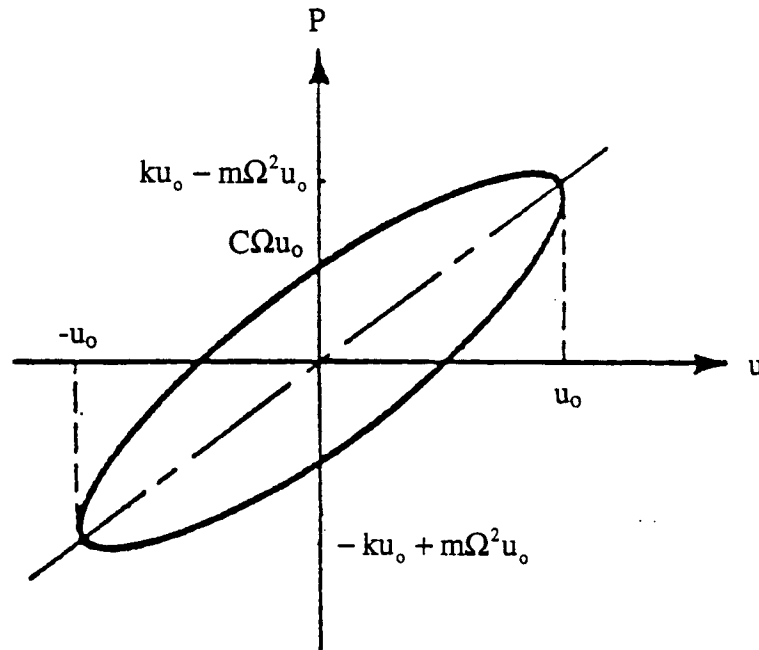
Figure 62 Hysteresis loop with respect to viscous damping for a body subjected to applied force

2. <u>Damping Ratio</u> The area bounded by damping force and amplitude in Figure 59 is denoted as W_D which can be written as

$$W_D = c\pi\Omega u_o^2 \tag{133}$$

From Eq. (133), damping coefficient c can be expressed in terms of

$$c = \frac{W_D}{\pi\Omega u_o^2} \tag{134}$$

Damping ratio ξ is defined as

$$\xi = \frac{c}{2\sqrt{km}} \tag{135}$$

or

$$\xi = \frac{c\omega_n}{2k} \tag{136}$$

where ω_n = undamped natural frequency of structure. From Eq. (132), it can be seen that spring constant k is

$$k = \frac{2W_{S1}}{u_o^2} = \frac{2W_{S2}}{u_o^2} \tag{137}$$

Thus substitute Eqs. (134) and (137) into Eq. (136),

$$\xi = \frac{c\omega_n}{2k} = \frac{W_D}{\pi\Omega u_o^2} \cdot \frac{\omega_n}{2\left(\frac{2W_{S1}}{u_o^2}\right)}$$

$$= \frac{W_D}{\pi\Omega u_o^2} \cdot \frac{\omega_n u_o^2}{4W_{S1}}$$

$$= \frac{\omega_n}{\Omega} \cdot \frac{W_D}{4\pi W_{S1}} \tag{138}$$

3. <u>Equivalent Damping Ratio</u> Now, apply the viscous damping concept to hysteretic damping (i.e., equivalent viscous damping). Use equivalent viscous damping in one full cycle which has a different peak amplitude at each half cycle (see Figure 63). If equivalent viscous damping vs. amplitude and equivalent spring vs. amplitude can be set up and shown in Figure 64 (these are derived later), then the work caused by damping force is
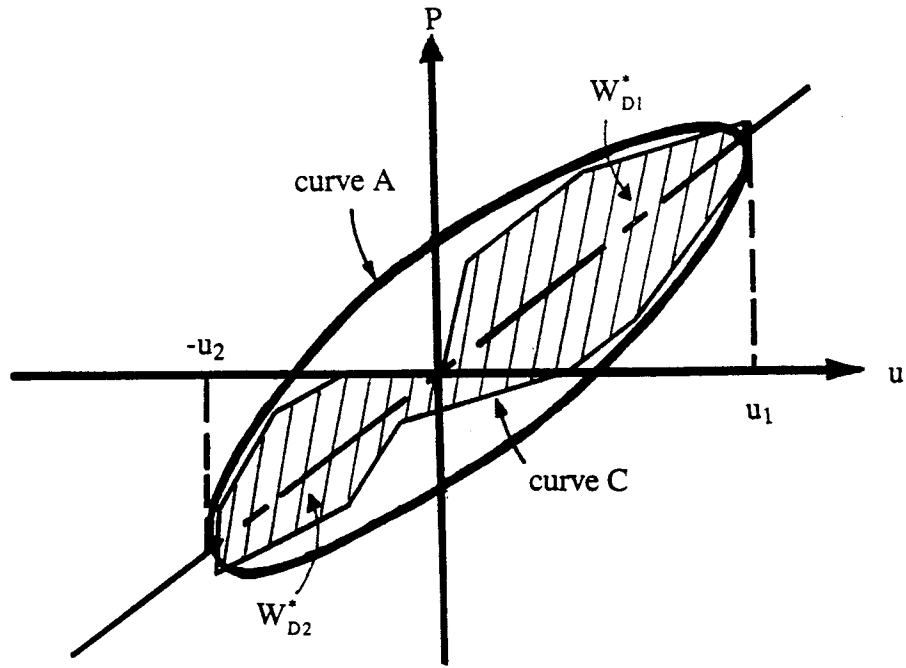
(a) a uncracked element
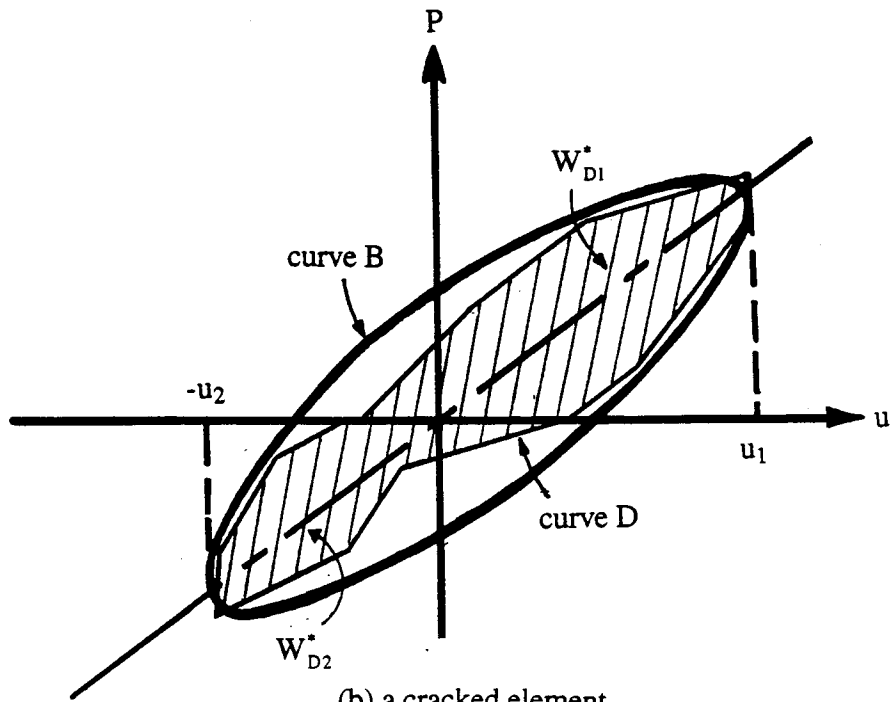
(b) a cracked element

Figure 63 Irregular load-displacement relationship and equivalent damping force vs. amplitude relationship for (a) uncracked element, (b) cracked element
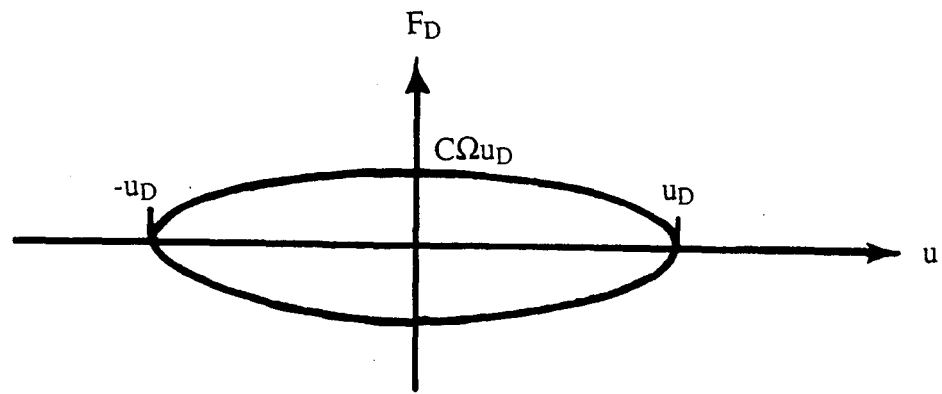
(a) Damping force
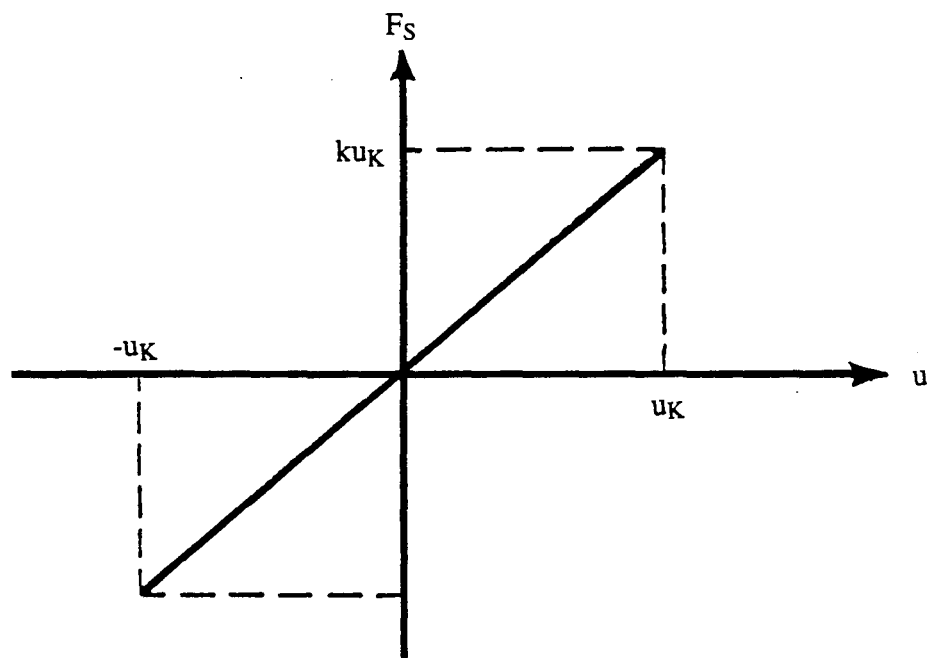
(b) Spring force

Figure 64   Damping force and spring force based on equivalent viscous damping

$$W_D = c_{eg}\pi\Omega u_D{}^2 \tag{139}$$

From Eq. (139), equivalent damping coefficient c_{eg} and amplitude u_D is

$$c_{eg} = \frac{W_D}{\pi\Omega u_D{}^2} \tag{140}$$

and

$$u_D{}^2 = \frac{W_D}{c_{eg}\pi\Omega} \tag{141}$$

Equivalent amplitude from spring force is expressed as

$$W_{S1} = \frac{1}{2} u_K{}^2 k \tag{142}$$

Spring constant k and amplitude u_K can be written from Eq. (142) as

$$k = \frac{2W_{S1}}{u_K{}^2} \tag{143}$$

$$u_K{}^2 = \frac{2W_{S1}}{k} \tag{144}$$

Therefore

$$\text{damping ratio } \xi = \frac{c\omega_n}{2k} = \frac{W_D}{\pi\Omega u_D{}^2} \cdot \frac{\omega_n}{2\left(\dfrac{2W_{S1}}{u_K{}^2}\right)}$$

$$= \frac{\omega_n}{\Omega} \cdot \frac{W_D}{4\pi W_{S1}} \cdot \frac{u_K{}^2}{u_D{}^2} \tag{145}$$

Since hysteretic damping is related to displacement, it is independent of frequency of motion. Here assume one critical point and let $\omega_n/\Omega = 1$. Damping ratio ξ then becomes

$$\xi = \frac{W_D}{4\pi W_{S1}} \cdot \frac{u_K^2}{u_D^2} \tag{146}$$

As noted above, hysteretic damping is independent of frequency of motion. The equation of motion under hysteretic damping is formulated

$$m\ddot{u} + f_h(u) = P \tag{147}$$

where $f_h(u)$ is nonlinear function of displacement.

For simplicity, total spring force $f_h(u)$ may consist of two components: equivalent spring force $f_s = ku$, (k is average spring constant) and equivalent damping force f_D. In view of the fact that hysteretic damping is not related to force frequency Ω, assume

$$c_{eg}\Omega = \eta k \tag{148}$$

Then equivalent damping coefficient c_{eg} can be expressed as

$$c_{eg} = \frac{\eta k}{\Omega} \tag{149}$$

Therefore, if $u_K = u_D = u$ is assumed, the ratio of dissipated energy W_D to energy by spring W_{S1} is

$$\frac{W_D}{W_{S1}} = \frac{c\pi\Omega u^2}{\frac{1}{2}ku^2} = 2 \cdot \frac{c\Omega}{k} \cdot \pi = 2\pi\eta \tag{150}$$

130

and

$$\text{constant } \eta = \frac{W_D}{2\pi W_{S1}} \tag{151}$$

From Eq. (146), equivalent damping ratio ξ becomes

$$\xi = \frac{W_D}{4\pi W_{S1}} \cdot \frac{u_K{}^2}{u_D{}^2} = \frac{1}{4\pi}(2\pi\eta) \cdot \frac{u_K{}^2}{u_D{}^2} = \frac{\eta}{2} \cdot \frac{u_K{}^2}{u_D{}^2} \tag{152}$$

if

$$u_K = u_D, \text{ then } \xi = \frac{\eta}{2} \tag{153}$$

4. **Near-Harmonic Motion** Near-harmonic motion is now explored. In Figure 63(a) and (b), the former's half cycle has amplitude u_1 and latter's half cycle has amplitude u_2. In a manner similar to the analysis of viscous damping, Figure 65(a) shows the relationship between equivalent damping force F_D and amplitude. If amplitude u_1 is assumed to be larger than amplitude u_2, then Figure 65(a) represents a larger half ellipse on the right side. Figure 65(b) shows idealized ellipse which has amplitude u_1^* and u_2^*. From this, two equations for dissipated energy can be derived as

$$W_{D1}^* = \frac{1}{2} c_{eg}\pi\Omega u_1^{*2} \tag{154}$$

$$W_{D2}^* = \frac{1}{2} c_{eg}\pi\Omega u_2^{*2} \tag{155}$$

As noted, the dissipation loop is a smooth skew ellipse. It is shown as curves A and B in Figure 63(a) and (b). From a practical viewpoint, a solid skew ellipse-like curve (i.e.,

(a) Irregular damping force

(b) Irregular equivalent damping force

(c) Equivalent damping force
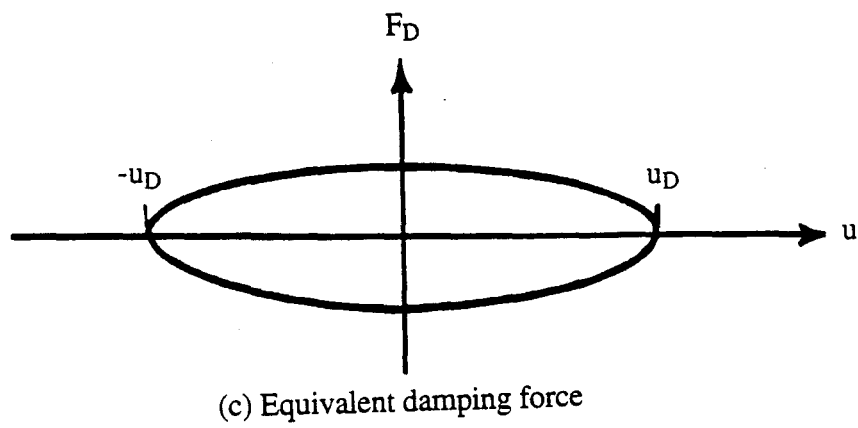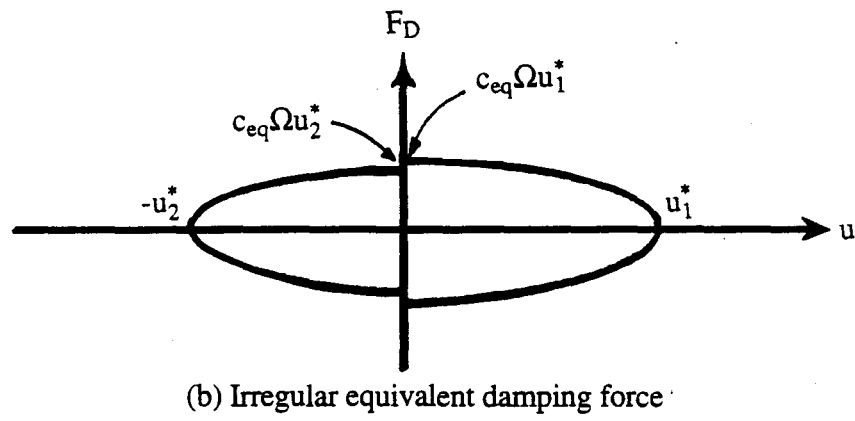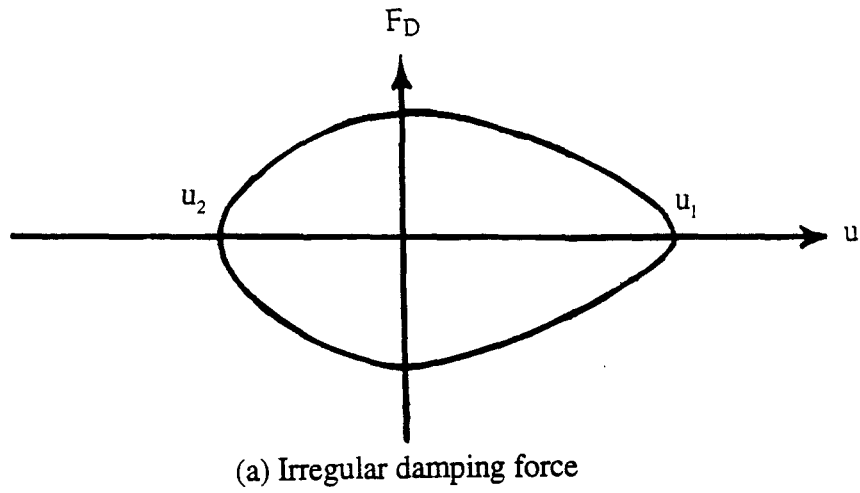
Figure 65   Irregular damping force and equivalent damping force vs. amplitude
relationship

curve C and D in Figure 63(a) and (b)) is a possible response and does occur in the experimental results for NCKU RC shear walls. In an attempt to obtain another equivalent ellipse (see Figure 65(b)), an irregular ellipse is formed (Figure 65(b)); u_D is assumed to be a new amplitude for both sides of the ellipse. Note that total dissipated energy in Figure 65(b) is equal to total dissipated energy in Figure 65(c). The formulation is

$$\frac{1}{2} c_{eg} \pi \Omega (u_1{}^*)^2 + \frac{1}{2} c_{eg} \pi \Omega (u_2{}^*)^2 = c_{eg} \pi \Omega u_D{}^2 \tag{156}$$

and equivalent amplitude u_D can be obtained as

$$u_D = \frac{1}{\sqrt{2}} \sqrt{(u_1{}^*)^2 + (u_2{}^*)^2} \tag{157}$$

Concerning the relationship between equivalent spring force and amplitude (see Figure 66), energy W_{S1} and W_{S2} can be given by

$$W_{S1}^* = \frac{1}{2} k_1 u_1^{*2} \tag{158}$$

$$W_{S2}^* = \frac{1}{2} k_2 u_2^{*2} \tag{159}$$

Total energy by spring force is

$$W_S = W_{S1}^* + W_{S2}^* = \frac{1}{2}\left(k_1 u_1^{*2} + k_1 u_2^{*2}\right)$$

$$= 2W_{S4} = k_f u_K{}^2 \tag{160}$$

If $k_f = \frac{k_1 + k_2}{2}$ is assumed, then

133
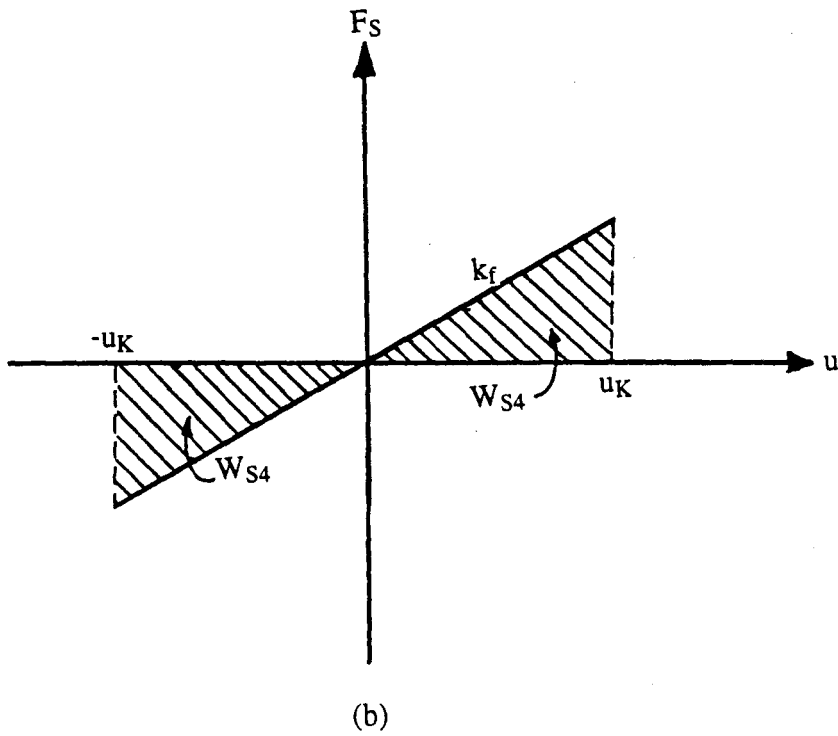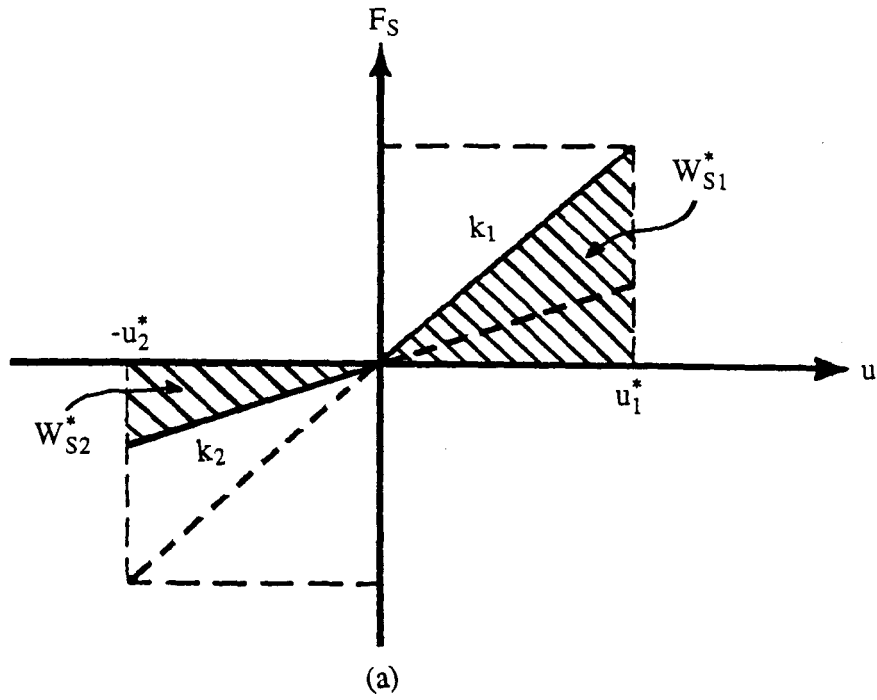
Figure 66 Equivalent spring force vs. displacement relationship

$$\tfrac{1}{2}(k_1 + k_2)u_K{}^2 = \tfrac{1}{2}\left(k_1 u_1{}^{*2} + k_1 u_2{}^{*2}\right) \tag{161}$$

$$u_K{}^2 = \frac{k_1 u_1{}^{*2} + k_2 u_2{}^{*2}}{k_1 + k_2} \tag{162}$$

By using Equation (146) (corresponding W_{S1} shown in Figure 60) and substituting W_{S4} into W_{S1}, equivalent damping ratio for irregular load-displacement can thus be obtained as

$$\begin{aligned}
\xi_{eg} &= \frac{W_D}{4\pi W_{S1}} \cdot \frac{u_K{}^2}{u_D{}^2} \\[2em]
&= \frac{W_D}{4\pi W_{S4}} \cdot \frac{\dfrac{k_1 u_1{}^{*2} + k_2 u_2{}^{*2}}{k_1 + k_2}}{\dfrac{1}{2}u_1{}^{*2} + \dfrac{1}{2}u_2{}^{*2}} \\[2em]
&= \frac{2W_D}{4\pi W_{S4}}\left[\frac{k_1}{k_1 + k_2}\,\frac{u_1{}^{*2}}{u_1{}^{*2} + u_2{}^{*2}} + \frac{k_2}{k_1 + k_2} \cdot \frac{u_2{}^{*2}}{u_1{}^{*2} + u_2{}^{*2}}\right] \tag{163}
\end{aligned}$$

Rewrite Eqs. (158) and (159) as

$$k_1 = \frac{2W_{S1}^*}{u_1^{*2}} \;;\; k_2 = \frac{2W_{S2}^*}{u_2^{*2}} \tag{164}$$

Then

$$\frac{k_1}{k_1 + k_2} = \frac{\dfrac{2W_{S1}^*}{u_1^{*2}}}{\dfrac{2W_{S1}^*}{u_1^{*2}} + \dfrac{2W_{S2}^*}{u_2^{*2}}} = \frac{\dfrac{2W_{S1}^*}{\tfrac{1}{2}c_{eg}\Omega u_1^{*2}}}{\dfrac{2W_{S1}^*}{\tfrac{1}{2}c_{eg}\Omega u_1^{*2}} + \dfrac{2W_{S2}^*}{\tfrac{1}{2}c_{eg}\Omega u_2^{*2}}}$$

$$= \cfrac{\cfrac{W_{S1}^*}{W_{D1}^*}}{\cfrac{W_{S1}^*}{W_{D1}^*} + \cfrac{W_{S2}^*}{W_{D2}^*}} \tag{165}$$

Since $c\Omega = \eta_1 k_1$ and $c\Omega = \eta_2 k_2$ are assumed

$$\frac{W_{S1}^*}{W_{D1}^*} = \frac{\frac{1}{2}k_1 u_1^{*2}}{\frac{1}{2}c_{eg}\pi\Omega u_1^{*2}} = \frac{1}{\pi} \cdot \frac{k_1}{c_{eg}\Omega} = \frac{1}{\pi} \cdot \frac{1}{\eta_1} \tag{166}$$

In the same manner

$$\frac{W_{S2}^*}{W_{D2}^*} = \frac{1}{\pi\eta_2} \tag{167}$$

Equation (5.44) becomes

$$\frac{k_1}{k_1+k_2} = \cfrac{\cfrac{1}{\pi\eta_1}}{\cfrac{1}{\pi\eta_1} + \cfrac{1}{\pi\eta_2}} = \frac{\eta_2}{\eta_1+\eta_2} \tag{168}$$

Similarly

$$\frac{k_2}{k_1+k_2} = \frac{\eta_1}{\eta_1+\eta_2} \tag{169}$$

Furthermore

$$\frac{u_1^{*2}}{u_1^{*2}+u_2^{*2}} = \frac{\frac{1}{2}c_{eg}\Omega\pi u_1^{*2}}{\frac{1}{2}\pi c_{eg}\Omega\left(u_1^{*2}+u_2^{*2}\right)} = \frac{W_{D1}^*}{W_{D1}^*+W_{D2}^*} = \frac{W_{D1}^*}{W_D} \tag{170}$$

and

$$\frac{u_2^{*2}}{u_1^{*2}+u_2^{*2}} = \frac{W_{D2}^*}{W_{D1}^*+W_{D2}^*} = \frac{W_{D2}^*}{W_D} \qquad (171)$$

Using Eqs. (166) through (171) in Eq. (163), equivalent damping ratio ξ_{eg} thus reduces to

$$\xi_{eg} = \frac{W_D}{2\pi W_{S4}} \cdot \left[\frac{\eta_2}{\eta_1+\eta_2} \cdot \frac{W_{D1}^*}{W_D} + \frac{\eta_1}{\eta_1+\eta_2} \cdot \frac{W_{D2}^*}{W_D} \right]$$

$$= \frac{1}{2\pi W_{S4}(\eta_1+\eta_2)} \left[\eta_2 W_{D1}^* + \eta_1 W_{D2}^* \right]$$

$$= \frac{1}{\pi\left(W_{S1}^*+W_{S2}^*\right)(\eta_1+\eta_2)} \left[\frac{W_{D2}^* W_{D1}^*}{\pi W_{S2}^*} + \frac{W_{D1}^* W_{D2}^*}{\pi W_{S1}^*} \right]$$

$$= \frac{1}{\pi^2(\eta_1+\eta_2)} \left(W_{D1}^* W_{D2}^*\right) \frac{1}{W_{S1}^*+W_{S2}^*} \left[\frac{1}{W_{S1}^*} + \frac{1}{W_{S2}^*} \right]$$

$$= \frac{1}{\pi^2(\eta_1+\eta_2)} \left(W_{D1}^* W_{D2}^*\right) \frac{1}{W_{S1}^*+W_{S2}^*} \left[\frac{W_{S1}^*+W_{S2}^*}{W_{S1}^* W_{S2}^*} \right]$$

$$= \frac{1}{\pi^2(\eta_1+\eta_2)} \frac{W_{D1}^* W_{D2}^*}{W_{S1}^* W_{S2}^*} = \frac{\pi^2 \eta_1 \eta_2}{\pi^2(\eta_1+\eta_2)} = \frac{\eta_1 \eta_2}{\eta_1+\eta_2} \qquad (172)$$

in which

$$\eta_1 = \frac{1}{\pi} \frac{W_{D1}^*}{W_{S1}^*} \ ; \eta_2 = \frac{1}{\pi} \frac{W_{D2}^*}{W_{S2}^*} \qquad (173)$$

as already given in Eqs. (166) and (167), and

$$0 \leq \eta_1, \eta_2 < 1/\pi \tag{174}$$

Substitution of Eq.(173) into Eq.(172), another form of equivalent damping ratio, ξ_{eg}, is

$$\xi_{eg} = \frac{1}{\pi^2(\eta_1+\eta_2)} \frac{W_{D1}^* W_{D2}^*}{W_{S1}^* W_{S2}^*}$$

$$= \frac{1}{\pi^2\left(\frac{1}{\pi}\frac{W_{D1}^*}{W_{S1}^*} + \frac{1}{\pi}\frac{W_{D2}^*}{W_{S2}^*}\right)} \frac{W_{D1}^* W_{D2}^*}{W_{S1}^* W_{S2}^*}$$

$$= \frac{1}{\pi} \frac{W_{D1}^* W_{D2}^*}{W_{S1}^* W_{D2}^* + W_{S2}^* W_{D1}^*} \tag{175}$$

For harmonic motion (see Figure 67(a)) damping ratio ξ (Eq. (153)) is

$$\xi = \frac{\eta}{2} \tag{176}$$

For near-harmonic motion (see Figure 67(b)), equivalent damping ratio is

$$\xi = \frac{1}{\pi} \frac{W_{D1}^* W_{D2}^*}{W_{S1}^* W_{D2}^* + W_{S2}^* W_{D1}^*} = \frac{\eta_1\eta_2}{\eta_1+\eta_2} \tag{177}$$

B. NUMERICAL OBSERVATION BASED ON EXPERIMENTAL RESULTS

Two perforated shear walls and one solid shear wall are represented in this section. SWO-4E and SWO-6E, the former, are described in Section II. SW5, the latter, is from Mertz's study [44]. All three walls are subjected to earthquake loading.

138
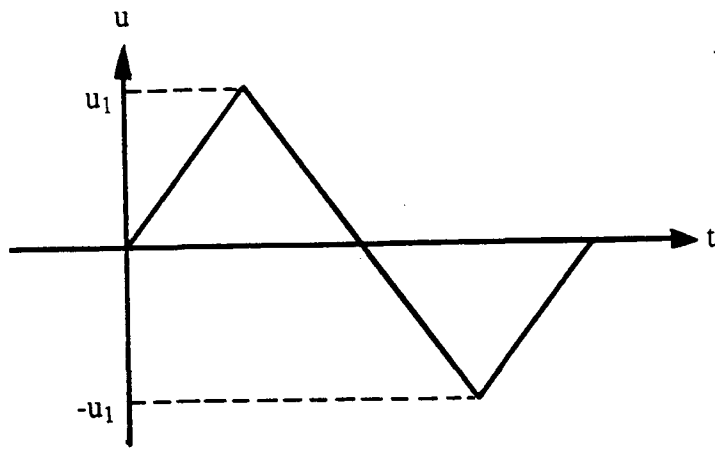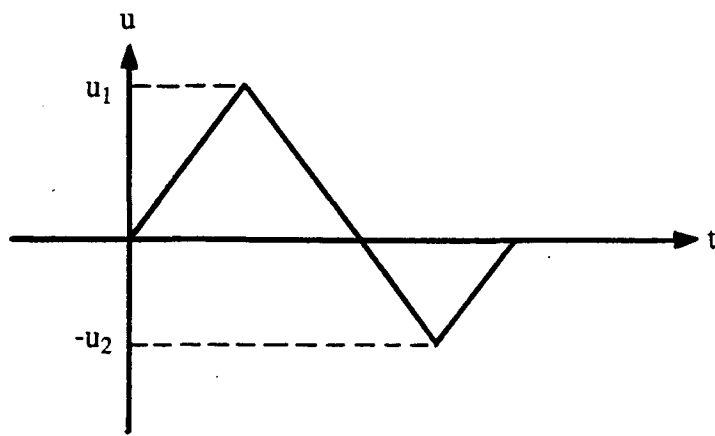
(a) Harmonic motion

(b) Near-harmonic motion

Figure 67 Harmonic motion and near-harmonic motion

Based on previous derivations, the amplitude(u), dissipated energy $\left(W_{D1}^* \text{ and } W_{D2}^* \right)$, energy of spring force $\left(W_{S1}^* \text{ and } W_{S2}^* \right)$ and corresponding damping ratio ξ for all cycles of the three shear walls are summarized in Tables XI, XII and XIII. From these tables, it can be seen that damping ratio generally increases with maximum amplitude(u), ductility, dissipated energy $\left(W_{D1}^* \text{ and } W_{D2}^* \right)$ and energy of spring force $\left(W_{S1}^* \text{ and } W_{S2}^* \right)$ in the NCKU shear wall experiments. Figure 68 further shows the relationship between damping ratio and ductility of shear walls while Figure 69 presents the definition of ductility μ as $\mu = \delta / \delta_y$. The trend of damping ratio is depicted in Figure 68. Bert [43] stated that there is no hysteresis damping unless displacement amplitude exceeds a certain threshold value. For RC shear walls, it can be assumed that there is no hysteretic damping before the cracking point. As shown in Figure 68, damping ratio gradually increases with maximum ductility of a shear wall. This ratio goes as high as 15.7%. Furthermore, it can be observed that the initial damping ratio for hysteretic damping is in the range of 5 to 6, a good agreement with practical design.

Table XI Summary of amplitude, dissipated energy, energy by spring, and damping ratio for all cycles of shear wall SWO-4E

D_{max}	0.268	0.938	2.68	3.819	5.527	13.668	7.437
Ductility	0.109	0.382	1.090	1.554	2.249	5.561	3.026
W_{D1}	0	2.207	19.868	28.86	45.70	54.9	80
W_{D2}	0	2.975	23.74	34.05	57.6	66.247	0.4
W_{S1}	0.5853	5.146	26.958	48.91	70.4	66.3	104.3
W_{S2}	0.3292	6.057	36.63	57.35	82	70.2	0.5
ξ	---	7.28	10.98	9.42	10.74	14.04	12.46

Table XII Summary of amplitude, dissipated energy, energy by spring, and damping ratio for all cycles of shear wall SWO-6E

D_{max}	1.306	2.680	3.517	4.355	8.274	17.65
Ductility	0.564	1.157	1.518	1.880	3.571	7.619
W_{D1}	2.396	21.00	27.97	34.76	83.8	123.3
W_{D2}	2.948	18.57	22.36	0.1	58.3	77.3
W_{S1}	8.507	28.356	50.59	60.86	111.6	125.4
W_{S2}	7.054	34.07	45.82	0.2	80.5	78.1
ξ (%)	5.36	9.99	8.25	8.49	11.73	15.70

Table XIII Summary of amplitude, dissipated energy, energy by spring, and damping ratio for all cycles of shear wall SW5

Dmax	0.0954	0.1010	0.1027	0.1027	0.1043	0.3629	0.3696	0.3742	0.3856	0.3856	0.3967
Ductility	0.0954	0.1010	0.1027	0.1027	0.1043	0.3629	0.3696	0.3742	0.3856	0.3856	0.3967
W_{D1}	0.01091	----	0.03547	0.0182	0.0182	1.2073	1.2073	1.065	1.115	1.159	1.249
W_{D2}	0.01848	----	0.01318	0.0207	0.0207	1.561	1.561	1.108	1.124	1.122	1.2
W_{S1}	0.2946	0.11541	0.33625	0.318	0.318	2.2653	2.6253	2.669	2.756	2.85	2.939
W_{S2}	0.30239	----	0.29928	0.3216	0.3216	3.16	3.16	2.706	2.748	2.741	2.9
ξ (%)	0.734	----	0.99	0.96	0.96	7.58	7.58	6.44	6.53	6.49	6.67

Dmax	0.7748	0.833	0.851	0.8586	0.8799	1.123	1.171	1.212	1.262	1.302
Ductility	0.7748	0.833	0.851	0.8586	0.8799	1.123	1.171	1.212	1.262	1.302
W_{D1}	4.15	3.67	3.47	3.68	3.75	6.24	6.02	6.39	6.85	7.29
W_{D2}	3.69	3.51	3.7	3.47	3.65	5.63	5.48	5.87	6.58	6.9
W_{S1}	8.63	8.64	8.58	8.77	9.1	13.73	13.94	14.42	15.08	15.59
W_{S2}	8.4	8.62	8.79	8.24	8.98	13.34	13.32	13.87	14.47	15.3
ξ (%)	7.31	6.62	6.57	6.69	6.51	6.97	6.71	6.89	7.23	7.31

142
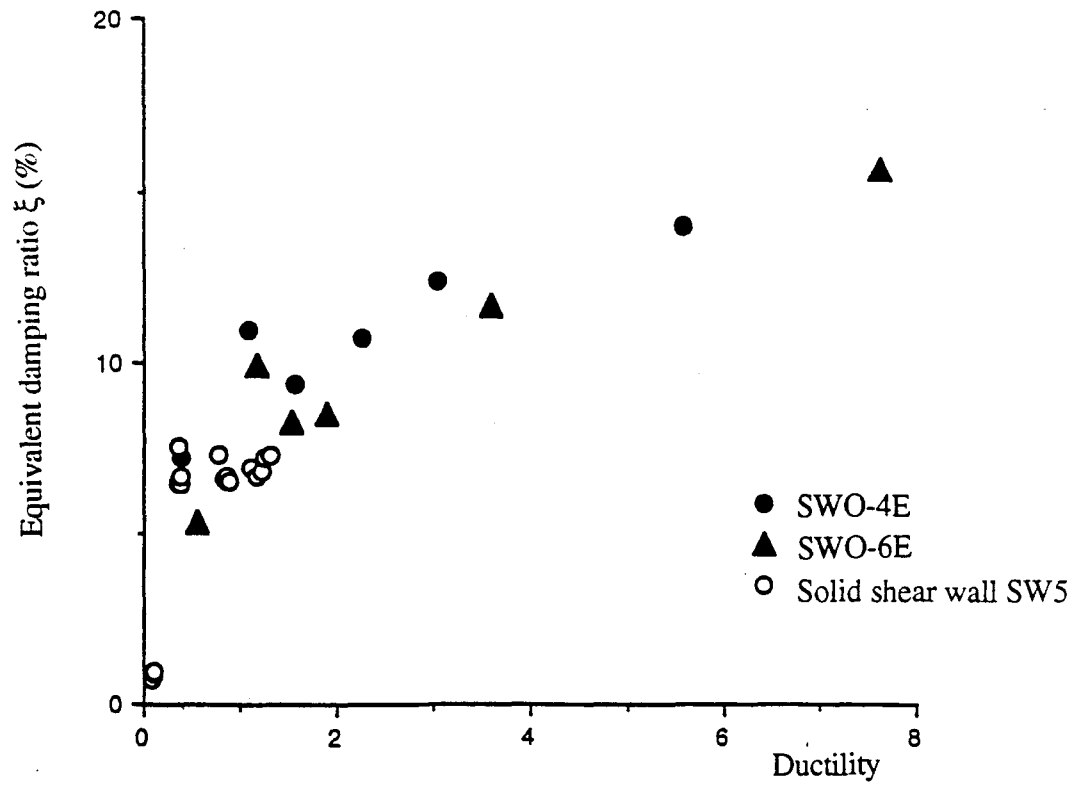
Figure 68 Relationship between damping ratio and ductility for shear wall
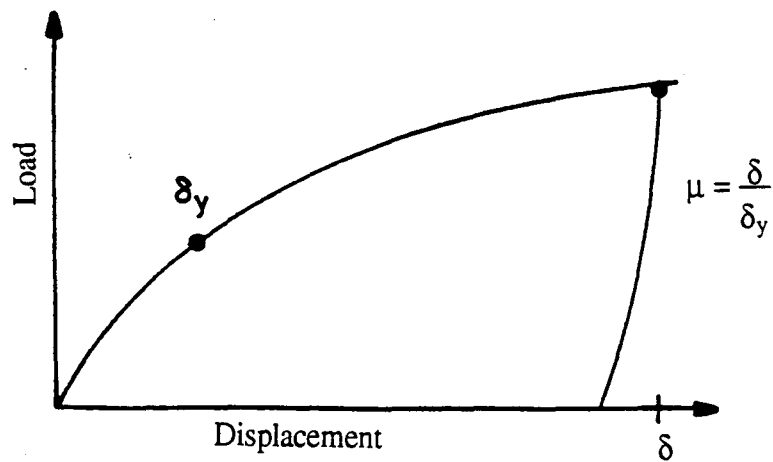
Figure 69 Displacement definition of ductility

VI. SOME OBSERVATIONS ON DESIGN PARAMETERS

When a structure is subjected to earthquake excitation, the system may deform into the inelastic range. Building codes use design parameters to include inelastic response in elastic design. Force reduction factor and displacement amplification factor are two key parameters. Response modification factor R is related to force reduction factor. It is used in the National Earthquake Hazards Reduction Program (NEHRP) recommended provisions [46] as is displacement amplification factor C_d . R_w is the force reduction factor used in Uniform Building Code (UBC) [47]. UBC code also uses the displacement amplification factor to compute an actual structure's drift. Force reduction factor, expressed as R or R_w, generally serves to reduce linear elastic design response spectra.

Story response on the critical story of a building is shown in Figure 70. Here the critical story exhibits stability vis-a-vis energy dissipation until it fails. Elastic response is also illustrated in Figure 70. For simplicity in obtaining design parameters, the actual response is idealized as a linearly elastic-perfectly plastic curve. On this idealized curve, the point where critical story enters the inelastic range is defined as yielding point which has load capacity, $(V_i)_f$, and associated yielding story drift, δ_y. Since load capacity encompasses the failure point (point D at the end of the plastic range on this response curve), load capacity $(V_i)_f$ at yielding strength refers to the structural collapse level. Maximum inelastic displacement at the end of the response curve refers to failure story drift which is maximum story drift, δ_{max}. Failure (or ultimate) load capacity, $(V_i)_f$, means the maximum ultimate base shear taken by the structure equals $(V_i)_f$.

For design purposes, actual maximum load level is reduced to the level where global structural response significantly initiates deviation from previous elastic response. First significant yield level is the usual term for this level. Prior to it, inelastic response is the same as elastic response. Being consistent with strength design approach for building codes, this level is adopted by NEHRP provisions. Base shear corresponding to this load

144
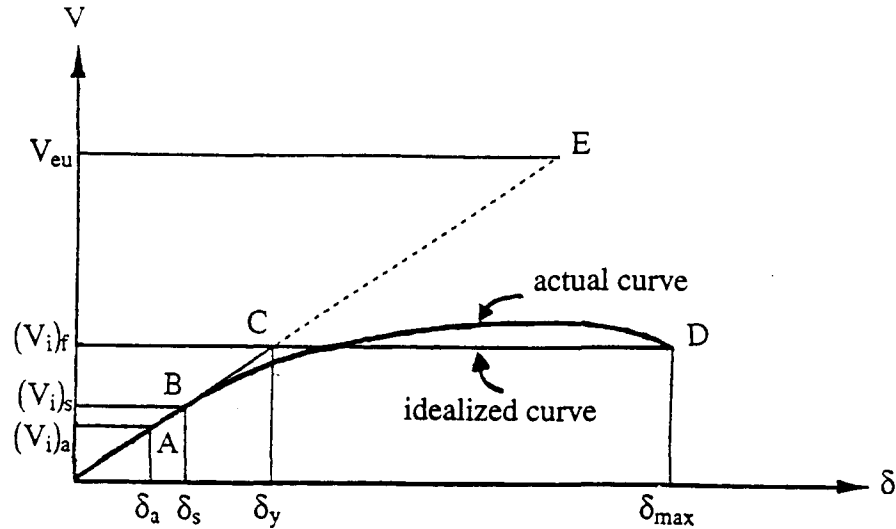
Figure 70 General story response of a structure

level is denoted as $(V_i)_s$ which has corresponding story drift, δ_s. UBC code further reduces this value from significant yield to serviceable load level. The latter is basically compatible with allowable (or working) stress design approach. Allowable base shear, $(V_i)_a$, represents this load level. Related allowable story drift is expressed as δ_a.

UBC design code has summarized formulae to estimate maximum design force based on extensive earthquake data with statistical analysis. When desirable seismic strength is determined and a simulated earthquake is applied to a structure, an elastic response is then obtained. Elastic response is shown in Figure 70, which has maximum elastic base shear, V_{eu}. UBC design code also provides a chart of normalized acceleration response spectrum. If the natural period of a structure is given, maximum design intensity can be applied. Here the idealized design response spectrum is called smooth linear elastic design response spectrum.

Based on Figure 70, some pertinent factors can be defined as follows.

(1) Ductility reduction factor, R_μ, represents the capacity to dissipate hysteretic energy by ductility characteristics of material. It is defined as

145

$$R_\mu = \frac{V_{eu}}{(V_i)_f} \tag{178}$$

(2) System ductility factor, μ_s, is based on the idealized linearly elastic-perfectly plastic curve. It is expressed as the ratio of maximum story drift to yield story drift and has the form of

$$\mu_s = \frac{\delta_{max}}{\delta_y} \tag{179}$$

The relationship between μ_s and R_μ was established for single degree-of-freedom by Newmark and Hall [48]. They stated that the ratio of R_μ/μ_s is smaller than or equal to 1.0.

(3) Overstrength factor, Ω, is the reserve load capacity existing between the actual structural collapse level and first significant yield level. If this range is larger, the overstrength factor increases. Larger overstrength factor offers more protection to structures subjected to seismic motion. This factor is expressed as

$$\Omega = \frac{(V_i)_f}{(V_i)_s} \tag{180}$$

(4) Load factor, Y, reflects the difference between strength design approach and allowable stress approach. This factor is 1.4 for reinforced concrete structures [49].

Formulations by Uang [50] elaborate on these factors and can be summarized as follows

(i) NEHRP force reduction factor (NEHRP called response modification factor)

$$R = R_\mu\Omega \tag{181}$$

(ii) UBC force reduction factor $R_w = R_\mu\Omega Y$ \hfill (182)

(iii) NEHRP displacement amplification factor $C_d = \dfrac{\delta_{max}}{\delta_s} = \mu_s \Omega$ (183)

(iv) $R/C_d = R_\mu/\mu_s$ (184)

where the ratio of R_μ to μ_s is equal to or smaller than 1.0 as cited earlier in Newmark and Hall's study [48].

These derivations as observed by Uang [50] illustrate that both force reduction factor R (or R_w) and displacement amplification factor C_d are functions of overstrength factor, system ductility factor, and damping (the effect of damping is involved in ductility reduction factor (R_μ)). Equations (181) through (183) show that the overstrength factor plays an important role in controlling structural response. An overstrength factor of 2.4~2.8 is observed in a six-story braced steel frame [45, 51].

Some researchers [45, 50, 51] note that the current UBC design procedure does not explicitly take the overstrength factor into account. This factor may be influenced by redundancy (internal stress redistribution), higher material strength, multiple loading conditions, strain hardening, and so forth. Also, displacement amplification factor/force reduction factor (DAF/FRF) ratio has a further advantage. Different design algorithms used in many countries make this ratio a more rational approach to the appropriate range for displacement amplification factor. Based on Uang's study [28], a DAF/FRF ratio of 1.0 is adequate for design purposes.

Some relationships discussed below shed light on the overstrength and related factors. The work herein attempts to explore a rational range for factors and their physical application.

A. RELATIONSHIP BETWEEN DUCTILITY REDUCTION FACTOR AND OVERSTRENGTH FACTOR

Recall Eq. (182)

$$R_w = R_\mu \Omega Y$$

It can be rewritten as

$$R_\mu = \left(\frac{R_w}{Y}\right)\frac{1}{\Omega} = \left(\frac{R_w}{1.4}\right)\frac{1}{\Omega} \tag{185}$$

where load factor, Y, is assumed to be 1.4 [50].

From Eq. (182), ductility reduction factor, R_μ, is inversely proportional to overstrength factor, Ω, if UBC-specified force reduction factor, R_w, is given. Figure 71 shows this relationship for some presumed UBC-specified force reduction factor of interest. Overstrength factor, Ω, is defined as the ratio of actual base shear at collapse level to NEHRP design base shear at first significant yield level, and actual base shear at collapse level should be greater than (or equal to) design base shear at first significant yield level. Thus the overstrength ratio, Ω, has a minimum value of 1.0. In the chart the overstrength factor of interest ranges from 1.0 to 2.5. UBC design force reduction factor, R_w, ranges from 2 to 15. It can be seen that ductility reduction factor becomes stable when overstrength factor is close to 2.5. Further observations from this chart appear in the next figure.

Turning to Figure 72(a), a reinforced concrete shear wall is examined. UBC-specified force reduction factor, R_w, is specified as 6 and overstrength factors, Ω, of 1.0, 1.5, 2.0, and 2.5 are selected. As shown in Figure 72(a), when overstrength factor is 1.0, ductility reduction factor is 4.28. Actual base shear at collapse level is the same as base shear at first significant yield level. There is no evidence of a gradual change in elastic

148
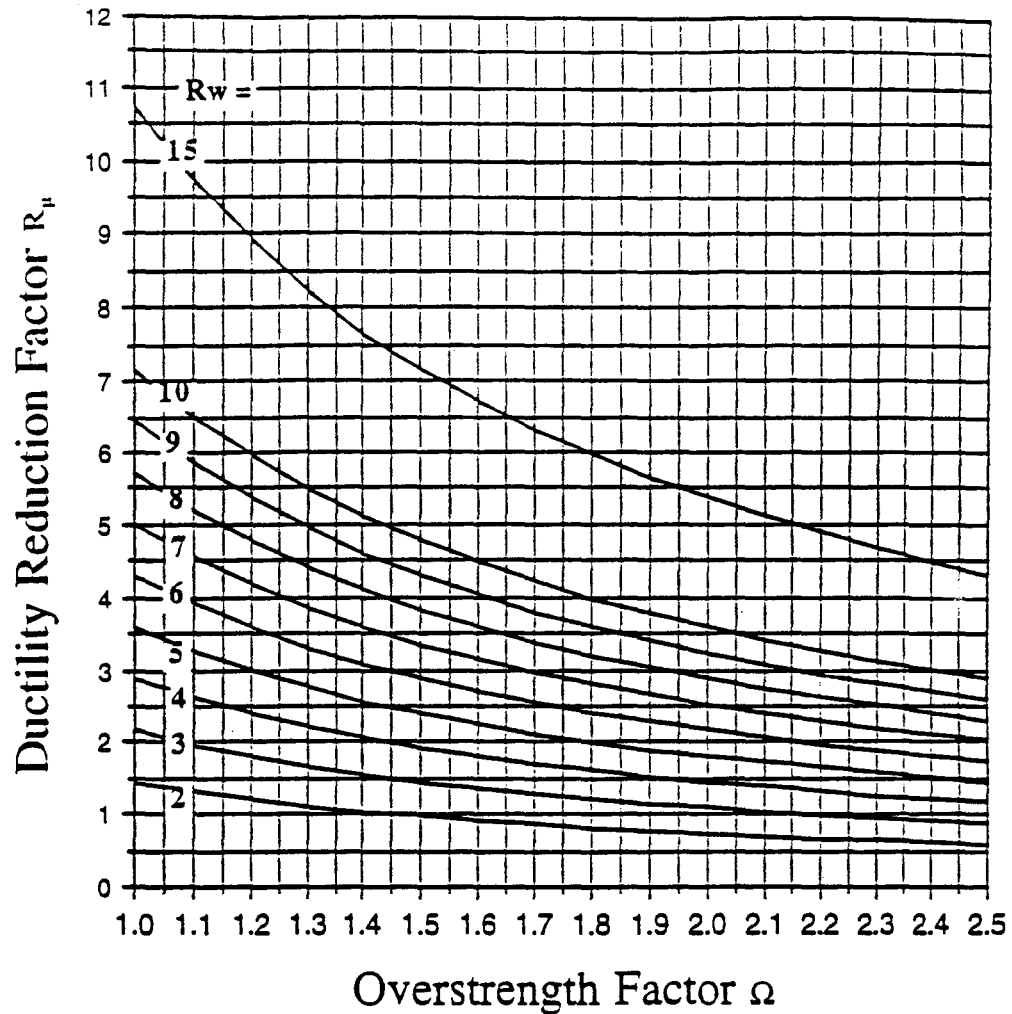
Figure 71 Relationship between ductility reduction factor and overstrength factor

range with inelastic range of higher ductility. The building's critical story displays a linearly elastic-perfectly plastic response. Ductility reduction factor (R_μ) does not appear to correlate with system ductility factor (μ_s). In Figure 72(a), the response of higher ductility remains unknown.

When the overstrength factor increases to 1.5, an obvious change in the load capacity of the structure's system can be observed. A gradual trend toward high inelasticity can be expected. In this case, a slight increment of overstrength factor at a low level can provide more load resistance for the structure against external excitation. When the
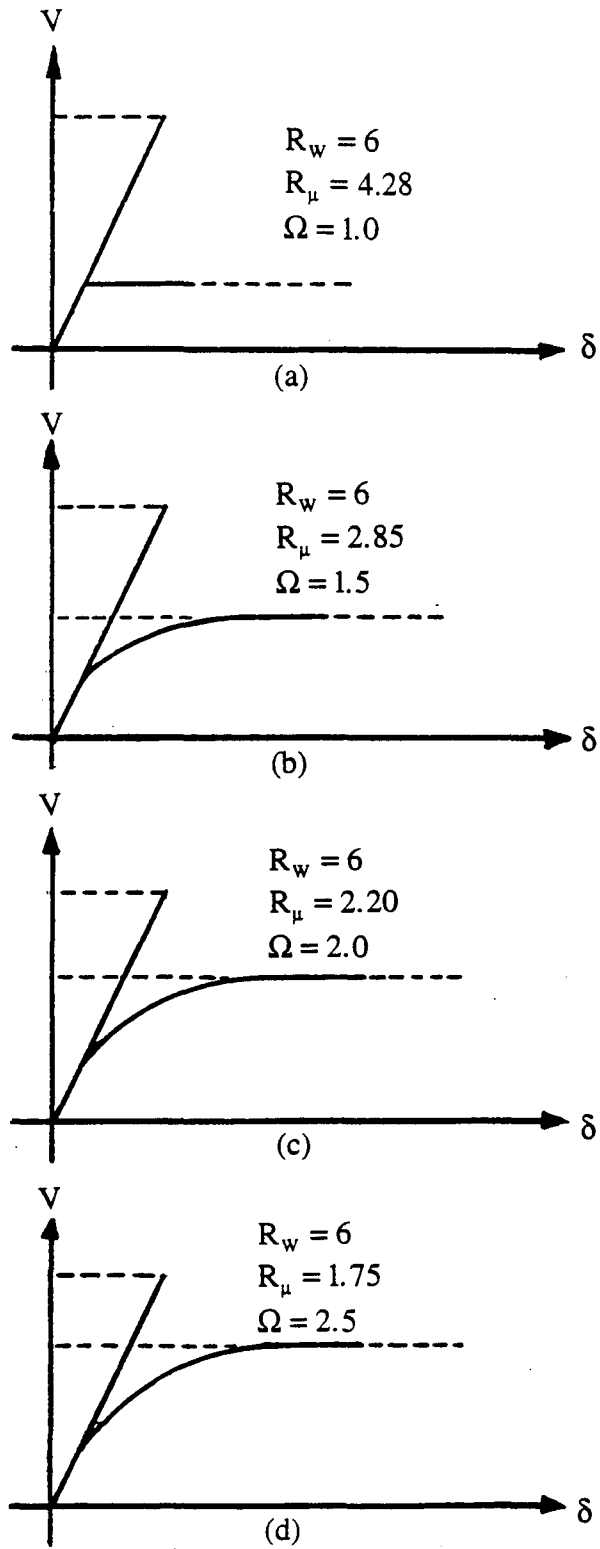
Figure 72 Structural response on critical story with respect to R_w of 6 for overstrength factor equal to (a) 1.0; (b) 1.5; (c) 2.0; (d) 2.5

overstrength factor goes up to 2.0, it provides more load capacity for the system but not as much as in the previous case. Similarly, when overstrength factor goes up to 2.5, load capacity of the structure increases to some extent. Generally, a higher overstrength factor can give enough reserve strength capacity for a structure to develop more material ductility and absorb more hysteretic energy. A higher overstrength factor also ensures that the structure can sustain higher base shear capacity.

Recall Eq. (185)

$$R_\mu = \left(\frac{R_w}{1.4}\right)\frac{1}{\Omega}$$

Overstrength factor is defined for the critical story. For a sound existing building or one under design, the overstrength factor can be approximately determined. The above formulation can be rewritten as

$$R_\mu = \left(\frac{1}{1.4\Omega}\right)R_w \tag{186}$$

or

$$R_\mu = C_1 R_w \tag{187}$$

where $C_1 = 1/(1.4\Omega)$ is constant.

Ductility reduction factor, R_μ, is defined in Eq. (178) as

$$R_\mu = \frac{V_{eu}}{(V_i)_f}$$

151

R_μ in the above formulation is strongly affected by the seismic intensity of an earthquake. From Equation (187)

$$R_w = \frac{R_\mu}{C_1} \qquad (188)$$

UBC-specified force reduction factor (R_w) is also influenced by seismic intensity.

Smoothed linear elastic design response spectrum, as mentioned earlier, is proposed by UBC design code. It is shown as curve SLEDRS in Figure 73. UBC provides the following formula for design force, based on allowable stress design approach

$$V = \frac{ZIC}{R_w}W \qquad (189)$$

where Z is seismic zone factor; I is importance factor; C is function of both site coefficient and structure's fundamental period; and W is active weight of the system. It is also shown as curve IDRS, which considers the nonlinear behavior of a system, in Figure 73. Here a general form of Eq. (189) is expressed as

$$V = \frac{ZIC}{R_g}W \qquad (190)$$

where R_g is a factor to assess base shear for a different design approach. It is noteworthy that if R_g is assumed to be unity, Eq. (190) becomes

$$V = (ZIC)W \qquad (191)$$

or
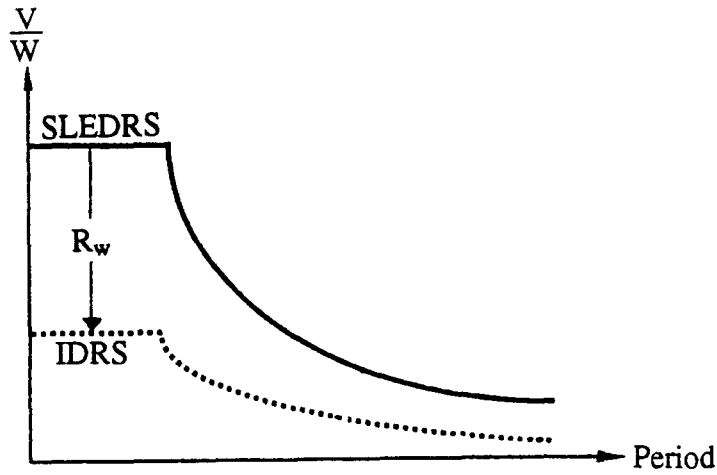
Figure 73   Schematic diagram of design response spectrum

$$\frac{V}{W} = ZIC \tag{192}$$

Equation (192) is physically the same as the maximum normalized design earthquake on the smoothed linear elastic design response spectrum (SLEDRS). If force reduction factor (R_g) is not considered in Eq. (190), this factor represents the elastic response which is identical to UBC's definition of SLEDRS curve. Eq. (192) can thus be expressed as

$$\frac{V_{eu}}{W} = \frac{V}{W} = (SLEDRS) \tag{193}$$

where (SLEDRS) is maximum intensity of normalized design earthquake for elastic analysis in accordance with the natural frequency of the structure's system.

Now Eq. (193) can be reformulated as

$$\frac{V_{eu}}{W} = (SLEDRS) = f_{eu} \tag{194}$$

where f_{eu} is constant.

If the most severe earthquake is chosen, f_{eu} becomes

$$f_{eu} = ZIC = 1.1 \qquad (195)$$

where $Z = 0.4$; $I = 1.0$; $C = 2.75$.

From Eqs. (194) and (195), maximum V_{eu} is obtained as $V_{eu} = f_{eu}W = 1.1W$ and $V_{eu} = f_{eu}W$. Ductility reduction factor then becomes

$$R_{\mu} \leq \frac{f_{eu} \cdot W}{(V_i)_f} = \frac{1.1W}{(V_i)_f} \qquad (196)$$

If a smaller seismic region is considered, and $f_{eus} = ZIC$ is defined for $Z \leq 0.4$, ductility reduction factor becomes

$$R_{\mu} = \frac{f_{eus} \cdot W}{(V_i)_f} \qquad (197)$$

B. RELATIONSHIP BETWEEN MAXIMUM BASE SHEAR RATIO AND OVERSTRENGTH FACTOR

Comparing Eq. (186) with (178), it yields

$$R_{\mu} = \frac{V_{eu}}{(V_i)_f} = \left(\frac{R_w}{1.4}\right)\frac{1}{\Omega} \qquad (198)$$

Maximum elastic base shear can be derived from Eq. (198) as

$$V_{eu} = \left(\frac{(V_i)_f R_w}{1.4}\right)\frac{1}{\Omega} = \left(\frac{(V_i)_f}{\Omega}\right)\left(\frac{R_w}{1.4}\right) \qquad (199)$$

154

For the most severe earthquake, V_{eu} equals 1.1 W (i.e., $f_{eu} = 1.1$) (see Eqs. (194) and (195)) and is the maximum elastic base shear. Eq. (199) then becomes

$$V_{eu} = \left(\frac{(V_i)_f}{\Omega}\right)\left(\frac{R_w}{1.4}\right) \leq 1.1W \qquad (200)$$

Equation (200) can be rewritten as

$$\left(\frac{R_w}{1.4}\right)\frac{1}{\Omega} \leq 1.1\frac{W}{(V_i)_f} \qquad (201)$$

or

$$\frac{W}{(V_i)_f} \geq \left(\frac{R_w}{1.54}\right)\frac{1}{\Omega} \qquad (202)$$

and further $(V_i)_f$ is normalized and defined as

$$\frac{(V_i)_f}{W} = C_f \qquad (203)$$

where C_f is called failure (or collapse) base shear ratio. From Eq.(199), $(V_i)_f = \frac{(1.4)\,V_{eu}}{R_w}\Omega$

$$= \frac{(1.4)\,ZICW}{R_w}\Omega.$$

Then C_f becomes

$$C_f = \frac{1.4ZIC}{R_w}\Omega \qquad (204)$$

$$= \frac{1.4f_{eu}}{R_w}\Omega \qquad (205)$$

Furthermore, Eq. (203) then reduces to

$$C_f \leq \left(\frac{1.54}{R_w}\right)\Omega \qquad\qquad (206)$$

For the most severe earthquake (i.e., Z = 0.4; I = 1.0; C = 2.75)

$$C_f = \left(\frac{1.54}{R_w}\right)\Omega \qquad\qquad (207)$$

Figure 74 shows relationship between C_f and Ω for some UBC-specified force reduction factors while Figure 75 is the same except Z = 0.3 (i.e., Z=0.3, I=1.0, C=2.75), C_f is written as

$$C_f = \frac{1.155}{R_w}\Omega \qquad\qquad (208)$$

If UBC-specified force reduction factor (R_w) is equal to 6.0 in Figure 74, then C_f will be less than or equal to 0.26, 0.51, and 0.64 for overstrength factors of 1.0, 2.0, and 2.5, respectively. In these cases, ductility reduction factor, R_μ (i.e., $= \frac{V_{eu}}{(V_i)_f} = \frac{1.1W}{C_f W} = \frac{1.1}{C_f}$ $= \frac{f_{eu}}{C_f}$), is less than 4.23, 2.16, and 1.72, respectively. For an overstrength factor of 2.5 with Z=0.4, C_f is 0.64. From Eq. (203), base shear for a structure's system is

$$(V_i)_f = C_f W = 0.64W \qquad\qquad (209)$$

In Eq. (209) the total base shear resisted by the structure's system at collapse level is 64 percent of structural active weight.

Also, Figure 74 is based on severe seismic situation with $f_{eu} = 1.1$ for a short period. For a structure's system with a long period, point A in Figure 76 illustrates design base shear ratio $(f_{eu})_a$. From Eq. (205), C_f is $\frac{1.4(f_{eu})_a}{R_w}\Omega$. In Figure 74 C_f is $\frac{1.4f_{eu}}{R_w}\Omega$ and
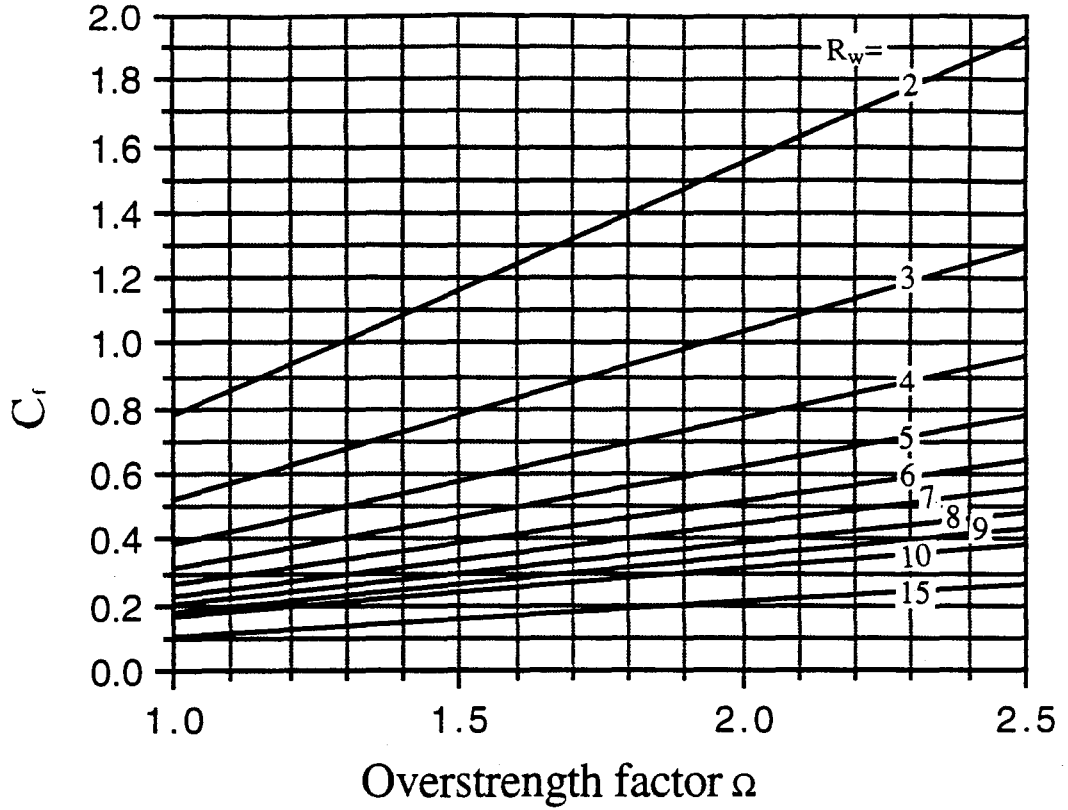
Figure 74 Relationship between failure base shear ratio and overstrength factor for severe earthquake with Z=0.4

f_{eu} equals 1.1. If Figure 74 is applied to the structure's system with a long fundamental period (let $C_{f_1}=\dfrac{1.4(f_{eu})_a}{R_w}\Omega$), then C_{f_1} in relation to C_f becomes

$$C_{f_1}=\frac{1.4(f_{eu})_a}{R_w}\Omega=\frac{1.4f_{eu}}{R_w}\Omega\left(\frac{(f_{eu})_a}{f_{eu}}\right)=C_f\frac{(f_{eu})_a}{1.1} \qquad (210)$$

It means that with the chart in Figure 74 failure base shear $(V_i)_f$ is

$$(V_i)_f=C_f\frac{(f_{eu})_a}{1.1}W \qquad (211)$$

where C_f is obtained from Figure 74.
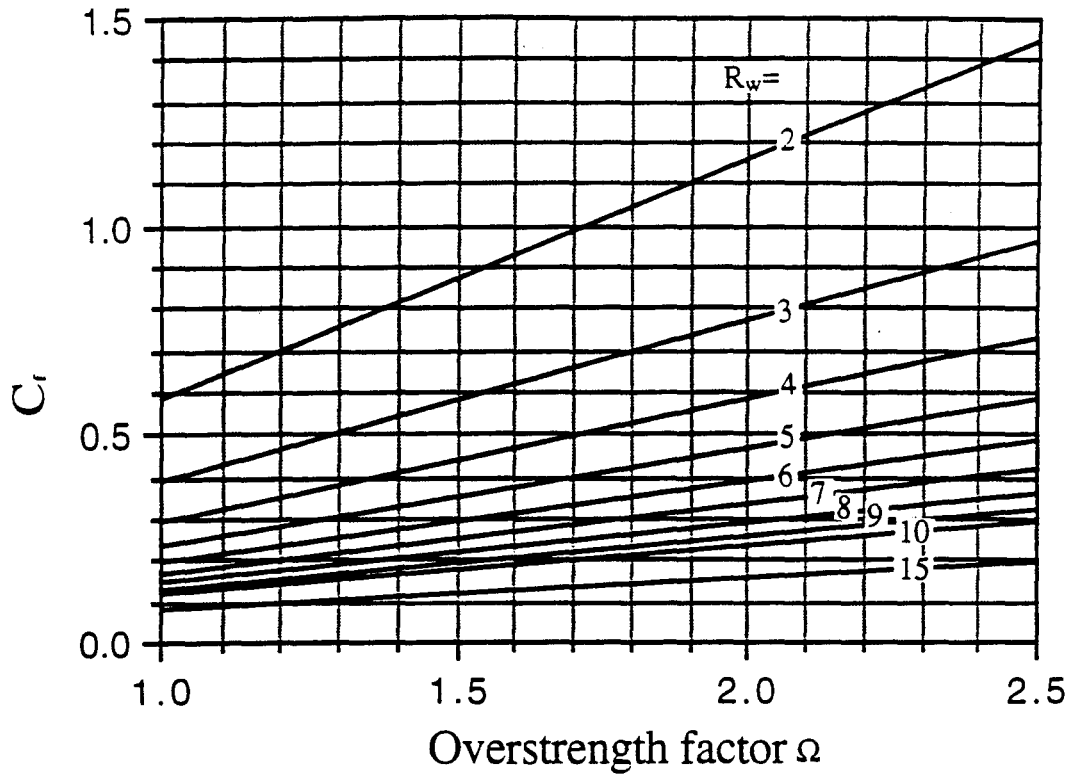
Figure 75 Relationship between failure base shear ratio and overstrength factor for earthquake with Z=0.3

C. RELATIONSHIP BETWEEN DAF/FRF RATIO AND OVERSTRENGTH FACTOR

DAF/FRF ratio is defined as the ratio of displacement amplification factor (DAF) to force reduction factor (FRF) for a structure subjected to external excitation. In Figure 77(a), (b), and (c) the relationship between DAF/FRF and overstrength factor for system ductility factor, μ_s, equals 1.5, 2.0, and 2.5, respectively. Comparison and derivation in this section use NEHRP recommended provisions.
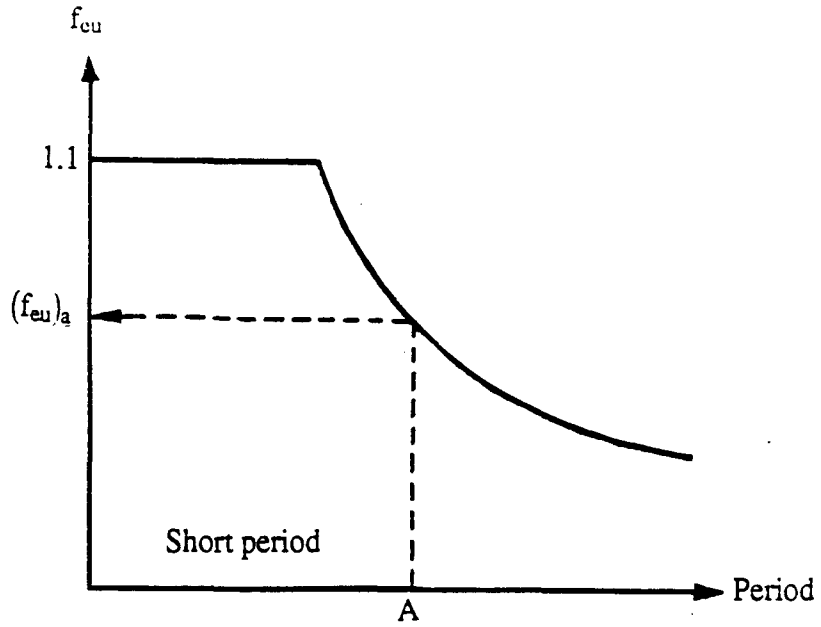
Figure 76 Design base shear ratio for structure within long period

(a) $\Omega = 1.5$
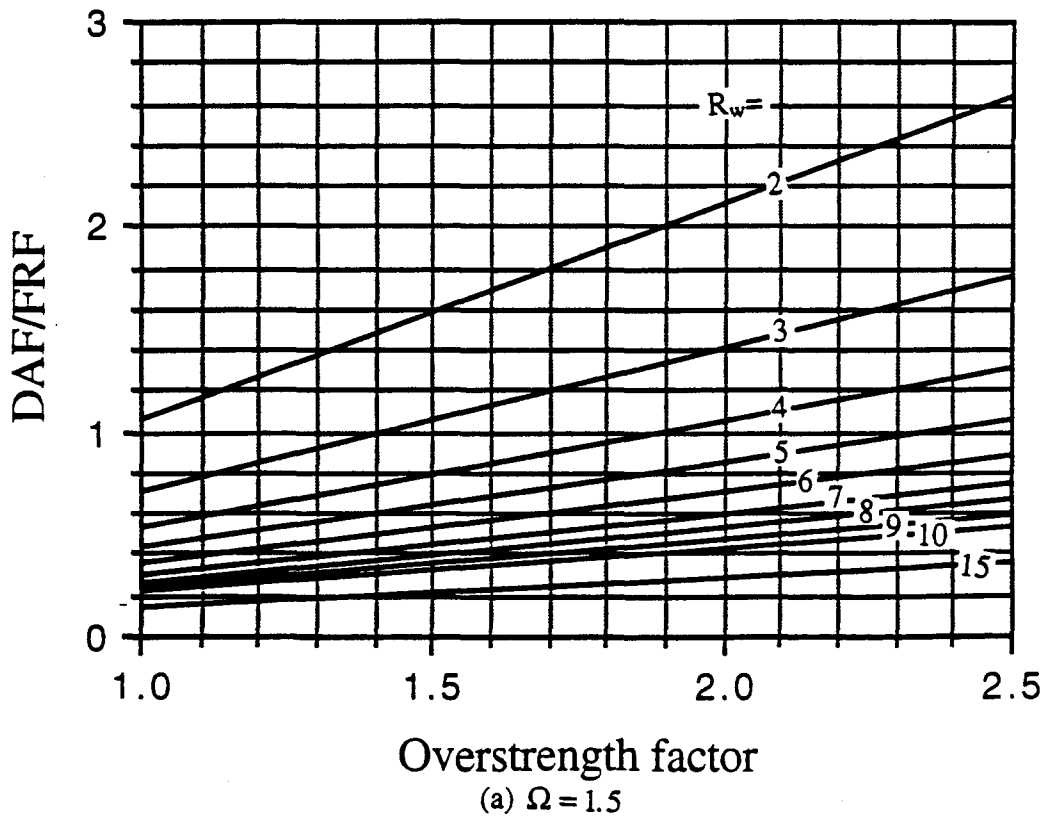
Figure 77 Relationship between DAF/FRF ratio with overstrength factor for system
ductility factor equal to (a) 1.5; (b) 2.0; (c) 2.5
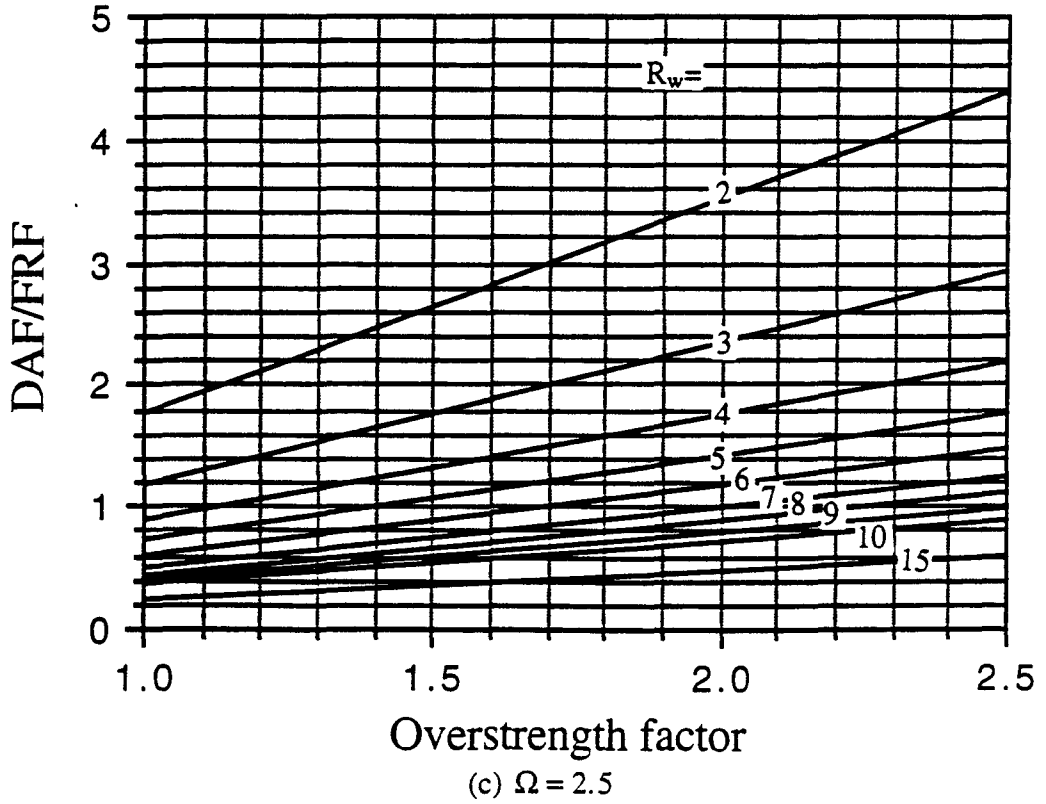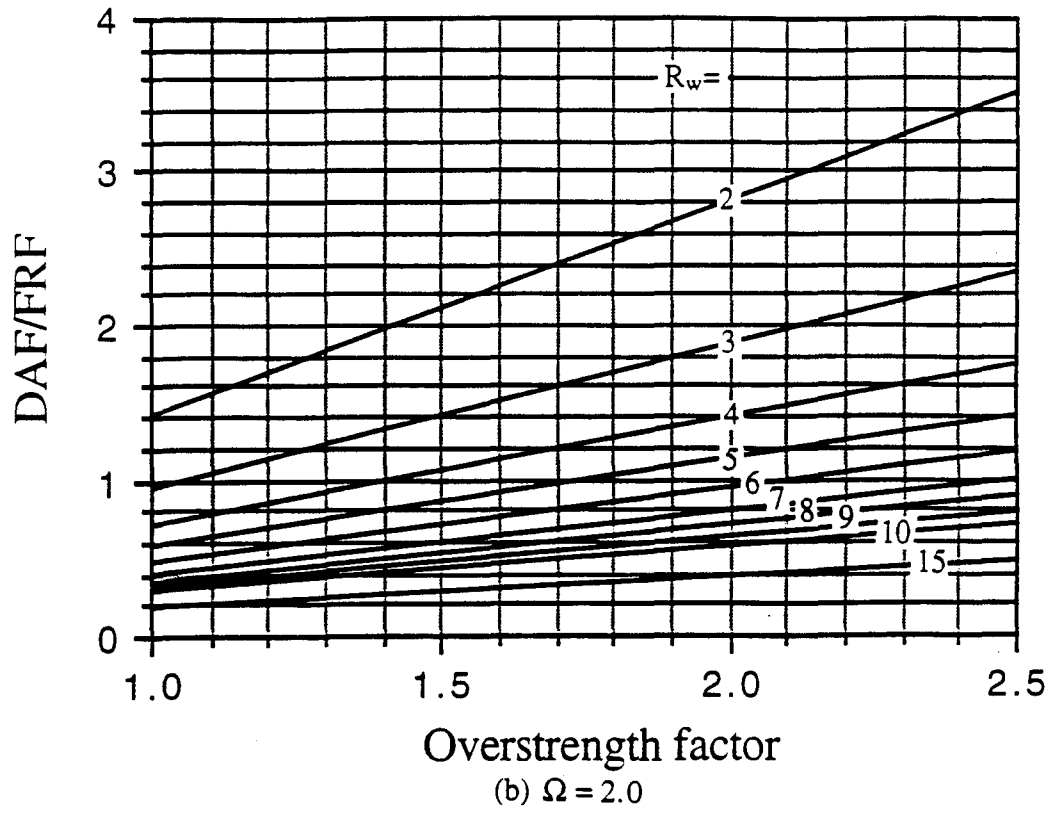
Figure 77 (continued) Relationship between DAF/FRF ratio with overstrength factor for system ductility factor equal to (a) 1.5; (b) 2.0; (c) 2.5

As stated before, NEHRP defines force reduction factor, FRF, as

$$FRF = R \tag{212}$$

Since all comparisons in this section use UBC-specified force reduction factor, R_w, R is expressed in terms of R_w, which is written as

$$R = R_w Y \tag{213}$$

Also, NEHRP defines displacement amplification factor, DAF, as

$$DAF = C_d \tag{214}$$

Substitution of Eq. (183) into Eq. (214) reduces this factor to

$$DAF = \mu_s \Omega \tag{215}$$

DAF/FRF ratio thus becomes

$$\frac{DAF}{FRF} = \frac{C_d}{R} = \left(\frac{\mu_s Y}{R_w}\right)\Omega \tag{216}$$

For structure ductility factor, μ_s, of 1.5, 2.0, and 2.5, and Y=1.4, $\frac{DAF}{FRF}$ equals $\left(\frac{2.1}{R_w}\right)\Omega$, $\left(\frac{2.8}{R_w}\right)\Omega$, and $\left(\frac{3.5}{R_w}\right)\Omega$, respectively.

From Figure 77(a), if UBC-specified force reduction factor (R_w) is 6.0, then DAF/FRF is less than 1.0. For μ_s of 2.0 and 2.5, (R_w) of 6.0 has a DAF/FRF ratio greater than 1.0 when the overstrength factor is close to 2.5. To obtain a minimum value of 1.0

for DAF/FRF ratio, as recommended by Uang [28], requires a lower force reduction factor (R_w or R), higher system ductility factor (μ_s), and higher overstrength factor (Ω).

From above discussion, relationships between maximum base shear ratio and overstrength factor as well as between DAF/FRF ratio and overstrength factor provide the following information:

i) if ranges of reduction factor and overstrength factor are known from analysis, the maximum base shear of a structure's system can be predicted from Eqs. (204) and (209).

ii) if force reduction factor and maximum base shear are estimated, overstrength factor for a structure's system can also be found from Eqs. (204) and (209).

Some correlations between the above factors are obvious in the structure's system. Later these correlations are checked with results for the RC shear-wall buildings which were analyzed by both monotonic and dynamic loading cases.

VII. ANALYTICAL FORMULATION FOR PERFORATED SHEAR WALL ELEMENT MODEL

Matrix formulation for analyzing 3-D structural systems is established and coded in the computer program, INRESB-3D-SUP, developed at UMR. This program can analyze elastic and inelastic building systems subjected to static loading, multi-component earthquake motion, and pseudo-static cyclic loading. It is also capable of calculating elastic natural frequency and buckling load [52-58].

Among major features of reinforced concrete and steel members of plane and 3-D buildings are elastic, inelastic, dynamic and stability analysis as well as various hysteresis rules of elasto-plastic, bilinear, Ramberg-Osgood, Takeda, and Cheng-Mertz. Other attributes of this computer program are listed as follows [29, 59,60]:

1) joint based degrees of freedom

2) rigid body and planar constraints

3) incremental nonlinear static solution

4) unbalanced load correction for overshooting

5) incremental nonlinear dynamic solution

6) mass and stiffness proportional damping

7) condensation to reduce size of dynamic problem

8) damage index

9) energy balance

10) ductility and excursion ratio for various definitions of displacement, constant strain energy, and variable strain energy

The RC perforated shear wall element consists of a panel with a joint at each corner. As shown in Figure 78, nonlinear equivalent shear spring and nonlinear axial spring account for nonlinear total lateral displacement and nonlinear axial displacement, respectively. Lumped nonlinear springs connect two bodies with two corner joints for each

163
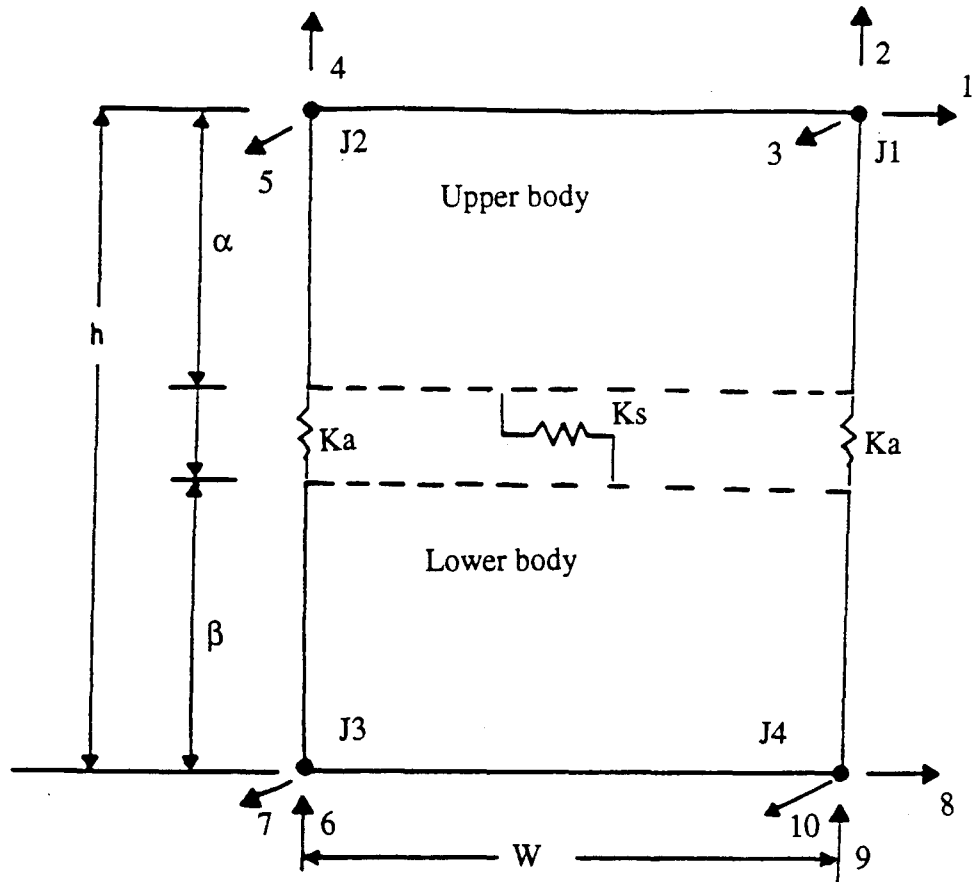
Figure 78 Perforated shear wall element model

body. Joints J1 and J2 are on the top corners of the upper body which has a height of α.

Joint J3 and J4 are on the bottom corners of the lower body which has a height of β. Total

height of the wall is the sum of the respective heights and can be written as

$$L = \alpha + \beta \tag{217}$$

Out of plane (i.e., perpendicular to the plane of the wall) stiffness is not considered. A

lumped parameter formulation of geometric stiffness with consideration of both in-plane

and out-of-plane P-Δ effect was also developed.

A. <u>ELEMENT COORDINATE SYSTEM AND DEGREES OF FREEDOM</u>

As shown in Figure 78, the perforated shear wall element has ten transitional degrees of freedom. Degrees of freedom 1 and 8 represent in-plane total lateral deformation. Note that total lateral deformation is the sum of shear deformation and flexural deformation with consideration of shear and bending effects. Degrees of freedom 2, 4, 6, and 9 represent axial deformation. In matrix form, these local forces and displacements in the element's coordinate system (ECS) are

$$[F_e] = [F_1 \ F_2 \ F_3 \ F_4 \ F_5 \ F_6 \ F_7 \ F_8 \ F_9 \ F_{10}]^T \tag{218}$$

$$[\Delta_e] = [\Delta_1 \ \Delta_2 \ \Delta_3 \ \Delta_4 \ \Delta_5 \ \Delta_6 \ \Delta_7 \ \Delta_8 \ \Delta_9 \ \Delta_{10}]^T \tag{219}$$

Figure 79 shows a perforated shear wall coordinate system. In this system, global coordinates for all four joints, J1, J2, J3, and J4, are denoted as (X_{g1}, Y_{g1}, Z_{g1}), (X_{g2}, Y_{g2}, Z_{g2}), (X_{g3}, Y_{g3}, Z_{g3}), (X_{g4}, Y_{g4}, Z_{g4}), respectively. Vectors $\vec{X_t}$ and $\vec{X_b}$ stand for orientation in the X direction from joint J2 to J1 and from joint J3 to J4 at the top and bottom of the wall expressed as

$$\vec{X_t} = (X_{g1}-X_{g2})\vec{i} + (Y_{g1}-Y_{g2})\vec{j} + (Z_{g1}-Z_{g2})\vec{k} \tag{220}$$

$$\vec{X_b} = (X_{g4}-X_{g3})\vec{i} + (Y_{g4}-Y_{g3})\vec{j} + (Z_{g4}-Z_{g3})\vec{k} \tag{221}$$

A vector $\vec{V_y}$, assumed along the mid-width of the wall in the longitudinal axis of the wall, is defined as

$$\vec{V_y} = \left[\frac{X_{g1}+X_{g2}}{2} - \frac{X_{g3}+X_{g4}}{2}\right]\vec{i} + \left[\frac{Y_{g1}+Y_{g2}}{2} - \frac{Y_{g3}+Y_{g4}}{2}\right]\vec{j} + \left[\frac{Z_{g1}+Z_{g2}}{2} - \frac{Z_{g3}+Z_{g4}}{2}\right]\vec{k} \tag{222}$$
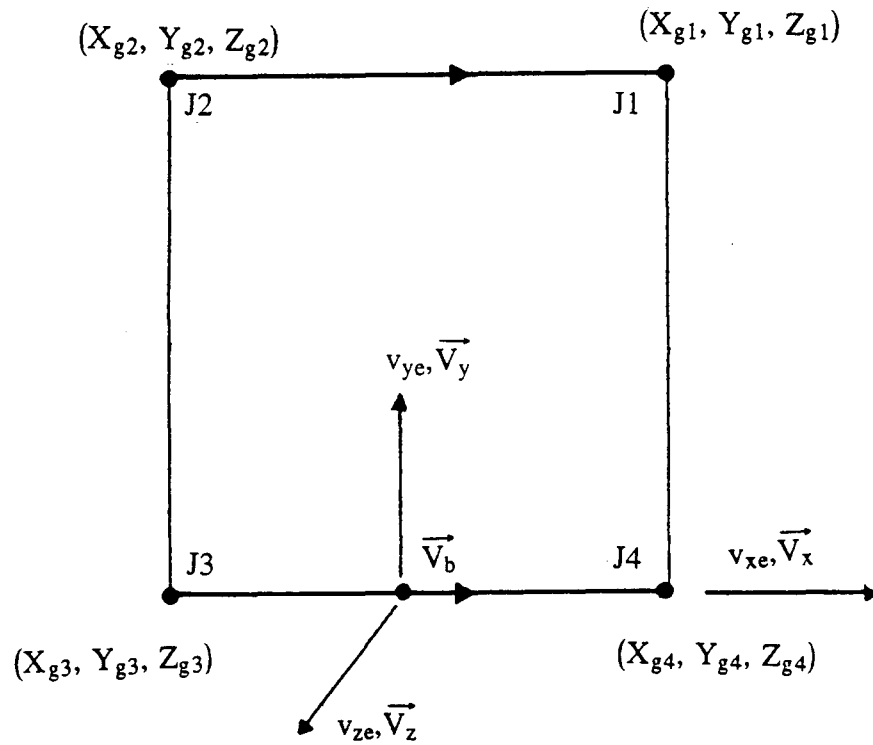
Figure 79   Perforated shear wall coordinate system

Vector $\overrightarrow{V_y}$ is oriented from mid-width at the bottom of the wall to mid-width at the top of the wall. Thus the span of vector $\overrightarrow{V_y}$ is the height of the wall, formulated as

$$L = \left|\overrightarrow{V_y}\right| \qquad\qquad (223)$$

Normalized $\overrightarrow{V_y}$ becomes

$$\overrightarrow{v_y} = \frac{\overrightarrow{V_y}}{L} \qquad\qquad (224)$$

where normalized $\overrightarrow{V_y}$ is a unit vector along the horizontal axis of the wall.

Vector $\overrightarrow{V_z}$, perpendicular to the wall, is defined as

$$\vec{V_z} = \vec{V_b} \times \vec{v_y} \qquad (225)$$

Unit vector $\vec{v_z}$ calculated by normalized $\vec{V_z}$ can be expressed as

$$\vec{v_z} = \frac{\vec{V_z}}{\left|\vec{V_z}\right|} \qquad (226)$$

where $\left|\vec{V_z}\right|$ is the length of vector $\vec{V_z}$.

Unit vectors $\vec{v_y}$ and $\vec{v_z}$ are established above. Unit vector $\vec{v_x}$, perpendicular to both unit vectors $\vec{v_y}$ and $\vec{v_z}$, yields

$$\vec{v_x} = \vec{v_y} \times \vec{v_z} \qquad (227)$$

Unit vectors $\vec{v_x}$, $\vec{v_y}$, and $\vec{v_z}$ form the basis of the element's coordinate system (ECS). This system with origin midway between joints J3 and J4 has three scalars denoted by v_{xe}, v_{ye}, v_{ze}. The three unit vectors that define ECS orientation are expressed in matrix form as

$$[\vec{v_e}] = \begin{bmatrix} \vec{v_x} \\ \vec{v_y} \\ \vec{v_z} \end{bmatrix} = \begin{bmatrix} c_{11} & c_{12} & c_{13} \\ c_{21} & c_{22} & c_{23} \\ c_{31} & c_{32} & c_{33} \end{bmatrix} \begin{bmatrix} \vec{i} \\ \vec{j} \\ \vec{k} \end{bmatrix} = [C_e] \begin{bmatrix} \vec{i} \\ \vec{j} \\ \vec{k} \end{bmatrix} \qquad (228)$$

where $[C_e]$ is the direction cosine matrix for the ECS.

B. ELEMENT STIFFNESS MATRIX IN THE ELEMENT COORDINATE SYSTEM

Stiffness derived here for perforated shear walls includes equivalent shear stiffness of the entire wall as well as axial stiffness of a unit height wall (in the computer program

noted earlier). Shear backbone curve and hysteresis model that determine shear stiffness are derived in terms of shear and shear displacement, but the axial hysteresis model is expressed as axial load vs. axial strain. The force deformation relationship for each of the springs is shown in Figure 80 and can be written as

$$V_a = K_s v_r = \frac{K_s}{L}(v_a - v_b) = -V_b \qquad (229)$$

and

$$P_a = K_a^* u_r = \frac{K_a^*}{L}(u_a - u_c) = -P_c \qquad (230)$$

$$P_b = K_a^* u_l = \frac{K_a^*}{L}(u_b - u_d) = -P_d \qquad (231)$$

where

$$K_a^* = \frac{K_a}{2} \qquad (232)$$

K_s is stiffness of the entire wall, shown in the shear hysteresis model in Section IV,

K_a^* is the axial stiffness on both the right and left sides of a unit height wall,

K_a is shown in the axial hysteresis model in Appendix B,

v_a, v_b are shear deformations at the top and bottom of the shear spring,

u_a, u_c are axial deformations at the top and bottom of the axial spring on the right side,

u_b, u_d are axial deformations at the top and bottom of the axial spring on the left side,

V_a, V_b are shears at the top and bottom of the shear spring,

P_a, P_b are axial forces at the top and bottom of the axial spring on the right side,
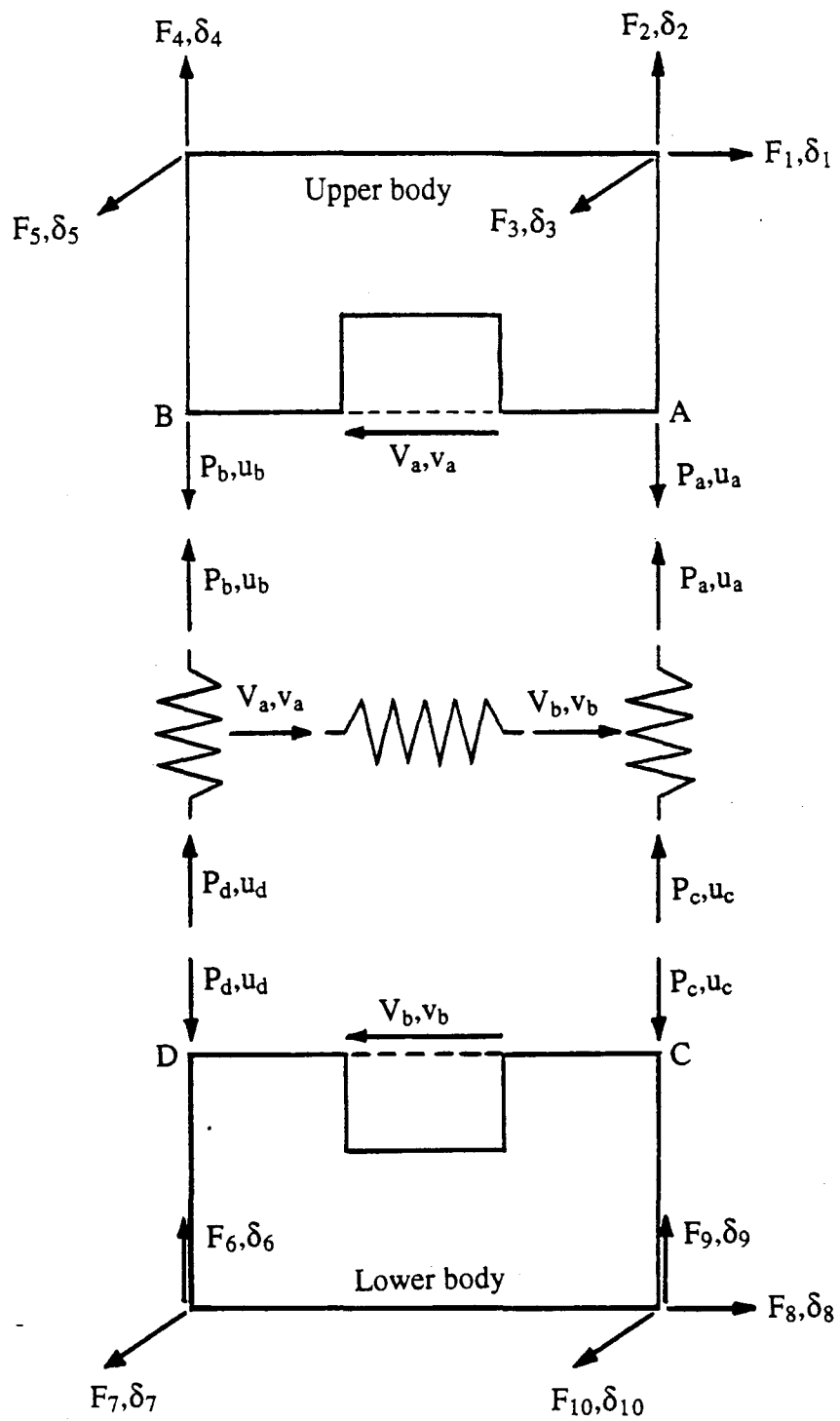
Figure 80 Shear wall forces and deformations

P_c, P_d are axial forces at the top and bottom of the axial spring on the left side,

v_r is relative unit shear deformation,

u_r is relative unit axial deformation on the right side, and

u_l is relative unit axial deformation on the left side.

Combining Eqs. (229) through (231) into the matrix form reduces them to

$$\begin{Bmatrix} V_a \\ V_b \\ P_a \\ P_b \\ P_c \\ P_d \end{Bmatrix} = \begin{bmatrix} 1 & 0 & 0 \\ -1 & 0 & 0 \\ 0 & 1 & 0 \\ 0 & 0 & 1 \\ 0 & -1 & 0 \\ 0 & 0 & -1 \end{bmatrix} \begin{Bmatrix} V_a \\ P_a \\ P_b \end{Bmatrix} = [A_1] \begin{Bmatrix} V_a \\ P_a \\ P_b \end{Bmatrix} \qquad (233)$$

Also the following expression holds

$$\begin{Bmatrix} V_a \\ P_a \\ P_b \end{Bmatrix} = [SI] \begin{Bmatrix} v_r \\ u_r \\ u_l \end{Bmatrix} = [SI][A_1]^T \begin{Bmatrix} v_a \\ v_b \\ u_a \\ u_b \\ u_c \\ u_d \end{Bmatrix} \qquad (234)$$

where $[SI]$ is the stiffness matrix

$$[SI] = \frac{1}{L} \begin{bmatrix} K_s & 0 & 0 \\ 0 & K_a^* & 0 \\ 0 & 0 & K_a^* \end{bmatrix} \qquad (235)$$

$$= \frac{1}{L} \begin{bmatrix} K_s & 0 & 0 \\ 0 & \dfrac{K_a}{2} & 0 \\ 0 & 0 & \dfrac{K_a}{2} \end{bmatrix} \qquad (236)$$

Applying the equilibrium of forces in Figure 80, some relationships between the spring and element forces can be determined.

Upper body becomes

$$\Sigma F_x = 0, \quad F_1 - V_a = 0 \tag{237}$$

$$\Sigma F_y = 0, \quad F_2 + F_4 - P_a - P_b = 0 \tag{238}$$

$$\Sigma M_B = 0, \quad F_1 \cdot \alpha + P_a \cdot W - F_2 \cdot W = 0 \tag{239}$$

These equations can be written as

$$F_1 = V_a \tag{240}$$

$$F_2 = \left(V_a \cdot \alpha + P_a \cdot W \right) / W$$

$$= \frac{\alpha}{W} \cdot V_a + P_a \tag{241}$$

$$F_4 = P_a + P_b - \frac{\alpha}{W} \cdot V_a - P_a = P_b - \frac{\alpha}{W} V_a \tag{242}$$

Lower body becomes

$$\Sigma F_x = 0, \quad F_8 - V_b = 0 \tag{243}$$

$$\Sigma F_y = 0, \quad F_6 + F_9 - P_c - P_d = 0 \tag{244}$$

$$\Sigma M_c = 0, \quad F_6 \cdot W - P_d \cdot W - F_8 \cdot \beta = 0 \tag{245}$$

171

These equations can be rewritten as

$$F_8 = V_b \tag{246}$$

$$F_6 = \frac{\beta}{W} V_b + P_d \tag{247}$$

$$F_9 = P_c + P_d - \frac{\beta}{W} V_b - P_d = P_c - \frac{\beta}{W} V_b \tag{248}$$

Equations (240) through (242) and (246) through (248) can be rewritten in matrix form

$$\{F_e\} = \begin{Bmatrix} F_1 \\ F_2 \\ F_3 \\ F_4 \\ F_5 \\ F_6 \\ F_7 \\ F_8 \\ F_9 \\ F_{10} \end{Bmatrix} = \begin{bmatrix} 1 & 0 & 0 & 0 & 0 & 0 \\ \dfrac{\alpha}{W} & 0 & 1 & 0 & 0 & 0 \\ 0 & 0 & 0 & 0 & 0 & 0 \\ \dfrac{-\alpha}{W} & 0 & 0 & 1 & 0 & 0 \\ 0 & 0 & 0 & 0 & 0 & 0 \\ 0 & \dfrac{\beta}{W} & 0 & 0 & 0 & 1 \\ 0 & 0 & 0 & 0 & 0 & 0 \\ 0 & 0 & 0 & 0 & 0 & 0 \\ 0 & \dfrac{-\beta}{W} & 0 & 0 & 1 & 0 \\ 0 & 0 & 0 & 0 & 0 & 0 \end{bmatrix} \begin{Bmatrix} V_a \\ V_b \\ P_a \\ P_b \\ P_c \\ P_d \end{Bmatrix}$$

$$= [A_2] \begin{Bmatrix} V_a \\ V_b \\ P_a \\ P_b \\ P_c \\ P_d \end{Bmatrix} \tag{249}$$

Combining Eqs. (233) and (249) reduces them to

$$\{F_e\} = [A_2][A_1]\begin{Bmatrix} V_a \\ P_a \\ P_b \end{Bmatrix} \tag{250}$$

The perforated shear wall's ECS stiffness is formulated as

$$[K_e] = [A_2][A_1][S_I][[A_2][A_1]]^T \tag{251}$$

C. ELEMENT STIFFNESS MATRIX IN GLOBAL DEGREES OF FREEDOM

Two steps occur in the transformation of degrees of freedom from the element coordinate system to global degree of freedom. First, rotate the degrees of freedom at each of the four ECS joints to their four counterparts in the joint coordinate system (JCS) at joints J1 through J4. Second, move degrees of freedom from each of the 'slave' joints to the 'master' joints for the constraint transformation. Global degree of freedom is defined at the master joints. Further discussion on the constraint transformation from the 'slave' joints to the 'master' joints can be found in Ref. 29.

Next the transformation explicitly focuses on the perforated shear wall. Element force of this wall is rotated to the four joints on an ECS basis and expressed as

173

$$\left\{\begin{matrix} F_{e1} \\ F_{e2} \\ F_{e3} \\ F_{e4} \end{matrix}\right\} = \left\{\begin{matrix} F_{e1x} \\ F_{e1y} \\ F_{e1z} \\ F_{e2x} \\ F_{e2y} \\ F_{e2z} \\ F_{e3x} \\ F_{e3y} \\ F_{e3z} \\ F_{e4x} \\ F_{e4y} \\ F_{e4z} \end{matrix}\right\} = \begin{bmatrix} 1 & 0 & 0 & 0 & 0 & 0 & 0 & 0 & 0 & 0 \\ 0 & 1 & 0 & 0 & 0 & 0 & 0 & 0 & 0 & 0 \\ 0 & 0 & 1 & 0 & 0 & 0 & 0 & 0 & 0 & 0 \\ 0 & 0 & 0 & 0 & 0 & 0 & 0 & 0 & 0 & 0 \\ 0 & 0 & 0 & 1 & 0 & 0 & 0 & 0 & 0 & 0 \\ 0 & 0 & 0 & 0 & 1 & 0 & 0 & 0 & 0 & 0 \\ 0 & 0 & 0 & 0 & 0 & 0 & 0 & 0 & 0 & 0 \\ 0 & 0 & 0 & 0 & 0 & 1 & 0 & 0 & 0 & 0 \\ 0 & 0 & 0 & 0 & 0 & 0 & 1 & 0 & 0 & 0 \\ 0 & 0 & 0 & 0 & 0 & 0 & 0 & 1 & 0 & 0 \\ 0 & 0 & 0 & 0 & 0 & 0 & 0 & 0 & 1 & 0 \\ 0 & 0 & 0 & 0 & 0 & 0 & 0 & 0 & 0 & 1 \end{bmatrix} \left\{\begin{matrix} F_1 \\ F_2 \\ F_3 \\ F_4 \\ F_5 \\ F_6 \\ F_7 \\ F_8 \\ F_9 \\ F_{10} \end{matrix}\right\} = [A_3]\{F_e\}$$

(252)

where the wall does not have transitional DOF along the ECS X axis. Some dummy degrees of freedom are included in the matrix form. $\{F_{ei}\} = \begin{bmatrix} F_{eix} & F_{eiy} & F_{eiz} \end{bmatrix}^T$ represents forces on the joints according to ECS and variable i can be 1, 2, 3 or 4. Then the forces at the four joints of the shear wall are rotated from ECS to JCS. Since both systems are the same in this case, the formulation becomes

$$\left\{\begin{matrix} F_{J1} \\ F_{J2} \\ F_{J3} \\ F_{J4} \end{matrix}\right\} = \left\{\begin{matrix} F_{j1x} \\ F_{j1y} \\ F_{j1z} \\ F_{j2x} \\ F_{j2y} \\ F_{j2z} \\ F_{j3x} \\ F_{j3y} \\ F_{j3z} \\ F_{j4x} \\ F_{j4y} \\ F_{j4z} \end{matrix}\right\} = \begin{bmatrix} 1 & & & \\ & 1 & & 0 \\ & & \ddots & \\ & & & \ddots \\ 0 & & & \\ & & 1 & \\ & & & 1 \end{bmatrix} \left\{\begin{matrix} F_{e1x} \\ F_{e1y} \\ F_{e1z} \\ F_{e2x} \\ F_{e2y} \\ F_{e2z} \\ F_{e3x} \\ F_{e3y} \\ F_{e3z} \\ F_{e4x} \\ F_{e4y} \\ F_{e4z} \end{matrix}\right\} = [A_4]\left\{\begin{matrix} F_{e1} \\ F_{e2} \\ F_{e3} \\ F_{e4} \end{matrix}\right\}$$

(253)

where $[F_{Ji}] = [F_{jix} \; F_{jiy} \; F_{jiz}]^T$ represents forces acting on joint i along X, Y, and Z direction. Based on JCS, i can be 1, 2, 3 or 4. An aspect of constraint transformation should be noted. If slave joints have the same coordinate system as master joints, then translational degrees of freedom for this perforated shear wall are found as follows. The transformation matrix is a unit matrix which can be written as

$$
\begin{Bmatrix} F_{J1M} \\ F_{J2M} \\ F_{J3M} \\ F_{J4M} \end{Bmatrix} = \begin{Bmatrix} F_{j1xm} \\ F_{j1ym} \\ F_{j1zm} \\ F_{j2xm} \\ F_{j2ym} \\ F_{j2zm} \\ F_{j3xm} \\ F_{j3ym} \\ F_{j3zm} \\ F_{j4xm} \\ F_{j4ym} \\ F_{j4zm} \end{Bmatrix} = \begin{bmatrix} 1 & & & \\ & 1 & & 0 \\ & & \cdot & \\ & & & \cdot \\ 0 & & & 1 \\ & & & & 1 \end{bmatrix} \begin{Bmatrix} F_{j1x} \\ F_{j1y} \\ F_{j1z} \\ F_{j2x} \\ F_{j2y} \\ F_{j2z} \\ F_{j3x} \\ F_{j3y} \\ F_{j3z} \\ F_{j4x} \\ F_{j4y} \\ F_{j4z} \end{Bmatrix} = [A_5] \begin{Bmatrix} F_{J1} \\ F_{J2} \\ F_{J3} \\ F_{J4} \end{Bmatrix}
\tag{254}
$$

where $[F_{Jim}] = [F_{jixm} \; F_{jiym} \; F_{jizm}]^T$ is translational degrees of freedom at joint i and i can be 1, 2, 3 or 4. Combining Eqs. (252), (253) and (254) yields

$$
\begin{Bmatrix} F_{J1m} \\ F_{J2m} \\ F_{J3m} \\ F_{J4m} \end{Bmatrix} = [A_5][A_4][A_3]\{F_e\}
\tag{255}
$$

Substitution of Eq. (250) into (255) reduces them to

$$\begin{Bmatrix} F_{J1m} \\ F_{J2m} \\ F_{J3m} \\ F_{J4m} \end{Bmatrix} = [A] \begin{Bmatrix} V_a \\ P_a \\ P_b \end{Bmatrix} \tag{256}$$

where $[A] = [A_5][A_4][A_3][A_2][A_1]$.

Stiffness matrix is thus transformed from spring stiffness to global degrees of freedom by

$$[K_{eg}] = [A][SI][A]^T \tag{257}$$

In the case of this perforated shear wall, computer results for $[K_{eg}]$ are as follows

$$[A][SI][A]^T = \begin{bmatrix} K_s & 0 & 0 \\ \frac{\alpha}{W}K_s & K_a^* & 0 \\ 0 & 0 & 0 \\ 0 & 0 & 0 \\ \frac{-\alpha}{W}K_s & 0 & K_a^* \\ 0 & 0 & 0 \\ 0 & 0 & 0 \\ \frac{-\beta}{W}K_s & 0 & -K_a^* \\ 0 & 0 & 0 \\ -K_s & 0 & 0 \\ \frac{\beta}{W}K_s & -K_a^* & 0 \\ 0 & 0 & 0 \end{bmatrix} \begin{bmatrix} 1 & \frac{\alpha}{W} & 0 & 0 & \frac{-\alpha}{W} & 0 & 0 & \frac{-\beta}{W} & 0 & -1 & \frac{\beta}{W} & 0 \\ 0 & 1 & 0 & 0 & 0 & 0 & 0 & 0 & 0 & 0 & -1 & 0 \\ 0 & 0 & 0 & 0 & 1 & 0 & 0 & -1 & 0 & 0 & 0 & 0 \end{bmatrix}$$

$$\tag{258}$$

176

$$[A][SI][A]^T =$$

$$
\begin{bmatrix}
K_s & \left(\dfrac{\alpha}{W}K_s\right) & 0 & 0 & \left(\dfrac{-\alpha}{W}K_s\right) & 0 & 0 & \left(\dfrac{-\beta}{W}K_s\right) & 0 & -K_s & \left(\dfrac{\beta}{W}K_s\right) & 0 \\
\left(\dfrac{\alpha}{W}K_s\right) & \left(\dfrac{\alpha^2}{W^2}K_s+K_a^*\right) & 0 & 0 & \left(\dfrac{-\alpha^2}{W^2}K_s\right) & 0 & 0 & \left(\dfrac{-\alpha\beta}{W^2}K_s\right) & 0 & \left(\dfrac{-\alpha}{W}K_s\right) & \left(\dfrac{\alpha\beta}{W^2}K_s-K_a^*\right) & 0 \\
0 & 0 & 0 & 0 & 0 & 0 & 0 & 0 & 0 & 0 & 0 & 0 \\
0 & 0 & 0 & 0 & 0 & 0 & 0 & 0 & 0 & 0 & 0 & 0 \\
\left(\dfrac{-\alpha}{W}K_s\right) & \left(\dfrac{-\alpha^2}{W^2}K_s\right) & 0 & 0 & \left(\dfrac{\alpha^2}{W^2}K_s+K_a^*\right) & 0 & 0 & \left(\dfrac{\alpha\beta}{W^2}K_s-K_a^*\right) & 0 & \left(\dfrac{\alpha}{W}K_s\right) & \left(\dfrac{-\alpha\beta}{W^2}K_s\right) & 0 \\
0 & 0 & 0 & 0 & 0 & 0 & 0 & 0 & 0 & 0 & 0 & 0 \\
0 & 0 & 0 & 0 & 0 & 0 & 0 & 0 & 0 & 0 & 0 & 0 \\
\left(\dfrac{-\beta}{W}K_s\right) & \left(\dfrac{-\alpha\beta}{W^2}K_s\right) & 0 & 0 & \left(\dfrac{\alpha\beta}{W^2}K_s-K_a^*\right) & 0 & 0 & \left(\dfrac{\beta^2}{W^2}K_s+K_a^*\right) & 0 & \left(\dfrac{\beta}{W}K_s\right) & \left(\dfrac{-\beta^2}{W^2}K_s\right) & 0 \\
0 & 0 & 0 & 0 & 0 & 0 & 0 & 0 & 0 & 0 & 0 & 0 \\
-K_s & \left(\dfrac{-\alpha}{W^2}K_s\right) & 0 & 0 & \left(\dfrac{\alpha}{W}K_s\right) & 0 & 0 & \left(\dfrac{\beta}{W}K_s\right) & 0 & K_s & \left(\dfrac{-\beta}{W}K_s\right) & 0 \\
\left(\dfrac{\beta}{W}K_s\right) & \left(\dfrac{\alpha\beta}{W^2}K_s-K_a^*\right) & 0 & 0 & \left(\dfrac{-\alpha\beta}{W^2}K_s\right) & 0 & 0 & \left(\dfrac{-\beta^2}{W^2}K_s\right) & 0 & \left(\dfrac{-\beta}{W}K_s\right) & \left(\dfrac{\beta^2}{W^2}K_s+K_a^*\right) & 0 \\
0 & 0 & 0 & 0 & 0 & 0 & 0 & 0 & 0 & 0 & 0 & 0
\end{bmatrix}
$$

$$(259)$$

The relationship between external force and external displacement with degrees of freedom based on the perforated shear wall's springs is

$$\{P\} = \begin{Bmatrix} P_1 \\ P_2 \\ P_4 \end{Bmatrix} = [A][SI][A]^T \begin{Bmatrix} X_1 \\ X_2 \\ X_4 \end{Bmatrix} = \left[K_{eg}\right]\{X\} \tag{260}$$

Equation (259) can be reduced to

$$
\begin{Bmatrix} P_1 \\ P_2 \\ P_4 \end{Bmatrix} =
\begin{bmatrix}
K_s & \dfrac{\alpha}{W}K_s & \dfrac{-\alpha}{W}K_s \\
\dfrac{\alpha}{W}K_s & \dfrac{\alpha^2}{W^2}K_s+\dfrac{K_a}{2} & \dfrac{-\alpha^2}{W^2}K_s \\
\dfrac{-\alpha}{W}K_s & \dfrac{-\alpha^2}{W^2}K_s & \dfrac{\alpha^2}{W^2}K_s+\dfrac{K_a}{2}
\end{bmatrix}
\begin{Bmatrix} X_1 \\ X_2 \\ X_4 \end{Bmatrix} \tag{261}
$$

This corresponds to Figure 81.

177

P_4, X_4 P_2, X_2

P_1, X_1

$X_1 = \delta_1$
$X_2 = \delta_2$
$X_4 = \delta_4$
$\delta_1, \delta_2, \delta_4$ refer to Fig.81.
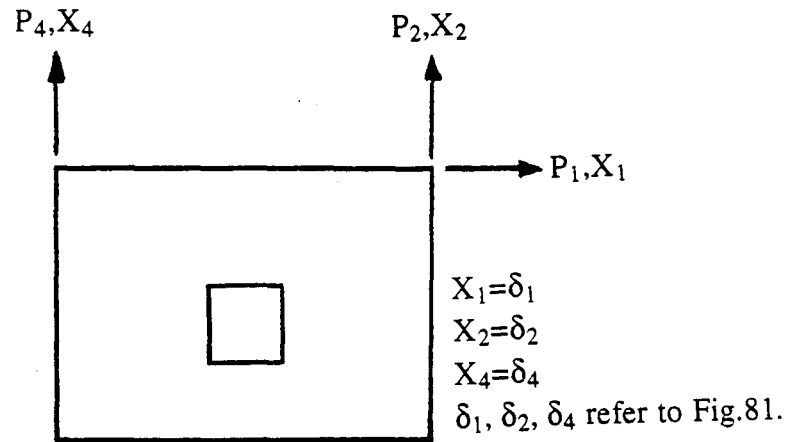
Figure 81 Unrestrained global degrees of freedom considered in the isolated system

D. FREE-BODY-DIAGRAM-BASED FORMULATION

In this case, three unit forces are applied to the perforated shear wall in relation to three kinds of springs. Formulations are then observed and established. To begin, unit force is applied at degree of freedom 1; the associated free-body diagram is shown in Figure 82. The bottom of the shear wall is fixed, and degree of freedom 1 is allowed one unit displacement. Degrees of freedom 2 and 5 are assumed to be fixed. Displacement matrix $[X]$ becomes

$$\{X\} = \begin{Bmatrix} X_1 \\ X_2 \\ X_4 \end{Bmatrix} = \begin{Bmatrix} 1 \\ 0 \\ 0 \end{Bmatrix} \tag{262}$$

This is shown in Figure 82(a).

Figure 82(b) depicts internal shear V which is equal to external force P_1. Note that a moment is induced within the upper free-body diagram. Internal shear is provided by the shear spring with stiffness of K_s. Force P_1 is thus

$$P_1 = K_s \cdot X_1 = K_s \cdot 1 = K_s \qquad (263)$$

Two forces, resisted by axial springs on both ends of the shear wall, balance the moment. As shown in Figure 82(c), these forces can be determined by equilibrium of moment and force as

$$\Sigma M_B = 0 \ , \ P_1 \cdot \alpha - P_2 \cdot W = 0 \qquad (264)$$

$$\Sigma F_Y = 0 \ , \ -P_4 + P_2 = 0 \qquad (265)$$

Forces P_2 and P_4 then become
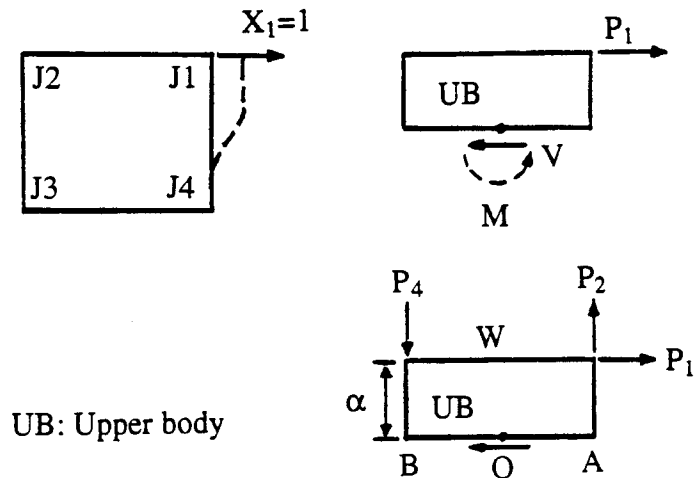
Figure 82   Free body diagram for unit force applied to degree of freedom 1

179

$$P_2 = \frac{\alpha}{W}P_1 = \frac{\alpha}{W}K_s \qquad\qquad (266)$$

$$P_4 = \frac{\alpha}{W}K_s \qquad\qquad (267)$$

External force can be rewritten as

$$\{P\} = \begin{Bmatrix} P_1 \\ P_2 \\ P_4 \end{Bmatrix} = \begin{Bmatrix} K_s \\ \dfrac{\alpha}{W} \cdot K_s \\ \dfrac{\alpha}{W} \cdot K_s \end{Bmatrix} \qquad\qquad (268)$$

If a unit force is applied to degree of freedom 2, as shown in Figure 83(a), degrees of freedom 1 and 4 are not allowed to move. The displacement matrix is thus written as

$$\{X\} = \begin{Bmatrix} X_1 \\ X_2 \\ X_4 \end{Bmatrix} = \begin{Bmatrix} 0 \\ 1 \\ 0 \end{Bmatrix} \qquad\qquad (269)$$

In Figure 83(b), X_2 is allowed to move one unit length upwards. Joint J1 (where degree of freedom 1 is located) then displaces ΔX to the left. Joint J2 rotates $\delta\theta$ and, with slight displacement of X_2 upwards, can be expressed by

$$W \cdot \delta\theta = 1 \qquad\qquad (270)$$

or

$$\delta\theta = \frac{1}{W} \qquad\qquad (271)$$

180
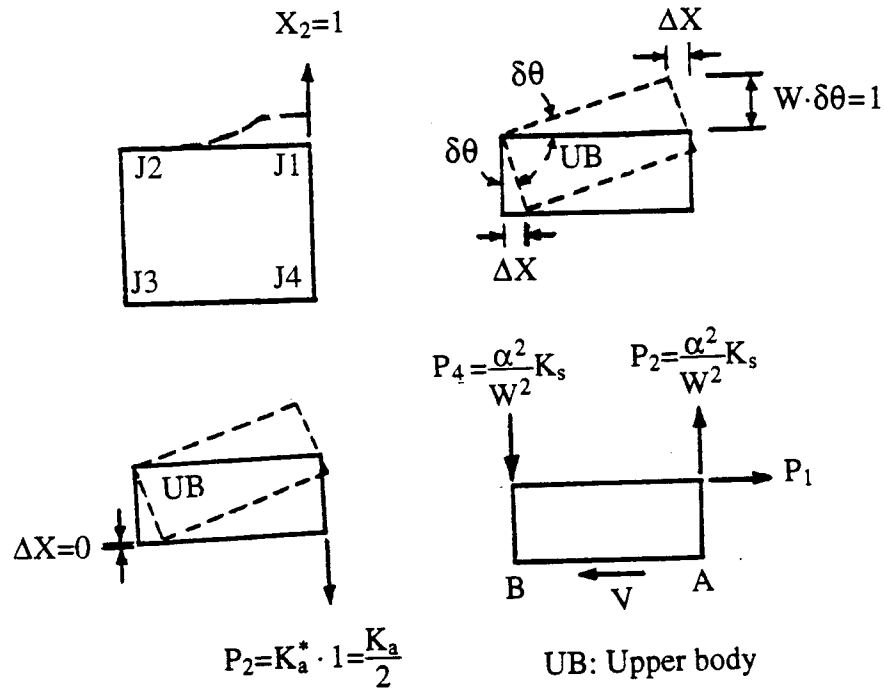
Figure 83 Free body diagram for unit force applied to degree of freedom 2

Lateral displacement of ΔX at joint J1 becomes

$$\Delta X = \alpha \cdot \delta\theta = \frac{\alpha}{W} \tag{272}$$

Thus external force P_1 becomes

$$P_1 = K_s \cdot \Delta X = \frac{\alpha}{W} K_s \tag{273}$$

External force P_2, caused by one unit displacement upwards at joint J1, reduces to

$$P_2 = K_a^* \cdot X_2 = K_a^* \cdot 1 = \frac{K_a}{2} \tag{274}$$

which is shown in Figure 83(c). Figure 83(d) illustrates associated external forces P_2 and P_4 due to the existence of external force P_1, which is obtained from equilibrium of moment. External force P_2 is formulated as

$$P_2 = \frac{\alpha^2}{W^2} K_s + \frac{K_a}{2} \tag{275}$$

where $\frac{K_a}{2}$ results from the action of axial spring (see Eq. (274)).

External force P_4 is written as

$$P_4 = \frac{\alpha^2}{W^2} K_s (\downarrow) = \frac{-\alpha^2}{W^2} K_s (\uparrow) \tag{276}$$

Here matrix form of external forces is

$$\{P\} = \begin{Bmatrix} P_1 \\ P_2 \\ P_4 \end{Bmatrix} = \begin{Bmatrix} \dfrac{\alpha}{W} K_s \\ \dfrac{\alpha^2}{W^2} K_s + \dfrac{K_a}{2} \\ \dfrac{-\alpha^2}{W^2} K_s \end{Bmatrix} \tag{277}$$

Similarly, when a unit force is applied to degree of freedom 4 (see Figure 84(a)), lateral displacement ΔX at joint J2 (see Figure 84(b)) caused by rotation $\delta\theta$ is

$$\Delta X = \alpha \cdot \delta\theta \tag{278}$$

Since

$$W \cdot \delta\theta = X = 1 \tag{279}$$

182

then

$$\delta\theta = \frac{1}{W} \qquad (280)$$

Substituting Eq. (280) into Eq. (278) yields

$$\Delta X = \frac{\alpha}{W} \qquad (281)$$

External force P_1 resisted by shear spring thus becomes

$$P_1 = K_s \cdot \Delta X = \frac{\alpha}{W} \cdot K_s \ (\leftarrow) = \frac{-\alpha}{W} \cdot K_s \ (\rightarrow) \qquad (282)$$

Due to the existence of P_1, forces P_2 and P_4 are
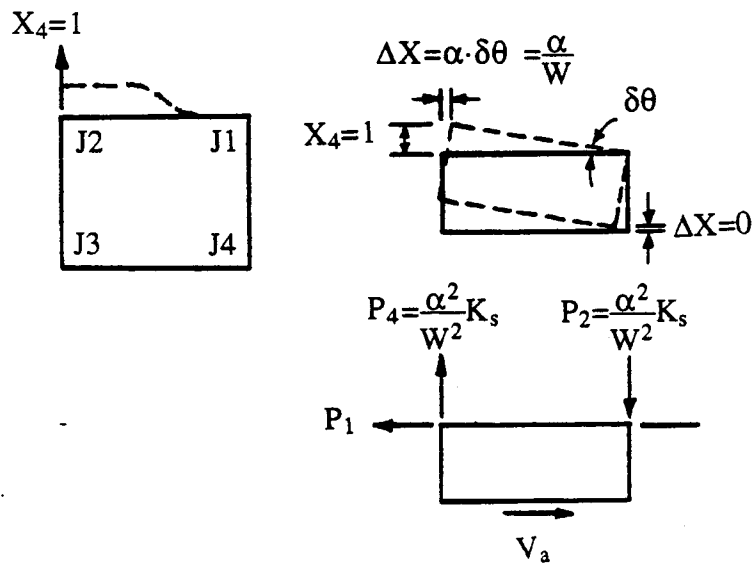
Figure 84   Free body diagram for unit force applied to degree of freedom 4

$$P_2 = \frac{\alpha^2}{W^2}K_s \ (\downarrow) = \frac{-\alpha^2}{W^2}K_s \ (\uparrow) \qquad (283)$$

$$P_4 = \frac{\alpha^2}{W^2}K_s \ (\uparrow) \qquad (284)$$

Furthermore, external force P_5 due to vertical unit displacement is

$$P_4 = K_a^* \cdot \Delta X = \frac{K_a}{2} \cdot 1 = \frac{K_a}{2} \qquad (285)$$

Total force P_4 then becomes

$$P_4 = \frac{\alpha^2}{W^2}K_s + \frac{K_a}{2} \qquad (286)$$

The final matrix force due to unit displacement at joint J2 thus reduces to

$$\{P\} = \begin{Bmatrix} P_1 \\ P_2 \\ P_4 \end{Bmatrix} = \begin{Bmatrix} \dfrac{-\alpha}{W}K_s \\ \dfrac{-\alpha^2}{W^2}K_s \\ \dfrac{\alpha^2}{W^2}K_s + \dfrac{K_a}{2} \end{Bmatrix} \qquad (287)$$

Combining Eqs. (268), (277) and (287), general global stiffness can be written as

$$\{P\} = \begin{bmatrix} K_s & \dfrac{\alpha}{W}K_s & \dfrac{-\alpha}{W}K_s \\ \dfrac{\alpha}{W}K_s & \dfrac{\alpha^2}{W^2}K_s + \dfrac{K_a}{2} & \dfrac{-\alpha^2}{W^2}K_s \\ \dfrac{-\alpha}{W}K_s & \dfrac{-\alpha^2}{W^2}K_s & \dfrac{\alpha^2}{W^2}K_s + \dfrac{K_a}{2} \end{bmatrix} \{X\} \qquad (288)$$

Comparing Eq. (288) with (261) shows that the stiffness matrix is the same for both approaches with the perforated shear wall.

VIII. RESPONSE STUDY OF FOUR-STORY INDUSTRIAL BUILDING

This section investigates the design parameters of force reduction and displacement amplification factors for a shear wall box-type building. Results are compared with UBC design parameters. Other parameters such as the ductility reduction factor R_μ, overstrength factor Ω and system ductility factor μ_s are also studied.

A. CONFIGURATION AND MASS CENTER

The structural system studied in this section is a reinforced concrete box-type building. The structural model is based on the building layout shown in Figure 85. Layout is for diesel power auxiliary building of the type used in nuclear plants as shown in Figure 86. Sixteen shear walls comprise the model for which the interior walls were not considered as structural elements[30].Table XIV shows the lumped mass at different levels. Level 1 represents the floor of the second story, Level 2 represents the floor of third story, and so on. Level 1 and Level 3 have heavier masses. At all levels, mass centers are located near the center of rigidity which is also the center of the floor. This means that the effect of torsion is small and can be neglected. In fact, only monotonic loading process is performed statically. Therefore the effect of masses is disregarded.

Having a basically square shape, this building system includes many kinds of shear walls. One set of shear walls along column lines C2-C4 has dimensions of 74'x26'x48" (SW9), 74'x12'x48"(SW10), 74'x13'x48"(SW11) and 74'x25'x48"(SW12). One set of shear walls(SW13, SW14, SW15, SW16) along column lines C1-C3 has the same dimensions as the previous set of shear walls along column lines C2-C4, except its thickness is 36". Perpendicular to these two sets of shear walls, the dimensions of shear walls along column lines C1-C2, C3-C4 are 75'x26'x30"(SW1), 75'x26'x36"(SW5), 75'x12'x36"(SW2, SW6), 75'x13'x36" (SW3, SW7), and 75'x25'x36" (SW4, SW8).

186
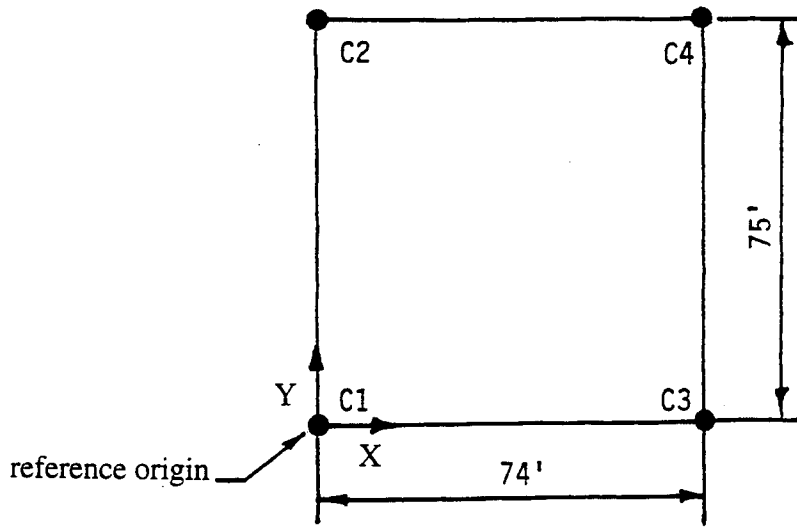
(a) Plan
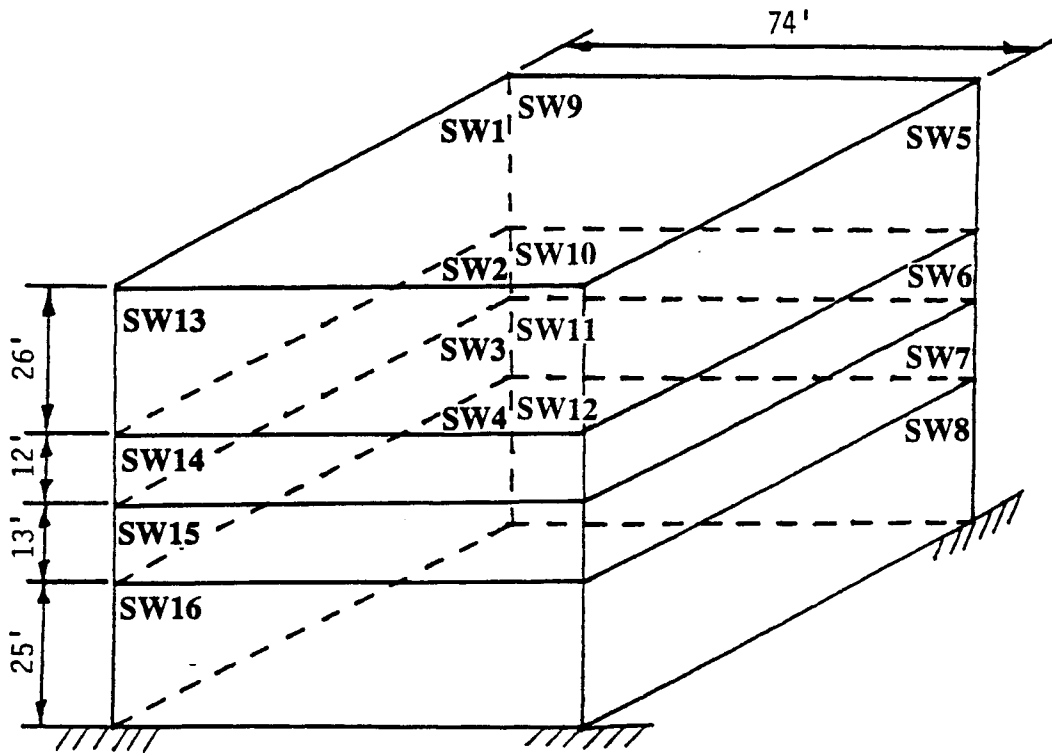
(b) Overall view

Figure 85 Structural configuration
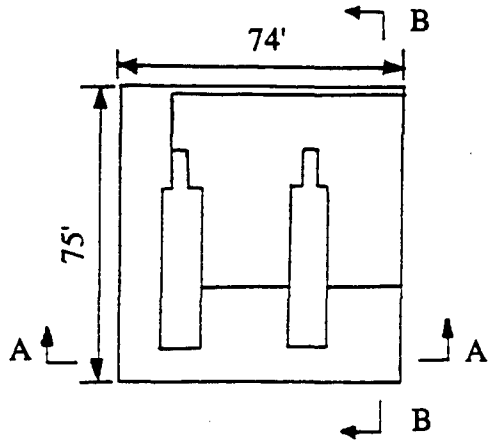
(a) Section C-C
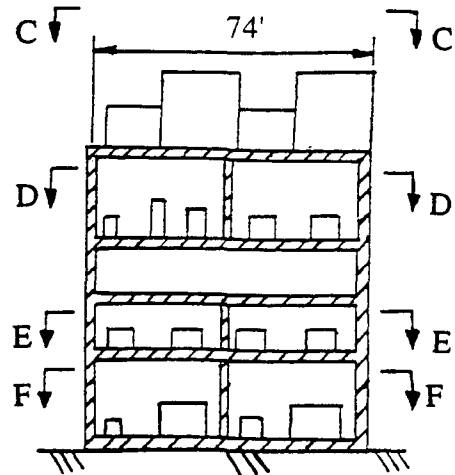
(b) Section A-A
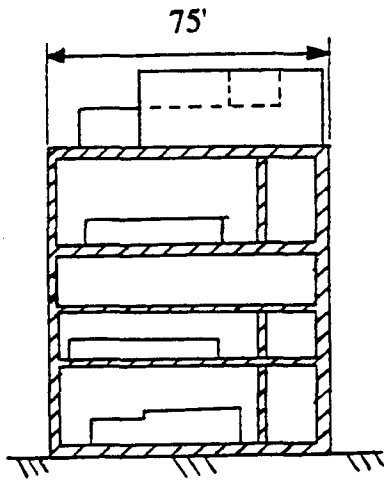
(c) Section B-B
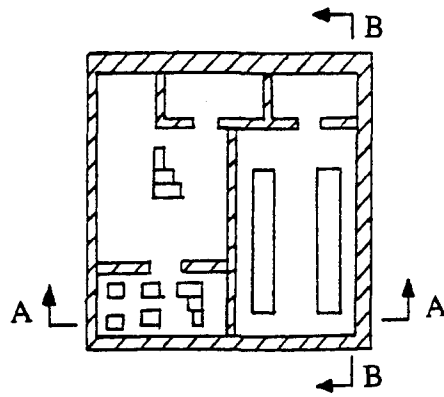
(d) Section D-D
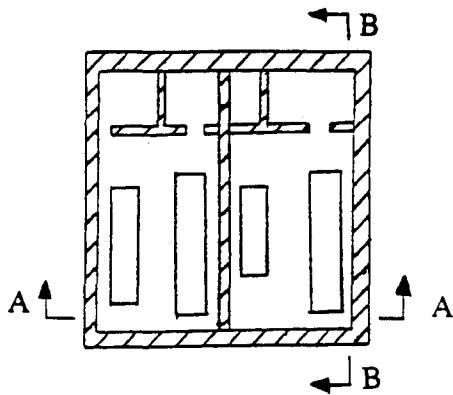
(e) Section E-E
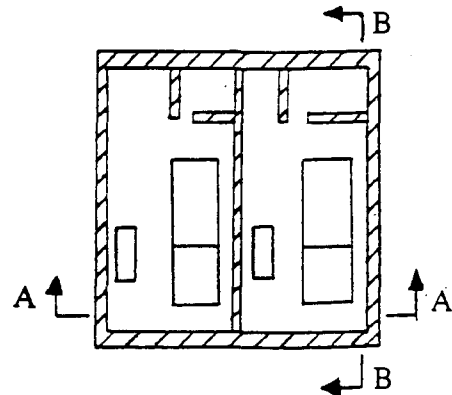
(f) Section F-F

Figure 86 Building layout

188

It can be seen that this box-type building system has sixteen large shear walls 74' (or 75') long and 30" to 48" thick. Shear walls denoted SW1 to SW16 above are shown in the Figure 85. Thickness of walls and floors are shown in Table XV.

Table XIV Mass distribution and mass center

LEVEL	MASS (k-sec^2/in)					MASS CENTER	
	COLUMN LINE 1	COLUMN LINE 2	COLUMN LINE 3	COLUMN LINE 4	TOTAL	X (in.)	Y (in.)
1	3.43	3.62	3.43	3.67	14.15	444.80	454.30
2	2.31	2.59	2.31	2.61	9.82	444.00	460.10
3	2.88	3.36	3.36	3.49	13.09	450.60	451.10
4	2.47	2.76	2.56	2.90	10.69	442.40	454.20

NOTE: The mass center is measured from the reference origin.

Table XV Thickness of walls and floors

PANEL POSITION		THICKNESS	
COLUMN LINES	LEVEL	WALL (in.)	FLOOR (in.)
1-2	1	36	18
	2	36	18
	3	36	18
	4	30	18
3-4	1	36	18
	2	36	18
	3	36	18
	4	36	18
1-3	1	36	18
	2	36	18
	3	36	18
	4	36	18
2-4	1	48	18
	2	48	18
	3	48	18
	4	48	18

NOTE: Level 4 is at the top of the structure.

189

B. LOAD-DISPLACEMENT RELATIONSHIP OF SHEAR WALLS

Based on the Cheng-Mertz solid shear wall model, the load-displacement relationship of solid shear walls is strongly dependent on moment/shear ratio (i.e., M/V). Because the box-type building has elements of the solid shear wall type, the building, as an indeterminate structure, has sixteen solid shear walls counteracting one another. The interaction between walls causes moment/shear ratios to change. Therefore elastic analysis is performed first to determine the actual moment/shear ratios for all walls in the box-type building. Initial stiffnesses of shear walls are based on load-displacement relationship of the isolated solid shear walls (i.e., moment/shear ratio of the wall equals wall height). Table XVI shows moment/shear ratios based on elastic analysis as well as the isolated wall itself for walls in force direction. From the study of Cheng-Mertz's solid shear wall model, moment-resistant capacity increases and shear-resistant capacity decreases when the moment/shear ratio becomes larger in a given isolated shear wall, and vice versa.

1. Bending Backbone Curves of Shear Walls From above elastic analysis, shear walls SW3, SW4, SW7 and SW8 in the direction perpendicular to force direction have small moment/shear ratios. These shear walls have far less moment capacity. Figure 87 shows moment-rotation relationship for rotational spring of unit wall length of SW12 and SW16. Rotation includes rotation of the wall itself due to flexural behavior and base rotation due to dowel action. Unit length shear wall represents shear wall with height equivalent to one unit. Those values are referred to as the bending backbone curves of shear walls in the analysis.

2. Shear Backbone Curves of Shear Walls Similar to previous cases, shear capacities of shear walls SW3, SW4, SW7, and SW8 are larger compared to other shear walls. This is caused by low moment/shear ratios. Figure 88 shows shear-shear displacement relationship for shear walls SW12 and SW 16. In general, shear capacities of shear walls in the force direction are smaller than those in the direction perpendicular

190

Table XVI   Comparison of moment/shear ratio for solid shear walls

Wall No.	Moment/shear ratio(M/V)*	Moment/shear ratio(M/V)**
9	3956.1	7924.8
10	2977.1	3657.6
11	2624.3	3962.4
12	5450.8	7620.0
13	1441.2	7924.8
14	2387.6	3657.6
15	4309.6	3962.4
16	5377.9	7620.0

(Unit: mm)

*results from elastic analysis
**results from isolated shear wall of the building

to force direction. Also, shear capacities of shear walls (SW12, SW16) on the first story in the force direction are smaller than those (SW9, SW10, SW11, SW13, SW14, SW15) elsewhere. As shown in Figure 88, those curves are referred to as the shear backbone curves of shear wall per unit length.

3. <u>Relationship between Bending, Shear and Total Lateral Displacement of Backbone Curves of Shear Walls</u> Figure 89 shows the relationship between lateral load and lateral displacement for typical walls SW12 and SW16. Lateral displacement includes bending displacement (Δ_b), shear displacement (Δ_s), and total displacement (Δ_t). Bending displacement Δ_b is derived from bending backbone curve which has the following relationship to rotation per unit length shear wall.

$$\Delta_b = \text{rotation/unit length shear wall x height x height} \qquad (289)$$

Rotation is referred to as bending backbone curve in the above section.
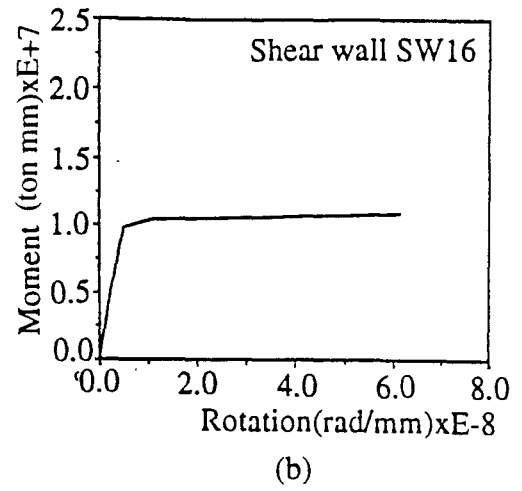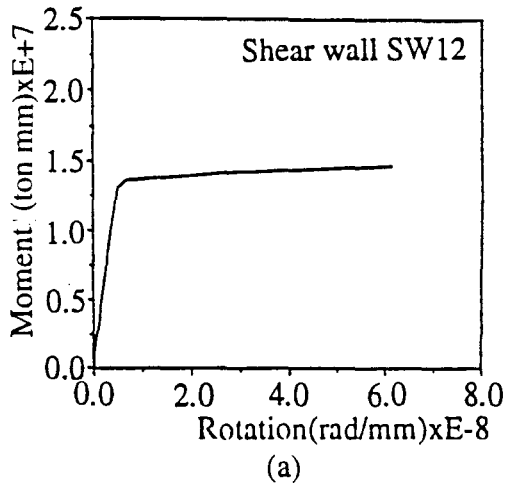
Figure 87 Relationship of moment vs. rotation for rotational spring of unit length shear walls (a) SW12 (b) SW16
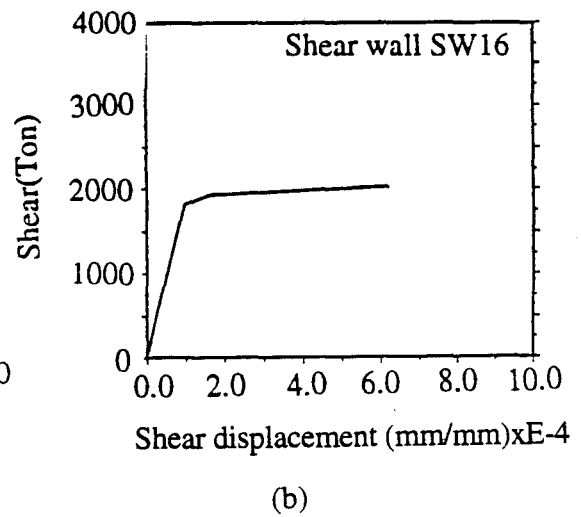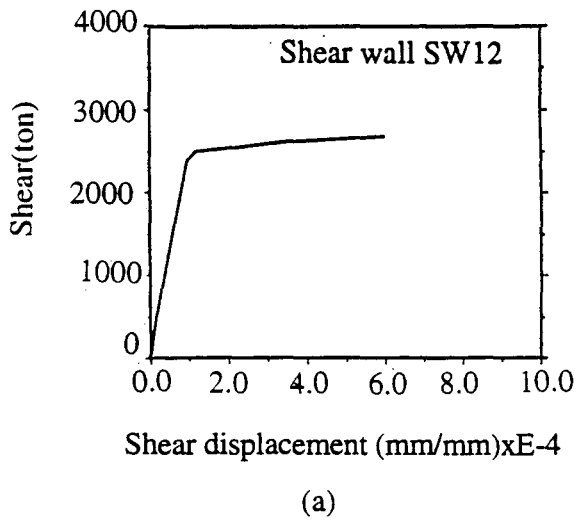
Figure 88 Relationship of shear vs. shear displacement for shear spring of unit length shear walls (a)SW12 (b) SW16
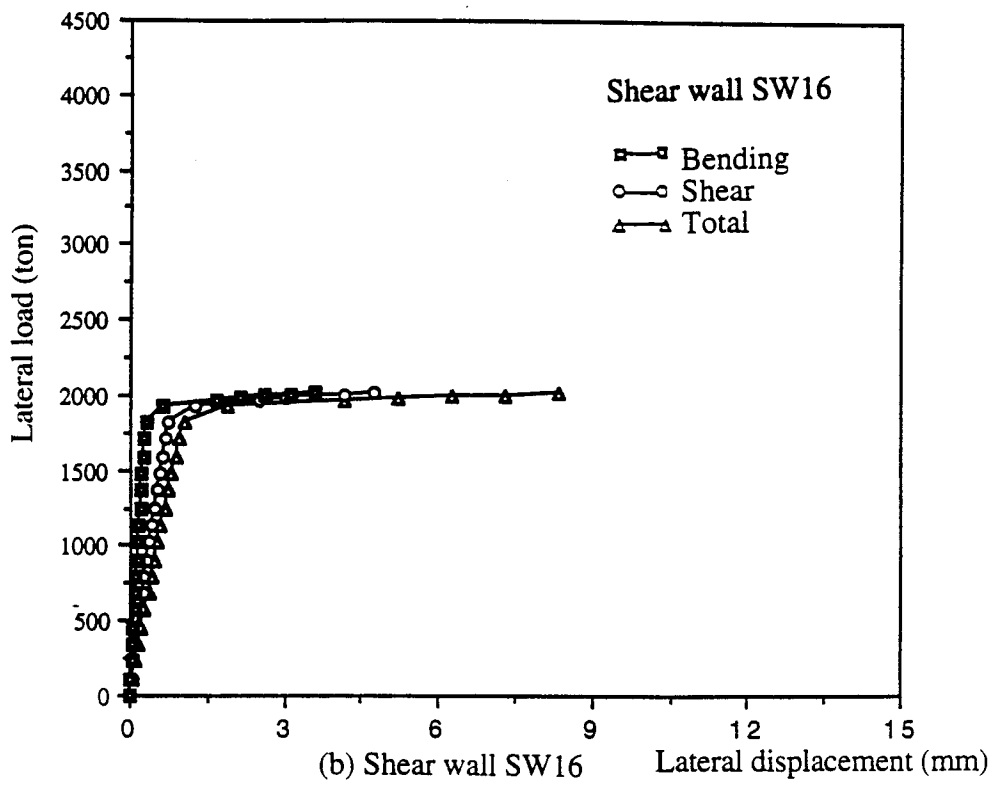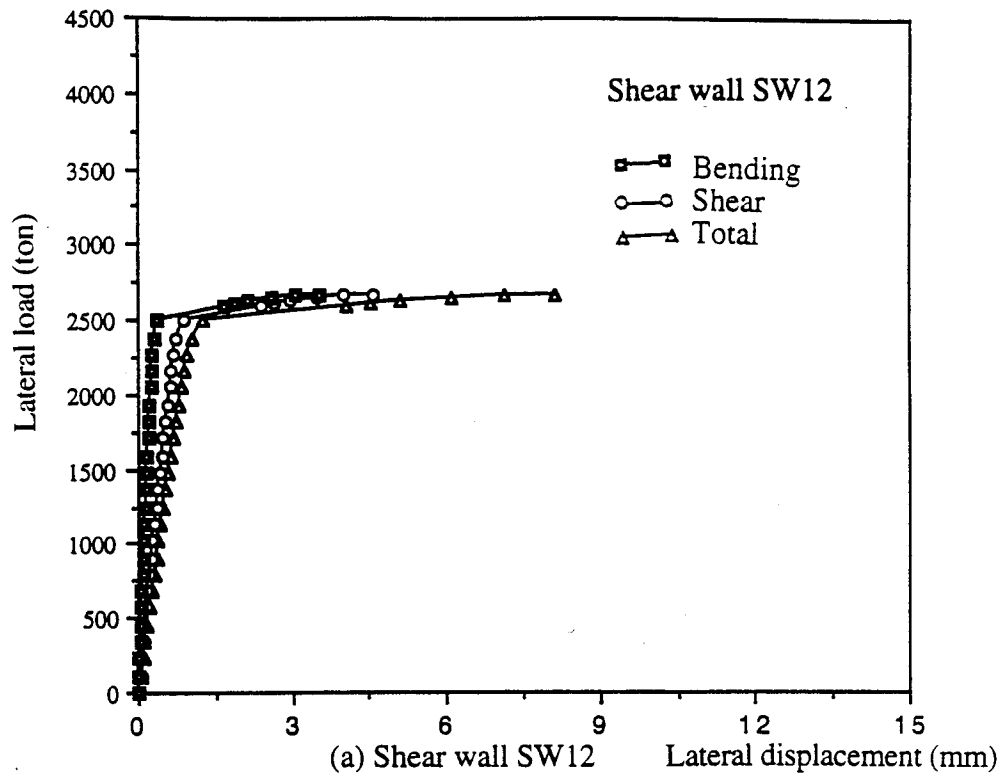
Figure 89 Comparison of bending, shear and total lateral displacements for backbone curve of shear walls

Shear displacement Δ_s is derived from shear backbone curve and is expressed as

$$\Delta_s = \text{shear displacement/unit length shear wall x height} \tag{290}$$

Total displacement Δ_t is composed of bending displacement Δ_b and shear displacement Δ_s as follows

$$\Delta_t = \Delta_b + \Delta_s \tag{291}$$

Figure 89 shows the relationship of lateral load to lateral displacement in which bending backbone curve has higher initial stiffness. With respect to lateral displacement, it can be seen that all shear walls in this building have larger ultimate shear displacement than ultimate bending displacement. This allows the shear wall's shear spring to displace further than its rotational spring.

C. MONOTONIC STATIC ANALYSIS

1. Lateral Force Distribution According to UBC design code, the total external force shall be distributed over the height of the building in the form of

$$V = F_t + \sum_{i=1}^{n} F_i \tag{292}$$

where V is the base shear of a building. At the top of the building, concentrated force F_t, in addition to F_n (i.e., lateral force applied to level n), is derived from

$$F_t = 0.07 \, TV \tag{293}$$

194

F_t cannot exceed $0.25V$ and may be considered as zero when the fundamental period T is 0.7 seconds or less. Other than force F_t, the base shear is distributed over the height of the structure, including level n, according to

$$F_x = \frac{(V-F_t)W_x h_x}{\sum_{i=1}^{n} W_i h_i} \qquad (294)$$

The force F_x, designated as x for each level, is applied over the floor of the building in accordance with the mass distribution at that level.

For this box-type building, the fundamental period T equals 0.12 second. Thus, as stated above, the concentrated force F_t is regarded as zero. Figure 90 shows the weight W_i for each floor and corresponding height h_i.

As shown in Figure 91, the distributed force F_i is computed as follows

$$F_1 = \frac{V \cdot W_1 \cdot h_1}{\sum_{i=1}^{4} W_i h_i} = \frac{18906134.4}{117250043.4} V = 0.162 \, V \qquad (295)$$

Similarly, distributed forces F_2, F_3, F_4 are calculated as 0.170 V, 0.298 V, 0.370 V, respectively.

2. Response Analysis Based on Ductility

    a. Overall response behavior To explore the response of shear walls, particularly for either rotational spring or shear spring of shear wall, the case of ductility equal to 4 is employed. The definition of ductility represents all shear walls having the same ductility for lateral load vs. total displacement relationship. For monotonic loading, the incremental loading procedure is used in which each load increment is eight tons. From the overall response in the force direction (X direction; see Figure 92), the rotational spring of shear wall SW12 reaches ultimate state when load is 4248 tons (=8

195

h_4=23164.8 mm; W_4=1874.43 tons

h_3=15240.0 mm; W_3=2295.25 tons

h_2=11582.4 mm; W_2=1721.88 tons

h_1= 7620.0 mm; W_1=2481.12 tons

$$\sum_{i=1}^{4} W_i h_i = 117250043.4 \text{ ton·mm}$$
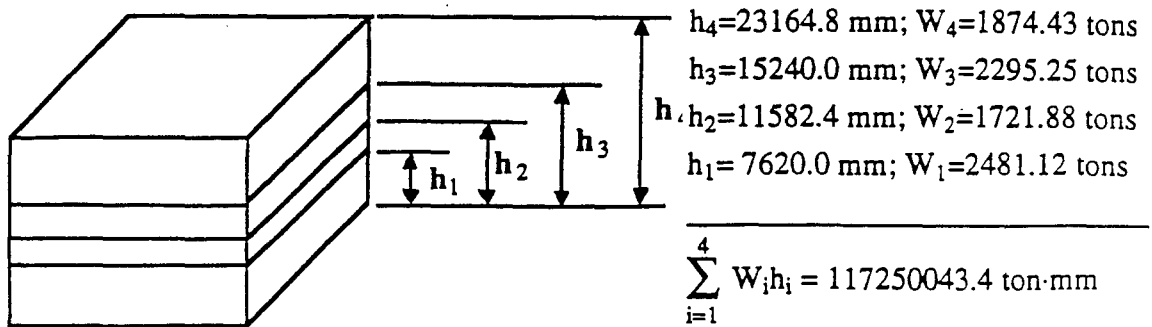
Figure 90   Diagram of height h_i and weight W_i for each floor

74'

75'

0.370V

0.298V

0.170V

0.162V
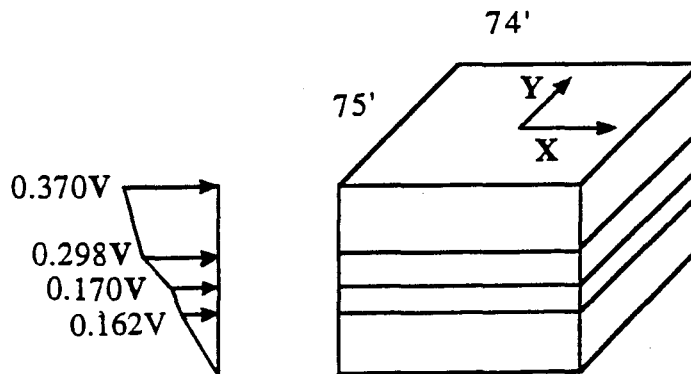
Figure 91   Lateral force distribution in force-applied direction for box-type industrial building based on UBC design code

tons times 531 steps). This is depicted at point A in Figure 92(a). At the same time, shear wall SW16 almost approaches ultimate state. When it goes one more step (load being 4256 tons), the rotational spring of shear wall SW12 drops dramatically to zero. When this happens, the rotational spring has failed already. Soon the rotational spring of shear wall SW16 reaches the ultimate state (see Figure 92(b)). With one more incremental load (load being 4264 tons), the rotational spring of shear wall SW16 fails. Examining the behavior of shear walls SW9, SW10, SW13 and SW14 on the higher

196
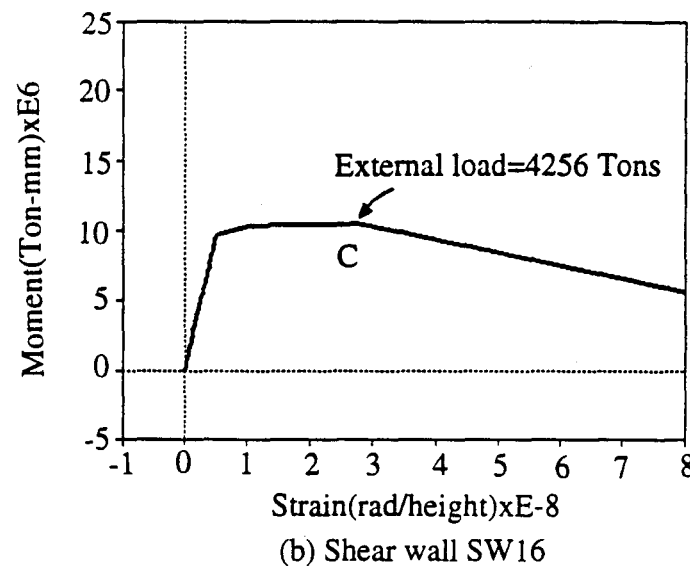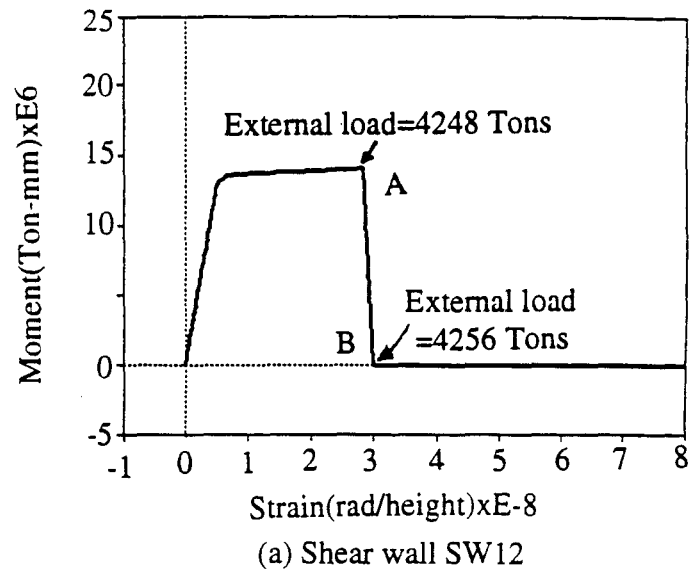
Figure 92 Response of rotational spring of shear walls for four-story box-type building
based on moment-strain relationship under monotonic loading

level of the building reveals that these walls are still in the elastic range. Shear walls

SW11, SW15 enter into the inelastic range slightly. It can be seen that the shear walls

(SW12, SW16) at the first story control overall response because they take much more

shear than those at other levels. Response may not be controlled by shear walls on the

first level if shear walls at higher levels are weak in resisting shear.

When one shear wall fails under monotonic loading, the other shear wall takes extra shear transferred from the failed shear wall. This occurs because the failed wall cannot take any more load. Therefore the other shear wall fails almost immediately, as shown in Figure 92(b) and, with more detail, in Figure 93. In the latter, when incremental load is small, shear wall SW16 fails soon after reaching ultimate state (point C).

In terms of story drift (or lateral displacement), after the first shear wall fails, that story exhibits more displacement. In a practical sense, this building can handle more seismic load yet exceed allowable drift. Due to its state of flexural failure, this building can be regarded as having failed already.

Shear walls in the direction perpendicular to force direction are not strong enough to control overall behavior. Since base shear is not exerted in this direction, shear walls are kept in the elastic range either for rotational spring or shear spring. The shear spring of shear walls of the building is discussed later.

b. <u>Moment development in shear walls during monotonic loading</u> Figure 94 shows moment development in shear walls SW12 and SW16 which have more flexural response than those at other levels. This is mainly because internal shear accumulates downward through the building. Increasing shear at the lower level creates more moment effect on shear walls.

An increase in internal moment continues until the rotational spring of shear wall reaches its ultimate capacity. At that point, the rotational spring of shear wall fails immediately. Then stress redistribution occurs until the building reaches stability again.

c. <u>Shear development in shear walls during monotonic loading</u> The internal moment occurring in the rotational spring of a shear wall is transformed into vertical forces at the joints on each side. But the internal shear occurs in the shear spring. Internal shear caused by external force is taken by the shear wall's shear spring. When the shear wall's rotational spring fails first, this wall can still withstand shear caused by
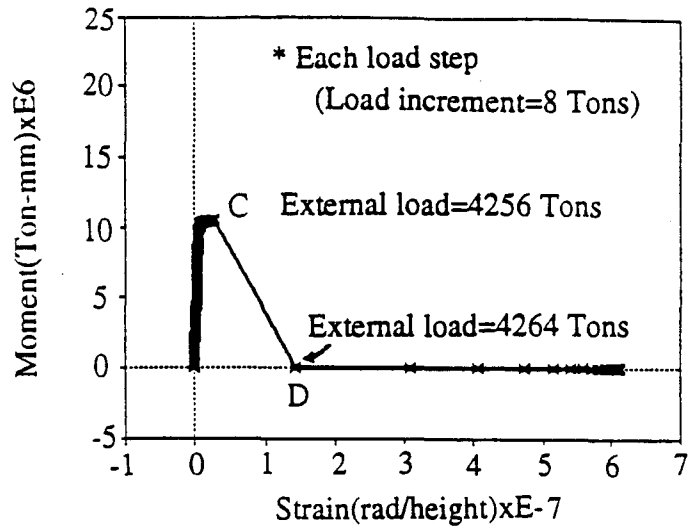
Figure 93   More detail of wall SW16 under monotonic loading
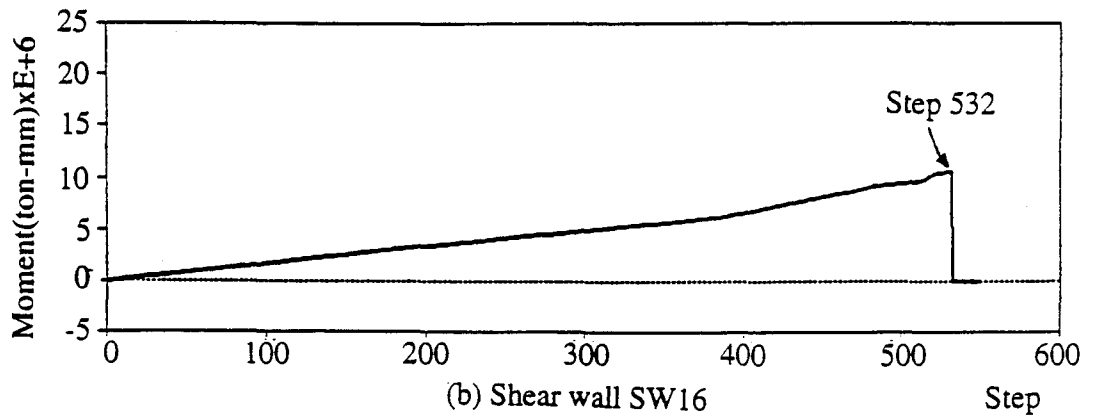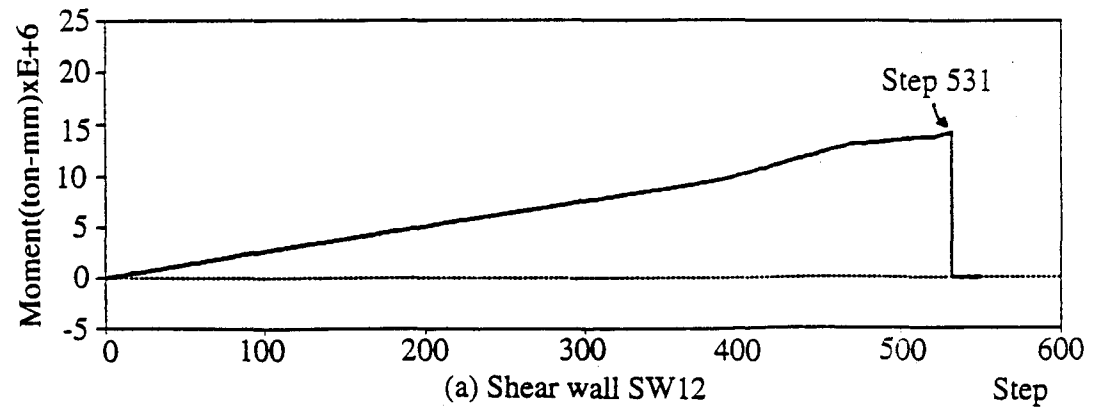
Figure 94   Moment development in shear walls during monotonic loading

199

external force even though the story drift owing to failure of the rotational spring is high. This phenomenon is shown in Figure 95.

In Figure 95, before flexural failure occurs on shear wall SW12 at load step 531(load=4248 tons), the shear response of the shear wall's shear spring proceeds steadily. After flexural failure of shear wall SW12, internal shear stress redistribution continues until stability is regained. Shear wall SW16 reaches shear failure at a load of 4384 tons (see Figure 95(b)), and fails at a load of 4392 tons thereafter.

d. Comparison of base shear-story drift relationship

i. Comparison of failure story drift As stated earlier, ductility is defined as the ductility of all shear walls of a building in accordance with the relationship between lateral load and total displacement. In Figure 96, the base shear-story drift relationship expresses the response of the first floor's mass center with ductility=4 and 8. For the first floor, story response is strongly related to the load-displacement relationship of shear walls at that level. In other words, the difference in maximum displacement of mass center from story to story depends on both wall height and backbone curve of shear walls. Since the shear walls of the first story fail first, this failure controls the behavior of the entire building. The first story is the so-called critical story. In Figure 96, maximum story drift $\Delta_{story,max}$ can be computed when all the shear walls fail completely. Based on an ideally linearly elastic-perfect plastic model, story drift $\Delta_{story,yield}$ at yielding point can also be calculated. Compared to the first story, the roof has considerable story drift; second and third stories have minor story drift. This is due to wall height and load-displacement relationship of shear walls, as noted earlier. Similar responses are also observed in the cases of other ductilities .

Two definitions for design parameters in the relationship between base shear and critical story drift are employed later, as shown in Figure 97. In the first definition, the initial significant yielding point occurs as soon as a main element fails. In the second definition, the initial significant yield point occurs when the behavior of the critical story
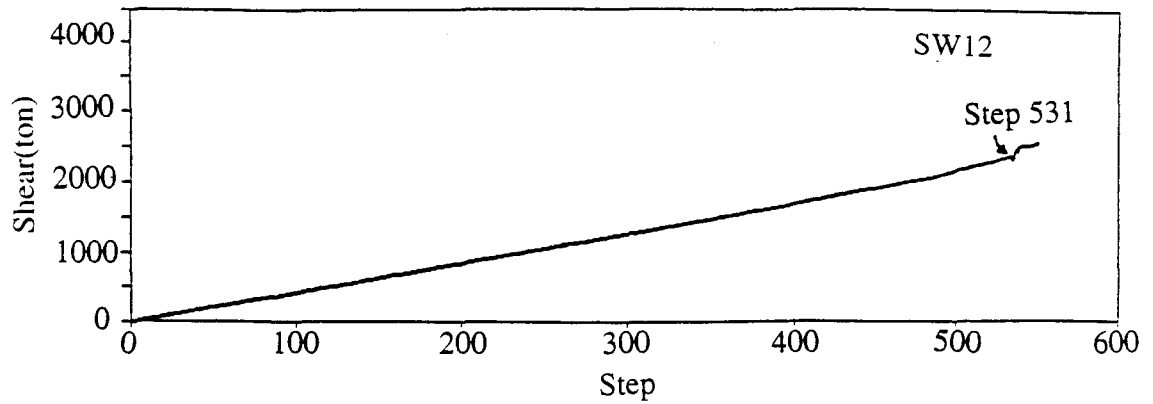
(a) Shear wall SW12
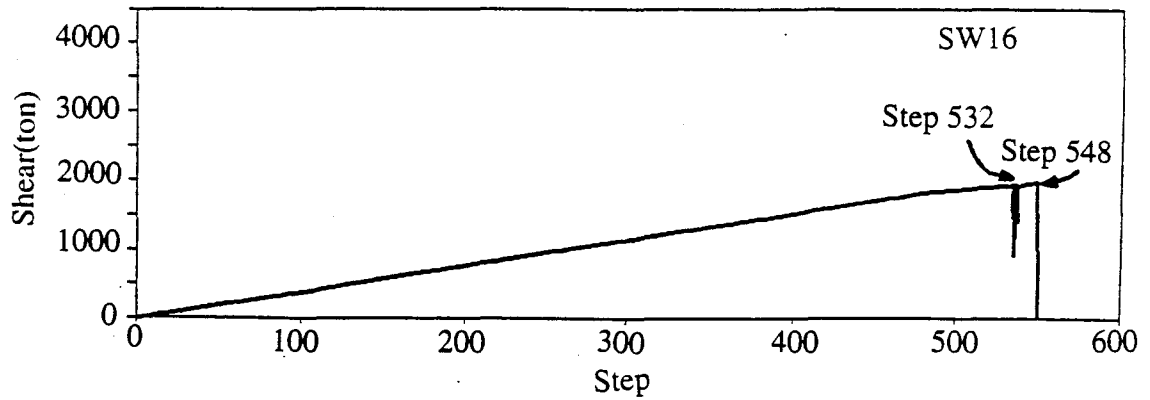
(b) Shear wall SW16

Figure 95 Shear development in shear walls during monotonic loading

deviates from elastic to inelastic range. Both definitions apply to an ideally linearly elastic-perfect plastic model.

Note maximum drift for ductility of 4.0 and 8.0 shown in Figure 96. In the second definition, maximum story drift $\Delta_{story,max}$ changes more than yielding story drift $\Delta_{story,yield}$ for each case of ductility. Story drift is almost the same in the first definition. As indicated by backbone curve of shear walls, if ductility of a shear wall is 4 or up to 8, this wall becomes partially inelastic and then almost fully inelastic after yielding point. Ultimate displacement of a shear wall increases radically even with small ductility
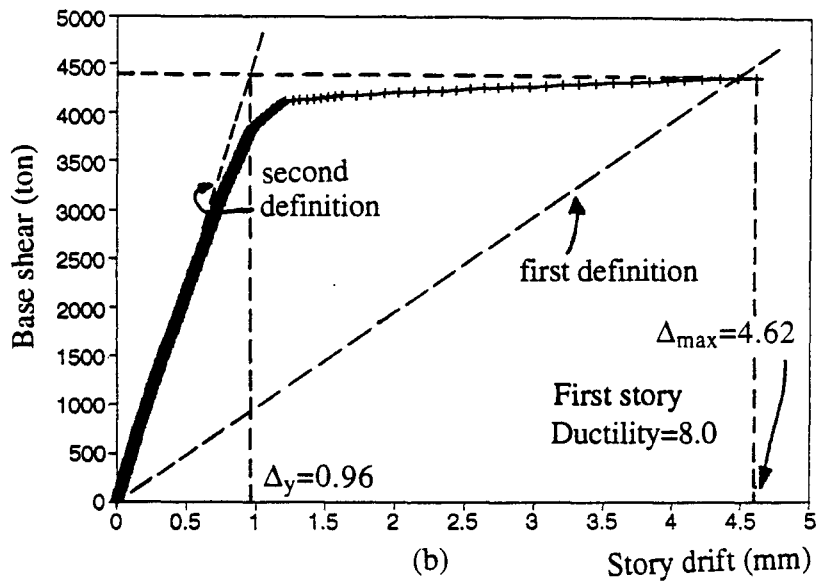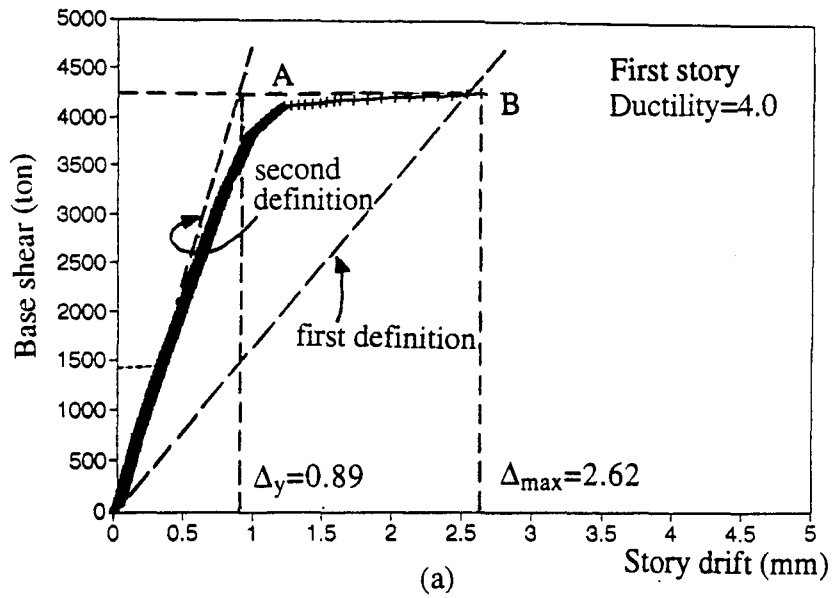
Figure 96 Relationship of base shear vs. story drift as critical story reaches flexural failure

increments. The highly plastic property of shear walls impacts on the entire behavior of a building. But ultimate lateral load does not change much due to high inelasticity. Thus, in the second definition, yielding story drift changes slightly.

V_y

$(V_s)1$

$(\Delta y)1$

$(\Delta s)1$

Δ_{max}

V

Δ

(a) First definition

V

V_y

$(V_s)2$

$(\Delta s)2$ $(\Delta y)2$

Δ_{max}

Δ

(b) Second definition
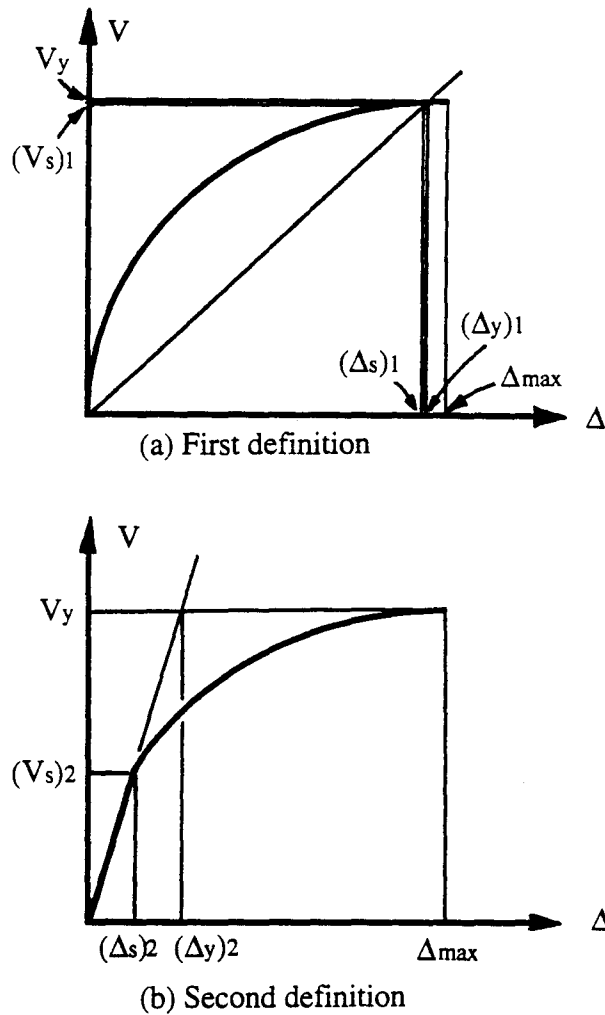
Figure 97 Two definitions in general response of a building

Table XVII shows that the range of maximum story drift $\Delta_{story,max}$ is much larger than that of yielding story drift $\Delta_{story,yield}$ (second definition). Comparing the cases of ductility=4 and ductility=8, maximum story drift $\Delta_{story,max}$ increases 76% (=(4.62-2.62)/2.62) while yielding story drift $\Delta_{story,yield}$ increases 7.8% ((0.96-0.89)/0.89). Based on first definition, yielding story drift is close to maximum story.(Assume antecedent of it is "yielding story drift".) The former results in the same high percentage ($\approx$7.6%) when comparing ductility of 4 with 8. As this table further shows, with the first definition, the corresponding allowable story drifts, Δ_s, have the same tendency as yielding story

Table XVII Summary of Δ_{max}, Δ_y and Δ_s

parameter / ductility	Δ_{max}	Δ_{y1}	Δ_{y2}	Δ_{s1}	Δ_{s2}
4.0	2.62	2.61	0.89	2.51	0.31
5.0	3.11	3.10	0.89	3.00	0.31
6.0	3.66	3.65	0.93	3.55	0.31
7.0	4.10	4.09	0.93	4.00	0.31
8.0	4.62	4.61	0.96	4.51	0.31

drift. With the second definition, allowable story drifts are the same due to the identical structure.

ii. <u>Comparison of failure story base shear</u> From Figure 96, corresponding to maximum story drift, maximum base shear can be obtained. Maximum base shear corresponds to story drift at yielding point in a linearly elastic-perfect plastic model. As these figures show, the maximum base shear for different cases of ductility is stable. As a shear wall enters into the highly inelastic range, uniform load capacity change only slightly. This results in fairly stable maximum story drift for the building.

iii. <u>Comparison of flexural and shear failure</u> Compare Figure 96 with Figure 98 for ductility=4. The former shows a building at flexural failure at the critical story while the latter shows building response at the stage of both flexural and shear failure. In Figure 96(a), story drift increases slowly until point A. After that point, shear walls SW12, SW16 go into a higher inelastic range. This causes story drift to increase more than the previous stage until point B. At that point, the critical story reaches flexural failure. If external force is still applied to the building, story drift shifts dramatically as shown at point C in Figure 98. This process continues through points D, E, F until point G is reached. During the period of story drift at points D, E, F and G, incremental story drift becomes smaller again as stress redistribution begins at point C and ends at point G. After point G, the shear wall's shear spring withstands the external force until the shear
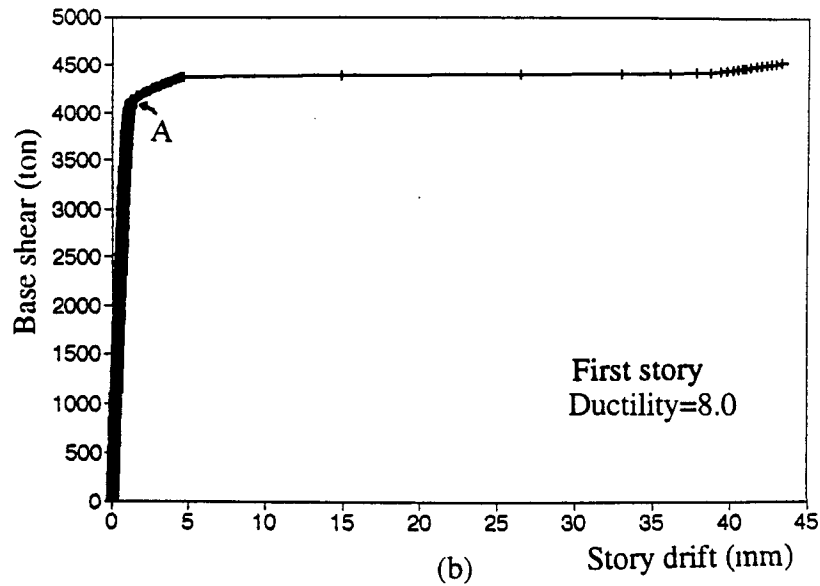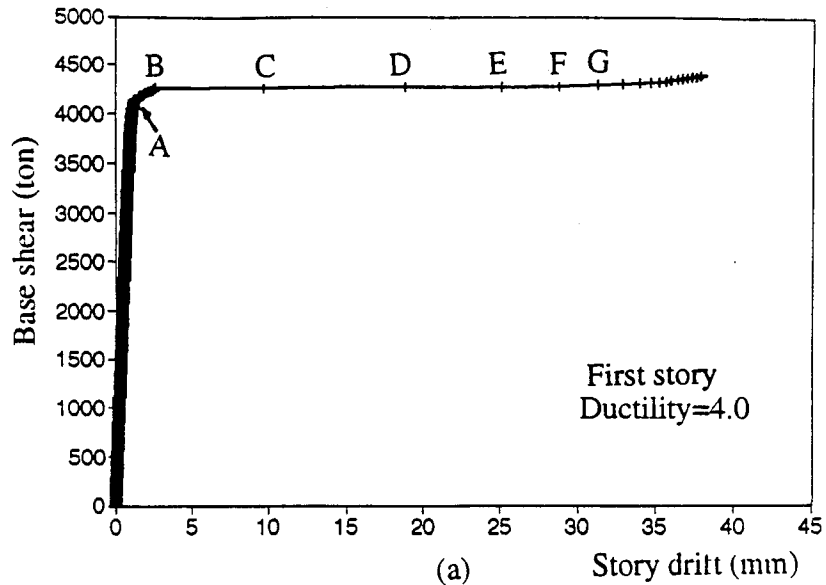
Figure 98 Relationship of base shear vs. story drift as critical story reaches both flexural and shear failure

spring of those shear walls on the critical story fails. For engineering purposes, the structure is assumed to have failed when it reaches point B.

e. Summary of observations Table XVIII shows base shear as the building reaches either flexural failure only or both flexural failure and shear failure. Comparing all cases, shear wall SW12 always fails earlier than shear wall SW16 in the flexural

Table XVIII   Summary of base shear

Ductility / Wall		4	5	6	7	8
12	(1)	4248	4280	4328	4344	4376
	(2)	4392	4432	4432	4504	4536
16	(1)	4256*	4288*	4336*	4352*	4384*
	(2)	4384	4424	4424	4496	4536

Note: (1) When rotational spring of shear wall fails
      (2) When rotational and shear springs of shear wall fail
      Unit: ton
      *Failure base shear (=V_y)

mode. Since ductility of shear walls increases, base shear also increases. But the rate of increase is slight, such as 0.75% in comparison between cases of ductility=4 and ductility=5.

If more load increments are applied to the building after the critical story fails in the flexural mode, failure in the shear mode occurs quickly. Thus little difference exists between the flexural failure mode vs. both flexural and shear failure mode. In the case of ductulity=5, shear wall SW12 failed in flexural mode with base shear of 4280 tons and failed in both flexural and shear modes with base shear of 4432 tons, a difference of only 3.55%. Identical results occur with shear wall SW16.

D. SENSITIVITY OF DESIGN PARAMETERS BASED ON DUCTILITY

Design parameter R_w and corresponding parameters, such as ductility reduction factor R_μ, overstrength factor Ω, system ductility factor μ_s and displacement amplification factor DAF are investigated under monotonic incremental loading analysis. A summary of design parameters is shown in Table XIX.

Table XIX Summary of design parameters

Parameter / Ductility	V_s	R_μ	μ_s	Ω	R_w	DAF	DAF/FRF
4.0	(a)4240	1.80	1.004	1.004	2.53	1.41	0.557
	(b)1425		2.940	2.987	7.53	12.29	1.632
5.0	(a)4272	1.79	1.003	1.004	2.52	1.41	0.560
	(b)1425		3.490	3.009	7.54	14.70	1.950
6.0	(a)4320	1.77	1.003	1.004	2.49	1.41	0.566
	(b)1425		3.940	3.043	7.54	16.79	2.227
7.0	(a)4336	1.76	1.002	1.004	2.47	1.41	0.571
	(b)1425		4.410	3.054	7.53	18.86	2.505
8.0	(a)4368	1.69	1.002	1.004	2.38	1.41	0.592
	(b)1425		4.810	3.076	7.28	20.71	2.845

(a) line based on first definition
(b) line based on second definition

1. Ductility Reduction Factor R_μ Ductility reduction factor is defined as the ratio of maximum base shear for an elastic analysis to yielding base shear for a nonlinear analysis. Here maximum base shear for elastic analysis V_{eu} is formulated as ZICW. Based on UBC design code, Z is seismic zone factor, I is important factor and C is numerical coefficient of $1.25S/T^{2/3}$ (S being site coefficient for soil characteristics and T being fundamental period). For analytic purposes, Z=0.4, I=1 and C=2.75. Thus elastic maximum base shear equals 8360 tons. As shown in Table XIX, R_μ is a stable factor with the range of 1.7~1.8. If the maximum base shear from elastic anaysis is 10,000 tons, the actual yielding wall is 5555.6~5882.4 tons (=10,000/R_μ), about 60% of elastic maximum base shear.

2. <u>Overstrength Factor Ω</u>   The ratio of the building's actual failure base shear to the base shear based on USD design is defined as overstrength factor Ω. In a dominant shear wall building, particularly with two main shear walls on the critical story, the overstrength factor is almost equal to 1.0 in the first definition and equal to 3.0 in the second definition.

3. <u>System Ductility Factor μ_s</u>   System ductility factor μ_s is the function of maximum critical story drift $\Delta_{story,max}$ and yielding critical story drift $\Delta_{story,yield}$ which is represented as $\Delta_{story,max}/\Delta_{story,yield}$. In the first definition, when yielding story drift is close to maximum critical story drift, the constant system ductility factor is equal to 1.0. In the second definition, the yielding critical story drifts $\Delta_{story,yield}$ are generally stable with a range of 0.89 to 0.96. If ductility of shear wall is changed here, maximum critical story drift $\Delta_{story,yield}$ is quite different. Therefore system ductility factor μ_s has a wide range of 2.94~4.81.

4. <u>Force Reduction Factor R_w</u>   Force reduction factor R_w is the ratio of maximum base shear for elastic analysis to base shear based on all allowable stress design. Force reduction factor R_w is also the function of ductility reduction factor R_μ, overstrength factor Ω and load factor Y (usually 1.4). All the factors R_μ, Ω and Y are stable. Force reduction factor R_w is likewise stable with a value of 2.53~2.70 based on the first definition and 7.28~7.54 based on the second definition. It can be treated as 3 for the first definition and 7.5 for the second definition. Compare these values with UBC-defined force reduction factor $R_w=6$ for the bearing wall structural system with the main element of concrete shear walls. The estimated force reduction factor is half the UBC design factor for this box-type industrial building in the first definition but larger by 25% than that of the UBC design factor in the second definition.

5. <u>Displacement Amplification Factor DAF</u>   Displacement amplification factor is defined as the ratio of maximum critical story drift to allowable critical story drift. This factor is also a function of system reduction factor μ_s, overstrength factor Ω and load

factor Y, represented as DAF=$\mu_s \Omega$Y. Since system reduction factor μ_s is stable, this parameter can be assumed to be load factor, Y, and equals 1.4, with other factors identical to 1.0. On the basis of second definition, system reduction factor μ_s is not stable (2.94~4.81). Thus the displacement amplification factor DAF is not stable, and ranges between 12.29 and 20.71, depending on ductility used in the analysis.

E. SUMMARY

Concerning static analysis with monotonic incremental load for box-type RC shear wall dominant structures, design parameter R_w is a stable value. This value is half the UBC-based design value(=6) in the first definition but 1.25 times the UBC design parameter in the second definition. System reduction factor μ_s(≈1.0) and displacement amplification factor DAF(1.40) in the first definition are stable constants. In the second definition a wide range occurs for system ductility factor (2.94~4.81) and displacement amplification factor DAF(12.29~20.71). Parameter of overstrength factor Ω is almost equal to 1.0 in the first definition and 3.0 in the second definition for a box-type RC shear wall building. DAF/FRF in the first definition is about 0.60, less than the value of 1.0 recommended by Uang [28]. DAF/FRF is 1.6~2.8 in the second definition. Furthermore, ductility reduction factor R_μ is stable, with a range of 1.7~1.8.

Generally, for frame type structures, occurrence of the first plastic hinge yields a definition of design parameters identical to the second definition in Figure 97. If the concept of the first plastic hinge applies to RC shear-wall-dominating buildings, then design parameters will not follow Figure 97(b) but Figure 97(a). Thus the concept of the first plastic hinge is not adequate to define design parameters for RC shear-wall-dominating structures.

IX. RESPONSE STUDY OF THREE-STORY COMMERCIAL BUILDING

A three-story building with RC solid shear walls and columns is studied to investigate the characteristics of low-rise shear wall structures. This building is for commercial use in Pleasant Hill, California [61]. Other structures with perforated shear walls (i.e., shear wall with openings), modified from the above building, are also used to obtain more information on design parameters based on monotonic static analysis. Conceptually, openings on a shear wall decrease its shear capacity. Behavior of columns, connected to shear walls in these buildings, is described later.

A. CONFIGURATION

This three-story commercial building (CSMIP Station No. 58348) in Pleasant Hill, California consists of shear walls, columns, wood-type floors, and plywood diaphragms on each story. Locations and corresponding directions of sensors on each story are shown in Figure 99. In Figure 99(a), a vertical profile of the building on N-S elevation shows that only one sensor was set up to measure vertical spectral response while two were used for horizontal measurement in N-S direction. Ground, third floor, and roof level have two sensors in E-W direction. The measurement near building's center in E-W direction is applied only to third floor and roof levels. Locations and directions of sensors are numbered as shown in Figure 99(b), (c), and (d).

Layout of the framing plan at ground level is shown in Figure 100. Shear walls SW1 and SW2 on both sides of the building are in X direction while SW3, SW4, SW5 and SW6 on both sides of the building are in Y direction. These walls are 20' x 16' x 6". Columns on both sides of the shear wall are 24" x 24". Others have a dimension of 18" x 18". A summary of columns is shown in Table XX. An 18" x 18" column was reduced to 12" x 18" at the joint where the floor connects to the column. This reduced column section was adopted for the load-displacement calculation of the column's top. The
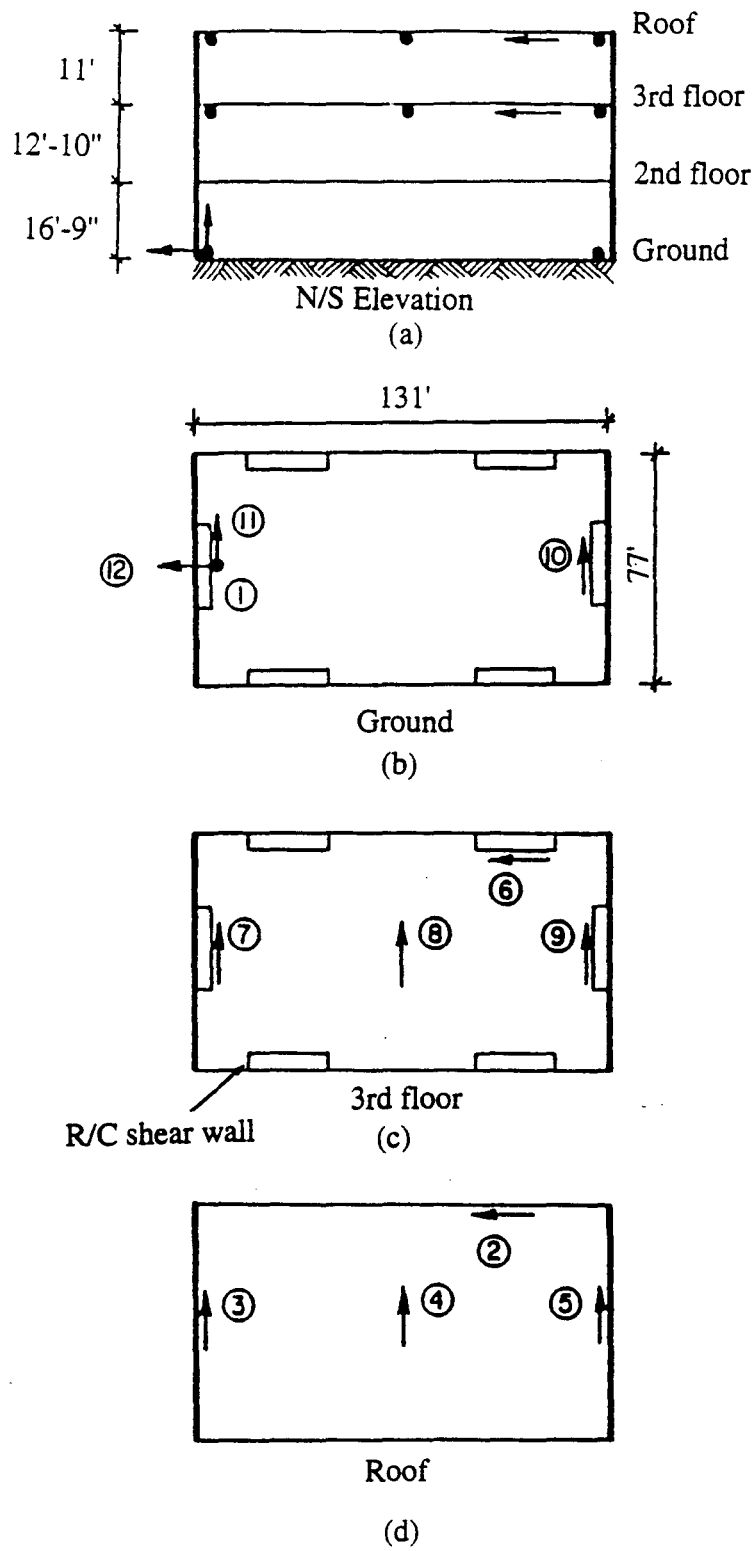
Figure 99 Location and orientation of sensors in three-story commercial building
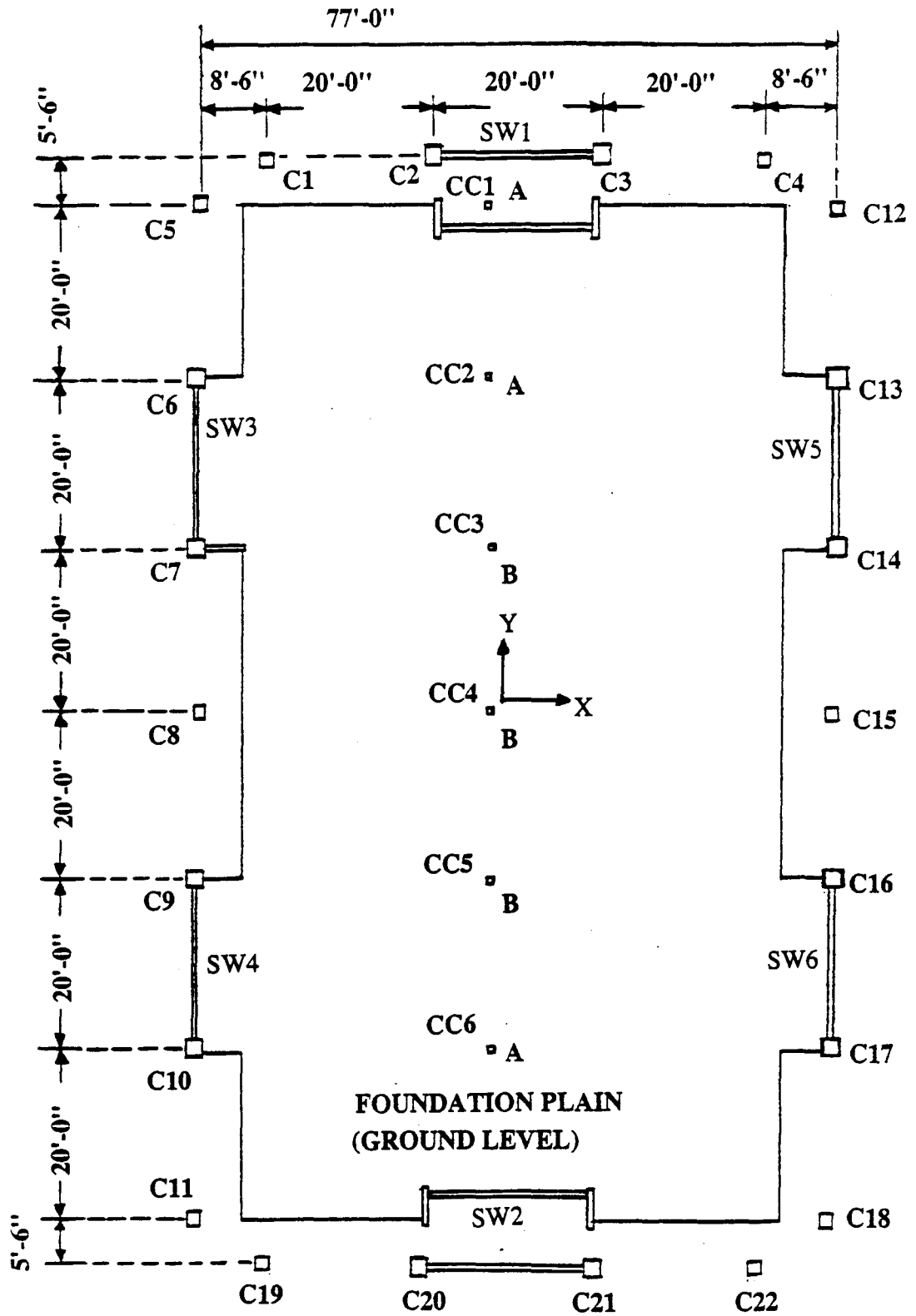
Figure 100 Layout of framing plan on ground level of three-story commercial building

Table XX Summary of columns on foundation plan (ground level)

Column	Size	Type
C1	18" x 18"	1
C2	24" x 24"	2
C3	24" x 24"	2
C4	18" x 18"	1
C5	18" x 18"	1
C6	24" x 24"	2
C7	24" x 24"	2
C8	18" x 18"	1
C9	24" x 24"	2
C10	24" x 24"	2
C11	18" x 18"	1
C12	18" x 18"	1
C13	24" x 24"	2
C14	24" x 24"	2
C15	18" x 18"	1
C16	24" x 24"	2
C17	24" x 24"	2
C18	18" x 18"	1
C19	18" x 18"	1
C20	24" x 24"	2
C21	24" x 24"	2
C22	18" x 18"	1

bottom of column thus has the material property based on an 18"x 18" section. In between the columns, glass curtain walls were installed to form all the exterior walls at the first story. Plywood diaphragms were used for interior walls. Six interior columns

213

made of steel tubing were put in the middle of the building's short span to support the dead load transferred from the above structural elements through beam.

Figure 101 shows the layout of the framing plan on the second floor. Shear walls SW7 and SW8 are on both sides of the building along the X direction. Shear walls SW9, SW10, SW11, and SW12 are on both sides of the building in Y direction. These walls are 18' wide, 12' high, and 6" thick. Columns on both sides of the shear wall are 24" x 24". The rest of columns are 18" x 18". A summary of columns is listed in Table XXI. A section of the 18" x 18" column is reduced to 12" x 18" at the connection of floor and column. For analytic concerns, this reduced section was input as a material property at both sides of column. Also, there are plywood diaphragms acting as interior walls.

As shown in Figure 102, the third floor framing plan has the same configuration as the second floor except a slightly different layout of interior diaphragms and smaller steel interior columns. Table XXII shows details of the exterior RC columns.

For the interior joint at the connection of columns and floor, the mixed design of welded and bolted subassemblages for this connection joint is not strong enough to transfer all the force. This is particularly true of subassemblages which are small in size. Thus the connection joint could be regarded as hinge. It should be noted that the connection between second and third floors is the same as that between roof and third floor.

B. MASS CALCULATION

The building's mass is mainly composed of walls, columns and floor. Walls include shear walls, curtain walls, and interior walls. Columns consist of exterior and interior columns. Floor is composed of plywood, joists and glue-laminated beams. Subassemblages such as stairs, penthouse, ceilings and precast concrete panels are also taken into account in the mass computation. Here a precast concrete panel was designed
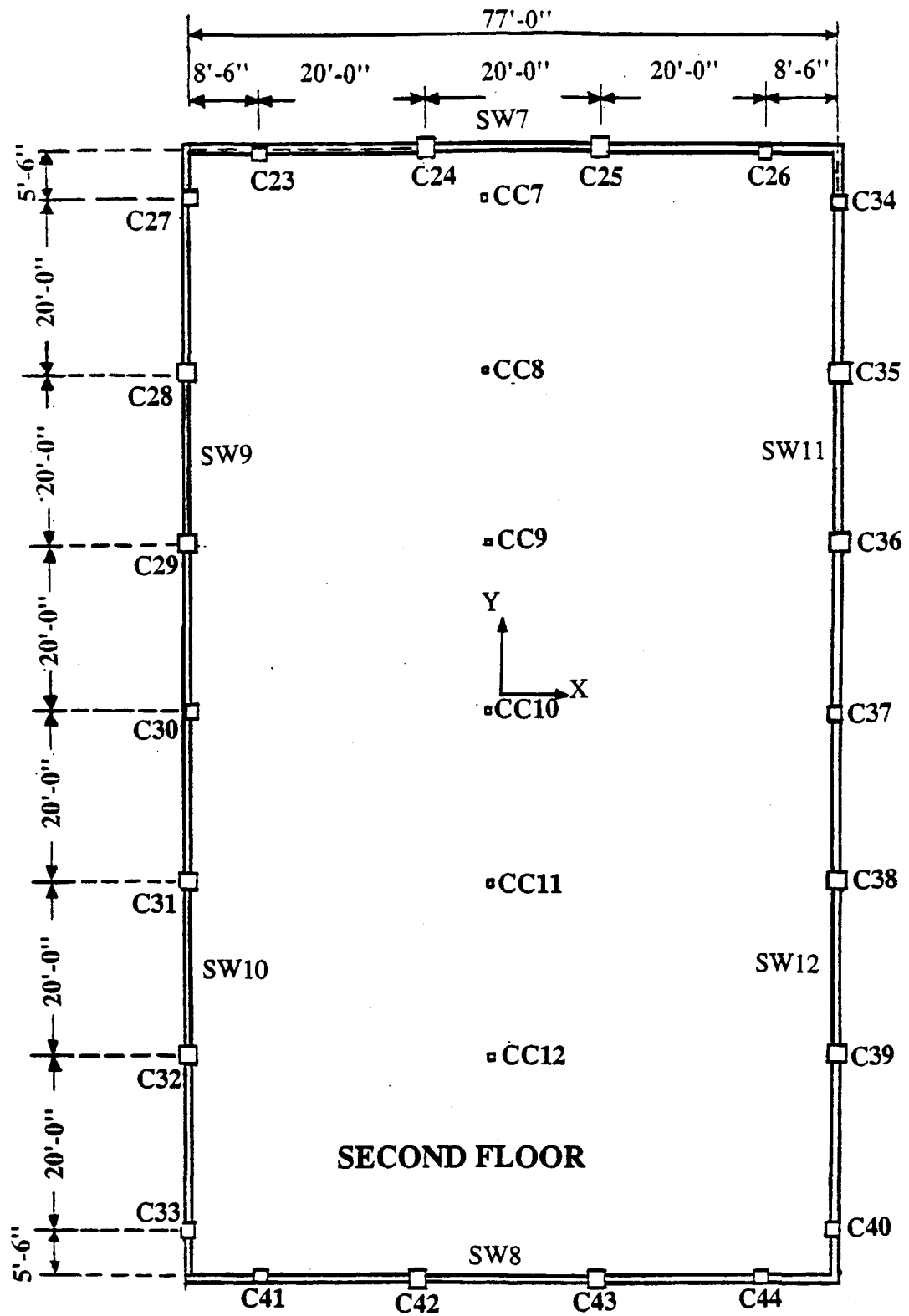
Figure 101 Layout of framing plan on second floor of three-story commercial building

Table XXI Summary of columns on second floor framing plan

Column	Size	Type
C23	18" x 12"	3
C24	24" x 24"	2
C25	24" x 24"	2
C26	18" x 12"	3
C27	18" x 12"	3
C28	24" x 24"	2
C29	24" x 24"	2
C30	18" x 12"	3
C31	24" x 24"	2
C32	24" x 24"	2
C33	18" x 12"	3
C34	18" x 12"	3
C35	24" x 24"	2
C36	24" x 24"	2
C37	18" x 12"	3
C38	24" x 24"	2
C39	24" x 24"	2
C40	18" X 12"	3
C41	18" X 12"	3
C42	24" x 24"	2
C43	24" x 24"	2
C44	18" X 12"	3
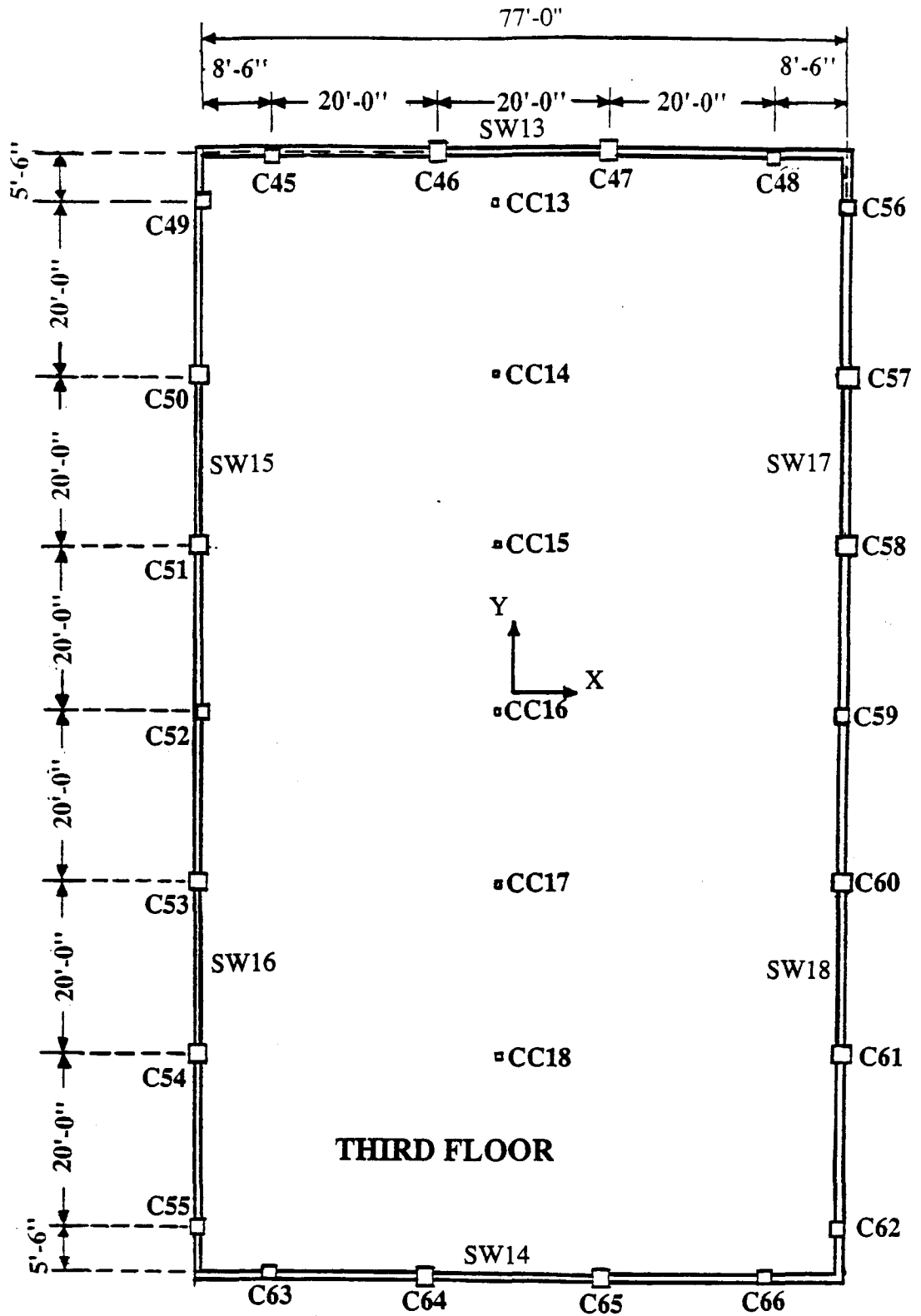
Figure 102 Layout of framing plan on third floor of three-story commercial building

Table XXII Summary of columns on third floor framing plan

Column	Size	Type
C45	18" x 12"	3
C46	24" x 24"	2
C47	24" x 24"	2
C48	18" x 12"	3
C49	18" x 12"	3
C50	24" x 24"	2
C51	24" x 24"	2
C52	18" x 12"	3
C53	24" x 24"	2
C54	24" x 24"	2
C55	18" x 12"	3
C56	18" x 12"	3
C57	24" x 24"	2
C58	24" x 24"	2
C59	18" x 12"	3
C60	24" x 24"	2
C61	24" x 24"	2
C62	18" X 12"	3
C63	18" X 12"	3
C64	24" x 24"	2
C65	24" x 24"	2
C66	18" X 12"	3

for decoration of the building. Masses and locations for all the joints of the building are shown in Table XXIII and Figure 103. The weight of each floor is

weight of second floor	= 221.547 tons
weight of third floor	= 200.702 tons
weight of roof	= 144.982 tons
total weight	= 567.231 tons

and mass centers are then obtained (see Table XXIV).

C. LOAD-DISPLACEMENT RELATIONSHIP OF SHEAR WALLS

1. Solid Shear Walls Eighteen shear walls comprise this three-story commercial building. They can be categorized as two types of shear walls. Category 1 refers to shear walls at the first story. Category 2 refers to shear walls at second and third story. Shear wall height mainly differentiates Category 1 and 2. Ductility equal to 4 and 8 was used in this building. Layout of shear walls of Category 1 and 2 is shown in Figure 104(a) and (b). Corresponding bending and shear backbone curves are represented in the Figure 106. Figures 105(a) and (b) indicate bending and shear backbone curves for Category 1 shear walls. Likewise, Figures 106(a) and (b) indicate bending and shear backbone curves for Category 2 shear walls. Because the shear walls are modified later for study of design parameters, these walls are given another notation system for simplicity (see Figure 107). Since shear walls SW1 to SW6 at the first story have identical load-displacement relationship, these walls are recognized as shear wall SWA or SWC. Shear walls at the second and third story with identical load-displacement relationship are denoted as shear wall SWD, SWF, SWG and SWH. Figures 105 and 106 show shear walls with a ductility of 4. Figures 108 and 109 indicate bending and shear backbone curves for shear walls with a ductility of 8. The above configuration of shear walls is called Case 1g, part of Group I. Two other groups with additive walls are also studied to investigate structural

Table XXIII Summary of masses and locations for all joints of three-story commercial building

Joint	Mass on 2nd floor (Ton*sec**2/mm)	Joint	Mass on 3rd floor (Ton*sec**2/mm)	Joint	Mass on roof (Ton*sec**2/mm)	X-Coordinate	Y-Coordinate
201	0.4077	301	0.3548	401	0.2776	-9144.0	19964.4
202	0.7567	302	0.6703	402	0.4028	-3048.0	20040.6
203	1.0120	303	0.8928	403	0.5259	3048.0	20040.6
204	0.4077	304	0.3548	404	0.2776	9144.0	19964.4
205	0.4095	305	0.3548	405	0.2776	-9144.0	-19964.4
206	1.1190	306	0.9984	406	0.6275	-3048.0	-20040.6
207	1.1190	307	0.9984	407	0.6275	3048.0	-20040.6
208	0.4095	308	0.3548	408	0.2776	9144.0	-19964.4
209	0.4315	309	0.3680	409	0.2763	-11734.8	18288.0
210	1.1850	310	1.0780	410	0.6883	-11811.0	12192.0
211	1.1850	311	1.0780	411	0.7043	-11811.0	6096.0
212	0.6194	312	0.5631	412	0.4763	-11734.0	0.0
213	1.1850	313	1.0780	413	0.7043	-11811.0	-6096.0
214	1.1850	314	1.0780	414	0.6883	-11811.0	-12192.0
215	0.4413	315	0.3761	415	0.2875	-11734.8	-18288.0
216	0.4386	316	0.3750	416	0.2824	11734.8	18288.0
217	1.1920	317	1.0850	417	0.6944	11811.0	12192.0
218	1.1920	318	1.0850	418	0.7113	11811.0	6096.0
219	0.6264	319	0.5702	419	0.4833	11734.8	0.0
220	1.1920	320	1.0850	420	0.7113	11811.0	-6096.0
221	1.1920	321	1.0850	421	0.6883	11811.0	-12192.0
222	0.4413	322	0.3761	422	0.2875	11734.8	-18288.0
223	0.6054	323	0.5408	423	0.3792	-1104.9	18288.0
224	0.7596	324	0.7299	424	0.6236	-1104.9	12192.0
225	0.7696	325	0.7336	425	0.6579	-1104.9	6096.0
226	0.7696	326	0.7336	426	0.8618	-1104.9	0.0
227	0.7696	327	0.7336	427	0.6579	-1104.9	-6096.0
228	0.7596	328	0.7299	428	0.6212	-1104.9	-12192.0

Note: (1) All the masses must be multiplied by 0.001
       (2) Coordinate unit: mm
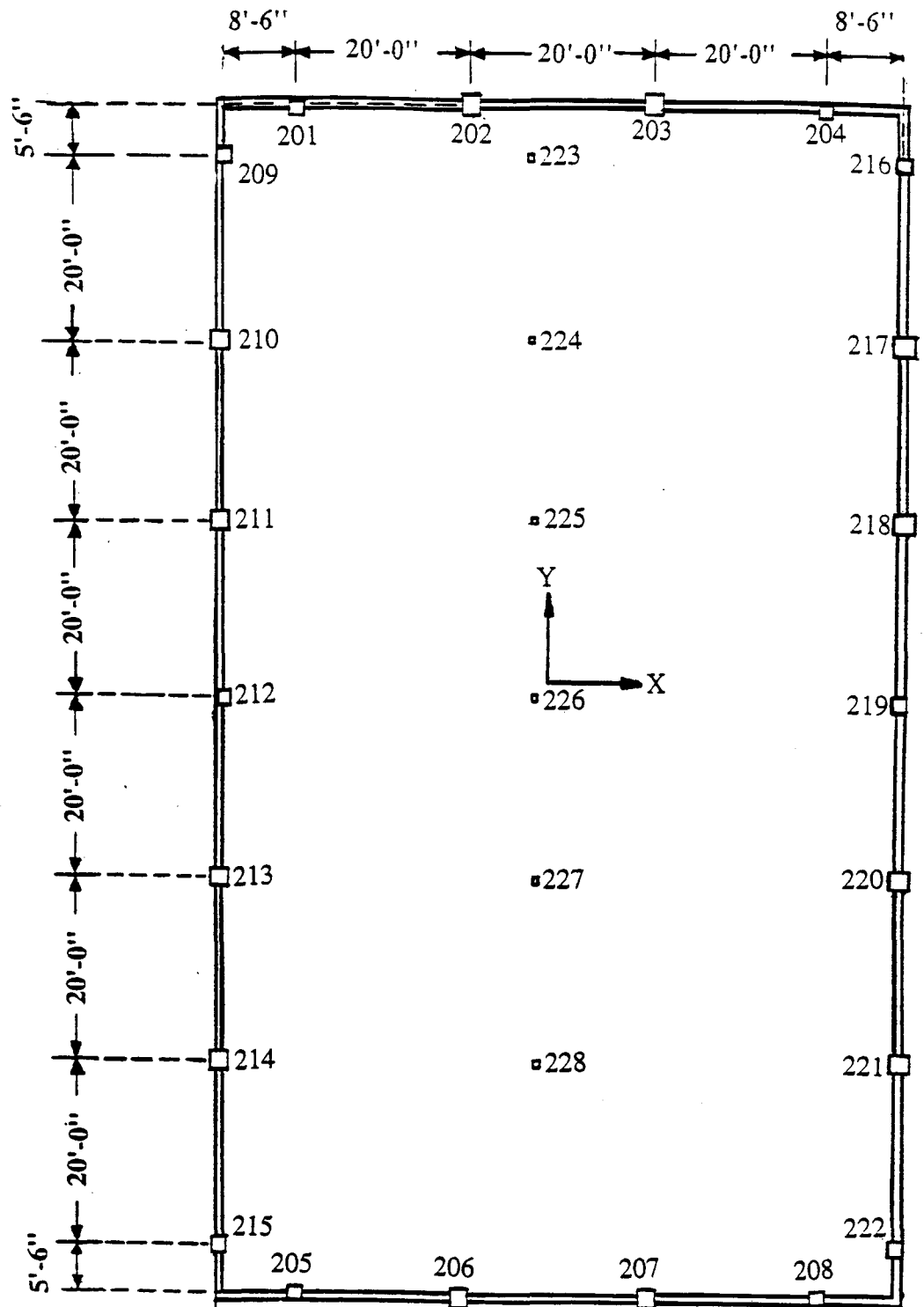
Figure 103 Location of all joints in three-story commercial building on second floor

Table XXIV Mass center on different levels of three-story commercial building

Mass center / Floor	X direction	Y direction
Second floor	-160.5	61.0
Third floor	-169.5	50.3
Roof	-232.3	13.6

* Unit = mm

responses and design parameters. Cases 2f (part of Group II) and 3f (part of Group III) have the same configuration (see Figure 110).

Groups II and III have two more shear walls than Group I. One, shear wall SWB, is in the center of the ground level, parallel to shear wall SWA. Another, shear wall SWE, is on second floor, just above shear wall SWB. Third floor walls are the same as Group I. Shear wall SWB is assumed to have one-and-a-half times the shear capacity of shear wall SWA, and three-fourths the maximum displacement of shear wall SWA (see Figure 111). Similarly, shear wall SWC has twice the shear capacity of shear wall SWA but half the maximum displacement of shear wall SWA (see Figure 112). For a ductility of 8, backbone curves of SWB and SWC are shown in Figures 113 and 114, respectively. On the second floor, shear walls SWE and SWD have identical load-displacement relationship. Note that external force is applied to the building in the X direction to study design parameters caused by different arrangement of shear walls in the same direction.
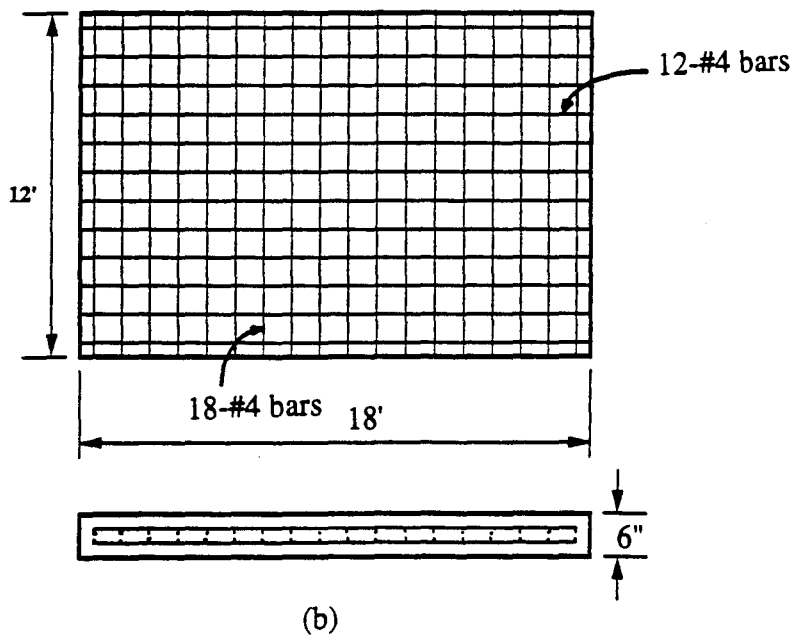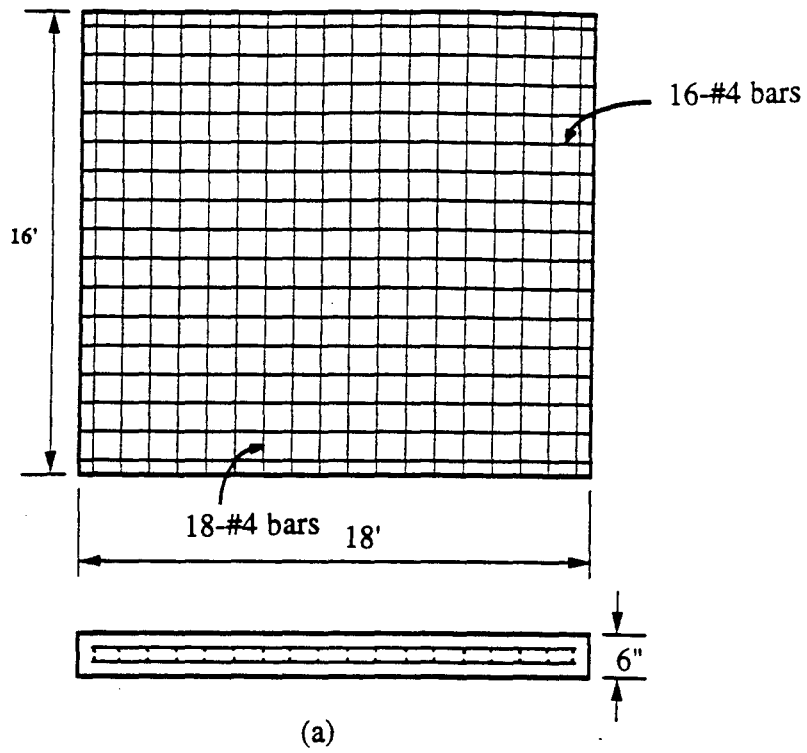
Figure 104   Layout of shear wall on (a) first (b) second story of three-story commercial building
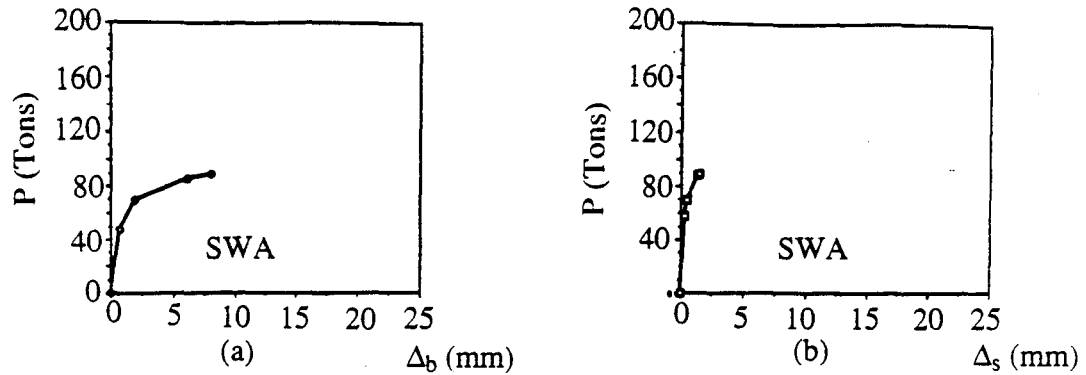
Figure 105   Bending and shear backbone curves for shear wall of Category 1
(ductility=4.0)
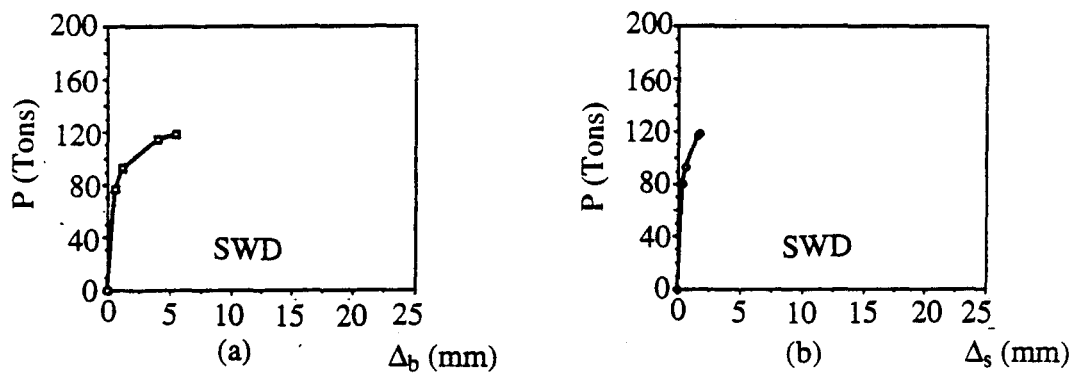
Figure 106   Bending and shear backbone curves for shear wall of Category 2
(ductility=4.0)

2. **Perforated Shear Walls** In practical terms, the use of perforated shear walls might be required for some buildings. To explore the effect of a shear wall opening on structural response of the building, some perforated shear walls are applied to the building. Table XXV summarizes the different cases in each group. Opening ratio of all perforated shear walls is assumed to be 0.1, as shown in Figure 115. Corresponding arrangement of steel as well as properties of both concrete and steel is shown in the figure. Walls are identical to solid shear walls in Group I except for openings.
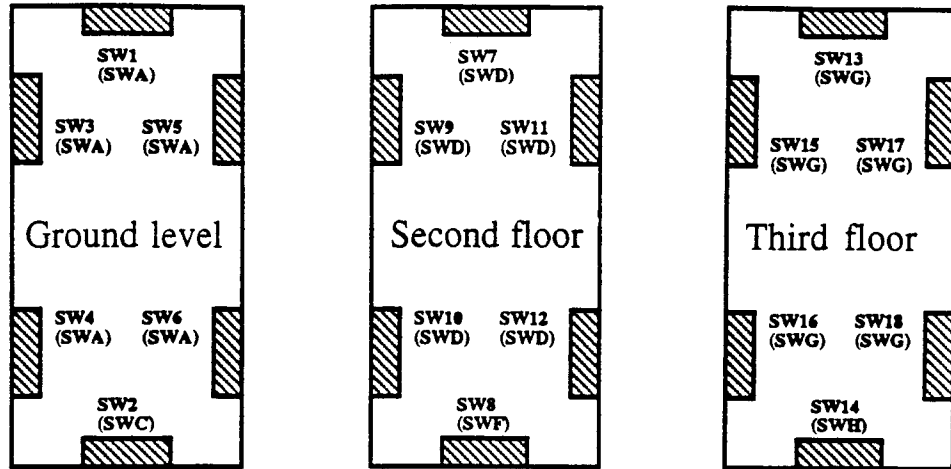
Figure 107 Notation sytstem of shear walls for three-story commercial building

(a) Δ_b (mm)   (b) Δ_s (mm)
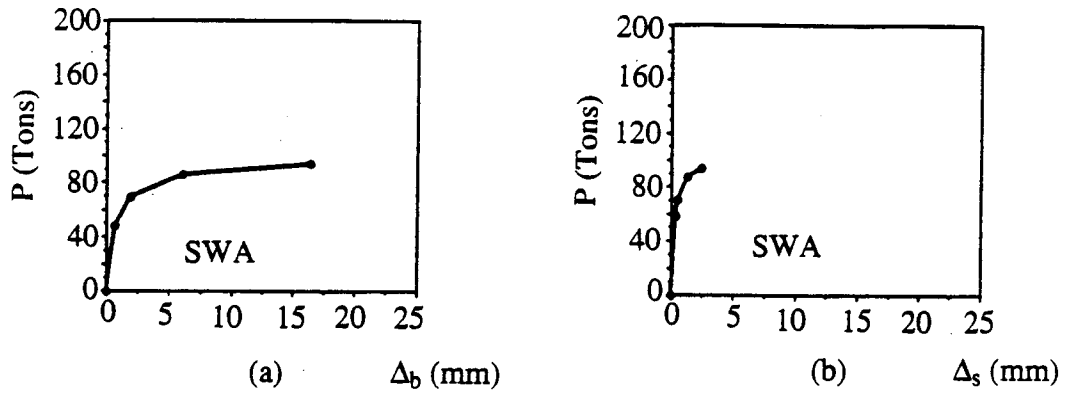
Figure 108 Bending and shear backbone curves of shear walls in Category 1
(ductility=8.0)

(a) Δ_b (mm)   (b) Δ_s (mm)
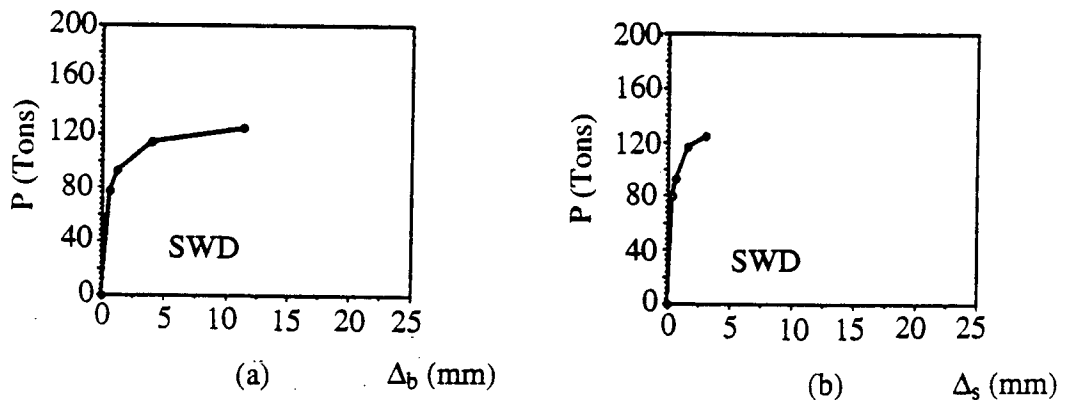
Figure 109 Bending and shear backbone curves for shear wall of Category 2
(ductility=8.0)
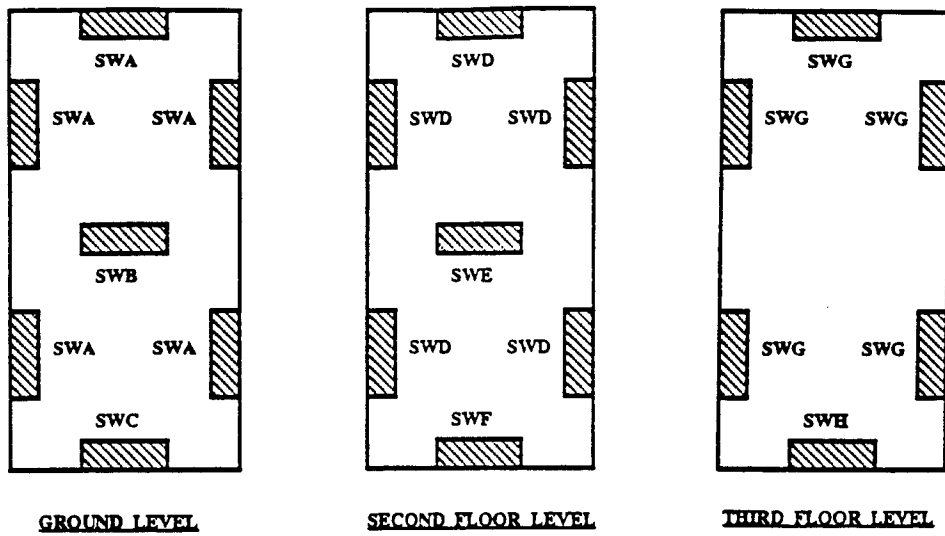
Figure 110   Layout of shear walls for cases 2a and 3a
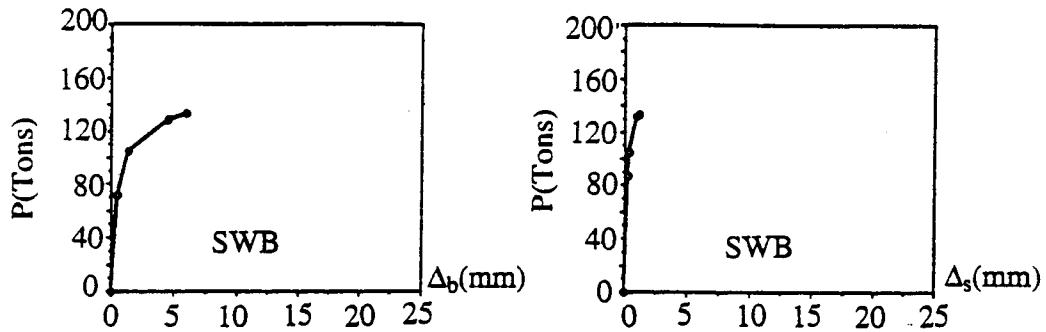
Figure 111   Bending and shear backbone curves of shear wall SWB (ductility=4.0)
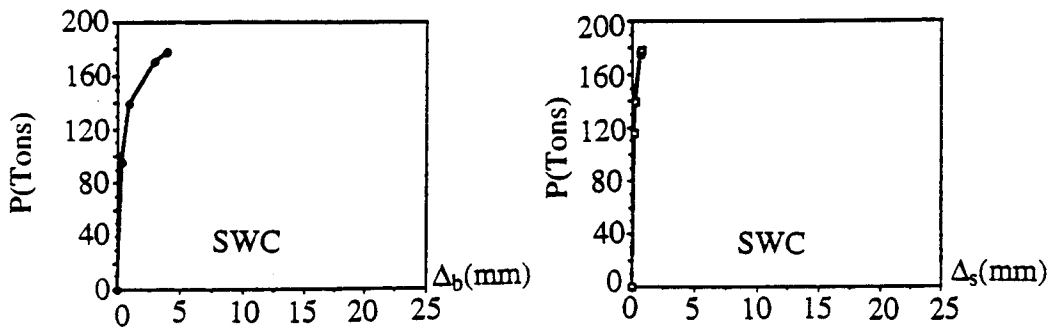
Figure 112   Bending and shear backbone curves of shear wall SWC (ductility=4.0)
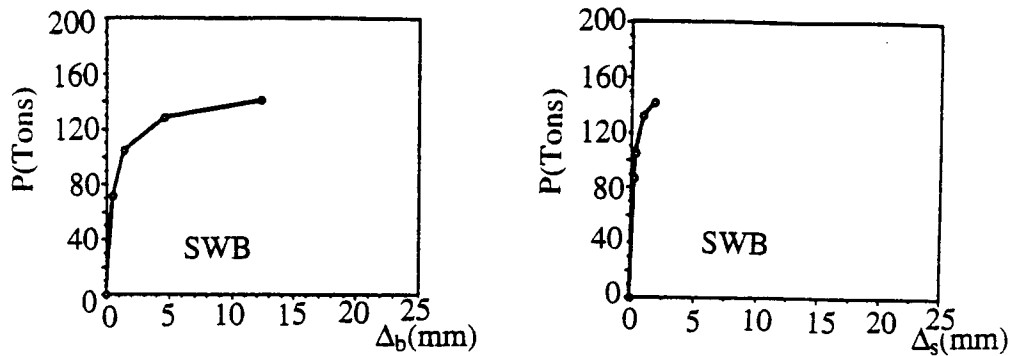
Figure 113   Bending and shear backbone curves of shear wall SWB (ductility=8.0)
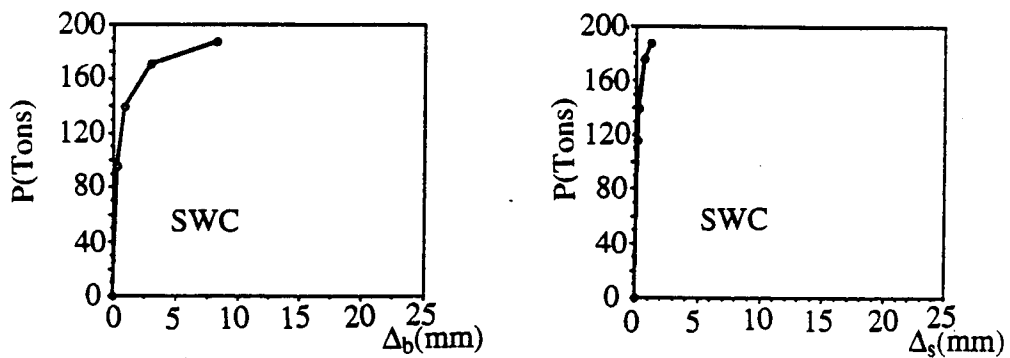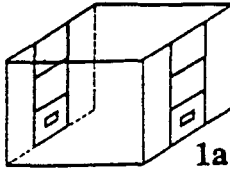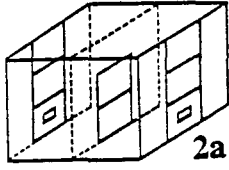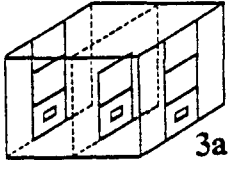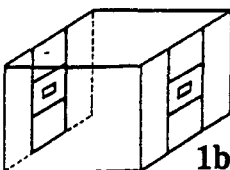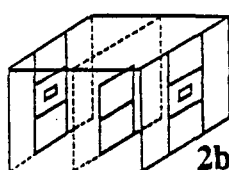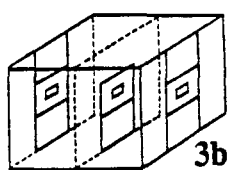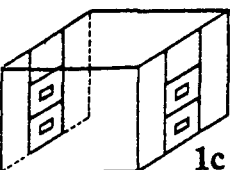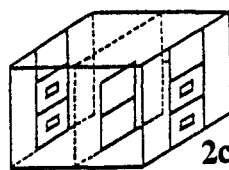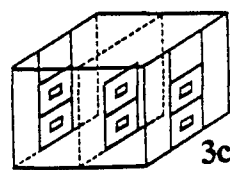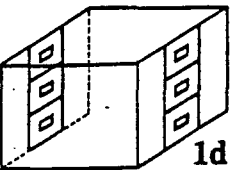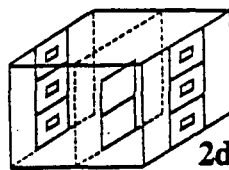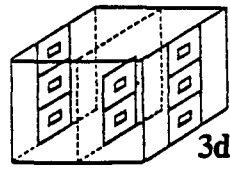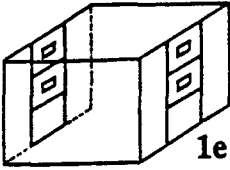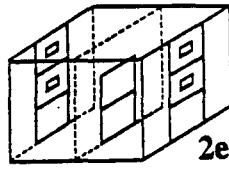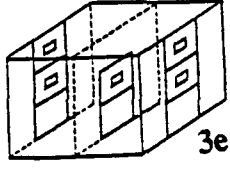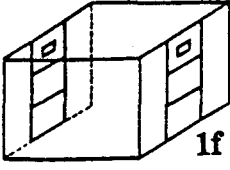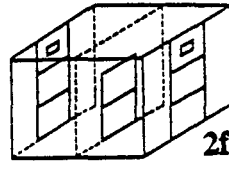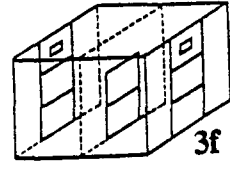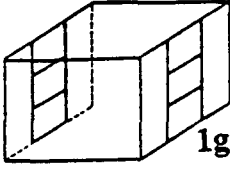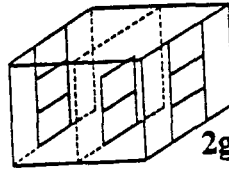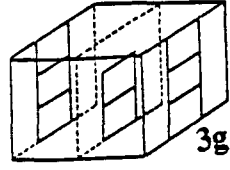
Figure 114   Bending and shear backbone curves of shear wall SWC (ductility=8.0)

Backbone curves of perforated shear walls were obtained in Figures 116 and 117. Figure 116(a) shows lateral load-total displacement $(p-\Delta_t)$ relationship (i.e., backbone curve) for a perforated shear wall, modified from shear wall SWA and called SWOA. Similarly, backbone curves of perforated shear walls SWOB, SWOC and SWOD, modified from solid shear walls SWB, SWC, and SWD, respectively, are shown in Figure 116(b). (c) and (d). Figures 116(b), (c) and (d) involve a ductility of 4.0. Figures 117(a),

Table XXV Buildings for Groups I, II and III

	Group I	Group II	Group III
a series	1a	2a	3a
b series	1b	2b	3b
c series	1c	2c	3c
d series	1d	2d	3d
e series	1e	2e	3e
f series	1f	2f	3f
g series	1g	2g	3g

Walls SWB, SWC | Walls SWD, SWE

H= 16'   H= 12'

H_o= 4' H_o= 3'

W= 18'   W= 18'

W_o= 7.2' W_o= 7.2'

Spacing= 1'   Spacing= 1'

Properties of steel and concrete refers to solid shear wall.
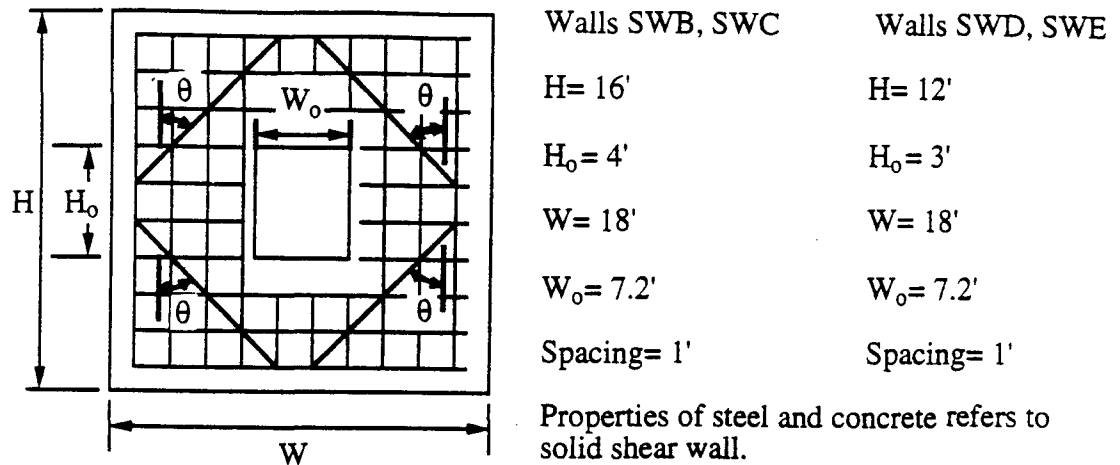
Figure 115   Schematic diagram of perforated shear wall for Groups II and III

(b), (c) and (d), with a ductility of 8.0, represent perforated shear walls SWOA, SWOB, SWOC, and SWOD, respectively.

D. LOAD-DISPLACEMENT RELATIONSHIP OF COLUMNS

Twenty-two exterior RC columns and six interior steel tubing columns are on each floor of the building. Sizes of the columns are 24" x 24" and 18" x 18". At the connection, given the precast RC wall added to the column, the size of 18" x 18" is reduced to 18" x 12". For all RC columns (18"x12" and 18"x18"), four #6 steel bars are used for vertical steel with #3 ties at a distance of 12" apart while eight #6 bars for 24"x24" columns. Steel tubings, from 7" x 7" to 5" x 3", support dead load from the floor only. The building is basically symmetric; its mass center is close to center of rigidity. When external force acts on the building, the influence of action of torsion can thus be neglected.

Due to symmetric structure and force direction along building's short span, the effect of biaxial bending in the columns is neglected [62]. As shown in Figure 118, when external load is applied in the X-direction, column bending occurs only at the Z axis of

229
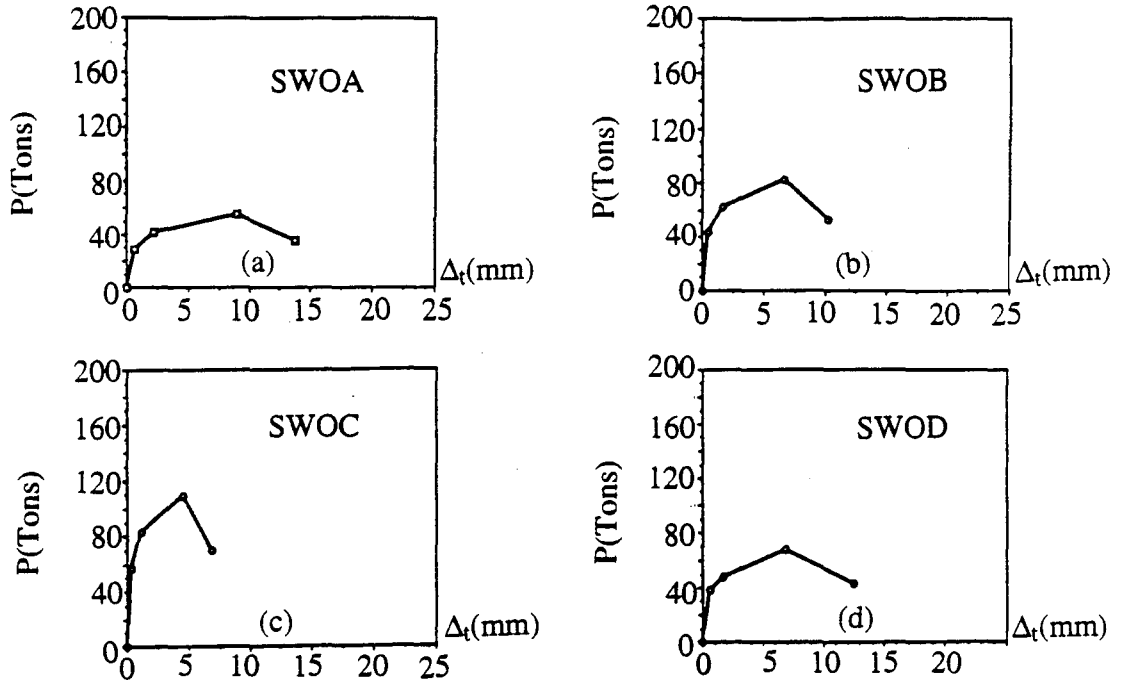
Figure 116 Lateral load vs. total lateral displacement for perforated shear walls
(ductility=4.0)
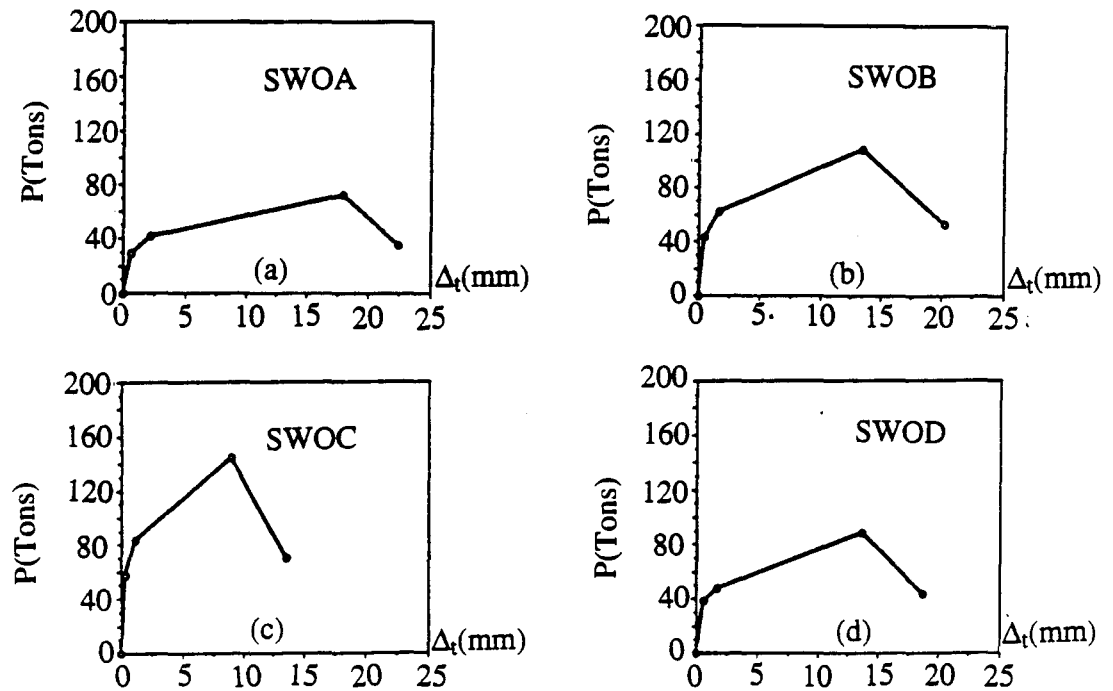
Figure 117 Lateral load vs. total lateral displacement for perforated shear walls
(ductility=8.0)
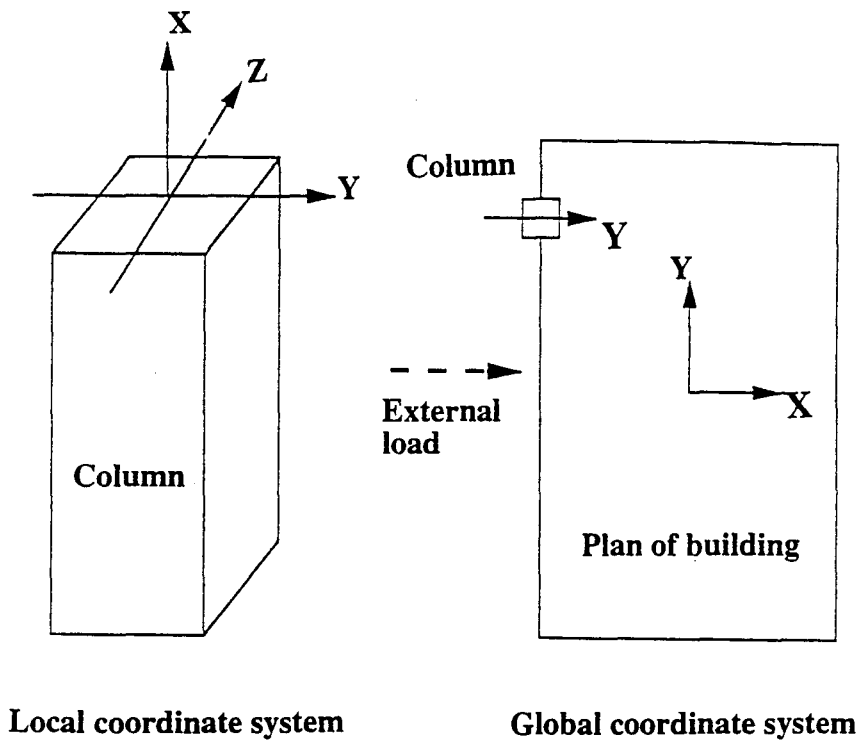
Figure 118   Relationship between local coordinate system of column and global
coordinate system

the local coordinate system. Load-displacement relationship of columns in the building
are henceforth investigated.

1. Sheikh's Model Columns with confined concrete, along with other factors,
have been studied by many researchers [63-73]. Here the analytical model for
confinement mechanisms in tied columns under flexure to large inelastic deformations
while simultaneously subjected to constant axial load, proposed by Sheikh and Uzumeri
[72], is used. In practice, confining-steel design, with axial force and shear, makes the
column exhibit ductile flexural behavior. Ductility of the column section under flexure is
strongly influenced by the level of axial load. Comparison between test and analytical
results reported by Sheikh et al. is good. This model is intended mainly to propose a
complete stress-strain relationship for confined concrete.

Based on the concept of an effectively confined concrete area within the nominal concrete core, the strength of the confined concrete can be calculated. Area of the effectively confined concrete is determined by tie spacing, distribution of longitudinal steel around the core perimeter and the resulting tie configuration. The curve of confined concrete consists of three parts. Further explanation of the curve is given to Appendix A.

Based on Sheikh's model of confined concrete, column C1 with dimensions of 24" x 24" is studied and this column's load-displacement relationship is obtained. Note that the extreme fiber concrete strain is assumed to be 0.003.

Column C1 is subjected to an axial load (i.e., dead load of 31.8 tons) typical for columns on both sides of the shear wall. For steel properties, yielding stress of 60,000 psi (strain = 0.0017) is assumed.

Strength design method was applied to the column's cross section with consideration of factored load, 1.4(dead load)+ 1.7(live load). Eighty psf was assumed as the live load. With different eccentricity, column C1 with a constant dead load of 31.8 tons results in the moment-curvature relationship shown in Figure 119. Material properties of confined concrete after plateau portion are not considered in Figure 119. Further detail about strength design method, see Wang and Salmon [62].

2. Theoretical Model Conventional strength of unconfined concrete was used in theoretical computation of structural elements or structures. This approach uses strength design method along with factored load acting on the specimen. Results of moment vs. curvature for column C1 are depicted in Figure 120. Point B in the figure shows that the strain of extreme fiber concrete reaches 0.003, maximum strain of concrete material property.

3. Result Comparison of Sheikh and Theoretical Models Figures 119 and 120 show that below a curvature near 5.9×10^{-5} rad/mm (0.0015 rad/in), two main parts constitute these curves. One is from origin to point a (Figure 119), the other from origin to point A (Figure 120), indicating the steel has not yielded yet. The slight difference
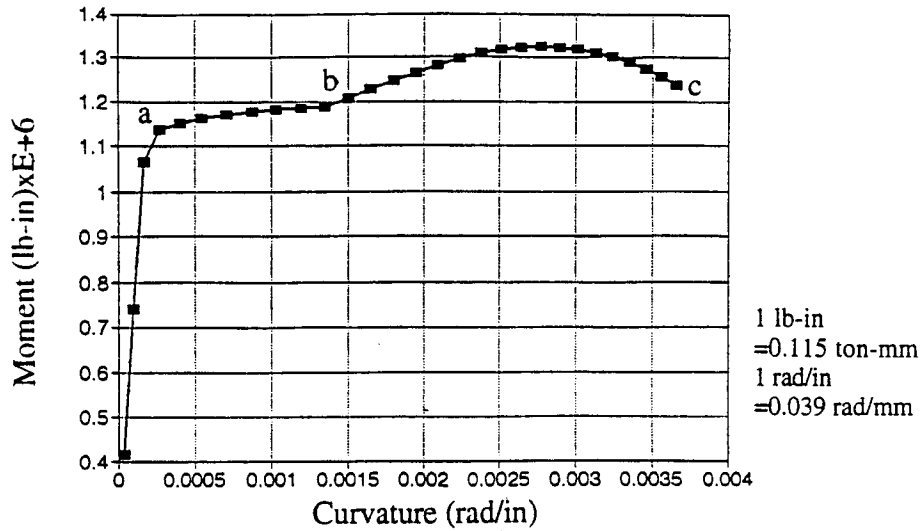
Figure 119 Moment-curvature relationship of column C1 concerning confined concrete
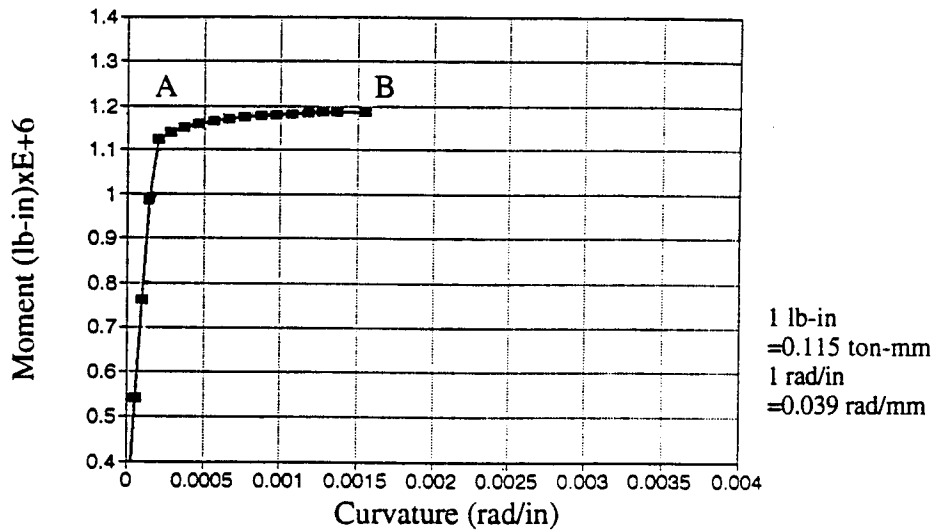
Figure 120 Moment-curvature relationship of column C1 concerning unconfined concrete

between these two parts (from origin to point a or A) arises mainly from the shape of the concrete at an early stage. Generally, the curvature from origin to point a or A is basically the same. When steel bars yield, the curves after point a (or A) reach a plateau stage. Behavior at this stage is fairly uniform until point B or b is reached. Based on

233

Sheikh's model, slightly higher strength capacity is predicted. One reason for this may be that confined concrete provides somewhat more strength than plain concrete. Sheikh's model allows confined concrete a larger ductility after concrete reaches a strain of 0.003. Thus the progression from point b to point c in Figure 119 shows that the column has greater strength and can bend more. A comparison of Figures 119 and 120 shows the main difference between confined and plain concrete. Before concrete reaches a strain of 0.003, both curves show little difference. When concrete strain is larger than 0.003, column behavior with confined concrete gains much more curvature ductility and somewhat more strength capacity. For analytic purposes, the theoretical model with plain concrete is used.

4. Load-Displacement Relationship of Other Columns Three groups of columns are studied based on their material and size as follows: (1) RC exterior columns with a size of either 18" x 18" or 18" x 12"; (2) RC exterior columns with a size of 24" x 24"; (3) interior steel columns with different sizes from floor to floor. RC columns are all exterior columns whose load-displacement relationship is computed based on the theoretical model just discussed. Steel columns can be checked by the design manual.

a. Columns of 18" x 12" or 18" x 18" type Figure 121 shows the layout of this type of column on ground, second and third floors. Size of columns is the same except the bottom of columns at the ground level. Previous studies [62-73] indicate that the effect of axial compression, combined with flexure, on the column is important. Material properties of the column might change to some extent. To explore the load-displacement relationship of columns in this building, axial load on columns (i.e., factored load) is summarized in Table XXVI.

Column C8 subject to a dead load of 16.27 tons and a live load of 26.73 tons would result in a total factored load of 97.47 tons (i.e., = 1.4 x 16.27 tons + 1.7 x 26.73 tons), approximately equal to 100 tons as shown in Table XXVI(f). Similar calculation is

C1 (1)   C4 (4)   C23(201)   C26(204)   C45(301)   C48(304)

C5 (9)   C12 (16)   C27 (209)   C34 (216)   C49 (309)   C56 (316)

C8 (12)   C15 (19)   (212)   C37 (219)   C52 (312)   C59 (319)

C11 (15)   C18 (22)   C33 (215)   C40 (222)   C55 (315)   C62 (322)

C19 (5)   C22 (8)   C41(205)   C44(208)   C63(305)   C66(308)

GROUND LEVEL   SECOND FLOOR LEVEL   THIRD FLOOR LEVEL
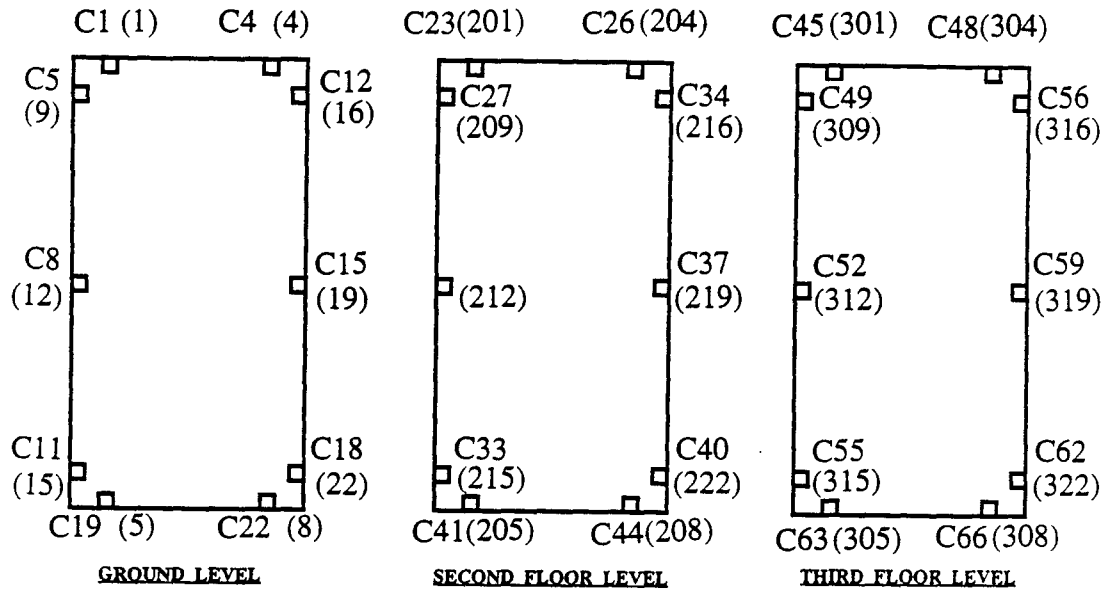
Figure 121   Layout of columns of 18" x 12" or 18" x 18" type

made for other columns. This table comprises small tables showing the same location of columns at different levels.

A cross section of rectangular form for this type of column is shown in Figure 122. It can be seen that load-displacement relationship differs along major or minor axis. Thus for each type of section (i.e., column under different axial load), the column could have two moment-curvature relationships based on the central axis shown in the cross section. This can be summarized as

(1) material properties identical to column C27: C23, C26, C41, C44, C33, C34, C40

(2) material properties identical to column C30: C37

235

Table XXVI Summary of axial load acting on columns

Column \ Load	P_u (Tons)
C45	5
C23	25
C1	50

(a)

Column \ Load	P_u (Tons)
C48	5
C26	25
C4	50

(b)

Column \ Load	P_u (Tons)
C63	5
C41	25
C19	50

(c)

Column \ Load	P_u (Tons)
C66	5
C44	25
C22	50

(d)

Column \ Load	P_u (Tons)
C49	5
C27	25
C5	50

(e)

Column \ Load	P_u (Tons)
C52	10
C30	50
C8	100

(f)

Column \ Load	P_u (Tons)
C55	5
C33	25
C11	50

(g)

Column \ Load	P_u (Tons)
C56	5
C34	25
C12	50

(h)

Column \ Load	P_u (Tons)
C59	10
C37	50
C15	100

(i)

Column \ Load	P_u (Tons)
C62	5
C40	25
C18	50

(j)
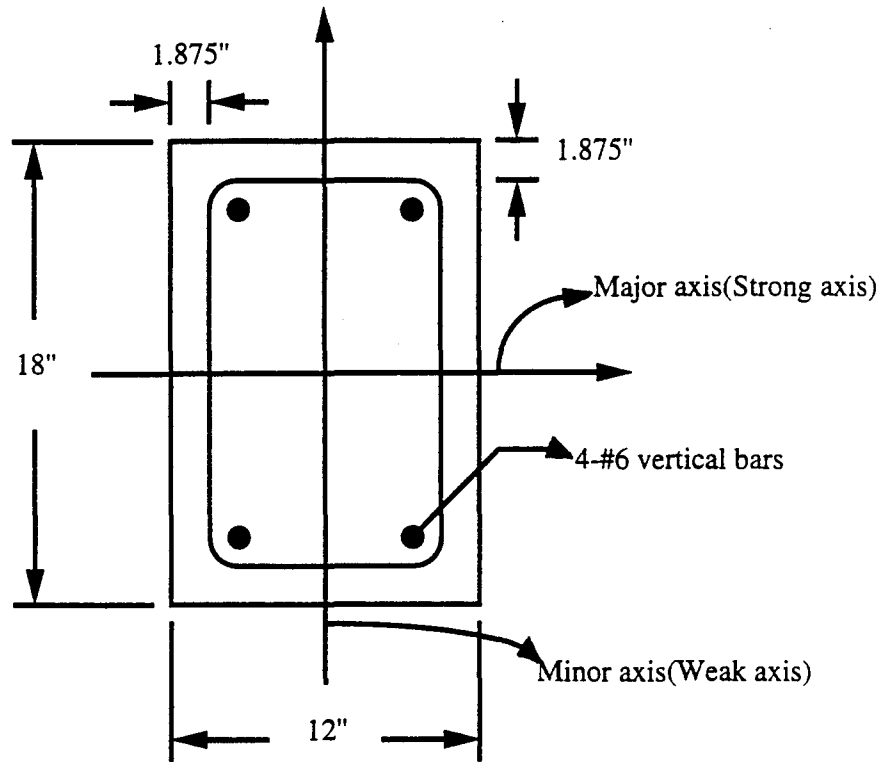
Figure 122 Cross section for column of 18" x 12" type

(3) material properties identical to column C49: C45, C48, C63, C66, C55, C56,

C62

(4) material properties of column C52

Note that all sections above (except the bottom of the column connected to ground) are the same as those shown in Figure 122.

The section of 18" x 18" is located at the ground level to which the column is connected (see Figure 123(a)). The connection at this spot is assumed to be a fixed point which can be determined from the original design. Size of the section is not reduced at this fixed connection. Two kinds of axial loads act on the same cross section of different columns. Figure 123(b) gives a clearer view of this cross section. This figure shows that

(a) Ground level   (b) vertical profile
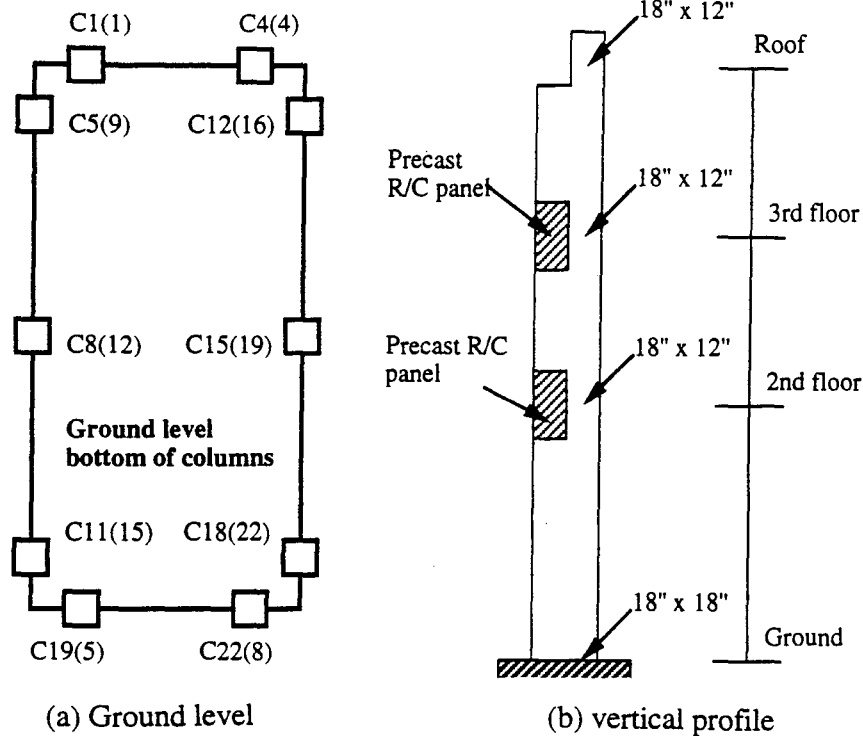
Figure 123   Layout of 18" x 18" column and its corresponding vertical profile

on the second and third floors as well as the roof, a reduced cross section of 18" x 12" was designed except for an 18" x 18" column on the ground level. Thus two groups of cross section exist with axial loads obtained as follows:

(1) material properties identical to column C1(b): C4(b), C19(b), C22(b), C5(b),C(11(b), C12(b)

(2) material properties identical to column C8(b): C15(b)

where (b) refers to the bottom cross section of the column.

Column C1's moment-curvature relationship was described in previous section. Column C8's moment-curvature relationship is shown in Figure 124. Comparing Figure 120 with 124 shows that the strength capacity of column C8 is 31% larger than that of column C1. In this case, column C8 is subjected to an axial load twice that of Column C1. As to curvature, Column C8's is 28% smaller than column C1's.

238

b. <u>Columns of 24" x 24" type</u> Figure 125 shows the layout of ⁺" x 24"

columns on different levels. In this figure, it can be seen that all the 24" x 24" columns are

the boundaries of shear walls, which provide more strength capacity to resist seismic

loads. Note that the arrangement of vertical steel bars for 24" x 24" columns is not

always the same, as shown in Figure 126, but is adjusted based on the configuration. If

seismic load acts on the building in X direction, then columns along A-C and B-D mainly

resist. If seismic load acts on the building in Y direction, then columns along A-B and C-

D mainly resist. Since the strong axes of columns (i.e., major axis) along A-C and B-D

are parallel to Y direction, these columns provide most resistance to external force in the

X direction. Behavior of columns along A-B and C-D follows the same logic.

To investigate the load-displacement relationship of 24" x 24" columns, axial

loads are calculated for all the columns on each floor. A summary of axial loads is shown

in Table XXVII.
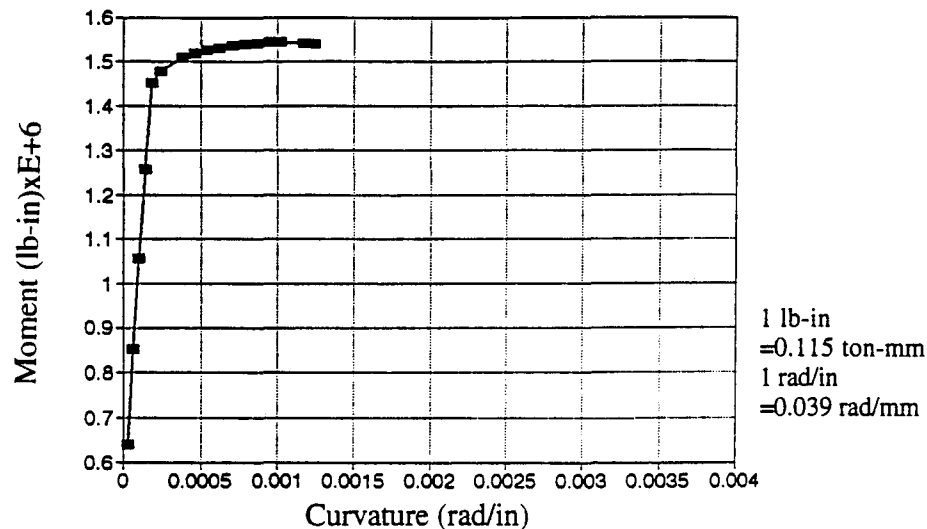
Figure 124 Relationship between moment and curvature for column C8
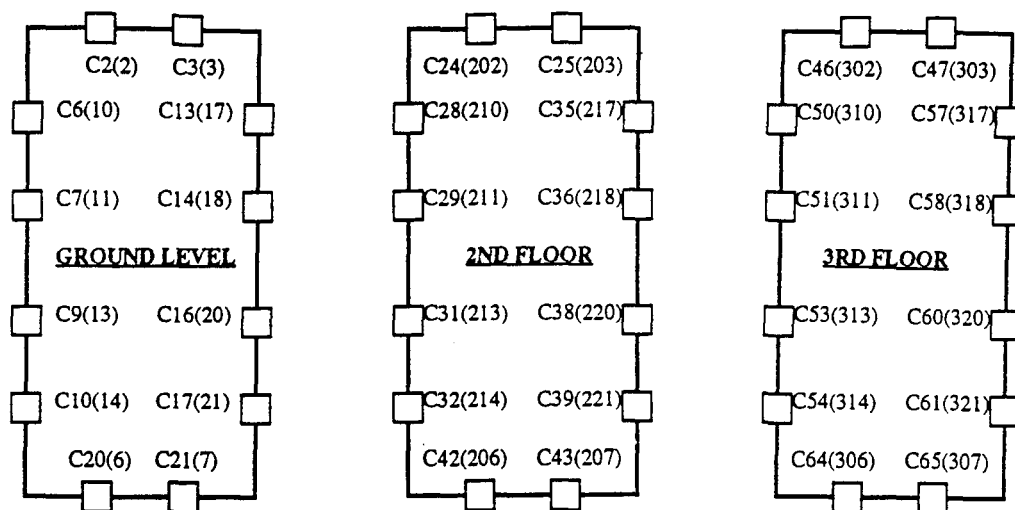
Figure 125 Layout of columns of 24" x 24" type

For analytical purposes, these columns are classified into five types on the basis of axial load (see Table XXVII). Types A, B, C, D and E refer to axial loads of 4.54 tons(=10 kips), 14.98 tons(=33 kips), 27.24 tons(=60 kips), 49.50 tons(=109 kips) and 55.84 tons(=123 kips), respectively. Corresponding moment-curvature relationship of column C2 is shown in Figures 127. In this figure, (a) refers to bending about the strong axis and (b) to bending about the weak axis. Other columns (Type A, B, D, E) have similiar moment-curvature relationship of Type C and are consequently not shown here.

c. Columns of steel tubing type All the interior columns in the building consist of steel tube, whose main purpose is to support the dead load. Material properties of these columns can be obtained from the design manual.

As noted earlier, both ends of all interior columns are assumed to be hinges. Thus all the internal moment cannot be transferred from one column to another. A ductility of 4.0 is proposed in this analysis.

240
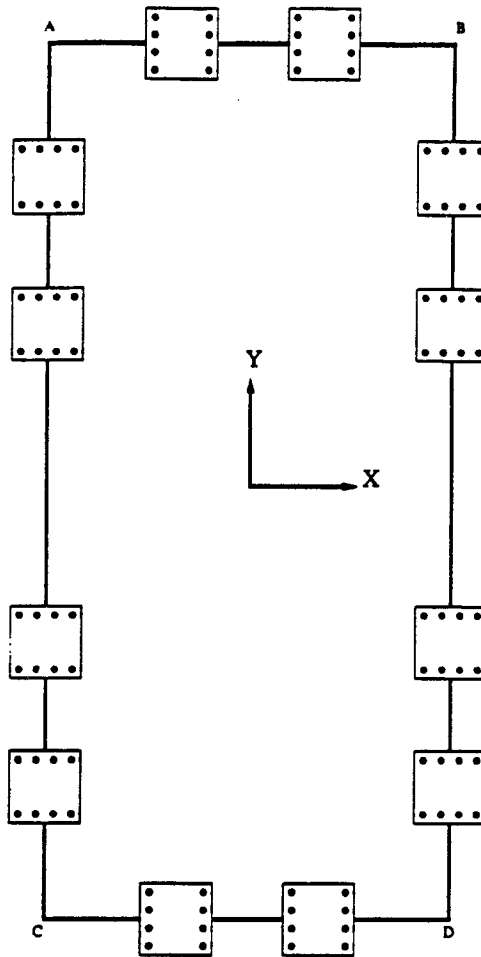
Figure 126   Configuration of vertical steel bars for 24" x 24" columns

E. MONOTONIC STATIC ANALYSIS

To analyze the response behavior of a three-story commercial building, some judgements and assumptions are made. For the floor system, $8\frac{3}{4}" \times 25\frac{1}{2}"$ beams were designed to transfer most of the dead load to exterior and interior columns for the load also partially carried by walls. Joists were connected to the beams to stablize and evenly distribute load from the plywood which covered the floor. The floor system was regarded as a rigid floor, allowing rigid-body motion in horizontal and vertical direction but not

Table XXVII   Summary of axial loads acting on columns of 24" x 24" type

Load / Column	P_u(Tons)	Type
C46	3.95	A
C24	15.00	B
C2	26.89	C

(a)

Load / Column	P_u(Tons)	Type
C47	5.16	A
C25	19.71	B
C3	35.44	C

(b)

Load / Column	P_u(Tons)	Type
C50	6.75	A
C28	30.69	C
C6	55.68	E

(c)

Load / Column	P_u(Tons)	Type
C51	6.87	A
C29	30.79	C
C7	55.80	E

(d)

Load / Column	P_u(Tons)	Type
C53	6.87	A
C31	30.81	C
C9	55.80	E

(e)

Load / Column	P_u(Tons)	Type
C54	6.75	A
C32	30.69	C
C10	55.68	E

(f)

Load / Column	P_u(Tons)	Type
C57	6.98	A
C35	31.00	C
C13	56.05	E

(g)

Load / Column	P_u(Tons)	Type
C58	6.98	A
C36	31.00	C
C14	56.05	E

(h)

Load / Column	P_u(Tons)	Type
C60	6.98	A
C38	31.00	C
C16	56.05	E

(i)

Load / Column	P_u(Tons)	Type
C61	6.98	A
C39	31.00	C
C17	56.05	E

(j)

Load / Column	P_u(Tons)	Type
C64	6.16	A
C42	27.21	C
C20	49.45	D

(k)

Load / Column	P_u(Tons)	Type
C65	6.16	A
C43	27.21	C
C21	49.45	D

(l)
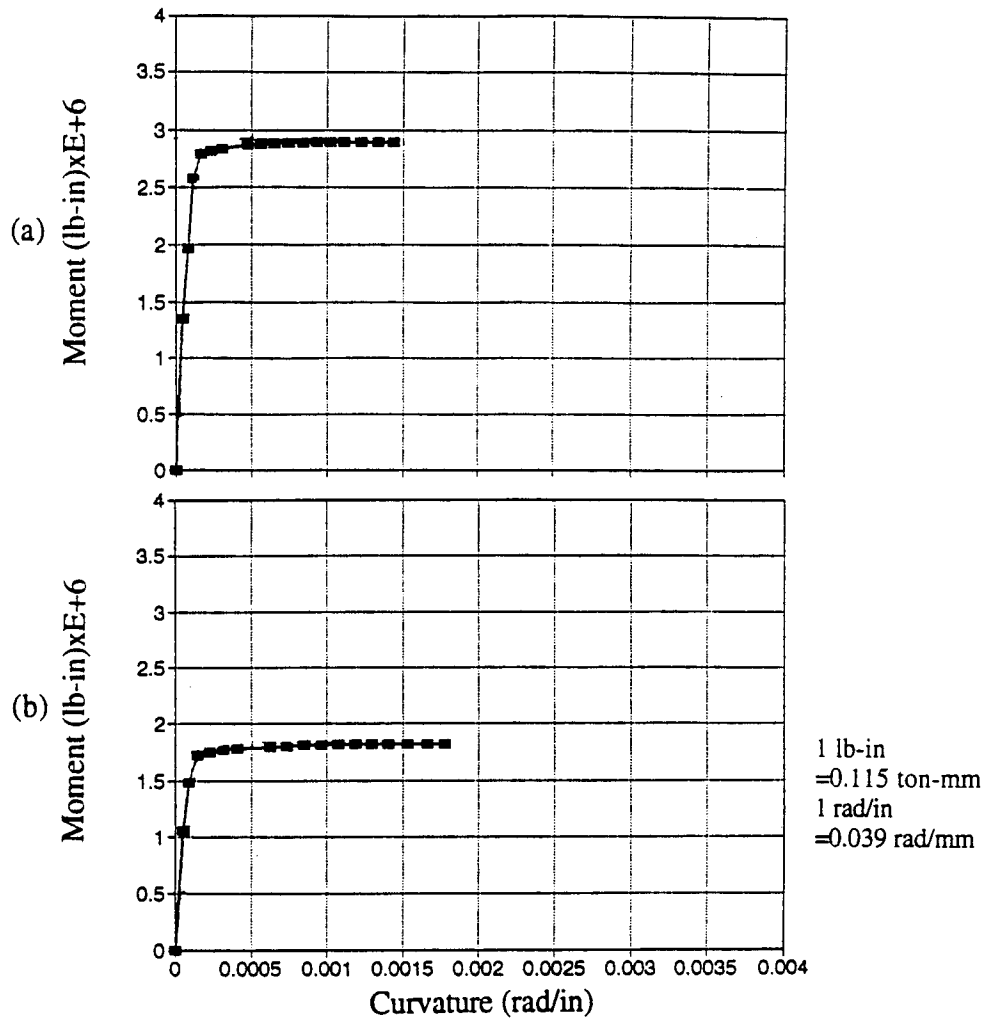
Figure 127 Moment-curvature relationship for 24" x 24" column of type C

resistance in vertical. Buckling of columns is not considered due to the small slenderness ratio. Columns and shear walls on the ground level are fixed except interior columns. Interior columns are hinged to the ground level. On the third floor, the top part of the columns is not welded to the roof. Those connections are treated as hinges.

Note that there are only two shear walls on each floor on the short span sides of the building as compared to four shear walls on the other sides. When subjected to external force, the direction parallel to the short span of the building becomes the critical

direction. As shown in Figure 128, external force is applied in the X direction. Based on UBC code design, force distribution is proportional to multiplication of weight and corresponding height for each floor because fundamental period T, equal to 0.22 second, is smaller than 0.7 second. Force distribution is thus calculated for each floor as

$$F_x = \frac{V \cdot W_x \cdot h_x}{\sum\limits_{i=1}^{n} W_i \cdot h_i} \tag{296}$$

where the notations refer to the description in the previous section.

1. <u>Overall Response Behavior</u> For simplification, shear walls applied in the force direction are denoted in Figure 129. Incremental load is 0.25 ton. Case 1b is studied here, as shown in Table XXV. The second floor has two perforated shear walls on each side of the building's short span. All others in the building are solid shear walls.

Under monotonic static loading, shear wall SW1 fails first at step 739 where base shear equals 184.75 tons, as shown at point A in Figure 130. After the first shear wall fails, first story drift increases abruptly. Simultaneously shear wall SW2 fails at the next step (i.e., base shear= 0.25 ton x 740 step = 185 tons) which is shown at point B in the figure. After point B (step 740), first story drift becomes quite large. Base shear increases slightly and more displacement occurs at the mass center of story, as point C indicates. Thus, when base shear of 185 tons is reached (point B), all shear walls in the force direction (SW1 and SW2) on the first story fail completely. After shear walls SW1 and SW2 fail, the columns on the first story gradually take over the stresses (bending and shear) initially taken by shear walls and originating from increased external load. At point D, perforated shear walls SW7 and SW8 on the second floor fail simultaneously. At base shear of 185.5 tons, the second story fails. Note that first-story columns are always in elastic range before shear walls fail. Also note that the failure of shear walls occurs in the shear failure mode. This is because most of the moment is taken
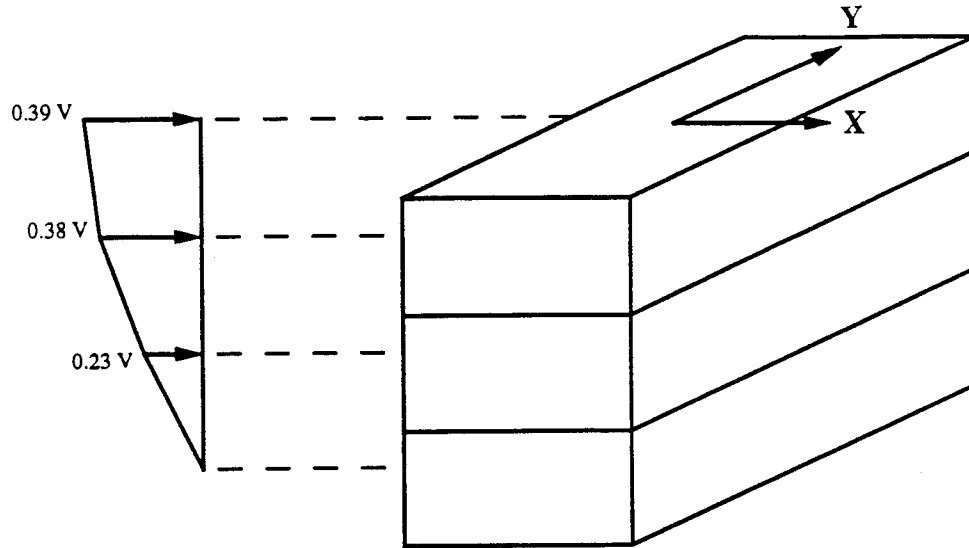
Figure 128 Vertical force distribution based on UBC code
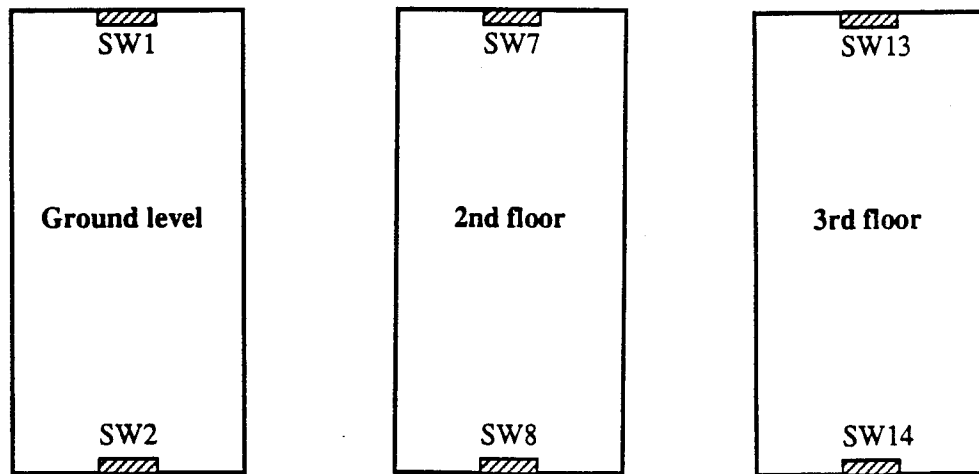
Figure 129 Notation for shear walls along short span of three-story commercial building

by columns which means shear walls then take very little moment. After shear failure occurs at the shear wall, the moment taken by columns increases dramatically and the corresponding shear can no longer be taken by the failed shear wall.

Figure 130 further illustrates shear wall control occurs before step 740, when story drift is slight. After step 740, stress redistribution occurs and columns on the first

245
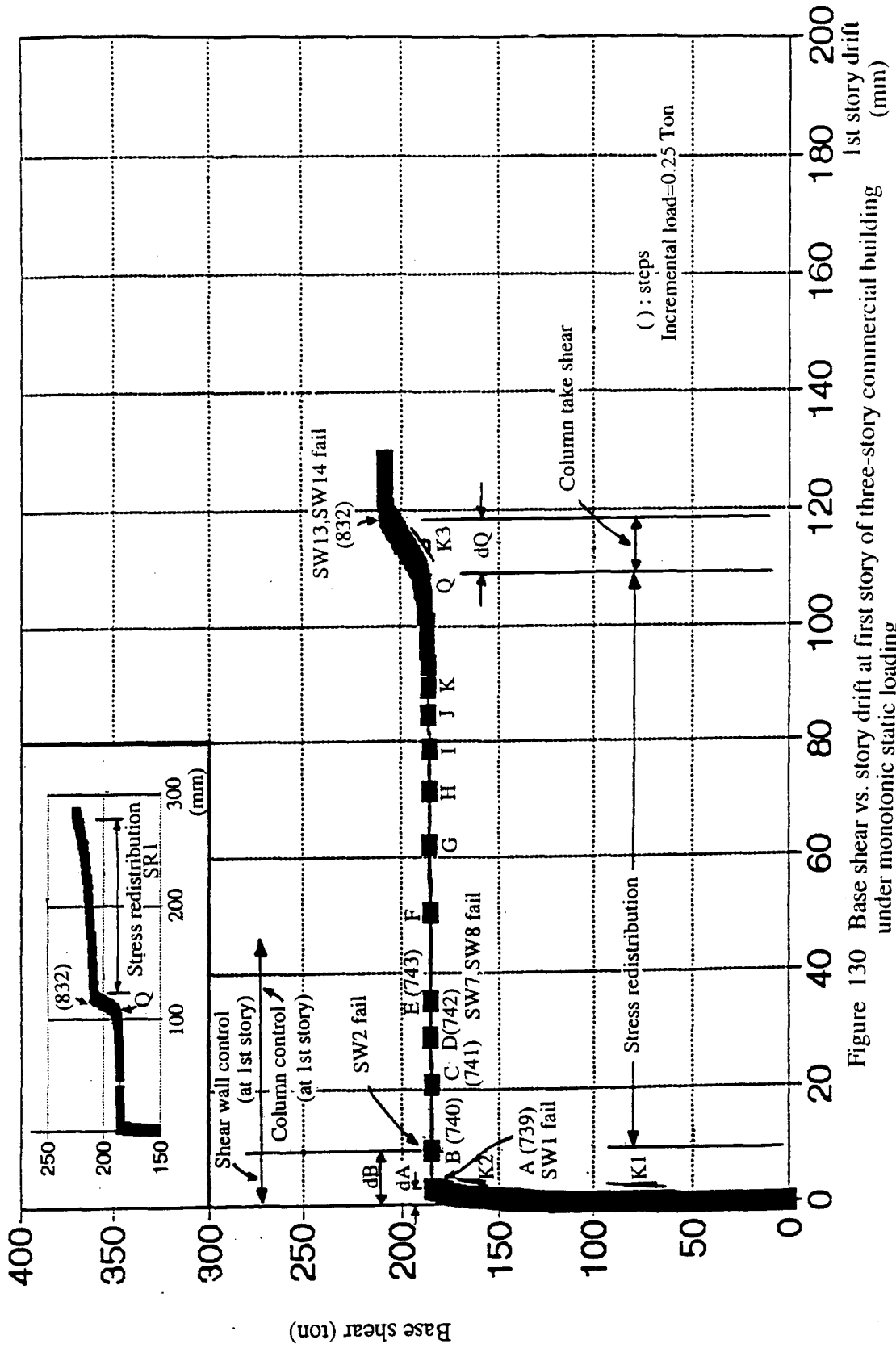
Figure 130 Base shear vs. story drift at first story of three-story commercial building under monotonic static loading

246

story control the behavior of the entire building. During stress redistribution, each incremental load step might result in significant displacement of the second floor's mass center (to account for first-story drift). Points C, D, E, F, G, H, I, J and K are among these steps which exhibit large story drift. Relative story drift between D and E, E and F, F and G, G and H, H and I, I and J, J and K is defined as d_{DE}, d_{EF}, d_{FG}, d_{GH}, d_{HI}, d_{IJ} and d_{JK}, respectively. Note that after point B story drift increases until largest relative story drift d_{EF} is reached. After point F, relative story drift decreases, so d_{FG} is smaller than d_{EF}, d_{GH} smaller than d_{FG}, through d_{JK} smaller than d_{IJ}. This decrease in relative story drift shows the stresses are redistributed to other elements, mainly first-story columns.

Until point Q, first-story columns take most of the base shear. After point Q, as more incremental loads are imposed on the building, shear walls SW13 and SW14 fail when load step reaches 832 (base shear=0.25 x 832= 208 tons). It can be seen that all the shear walls in the force direction fail completely. Subsequently a flat plateau curve appears and stress redistribution continues. Stress redistribution represents force transition from shear walls to columns mainly on the third floor.

Figure 130 hints at further information about the capacity of shear resistance to external lateral load. Before point A, shear wall SW1 has not yet failed and the curve has two parts distinguished by yielding point. From origin to yielding point, where it deviates from elastic behavior, the curve represents base shear increasing proportionally with respect to story drift. Relative story drift is slight since the elastic material property of the shear walls' shear spring controls first-story behavior. The slope in this part of the curve, reflecting story stiffness by shear walls, is denoted by K1.

Before point A, the adjacent part of the curve shows first-story yield behavior in terms of base shear and story drift. The slope in this part of the curve, reflecting the shear walls' yielding property, is denoted by K2. At the part of curve after point Q, the same situation arises. There, increasing base shear with respect to story drift represents story stiffness, which reflects the shear resistance of columns on the first floor. The slope in

this part of the curve is designated K3. From its response, story stiffness K3 is clearly much less than K1, even K2. For this, the most plausible reason is shear walls are designed to resist shear whereas columns are designed to resist moment and axial load. This can be seen from the configuration and size of columns. Figure 130 indicates an important phenomenon. A given story's mass center displaces quickly, as shown by comparing the curve after point Q to the curve before point A. Considering serviceability of the structure, failure of the building can be marked at point B. Critical story failure occurs there. After point B, story drift continues.

2. Moment Development of Columns during Loading Process Figure 131 indicates the response of moment with respect to step for columns C1 and C2 on the first story. Both are examples of column behavior in the force direction. Column C1 is 18" x 18" at the start joint (i.e., bottom side) of the column in the force direction, and 18" x 12" at the end joint (i.e., top side) of the column. Column C2 is 24" x 24" at the start and end joints of the column in the force direction. A schematic diagram of the columns is shown in Figure 132. As shown in Figure 118, external force acts on the global X direction; local Y and Z directions correspond to global X and Y directions, respectively. Moment vs. rotation relationships of two columns are shown in Figure 133. Points A and D of Figure 133 are compatible with points A and D in Figure 131.

Comparing these four charts in Figure 131 and Figure 133 shows that before point A the moment taken by the columns is relatively small. After point A, when shear walls SW1 (739 steps), SW2 (740 steps) and then SW7 as well as SW8 (742 steps) fail, the columns increase moment quickly. This is due to shear originally taken by shear walls being transferred to columns. Shear thus transferred to the columns will increase corresponding moment of columns. During stress redistribution, the moment taken by C1 and C2, increases dramatically at the force direction. For column C1 with the same cross section but slightly different moment capacity, moment goes up to 25,000 ton-mm.

(a) Column C1
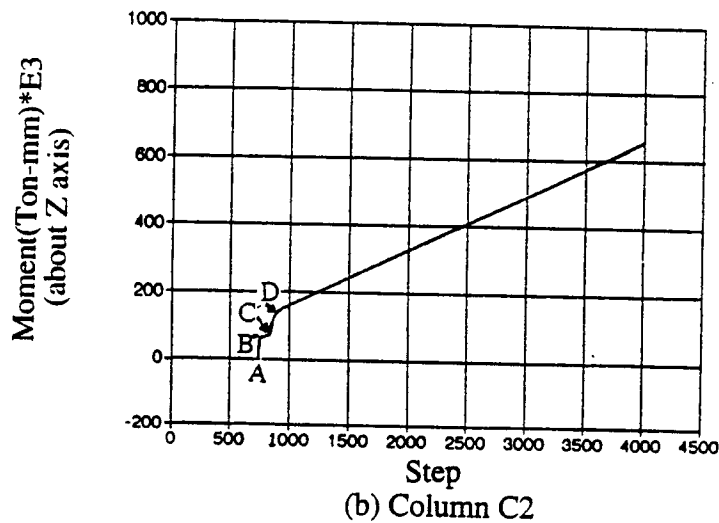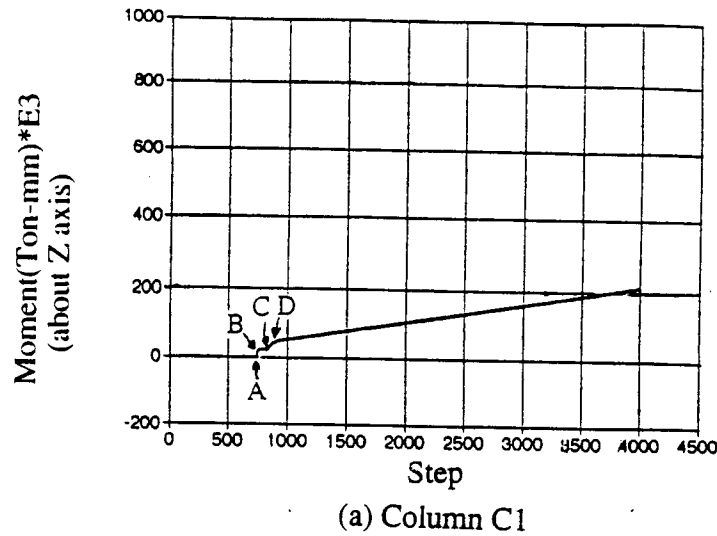
(b) Column C2

Figure 131 Response of moment with respect to step on bottom side of column of first story (a) column C1 (b) column C2

Similarly, moment goes as high as 75,000 tons-mm for column C2. Segment AB in these charts (see Figure 131) is shown for the above responses. After point B, the moment drives continuously until shear walls SW13 and SW14 on the third floor fail, shown as point C in the figure. Segment CD, similar to segment AB, continues the stress redistribution behavior. After point D, columns take over almost all the shear resulting from external load. Moment resistance for columns differs, depending on material property. For column C1, moments exceed 200,000 tons-mm at step 4000 (equivalent

249
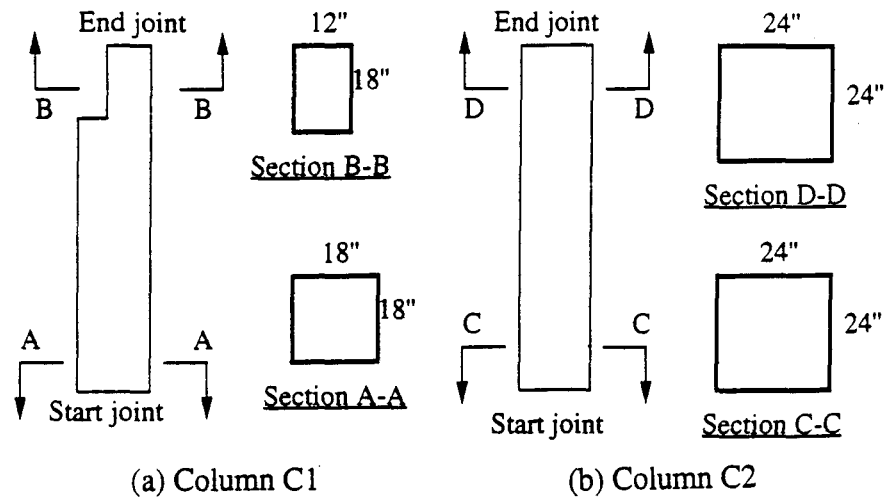
Figure 132 Schematic diagram for columns of both 18" x 18" and 24" x 24"

base shear= 0.25 ton x 4000 = 1000 tons). For column C2, ultimate moments approximate 600,000 tons-mm at step 4000. Note that, after step 4000 in Figure 133, application of more incremental loads to the building causes the moment-rotation relationship of columns to follow the material properties of columns and ends in column failure.

3. Shear Development of Columns during Loading Process In Figure 134, (a) and (b) represent shear response of columns C1 and C2 at the start joint of the column in local Y direction. Points A, B, C and D are compatible with the points in Figure 131 where the same steps occur. Before point A, shear in these figures is quite small. Segment AB, just after point A, has a steep curve. This curve illustrates the failure of shear walls SW1, SW2, SW7 and SW8 around point A caused by transferral of internal forces such as shear and moment. In this case, similar to moment development in Figure 131, shear is transferred quickly from shear walls to columns in the force direction. When force transmission is complete, the shear taken by columns, shown as segment BC in the figures, increases steadily. Note the similarity between moment response and shear in Figure 131. Shear at point C for column C1, 18" x 18", is smaller than for column C2.

250
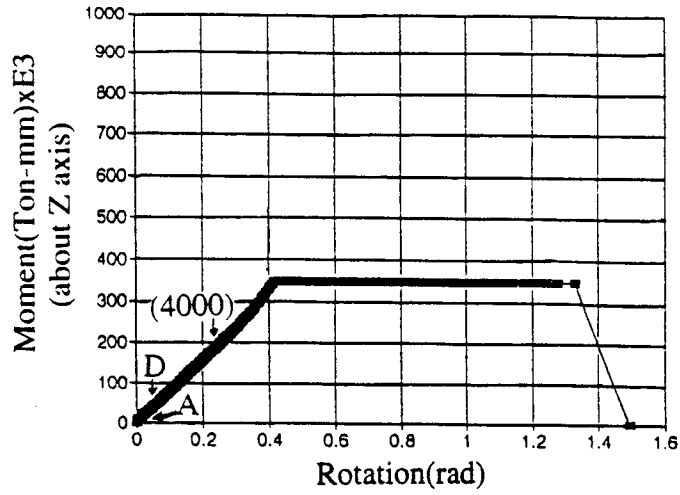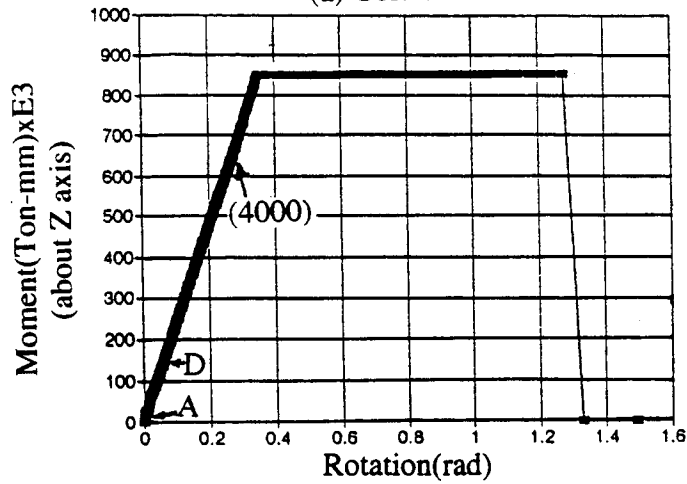
Figure 133 Moment vs. rotation relationship at start joint of column on first story
(a) column C1 (b) column C2

Column C1 has only about five tons whereas column C2 obtains shear up to 15 tons. Ultimate strength of the material is the most important factor there.

Point C, at which shear walls SW13 and SW14 fail on the third floor, is the critical point in another stress redistribution. Shear walls SW13 and SW14 on the third floor lose the capacity of shear resistence. Internal shear is shifted to columns on third floor. At the same time, the abrupt extra shear taken by those columns directly affects columns on the second floor and ground level. In Figure 131, the segment after C shows
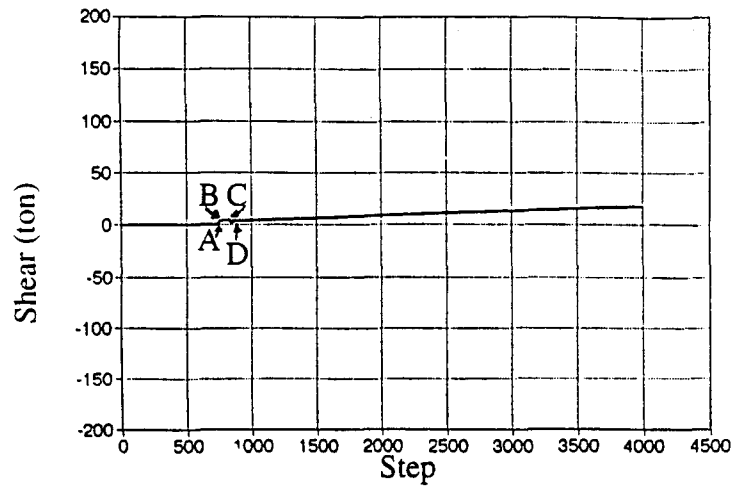
(a) Column C1
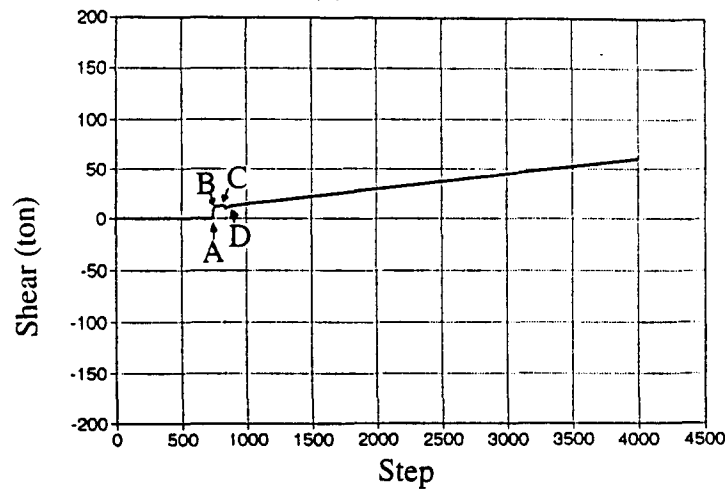
(b) Column C2

Figure 134 Response of shear with respect to step on start joint of column on first story (a) column C1 (b) column C2

the above response. The change in shear is clear. This is compensated by rotational spring of shear walls. Moment development after point D in Figure 131 is not compatible with shear development after point D in Figure 134. Internal moment after D in Figure 131 increases steadily while internal shear after that same point decreases slightly and then increases steadily. In fact, the column has internal shear and moment at each end. Due to the existence of other elements, the force equilibrium condition for a column may not ensure that internal shear is always proportional to internal moment. In this case,

rotational spring of a shear wall takes on more shear which causes the drop in shear after point C in the column.

If more incremental loads are applied to the building reaching 1000 tons (4000 steps), column C1 resists shear to about 18 tons while column C5 resists up to 35 tons. Shear in columns C2 and C6 can go to 60 and 50 tons, respectively. In general, the larger the cross section of column, the more shear resistance the column takes. Overall shear response has another characteristic here. Before point A in the figures, shear is relatively slight and can even be neglected. This illustrates that shear walls SW1 and SW2 take all the shear from the external load.

4. Effect of Shear and Rotational Springs on Shear Wall As stated earlier, there are six shear walls in the three-story building in the force direction. Shear walls SW1 and SW2 are on ground level, SW7 and SW8 are on second floor, and SW13 and SW14 are on third floor. Response of the building to monotonically static incremental load exhibits distinct behavior on each story. The shear wall itself has two types of resistance systems based on Cheng-Mertz's element model of solid shear wall. One is shear spring; the other is rotational spring. Under an external load, shear spring takes shear force while rotational spring resists the moment to prevent bending.

The walls of SW1 and SW2 on the first story take shear proportionally until SW1 fails at a load of 92 tons, which is ultimate shear capacity of both these walls. Figure 135(a) shows that incremental load imposed on the building is constant for each step. But the shear resisted by SW1 increases proportionally up to its final resistance of almost half the total incremental load. The other half is taken by shear wall SW2. SW1 and SW2 take almost all the shear applied by external load increments. Shear walls are the main elements to resist external load for this building. SW1, however, fails sooner than SW2. Shear wall SW1 fails at a load of 184.75 tons and SW2 at a load of 185.0 tons. After step 739 in Figure 136(c), slightly more external load causes significant lateral displacement due to the shear wall's shear spring. Therefore, considerable story drift occurs.
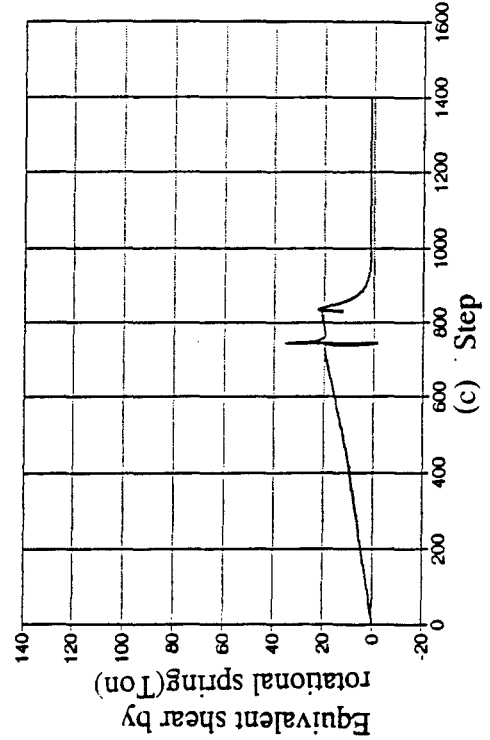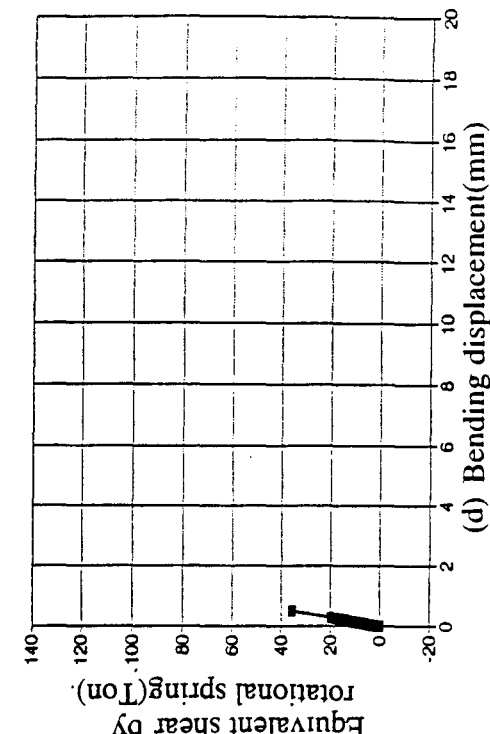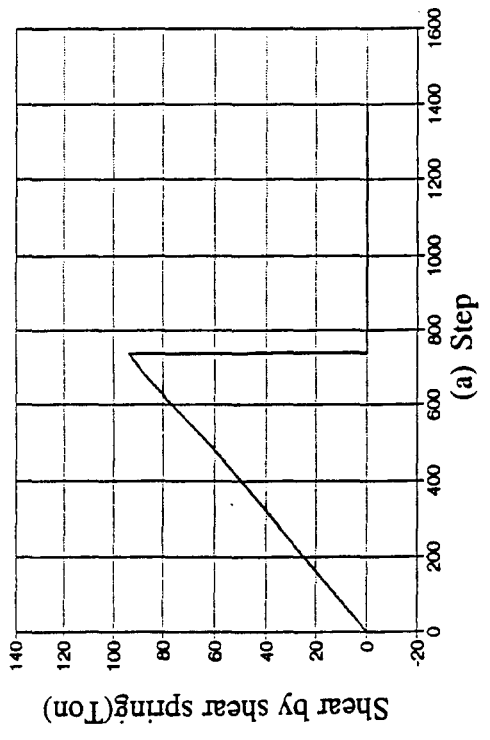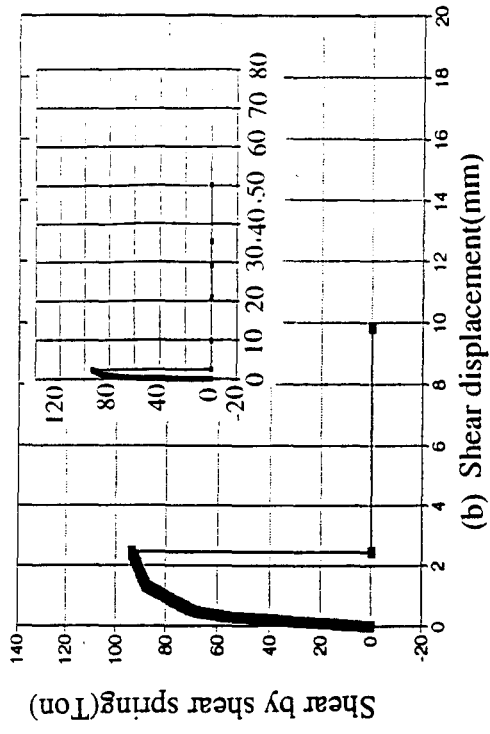
Figure 135 Shear response and shear vs. displacement by shear spring as well as shear response and shear vs. displacement by rotational spring of shear wall SW1

254

5. Base Shear-Story Drift Comparison of Different Stories for Buildings in Group I   Figure 136 shows that, as the shear walls fail, the behavior of the building is dominated by columns at the first, second or third story. The figure shows the proportional straight line at each story, representing **influence of columns on the building** after 300 mm for first story and 700 mm for second and third story. Story drift, the critical point for the column to control story behavior, is less on the first than on the second and third story. Before the critical point is reached, shear walls, for the most part, and columns, give resistance. Displacement of 300 mm is small enough that shear walls on the first story take significant internal shear after a given external force. In terms of critical point, the second story takes more shear than the third story. This causes longer duration in the combined effect of shear walls and columns on the building.

The slope of the straight line, after the critical point is reached in each case, shows the rigidity of columns on each story. This slope expresses the base shear vs. story drift relationship. Figure 136 shows that the slope is largest on the first floor and smallest on the third floor. It follows that first-floor columns have the highest rigidity and third floor columns the lowest rigidity. Higher rigidity of a column demonstrates higher initial stiffness. It makes the story less likely to shift. In seven cases investigated, response of the first floor is the same after shear walls in the building totally fail because only columns remain to take **external load.** For the second and third story, the relationship between base shear and story drift after the critical point is likewise.

6. Comparison of Base Shear vs. Critical Story Drift

    a. Comparison of failure base shear

        i. Building of Group I   Buildings with perforated shear walls on the ground level and those with solid shear walls on the ground level are compared first. Cases 1a, 1c, and 1d comprise the former. As shown in Table XXVIII, **cases** 1a, 1c and 1d, with ductility of 4.0, have a base shear ranging from 139.5 to 147 tons. Cases 1a,1c and 1d, with ductility of 8.0, have a base shear ranging from 197.75 tons to 218.75 tons. Case 1a,
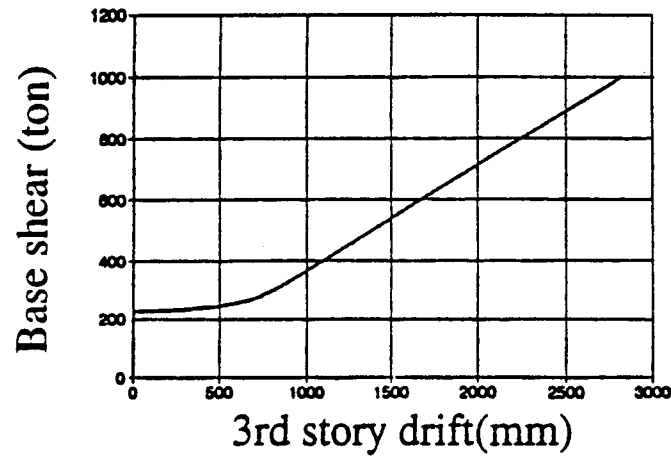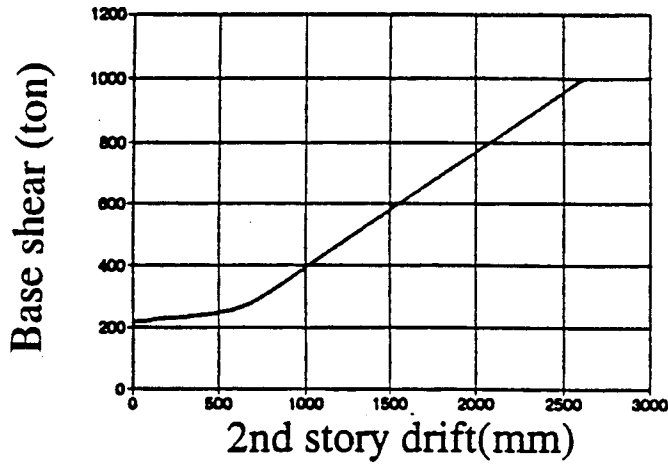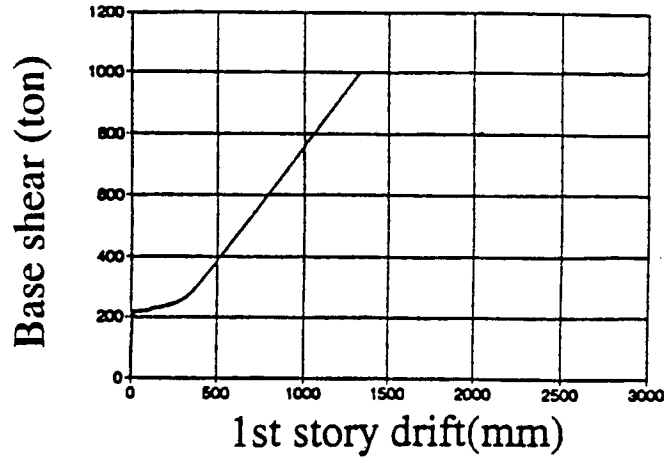
Figure 136 Base shear vs. story drift relationship of different stories for building 1a of Group I

Table XXVIII Maximum base shear at critical story for all the cases of Group I

Wall	Spring	Case 1a		Case 1b		Case 1c		Case 1d		Case 1e		Case 1f		Case 1g	
	Duct.	4.0	8.0	4.0	8.0	4.0	8.0	4.0	8.0	4.0	8.0	4.0	8.0	4.0	8.0
SW1	Shear	146.75	218.25	173.75	184.25	139.25	197.50	139.50	197.75	172.75	183.50	184.25	198.25	185.00	198.75
	Rotational	NO**	NO	—*	—	NO	NO	NO	NO	—	—	—	—	—	—
SW2	Shear	147.00	218.50	174.00	184.50	139.50	197.75	139.75	198.00	173.00	183.50	184.50	198.25	185.25	199.00
	Rotational	NO	NO	—	—	NO	NO	NO	NO	—	—	—	—	—	—
SW7	Shear														
	Rotational														
SW8	Shear														
	Rotational														
SW13	Shear														
	Rotational														
SW14	Shear														
	Rotational														

Shaded area indicates that SW7, SW8, SW13, and SW14 haven't failed yet.

* Rotational spring never reaches failure state.
** There is no rotational spring for perforated shear wall.

257

with ductility of 8.0, could attain base shear up to 218.5 tons, which is 32.7% (= (218.5-147)/218.5) higher (147 tons) than that of case 1a with ductility of 4.0. Similar comparison holds true for cases 1c and 1d. Percentages of increase in base shear for cases 1c and 1d with ductility of 4.0 to 8.0 are 29.5% (i.e., (197.75-139.5)/197.75) and 29.4% (i.e., (198-139.75)/198), respectively. Average of these increases is 30.5%. A difference of 30.5% in base shear is so large. It is caused mainly by the ductility of perforated shear wall SWOA. The strength capacity of perforated shear wall SWOA, with ductility of 4.0, is one-third less than that of perforated shear wall SWOA, with ductility of 8.0. Maximum displacement less by 67%. Both influences result in a deviation of maximum base shear as high as 30.5%.

Note that the backbone curve of solid shear wall SWA with ductility of 4.0 is 4% less than that with ductility of 8.0 in strength capacity, but about two-thirds less for maximum displacement. Buildings with solid shear wall SWA on the ground level range in maximum base shear from 138 to 185.25 tons and from 183.5 to 199 tons with ductility of 4.0 and of 8.0, respectively. In terms of strength capacity, it can be computed that the deviation is 5.69% (=(184.5-174)/184.5) for case 1b, 5.72% (=(183.5-173) /183.5) for case 1e, 6.94% for case 1f and 7.16% for case 1g. Average increase in maximum base shear for the building with solid shear walls at ground level is about 6.8%. This is due to a difference of only 4% shear capacity of solid shear walls when ductility is between 4.0 and 8.0.

Cases 1a, 1c and 1d (building with perforated shear walls at ground level) are compared with cases 1b, 1e, 1f and 1g (building with solid shear walls at ground level) with ductility of 4.0. For cases 1a, 1c and 1d maximum base shear ranges from 140 to 147 tons. For cases 1b, 1e, 1f and 1g it ranges from 173 to 185.25 tons. The latter have a maximum base shear 1.25 times the former. Thus a building with solid shear walls at ground level, where ductility is 4.0, has 25 percent more base shear than a building with perforated shear walls on ground level.

Making the same comparison, where ductility is 8.0, shows that maximum base shear for the building with perforated shear walls at ground level is slightly larger than that for the building with solid shear walls at ground level. Buildings with perforated shear walls at ground level range from 197.75 to 218.50 tons for maximum base shear. Buildings with solid shear walls on ground level range from 183.50 to 199 tons for maximum base shear. Comparatively, the result with ductility of 8.0 is quite different from that with ductility of 4.0.

Mechanisms involved in the above behavior with ductility of 8.0 also differ. As noted, the coupling effect could result from the connection of shear walls to boundary columns at both sides. If a shear wall has larger horizontal displacement, it could induce more rotation in the boundary columns. More rotation in the columns introduces more internal shear. A perforated shear wall exhibits more flexible behavior in the elastic stage since it has smaller initial stiffness than a solid shear wall. Its smaller initial stiffness causes more lateral displacement which in turn shifts the top of the column. Increased lateral displacement here makes the column rotate. Internal moment is then developed due to column rotation. Simultaneously the equivalent internal shear occurs in the column. Here internal shear gives the building more shear strength capacity against an external load. Due to this force combination of column and shear wall, buildings with perforated shear walls at ground level can better resist external lateral load. Supplemental reaction from the column thus strengthens and protects the building.

Also note what happens when the backbone curve of perforated shear walls degrades. As the backbone curve degrades, more internal shear can transfer to columns. These columns are then able to bend more. Backbone curve and its ductility thus play an important role in maximum base shear capacity of the building.

ii. <u>Buildings in Group II</u>   Compared with buildings in Group I, buildings in Group II have two additional shear walls. One is in the middle of the ground floor along global X direction. The other is in the middle of the second floor along global X

direction. Figure 110 shows this configuration. The wall in the middle of the ground floor has one-and-a-half times the shear strength of shear wall SWA (see Figures 105 and 108) but three-fourths the maximum displacement of shear wall SWA. The wall in the middle of the second floor has the same material properties as side walls SWD or SWF. Recall that the middle walls on the ground floor and second floor are SWB and SWE, respectively. On the opposite side of the building, the wall symmetrical to shear wall SWA at ground level has twice the shear strength of shear wall SWA but half the maximum displacement of shear wall SWA. Perforated shear walls corresponding to solid shear walls SWA, SWB, SWC, SWD, SWE and SWF are denoted as SWOA, SWOB, SWOC, SWOD, SWOE and SWOF, respectively. Alternative building configurations in other cases of Group II and III use some of these perforated shear walls. Material properties of perforated shear walls are stated earlier.

Group I and Group II differ in terms of critical story changes in building configuration. Table XXIX shows maximum base shear at the critical story for all Group II cases. In Group I, buildings always fail at ground level where shear walls, either perforated or solid, reach shear failure first. Note the critical story location for Group II buildings. Those with perforated shear walls on the second floor, including cases 2b, 2c, 2d and 2e, likewise have the critical story on the second floor. Those with perforated shear walls at ground level (case 2a only) likewise have their critical state at ground level. Those with perforated shear walls on the third floor (case 2f only) have their critical state on the third floor with a ductility of 4.0, but on the first floor with a ductility of 8.0 case. For case 2g, which has all the solid shear walls in the building, the building fails at ground level first. These differences in behavior might be due to more stiff shear walls are at ground level than on the second floor. Buildings in Group II could thus have more strength capacity at ground level. In addition, the arrangement of perforated shear walls is a controlling factor in maximum base shear.

Table XXIX Maximum base shear at critical story for all the cases of Group II

Wall	Spring	2a 4.0	2a 8.0	2b 4.0	2b 8.0	2c 4.0	2c 8.0	2d 4.0	2d 8.0	2e 4.0	2e 8.0	2f 4.0	2f 8.0	2g 4.0	2g 8.0
SW1	Shear	312.50	383.25										422.00	393.25	422.25
SW1	Rotational	NO**	NO										—	—	—
SW19	Shear	312.50	383.25										422.75	394.50	422.75
SW19	Rotational	—*	—										—	—	—
SW2	Shear	312.25	383.00										422.25	393.50	422.00
SW2	Rotational	NO	NO										—	—	—
SW7	Shear			304.75	331.50	292.75	313.75	283.75	302.50	293.00	316.25				
SW7	Rotational			NO	NO	NO	NO	NO	NO	NO	NO				
SW20	Shear			304.50	331.00	292.50	313.25	283.50	302.00	292.75	315.75				
SW20	Rotational			—	—	—	—	—	—	—	—				
SW8	Shear			304.75	331.50	292.75	313.75	283.75	302.50	293.00	316.25				
SW8	Rotational			NO	NO	NO	NO	NO	NO	NO	NO				
SW13	Shear											375.50			
SW13	Rotational											—			
SW14	Shear											372.75			
SW14	Rotational											—			

Shaded area indicates that shear walls haven't failed yet.

* Rotational spring never reaches failure state.
** There is no rotational spring for perforated shear wall.

Maximum base shear is generally proportional to total shear strength capacity of shear walls at the critical story. Other shear walls or columns at adjacent stories influence maximum base shear to some extent. Table XXIX shows that the maximum base shear ratio of Group II/ Group I for cases 2a through 2e is between 1.53 and 2.13. It varies from case to case for those buildings with perforated shear walls except case 2f. For cases 2f and 2g, where response is controlled mainly by solid shear walls at ground level and on the second floor, maximum base shear ratio is about 2.04 to 2.13. This range is comparable to the shear strength capacity ratio of about 2.25 for cases 2f/1f and 2g/1g. For cases 2b to 2e, response is weakest on the second story (or critical story) which has a shear strength capacity ratio of 1.5 due to additional shear resistance from shear wall SWE (solid) or SWOE (perforated) . As noted, more shear strength capacity could come from adjacent columns, from other shear walls, or from columns on other stories. These sources of resistance cause maximum base shear ratios to vary from 1.53 to 2.13. For cases 2b through 2e, 1.53 to 2.13 is larger than 1.5 while for cases 2f and 2g, 2.04 to 2.13 is less than 2.25 .

Comparing case 2a to cases 2c and 2d, with ductility of 4.0 or 8.0, shows a significant difference. Case 2a with only perforated shear walls at ground level has a higher maximum base shear. Cases 2c and 2d have perforated shear walls at ground level and on second or third floors, which could decrease building's stiffness (i.e., rigidity). Another look at maximum base shear in all three cases **with ductility between 4.0 and 8.0**, shows further differences. In case 2a maximum base shear of a building with ductility of 4.0 is greater than that of a building with ductility of 8.0 by 18% (i.e., (383.25-312.5)/383.25). In cases 2c and 2d, maximum base shear increments are 6.7% ((313.75-292.75) / 313.75) and 6.2% ((302.5-283.75) / 302.5), respectively. Thus perforated shear walls on second floor decrease the the building's maximum base shear.

For cases 2b, 2e, 2f and 2g, with ductility of 4.0 and 8.0, comparison shows less difference. Maximum base shear increments are small, 8.07% ((331.5-304.75)/331.5),

7.35% ((316.25-293)/316.25), 11.18% ((422.75-375.5)/422.75) and 6.68% ((422.75-394.5)/422.75) for cases 2b, 2e, 2f, and 2g, respectively. Less difference in maximum base shear, particularly for cases 2b and 2e, is probably due to solid shear walls in the middle of the second floor and other solid shear walls at ground level. These solid shear walls in the middle restrict the resistance otherwise taken over by the active shear walls. (See discussion of Group III buildings in next section for this phenomenon.)

With ductility of 4.0, cases 2b, 2e, 2f and 2g (293 to 394.5 tons) obtain maximum base shear 1.03 to 1.26 times that of cases 2a, 2c and 2d, an average of 1.157. Buildings with solid shear walls at ground level have 16% more maximum base shear than those with perforated shear walls at ground level. With ductility of 8.0, there is about 7% more maximum base shear for solid shear walls at ground level than for perforated shear walls at ground level. Case 2a has more maximum base shear than cases 2b and 2e, but less than cases 2f and 2g.

iii. **Buildings in Group III** A major difference between these buildings and those of Group II and III is that all cases in Group III have perforated shear walls at ground level and second floor in the middle. This change of configuration might increase maximum base shear for two reasons. First, more perforated shear walls at the critical story would provide more flexibility. Second, other elements , such as adjacent columns, might also take some resistance. This supplemental shear strength can increase the building's capacity for external load. At issue is the arrangement of perforated and solid shear walls.

Table XXX represents maximum base shear at the critical story for all cases in Group III. Critical story for Groups II and III is compared. Group III has the same critical story in all cases except building 3c, with first critical story, and building 3d, with both first and second critical stories. Buildings 3b and 3e are of second-critical-story type while 3f, with ductility of 4.0, is of third-critical-story type. The rest belong to first-critical-story type.

Table XXX   Maximum base shear at critical story for all the cases of Group III

Wall	Spring	Case 3a 4.0	3a 8.0	3b 4.0	3b 8.0	3c 4.0	3c 8.0	3d 4.0	3d 8.0	3e 4.0	3e 8.0	3f 4.0	3f 8.0	3g 4.0	3g 8.0
SW1	Shear	257.50	343.75			246.00	319.50	247.50	322.50				422.00	393.25	422.25
	Rotational	NO**	NO			NO	NO	NO	NO				—*	—	—
SW19	Shear	257.50	343.75			246.00	319.50	247.50	322.50				422.75	394.50	422.75
	Rotational	NO	NO			NO	NO	NO	NO				—	—	—
SW2	Shear	257.25	343.50			245.75	319.25	247.25	322.25				422.25	393.50	422.00
	Rotational	NO	NO			NO	NO	NO	NO				—	—	—
SW7	Shear			292.75	389.50			247.50	322.50	286.75	380.75				
	Rotational			NO	NO			NO	NO	NO	NO				
SW20	Shear			293.00	389.75			247.50	322.50	286.50	380.50				
	Rotational			NO	NO			NO	NO	NO	NO				
SW8	Shear			293.00	389.75			247.50	322.50	286.75	380.75				
	Rotational			NO	NO			NO	NO	NO	NO				
SW13	Shear											375.50			
	Rotational											—			
SW14	Shear											372.75			
	Rotational											—			

Shaded area indicates that shear walls haven't failed yet.

* Rotational spring never reaches failure state.
** There is no rotational spring for perforated shear wall.

Note that 3c has perforated shear walls in the middle of the second floor and at ground level along the building's short span. This contrasts with the solid shear walls in 2c. Building 3c, with its perforated shear wall in the middle of the second floor, provides more flexibility and less shear strength capacity than building 2c. Here, 2c begins to fail at the second story while 3c begins to fail at the first story. A decrease in shear strength capacity of the middle shear wall on the second floor can control the building's response. More flexibility, causing more maximum displacement, is also a factor and compensates for the loss of shear strength capacity to some extent. Compensation for loss of shear strength capacity means that more lateral displacement of a perforated shear wall increases bending effect on adjacent columns and, thereafter, shear resistance is induced in the columns as well. Note also what happens in building 3d. It fails on the first and second floor simultaneously. Its intensive collapse shows that building 3d is not as well designed as building 3c.

Compare maximum base shear for buildings 3a, 3c and 3d with ductility of 4.0 versus 8.0. **Building 3a has 25% more maximum base shear with ductility of 8.0** than with ductility of 4.0 ((343.75-257.5) / 343.75). Building 3c ((319.5-246) / 319.5) and building 3d ((322.5-247.5) / 322.5) both have 23% more maximum base shear with ductility of 8.0. Group II buildings are similar. Building 2a has 18% more maximum base shear with ductility of 8.0, lower than that for building 3a. But buildings 2c and 2d only increase 6.2% and 6.7%, respectively, in maximum base shear with ductility of 8.0. Note the difference between 2c and 3c or 2d and 3d. It comes from the effect of additional perforated shear walls on the behavior of building in Group III. Particularly significant for Group III is the combined influence of perforated shear walls and columns. This holds true for buildings 3b and 3e where more base shear, 24.8% ((389.75-293) / 389.75) and 24.7% ((380.75-286.75) / 380.75), respectively, is obtained with ductility of 8.0. Buildings 3f and 3g are the same as buildings 2f and 2g.

Note the change in maximum base shear with ductility of 4.0 for buildings 3a, 3c and 3d. Their maximum base shear ranges from 246 to 257.5 tons as compared to buildings 3b, 3e, 3f and 3g whose maximum base shear ranges from 286.75 to 394.5 tons. Ratios are 1.192 to 1.230 with an average of 1.35. This represents 35% more base shear in buildings with solid shear walls at ground level than buildings with perforated shear walls at ground level. Note also, with ductility of 4.0, that Group I has 25% more base shear and Group II has 16% more base shear in buildings with solid shear walls at ground level. Solid shear walls at a building's critical story can create more resistance than the same number of perforated shear walls at the same location.

Similarly, with ductility of 8.0, the maximum base shear ratio of buildings 3a, 3c and 3d (319.5~343.75 tons) to buildings 3b, 3e, 3f and 3g (380.75-422.75 tons) is 1.192 to 1.230, an average of 1.21. Thus 21% maximum base shear can be attained by Group III buildings which exceeds Group I and II, both having maximum base shear less than 10%. Again, perforated shear walls clearly occupy a crucial position in the building. Some elements, such as columns, develop more shear capacity by virtue of these more flexible perforated shear walls. The best possible arrangement for perforated shear walls and corresponding shear strength capacities is thus an important design factor.

Recall that a shear wall's backbone curve (see earlier Figures 105-117) reveals differences between perforated and solid shear walls. Compare the backbone curves of solid shear walls with ductility of 4.0 and 8.0. Shear capacity increases slightly and more displacement occurs with ductility of 8.0. For perforated shear walls, a ductility of 8.0 provides more shear capacity as well as maximum displacement. Particularly for the degrading portion of a perforated shear wall's backbone curve, a ductility of 8.0 offers more opportunity to transfer shear resistance from perforated shear wall to column. In this case, the column takes more shear due to the characteristics of strength decay in the degrading portion. Here larger displacement occurs in the backbone curve of a perforated shear wall. An observation can thus be made for Group III buildings with a perforated

shear wall at ground level, second floor or both (except building 3a) with ductility of 8.0:
columns develop significant shear and enable the structure to attain more shear strength
capacity. It can be concluded that the characteristics of a shear wall's backbone curve
play an important role in the response of a building subjected to external load. Further
research on the degrading portion and ductility is recommended.

b. Comparison of failure displacement Table XXXI shows failure displacement
at the critical story for each group. Buildings 1a through 1e in Group I vary in this
regard. Those with perforated shear walls at ground level, such as 1a, 1c and 1d, range
from 9.0 to 18.0 mm (9.0 mm for ductility of 4.0 and 18.0 mm for ductility of 8.0).
Failure displacement in buildings 1b and 1e starts at 1.6 mm with ductility of 4.0 and
goes up to 3mm with ductility of 8.0. Group II buildings, namely 2a through 2e, range
from 3mm to 13mm and vary more widely. Group III buildings, namely 3a through 3e,
range from 5mm to 13 mm. Groups II and III have a similar failure displacement range
with the former slightly less. This is due to solid shear walls in the middle of the ground
level and second floor in Group II but perforated shear walls in Group III.

Compare Groups II and III with Group I. For buildings with perforated shear
walls at ground level, failure displacements in Group II and III are about 55% of Group I
with ductility of 4.0 and 8.0. Buildings of this type in Group I are more flexible. Groups
II and III buildings of this type also have one more shear wall, either perforated or solid,
in the middle of the ground level or second floor. Thus their lateral displacement is more
limited. Groups II and III buildings with perforated shear walls at ground level have
significant deviation in maximum base shear, but only a slight difference in failure
displacement. Thus failure displacement might be controlled by perforated shear walls at
the critical story, not by the configuration change caused by the middle shear walls.

Failure displacement ratios with ductility of 4.0 and of 8.0 for buildings 1a
through 1e in Group I range from 1.574 to 1.998. These ratios (less than 2.2) are
determined by maximum displacement of a shear wall with ductility of 8.0 divided by

Table XXXI Comparison of failure displacement for Groups I, II, and III

Unit: mm

Buildings of Group I

Case	1a		1b		1c		1d		1e		1f		1g	
Story \ Duct.	4.0	8.0	4.0	8.0	4.0	8.0	4.0	8.0	4.0	8.0	4.0	8.0	4.0	8.0
First story	8.855	17.688	1.746	2.749	9.215	18.222	9.319	18.367	1.579	2.565	1.955	2.971	2.294	3.343
Second story														
Third story														

Shaded area indicates that shear walls haven't failed yet.

Buildings of Group II

Case	2a		2b		2c		2d		2e		2f		2g	
Story \ Duct.	4.0	8.0	4.0	8.0	4.0	8.0	4.0	8.0	4.0	8.0	4.0	8.0	4.0	8.0
First story	4.850	9.551										13.855	10.997	17.001
Second story			2.914	12.845	3.111	13.266	3.119	13.520	2.850	13.012				
Third story											6.407			

268

Table XXXI (continued) Comparison of failure displacement for Groups I, II, and III

Buildings of Group III

Case / Duct. Story	3a		3b		3c		3d		3e		3f		3g	
	4.0	8.0	4.0	8.0	4.0	8.0	4.0	8.0	4.0	8.0	4.0	8.0	4.0	8.0
First story	4.968	9.617			5.309	10.086						13.855	10.997	17.001
Second story			6.557	13.531			5.868	12.154	6.856	13.700				
Third story											6.407			

that of a shear wall with ductility of 4.0. **In Group II with ductility of 8.0 vs. ductility of 4.0,** failure displacement ratios range from 1.969 to 4.566 while Group III is 1.900~2.071. Overall failure displacement ratio of the critical story in all groups, with different ductility, is close to 2.0 except in Group II, where some cases go up to 4.6.

Buildings with all solid shear walls, such as 1g and 2g, exhibit a failure displacement ratio around 1.5. Note the variation in failure displacement for different groups: 2.3 to 3.3 mm for Group I; 11 and 17 mm for Group II (or III). Group II buildings' larger displacement might be the result of more torsion effect since their rigidity center shifts more than Group I's. Critical stories in buildings 1f, 2f and 3f are different due to a change in ductility for shear walls. Here the range of failure displacement ratio with ductility of 8.0 vs. 4.0 is from 1.5 to 2.2, an average of 1.8. Figure 137 shows these relationships. For buildings of the shear-wall-dominating type, the structure might exhibit the failure ductility close to the ductility characteristic of individual shear walls. For more complicated shear wall buildings, displacement response could depend on the combination of all shear walls at the critical story.

F. DESIGN PARAMETERS

By expressing the relationship of base shear vs. critical story drift in terms of actual story response and a corresponding bilinear model, Figure 137 shows design parameters. Response of the building under nonlinear analysis is demonstrated by the curvilinear curve. Before point B, the structure responds within the elastic range (i.e., base shear is linearly proportional to story drift). After point B the structure goes through a nonlinear process until the major resistance elements fail completely at the critical story. Earlier research work [50, 51, 74, 75] indicates that point B occurs as soon as the first plastic hinge **develops** in the structure. When this happens, the structure undergoes displacement and consequently deviates from the previous elastic linear curve. If a linearly elastic-perfectly plastic curve is used here, its first segment coincides with the
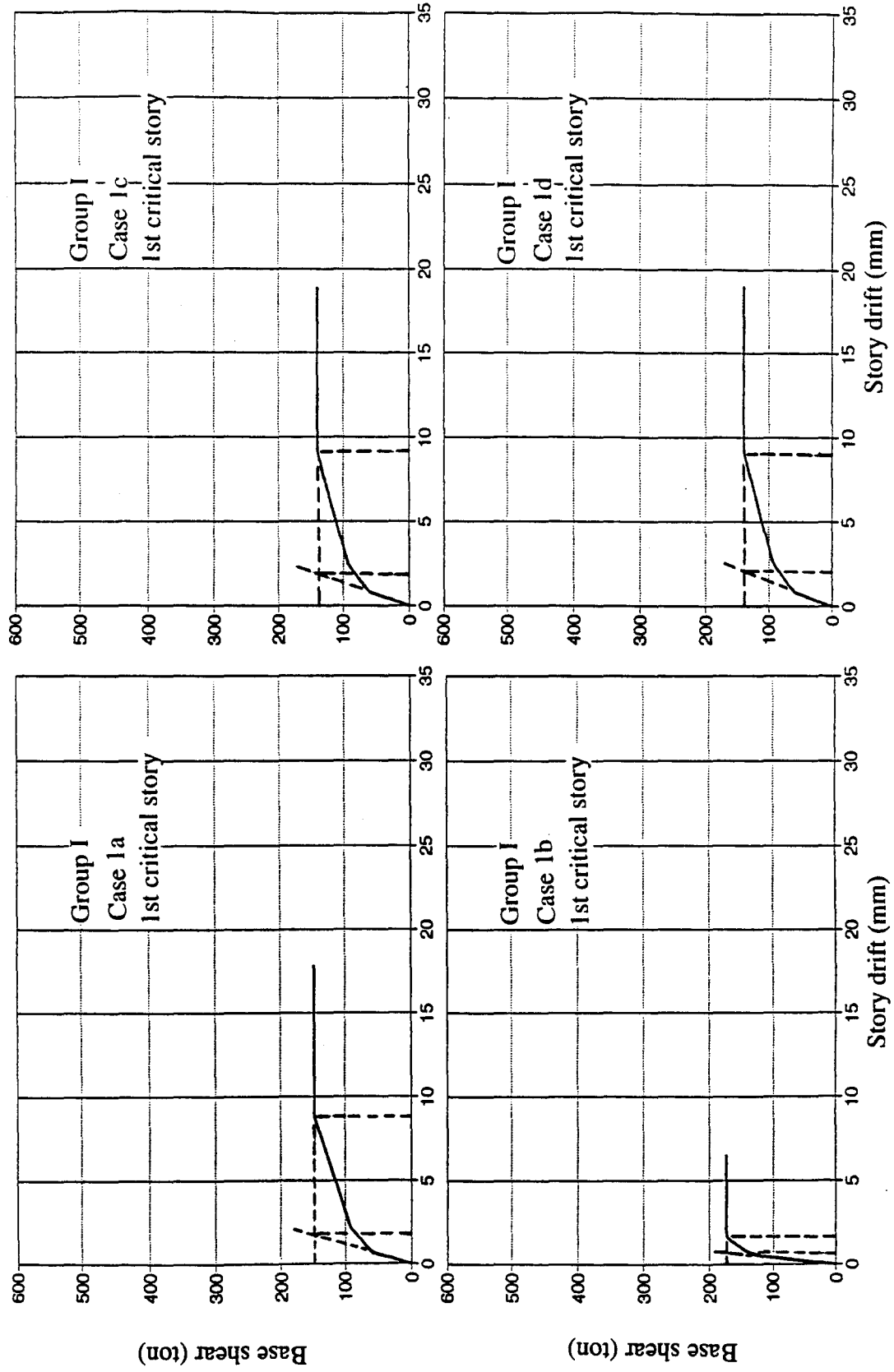
Figure 137 Relationship between base shear and critical story drift for buildings in Group I (ductility=4.0)
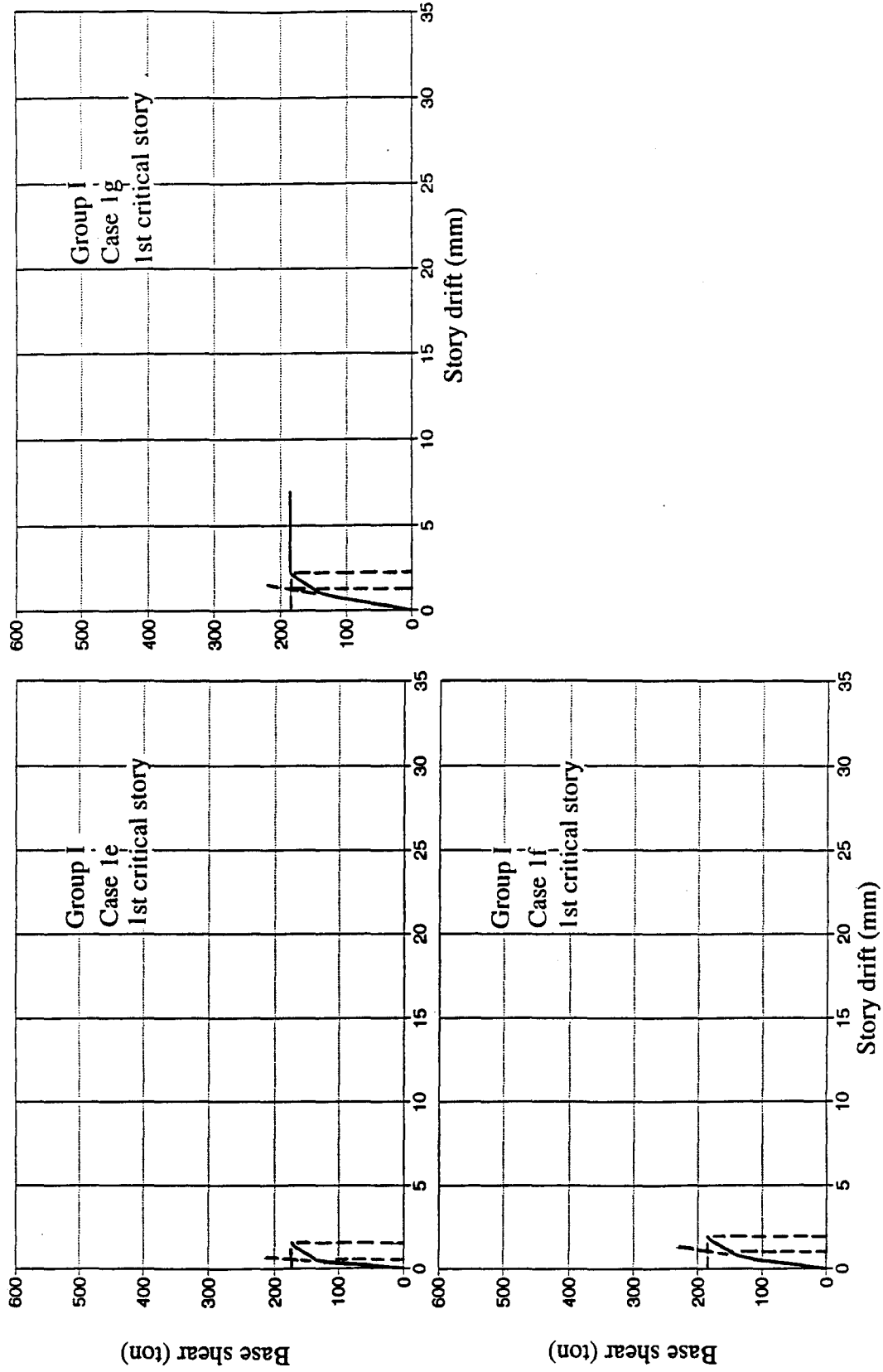
Figure 137 (continued) Relationship between base shear and critical story drift for buildings in Group I (ductility=4.0)

actual response curve between O and B. After point B, the linearly elastic-perfect plastic model allows the straight curve to go linearly up to point C where the model reaches the horizontal line passing through point C. Maximum displacement, located at lines O-C-D is then defined based on the linearly elastic-perfect plastic model.

For a structure with shear walls, as its main resistance elements, the critical floor may consist of two, three, or more shear walls, no matter what kind of configuration exists. Shear walls, composed of steel bars and concrete, have more steel bars in the horizontal direction. More shear strength to resist external load and more ductility are thus provided. Given a certain external load, first to crack is concrete in the wall. It causes the behavior of a shear wall to go beyond the elastic range. Clearly, the elastic segment is found in the shear wall's backbone curve. Beyond its elastic range, the shear wall can still provide strength and ductility. Due to this material property, the shear-wall-dominating building behaves in a similar way. Note that Group I has two shear walls at the critical story. After both of these walls fail, too much displacement occurs. In terms of serviceability, this building is assumed to have failed already. Recall the failure mechanism of the building in this type is when one shear wall fails, the other immediately fails.

One uses a ductility of 4.0, the other a ductility of 8.0, for the buildings of Groups I, II and III. Each ductility involves seven buildings. Tables XXXII summarizes design parameters and corresponding base shear and story drift for ductility of 4.0.

1. Ductility Reduction Factor R_μ Ductility reduction factor R_μ is the ratio of maximum base shear ,V_{eu} (by elastic analysis) to actual failure base shear ,V_y, (by nonlinear analysis). Elastic maximum base shear V_{eu} is the same with ductility of 4.0 or 8.0 in each group. Compare these ductilities in Group I: 4.0 obtains a ductility reduction factor of 3.37 to 4.47 (an average of 3.87), which is 22% higher than that of 8.0 ((3.87-3.17) / 3.17)(Table XXXIII). In Group II, 8.0 obtains a ductility reduction factor of 1.50~2.10 (average of 1.81), which is 10% higher than that of 4.0 ((2.00-1.81) / 1.81). In

Table XXXII Summary of design parameters and corresponding base shear for buildings of Group I with ductility of 4.0

Parameter \ Building	Δ_{max}	$(\Delta_y)_1$	$(\Delta_y)_2$	$(\Delta_s)_1$	$(\Delta_s)_2$	$(\mu_s)_1$	$(\mu_s)_2$	V_y	$(V_s)_1$	$(V_s)_2$	$(\Omega)_1$	$(\Omega)_2$	R_μ	$(DAF)_1$	$(DAF)_2$	$(R_w)_1$	$(R_w)_2$	$\frac{(DAF)_1}{(FRF)_1}$	$\frac{(DAF)_2}{(FRF)_2}$
1a	8.855	8.845	1.645	8.825	0.702	1.0011	5.383	147.00	146.75	57.69	1.0017	2.548	4.243	1.404	19.202	5.950	15.136	0.24	1.27
1b	1.746	1.740	0.789	1.730	0.581	1.0034	2.213	174.00	173.75	124.18	1.0014	1.401	3.584	1.407	4.341	5.025	7.030	0.28	0.62
1c	9.215	9.200	1.864	9.177	0.811	1.0016	4.944	139.50	139.25	58.79	1.0018	2.373	4.471	1.405	16.425	6.271	14.854	0.22	1.11
1d	9.319	9.300	1.974	9.282	0.833	1.0020	4.721	139.75	139.50	65.93	1.0018	2.120	4.463	1.405	14.012	6.259	13.246	0.22	1.06
1e	1.579	1.575	0.592	1.575	0.439	1.0025	2.667	173.00	172.75	116.48	1.0014	1.485	3.605	1.405	5.545	5.054	7.495	0.28	0.74
1f	1.955	1.950	0.987	1.950	0.658	1.0026	1.981	184.50	184.25	120.33	1.0014	1.533	3.380	1.406	4.252	4.739	7.254	0.30	0.59
1g	2.294	2.290	1.316	2.280	0.877	1.0017	1.743	185.25	185.00	121.98	1.0014	1.519	3.367	1.404	3.707	4.720	7.160	0.30	0.52

Case 1:

Case 2:
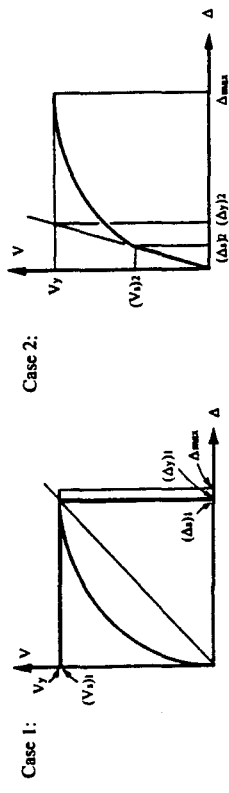
Notes: (1) Units in terms of mm, tons

(2) $(\mu_s)_1 = \Delta_{max}/(\Delta_y)_1$; $(\mu_s)_2 = \Delta_{max}/(\Delta_y)_2$; $(\Omega)_1 = V_y/(V_s)_1$; $(\Omega)_2 = V_y/(V_s)_2$; $R_\mu = V_{cu}/V_y$; $(DAF)_1 = (\mu_s)_1$; $(\Omega)_1$; $(DAF)_2 = (\mu_s)_2$; $(\Omega)_2$; $(R_w)_1 = R_\mu$; $(\Omega)_1$; $(R_w)_2 = R_\mu$; $(\Omega)_2$; $Y: \frac{(DAF)_1}{(FRF)_1} = \frac{(DAF)_1}{(R_w)_1}$; $Y: \frac{(DAF)_2}{(FRF)_2} = \frac{(DAF)_2}{(R_w)_2}$

274

Table XXXIII Summary of ductility reduction factor

Group	Range	Average
I	3.37~4.47	3.87
II	1.61~2.23	2.00
III	1.70~2.58	2.28

(Ductility=4.0)

(a)

Group	Range	Average
I	2.85~3.40	3.17
II	1.50~2.10	1.81
III	1.61~1.98	1.78

(Ductility=8.0)

(b)

Group III, 4.0 obtains a ductility reduction factor 28% higher than that of 8.0 ((2.28-1.78) / 1.78). Generally, when ductility of a shear wall increases, shear capacity increases to some extent. Thus the ductility reduction factor is smaller. If there are more shear walls at the critical story, then shear capacity increases and the ductility reduction factor decreases. On average, Groups II and III have a smaller ductility reduction factor than Group I. The reduction factor is also smaller, as noted in the above results, with ductility of 8.0 than 4.0.

Reviewing all cases in each group, I has an average ductility reduction factor, R_μ, around 3.50; II and III have an average of 2.0. In physical terms, actual failure base shear is about 1/3.5 of elastic maximum base shear for Group I while failure base shear is about half of elastic maximum base shear for both Groups II and III. The total average ductility reduction factor is about 2.3.

2. <u>Overstrength Factor Ω</u> This factor equals failure base shear divided by base shear corresponding to the first significant yield point of the response curve. Overstrength factors are based on two different definitions. Table XXXIV shows both. By the first definition (i.e., $(\Omega)_1$) overstrength factor is almost 1.0 with either ductility of 4.0 or 8.0. By the second definition, overstrength factor is stable at about 1.8 with ductility of 4.0 and 1.78 ~ 2.41 (an average of 2.2) with ductility of 8.0.

275

An overstrength of 1.0 (first definition) cannot guarantee the safety of the building. When the first main element fails, it has reached the first significant yielding point. Total failure of the structure soon occurs if external force continues to increase. An overstrength of 1.8 with ductility of 4.0 or 2.2 with ductility of 8.0 (second definition) can provide 80% up to 120% more shear capacity to prevent failure. This reserve capacity is an important factor in structural design. As noted, larger overstrength provides more shear capacity for the building. Overstrength of 1.8 or 2.2 could have significant practical value.

Table XXXIV Summary of overstrength factor

Group	Range	Average
I	1.40~2.55	1.85
II	1.56~2.02	1.78
III	1.70~1.94	1.87

(Ductility=4.0)

(a)

Group	Range	Average
I	1.49~3.68	2.41
II	1.45~2.19	1.78
III	1.59~2.59	2.32

(Ductility=8.0)

(b)

3. <u>System Ductility Factor μ_s</u> Maximum story drift at the critical story divided by story drift at the first significant yielding point is called system ductility factor, μ_s. This factor reflects the general characteristics of the building's ductility. As noted, based on the first definition (except Group II with ductility of 8.0), the system ductility factor equals 1.0 (see Table XXXV). No duration of inelasticity can then be detected for a shear-wall-dominating building. Before the behavior of the building's critical story reaches the yielding point, the critical story behaves elastically. After this point, the

Table XXXV Summary of system ductility factor

Group	Range	Average
I	1.001~1.003	1.002
II	1.002~1.005	1.003
III	1.001~1.002	1.002

(Ductility=4.0)

(a)

Group	Range	Average
I	1.001~1.003	1.001
II	1.002~5.80	3.060
III	1.001~1.053	1.011

(Ductility=8.0)

(b)

Group	Range	Average
I	1.74~5.38	3.38
II	2.19~6.79	3.70
III	3.67~6.79	4.81

Average ~ 4.00

(Ductility=4.0)

(c)

Group	Range	Average
I	2.35~7.20	4.83
II	8.50~12.15	9.76
III	5.48~8.39	7.78

Average ~ 7.50

(Ductility=8.0)

(d)

critical story fails abruptly. No other element in the building forestalls the inelastic stage. By the second definition, as noted, the system ductility factor has a wide range. Groups I, II and III are 3.38 ~ 4.81 with ductility of 4.0 (an average of 4.0) but 4.83 ~ 9.76 with ductility of 8.0 (an average of 7.5). Averages here show the building's system ductility approximately reflect the shear wall's ductility characteristics. Since buildings with all solid shear walls in Groups II and III have a larger system ductility factor, they are not taken into account here.

    4. Force Reduction Factor R_w This factor is defined as the ratio of elastic maximum base shear by elastic analysis to allowable base shear based on ASD design by nonlinear analysis. Force reduction factor, R_w, is also the function of ductility reduction factor R_μ, overstrength factor Ω, and load factor Y, expressed as $R_w = R_\mu \cdot \Omega \cdot Y$.

As shown in Table XXXVI, Group I with ductility of 4.0 or 8.0 has a larger force reduction factor than Group II for both definitions. In Group I, the ductility reduction factor is generally much larger than in Groups II and III due to Group I's smaller failure base shear.

Based on the first definition, the average force reduction factor with ductility of 4.0 is 3.81 but is 3.16 with ductility of 8.0. Average force reduction factor for these cases is about 3.49. For design purposes, 4.0 can be conservatively recommended, which is two-thirds of the UBC-based design parameter for a bearing wall system with shear walls. Based on the second definition, the average force reduction factor with ductility of 4.0 is about 6.05 but is 5.94 with ductility of 8.0. Average force reduction factor for these cases is about 6.0. The calculated design parameter is exactly the same as the UBC design parameter. As indicated, force reduction factor is generally stable in Table XXXII.

5. <u>Displacement Amplification Factor DAF</u> In order to obtain actual nonlinear story drift, this factor accounts for displacement which would somewhat amplify elastic maximum story drift. At the building's critical story, this factor is expressed as $\Delta_{max,SD}/\Delta_{all,SD}$. As multiplication of system ductility factor μ_s, overstrength factor Ω, and load factor Y, it is represented by $DAF = \mu_s \cdot \Omega \cdot Y$. Based on the first definition, most system ductility and overstrength factors equal 1.0. Therefore the displacement amplification factor is almost equal to load factor Y, which is assumed to be 1.4. Except for some buildings in Group II with ductility of 8.0, all other displacement amplification factors range from 1.404 to 1.407, which can be considered a constant (Table XXXVII).

Based on the second definition, displacement amplification factor ranges from 3.7 to 33.42 with ductility of 4.0 as well as 8.0. Average displacement amplification factor thus ranges widely from 4.46 to 24.94. Overall, factors of 1.4 (based on the first definition) and 3.7 ~ 33.42 (based on the second definition) are either too large or too small.

Table XXXVI Summary of force reduction factor

Group	Range	Average
I	4.72~6.27	5.43
II	2.26~3.13	2.80
III	2.38~3.61	3.19

(Ductility=4.0) Average ~ 3.81
(a)

Group	Range	Average
I	4.00~4.76	4.45
II	2.10~2.94	2.54
III	2.26~2.78	2.50

Ductility=8.0) Average ~ 3.16
(b)

Group	Range	Average
I	7.03~7.50	7.23
II	3.50~5.73	4.98
III	4.59~6.68	5.95

(Ductility=4.0) Average ~ 6.05
(c)

Group	Range	Average
I	7.03~7.91	7.48
II	3.05~5.73	4.53
III	3.57~6.68	5.80

(Ductility=8.0) Average ~ 5.94
(d)

6. Displacement Amplification Factor/Force Reduction Factor Ratio (DAF/FRF)

As noted earlier, displacement amplification factor has a wide range and force reduction factor is a stable number. The ratio of displacement amplification factor to force reduction factor could also have a wide range of value, particularly for Groups II and III based on the second definition. As shown in Table XXXVIII, this ratio has a range of 0.26~0.56, but an average of 1.27 for Group II, based on the first definition.

Uang [28] found a displacement amplification factor/force reduction factor ratio equal to or greater than 1.0. Here the range is generally less than 1.0, about 0.4. As shown in Table XXXVIII(c) and (d), based on the second definition. the DAF/FRF ratio has a wide range, averaging 1.82 with ductility of 4.0 and 3.37 with ductility of 8.0.

279

Table XXXVII Summary of displacement amplification factor

Group	Range	Average
I	1.404~1.407	1.405
II	1.406~1.412	1.407
III	1.403~1.404	1.404

(Ductility=4.0)

(a)

Group	Range	Average
I	1.400~1.407	1.403
II	1.404~4.118	3.520
III	1.402~1.475	1.417

(Ductility=8.0)

(b)

Group	Range	Average
I	3.707~5.545	4.460
II	4.916~8.025	6.384
III	8.723~18.329	12.68

(Ductility=4.0)

(c)

Group	Range	Average
I	5.311~10.023	7.254
II	18.666~33.420	24.941
III	17.719~30.425	24.267

(Ductility=8.0)

(d)

Based on monotonic static analysis, no DAF/FRF value can be recommended as a design parameter.

G. SUMMARY

As discussed, a shear wall's backbone curve is a key factor in determining the response of a building under monotonic static loading analysis, particularly for the degrading portion and ductility of a shear wall. Perforated shear walls have smaller initial stiffness, in general, which allows adjacent columns to take more shear vis-a-vis external load. Also a key factor is the arrangement of perforated and solid shear walls. This affects reserve capacity which makes a building more flexible and better able to absorb the energy from external force.

Table XXXVIII Summary of DAF/FRF ratio

Group	Range	Average
I	0.22~0.30	0.26
II	0.45~0.49	0.49
III	0.39~0.59	0.45

(Ductility=4.0)

(a)

Group	Range	Average
I	0.29~0.35	0.32
II	0.61~1.49	1.27
III	0.51~0.65	0.56

(Ductility=8.0)

(b)

Group	Range	Average
I	0.52~1.27	0.84
II	0.98~5.38	2.39
III	1.43~3.99	2.23

(Ductility=4.0)

(c)

Group	Range	Average
I	0.75~2.52	1.54
II	4.06~5.84	4.80
III	2.76~5.16	3.76

(Ductility=8.0)

(d)

With respect to design parameters, two factors in this chapter are applicable Generally, the force reduction factor has a stable value; 4.0 is recommended based on the first definition and 6.0 based on second definition, which is the same as the UBC code force reduction factor. Average ductility reduction factor is 2.3. Overstrength factor Ω by the first definition is almost 1.0, but varies from 1.8 to 2.2 by the second definition. System ductility factor μ_s is about 1.0 by the first definition while larger (4.0~7.5) by the second definition. Displacement amplication factor is 1.4 by the first definition, but has a wide range of 4.5~24.9 by the second definition. This factor is unsuitable for most of its range. DAF/FRF ratio is 0.40 by the first definition which is less than 1.0, the value suggested by other researchers. By the second definition, 1.82~3.37 for DAF/FRF is the range. All are summarized in Table XXXIX. It can be concluded that only force

reduction factor R_w and ductility reduction factor R_μ can be reasonably adopted for design purposes. More shear wall buildings could be tested and analyzed in the future for further evaluation of force reduction and ductility reduction factors.

Table XXXIX Summary of design parameters based on different definitions

Approach Design parameter	Based on first definition	Based on second definition
Ductility reduction factor	2.3	
Overstrength factor	1.0	1.8~2.2
System ductility factor	1.0	4.0~7.5
Force reduction factor	4.0	6.0
Displacement amplification factor	1.4	4.5~24.9
DAF/FRF ratio	0.40	1.82~3.37

X. RESPONSE STUDY OF THREE-STORY COMMERCIAL BUILDING-DYNAMIC ANALYSIS

To study the response of shear walls under seismic load, a three-story commercial building (case 1g in Section IX) at Pleasant Hill, California, subject to the 1989 Loma Prieta earthquake is studied. Several earthquakes are simulated and applied to a test version of this building. Those cases which involve seismic simulation are aimed to explore the role of shear walls and, thereafter, the recommendation of design parameters as well.

A. THREE-STORY COMMERCIAL BUILDING SUBJECTED TO LOMA PRIETA EARTHQUAKE

1. **Description of 1989 Loma Prieta Earthquake Records** This earthquake originated in the Loma Prieta, California, area in April of 1989 [61]. At that time, many buildings had sensors for recording structural responses. For the three-story building shown in Figure 99, sensors were located at different levels, including horizontal and vertical directions. Records from these sensors for the Loma Prieta earthquake in Figure 138 show the duration of the acceleration to be 20 seconds. Comparing acceleration records between vertical and two horizontal directions, the former is small, with its peak of about 0.025g occurring after 17.7 seconds. As to ground-level acceleration, records of sensors 10 and 11 are assumed to be in the X direction (see coordinate system in Section IX). These sensors, located on shear walls, have almost the same acceleration records with their peak of 0.13g at t = 15.1 seconds. Sensors 7, 8 and 9 in X direction are on the third floor. Sensors 3,4 and 5 in X direction are on the roof. Observe that sensors 7 and 9 on the third floor as well as sensors 3 and 5 on the roof are located on shear walls. Their peak acceleration of 0.13 g at t = 15.1 seconds matches that of sensors 10 and 11 also located on shear walls. But sensor 8 on the third floor, not located on a shear wall, has a larger peak

Max. Accel. = 0.03 g

1 Ground Floor: North Wall -- Up

2 Roof: East Wall -- N   0.14 g

3   "   North Wall -- E   0.16 g

4   "   Center -- E   0.23 g

5   "   South Wall -- E   0.15 g

6 3rd Floor: East Wall -- N   0.10 g

7   "   North Wall -- E   0.14 g

8   "   Center -- E   0.18 g

9   "   South Wall -- E   0.12 g

10 Ground Floor: South Wall -- E   0.12 g

11   "   North Wall -- E   0.13 g

12   "   North Wall -- N   0.08 g

Structure Reference Orientation: N=0°

0   1   2   3   4   5   10   15   20 Sec.
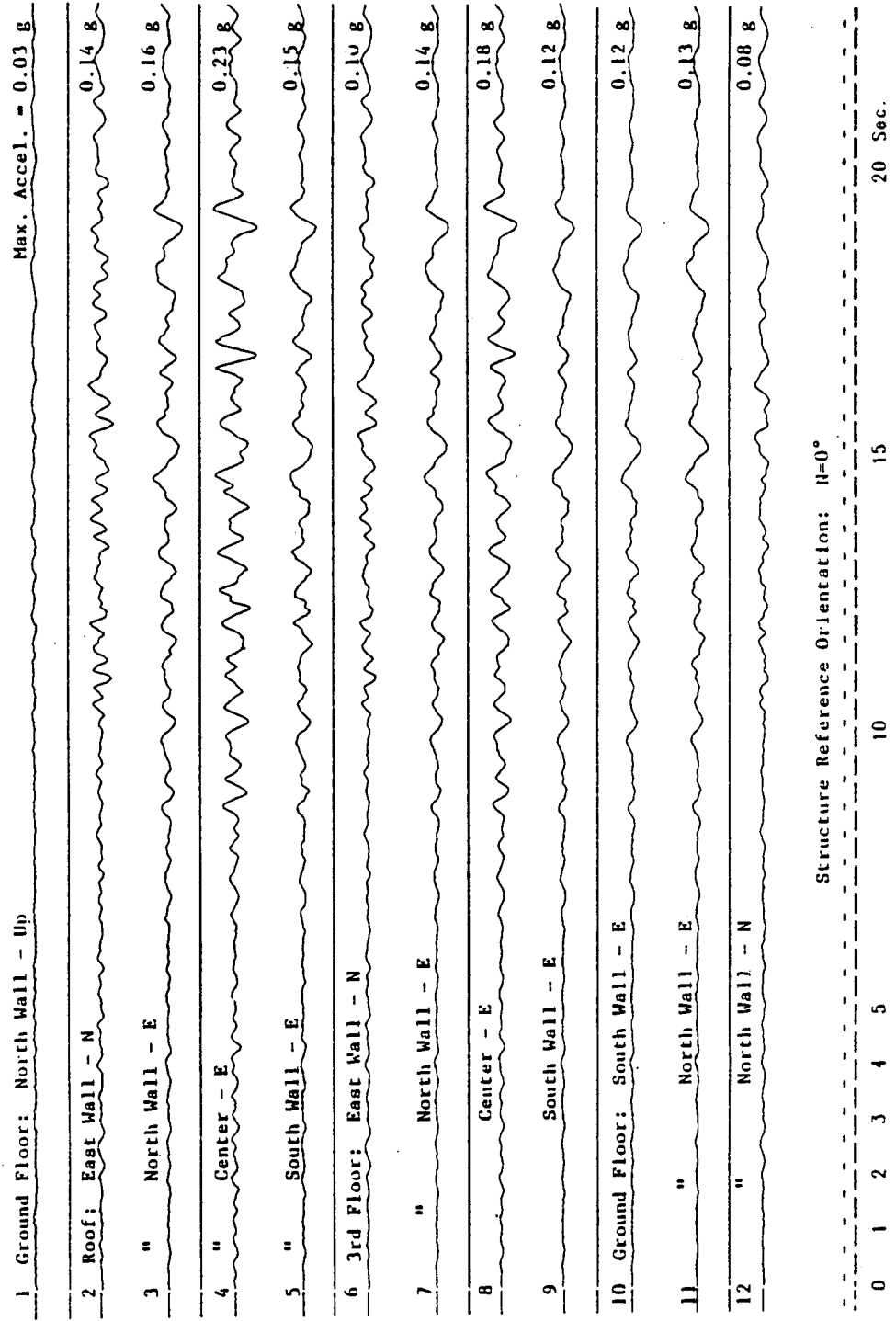
Figure 138   Earthquake records for three-story commercial building at Pleasant Hill, California

284

acceleration of 0.17 g. Sensor 4 on the roof, again not located on a shear wall, has an even larger peak acceleration of 0.23 g.

Sensor 12 at ground level, sensor 6 on the third floor, and 2 on the roof are in Y direction. Their peak accelerations, at time = 15 seconds, are 0.08 g, 0.11 g, and 0.15 g, respectively. At each end of the building, sensors 10 and 11 represent ground acceleration in X direction. Their sensors have close acceleration and their average is used here as input acceleration spectrum in X direction. Also, the acceleration of sensor 12 is used as input acceleration in Y direction. Otherwise, acceleration of sensor 1 is used as input for acceleration in the vertical direction. For simplicity, the floor is assumed to be rigid in this analysis. On the basis of multi-component earthquake input for this three-story commercial building, dynamic nonlinear analysis was done.

2. <u>Response Analysis</u> Structural analytical output of accelerations at all the sensor locations yielded the same acceleration results as actual earthquake records (shown in Figure 139 for sensor 7). To further test the response of building, the same procedure was implemented with elastic analysis. Results matched those of nonlinear analysis, as shown in Figure 139(b) for sensor 7. Elastic and nonlinear analyses indicate that the entire building behaves in the elastic range under conditions of the Loma Prieta earthquake, which has maximum ground acceleration of 0.15 g $(=\sqrt{(0.13)^2+(0.08)^2}$; 0.13 g in X direction and 0.08 g in Y direction).

As stated, peak accelerations at the centers of the third floor and roof are larger than accelerations at each end of the building whereas analytical results indicate the mass centers of the third floor and roof have the same response as each end of the building.
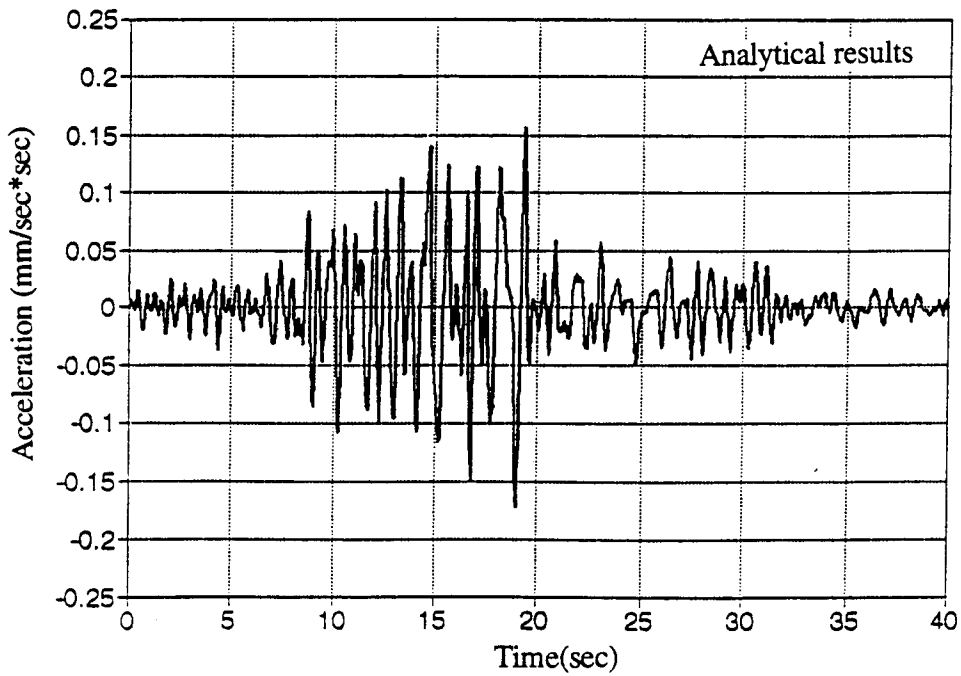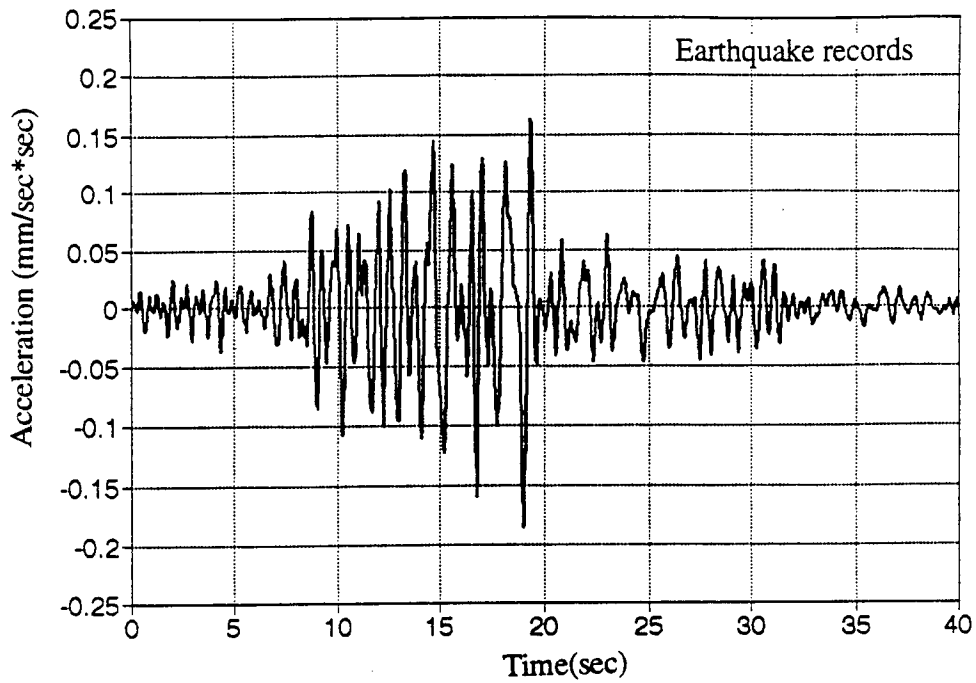
Figure 139 Acceleration response for sensor 7 of three-story building subjected to Loma Prieta earthquake

B. THREE-STORY COMMERCIAL BUILDING SUBJECTED TO SIMULATED EARTHQUAKE

1. Description of Simulated Earthquake   Normalized acceleration response spectrum adopted by UBC design code was used for simulation. Figure 140(a) shows this spectrum. Note that soil type 2 is assumed here. Normalized acceleration response spectrum is defined as acceleration response (with respect to period) divided by effective peak acceleration. If previous local maximum acceleration is set at 0.4 g, then effective peak acceleration is 0.4 g. Acceleration of the plateau portion in the acceleration response spectrum equals 1 g (=0.4 g × 2.5), or 386.2 in/sec^2 (see Figure 140(b)). When period of structure is small, which corresponding maximum acceleration in the acceleration response spectrum is constant, the structure's maximum design acceleration is 1 g.

SIMQKE, used to create a simulated earthquake, was developed at MIT [76]. This program inputs a velocity response spectrum expressing the characteristics of a simulated earthquake. Velocity response spectrum represents the UBC design code acceleration response spectrum. Also essential is input from the deterministic envelope function which is shown in Figure 141. As used in the program, this function confines the general shape of earthquake with respect to time. Other factors defining the function, such as time increment, duration of earthquake and maximum earthquake intensity, are also considered in SIMQKE.

Six simulated earthquakes created here can be classified into three types: (1) seismic intensity of 0.2 g, (2) seismic intensity of 0.3 g; (3) seismic intensity of 0.4 g. respectively. Earthquakes denoted as 'A' in all three types of simulated earthquakes are influenced by the same deterministic envelope function. Likewise earthquakes denoted as 'B' share another deterministic envelope function. Simulated earthquakes 1A and 1 B are shown in Figure 141. Major earthquake duration ranges from 1 second to 10 seconds. In this figure, earthquake 1A has the same velocity response spectrum as earthquake 1B. But
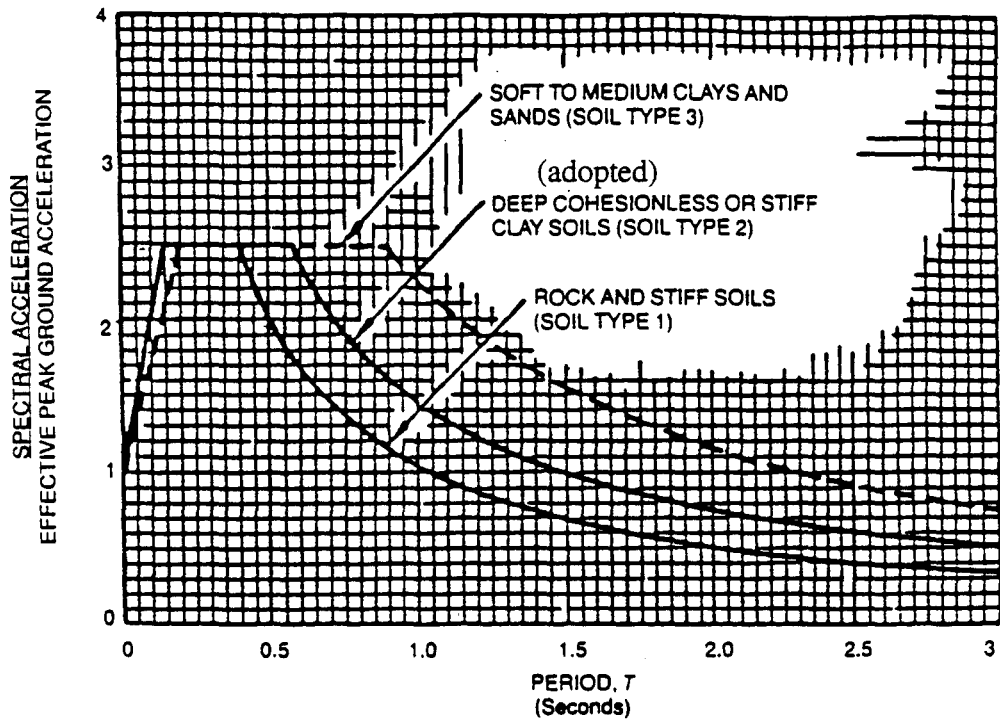
(a) Selected normalized spectrum
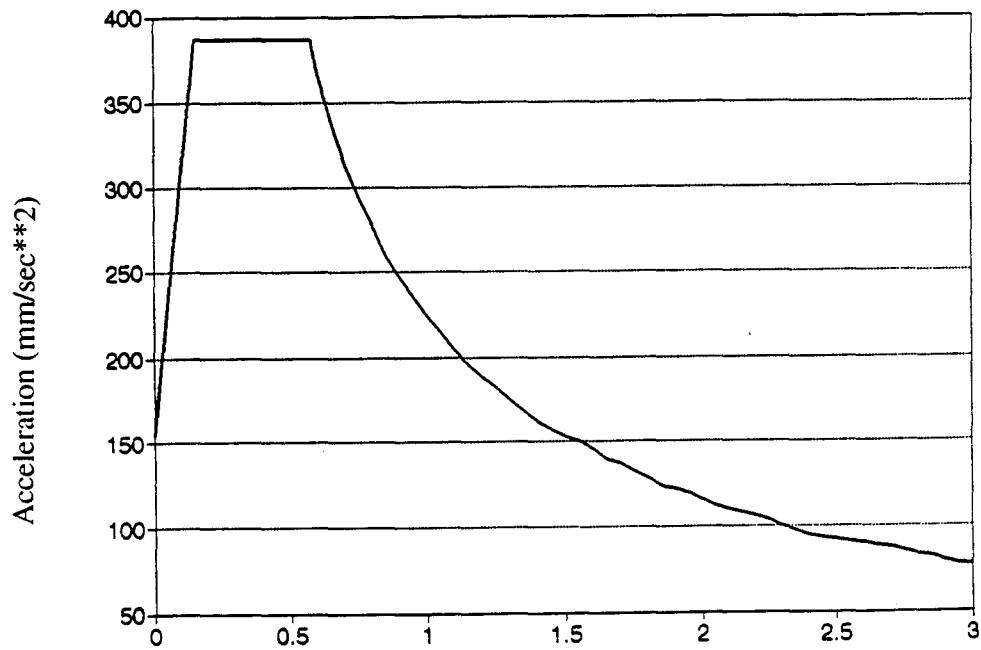
(b) actual spectrum

Figure 140 Selected normalized acceleration response spectrum for three-story building and actual acceleration response spectrum

288
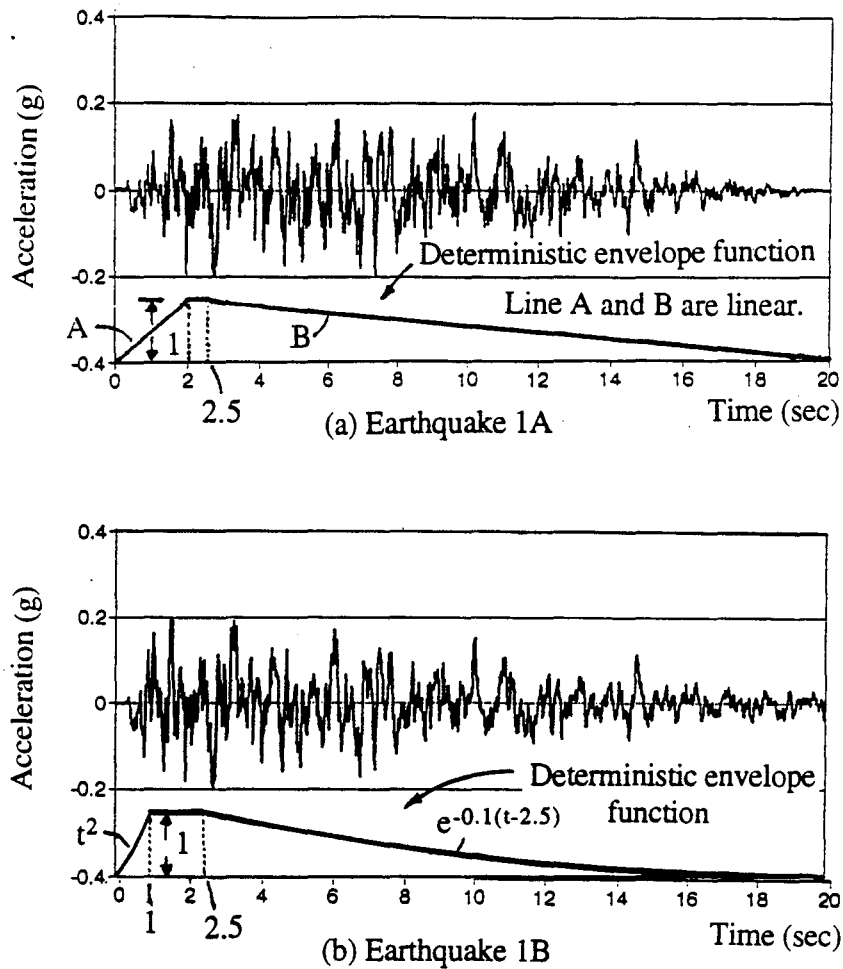
Figure 141 Simulated earthquakes for three-story commercial building

the difference between their acceleration histories is due to the deterministic envelope function.

2. Response Analysis

a. Definition of failure of building For RC shear-wall-dominating buildings, there are three types of failure structure modes as follows.

Shear failure mode If a building with RC shear walls is subjected to external excitation, the critical story's shear walls reach shear failure first. Based on strength and serviceability concerns, the building can be assumed to fail totally: slightly more excitation

will result in irreparable displacement. In this case, flexural displacement by a shear wall's rotational spring and shear displacement by a shear wall's shear spring characterize shear-wall-element behavior. Once a shear wall's shear spring reaches the ultimate state, the wall cannot take any more load.

Flexural failure mode   When a shear wall's rotational spring of shear wall reaches the maximum moment, the wall's flexural response is highly inelastic. With slight external excitation, the shear wall has significant story drift. In this situation, the building fails.

Flexural and shear failure   In some cases, both rotational spring and shear spring of RC shear walls on the critical story of a building reach the ultimate state at the same time. Then the building is on the verge of collapse. With slight external excitation, the building collapses immediately.

b. Shear response history caused by shear spring of critical story's shear wall As stated before, RC shear walls take the majority of shear resistance in a shear-wall -dominating building. The process by which the shear wall's shear spring takes shear is important for the building's behavior. If shear walls lack sufficient load capacity against external force, these walls soon take the shear resistance and cause other elements of the building to fail. Thereafter the entire building fails. For this investigation, the building is subjected to simulated earthquake 1A. Intensity of the earthquake is 0.2 g. It is demonstrated that the critical story of the building is on the ground level. Since the building is symmetrical, shear walls SW1 and SW2 have the same shear response from the shear wall's shear spring. Figure 142(a) shows shear response caused by shear wall SW1. In this figure, points A and B pass the cracking point of the shear wall's backbone curve. Thus the shear wall enters the inelastic range. Points C and D pass the yielding point of the shear wall's backbone curve. After time = 3.3 seconds, the shear wall enters the highly inelastic range. Subsequent to point D, shear response generally deviates from the horizontal axis of shear = 0 ton. The elastic behavior ranges from 0 to 3.3 seconds. It
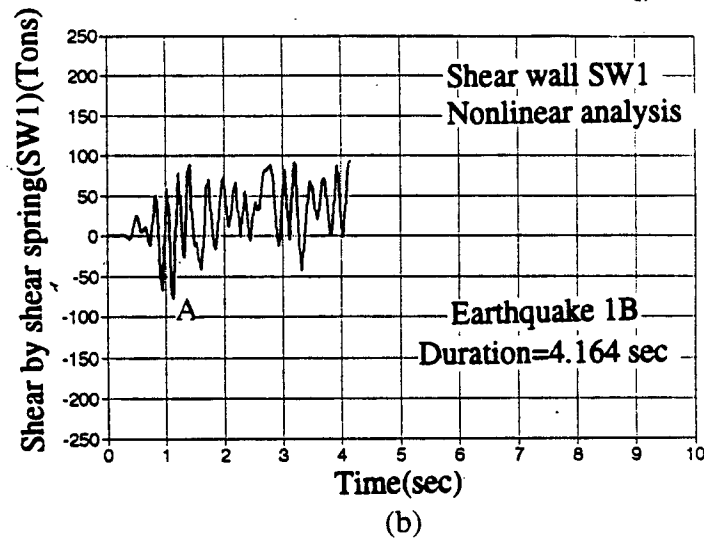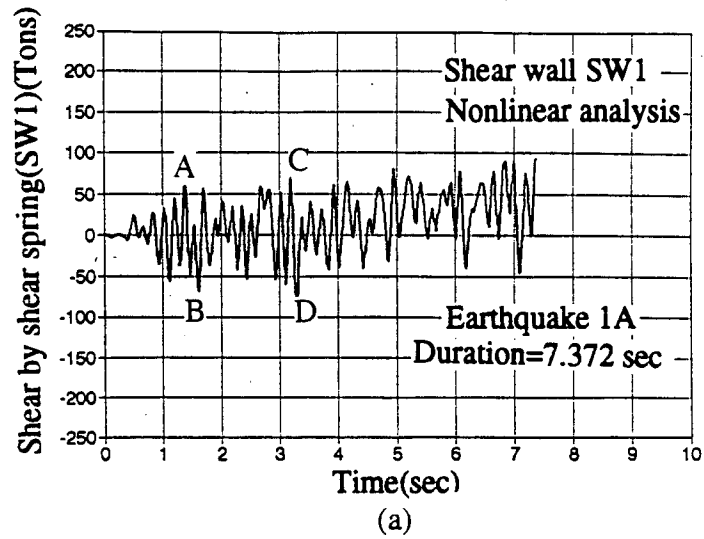
Figure 142   Shear by shear spring of shear wall SW1 vs. time relationship for three-story building under earthquake (a) 1A (b) 1B

marks shear wall displacement for the building which is small here. During this time span of 0~3.3 seconds, energy dissipation of both shear walls and the entire building is small. Beyond 3.3 seconds, highly inelastic behavior of shear walls on the building's critical story causes large energy dissipation there. If shear walls are characterized by large ductility, then even more energy dissipation can occur. As noted earlier, the simulation involves acceleration in a range of from 1 to 10 seconds. When subjected to simulated earthquake

1A, the building cannot last 10 seconds. It fails at 7.372 seconds with an intensity of 0.2 g for this particular seismic excitation.

For the building subjected to simulated earthquake 1B, Figure 142(b) shows an elastic behavior ranging from 0 to 1.1 seconds (point A). After point A the shear band goes upward. It represents the shear spring of shear wall SW1 entering a higher inelastic range. At 4.164 seconds, failure is reached. When shear wall SW1 fails, shear wall SW2 does likewise, and the whole building fails. Comparing shear responses between earthquake 1A and 1B indicates a difference in building response to earthquakes of different types with the same seismic intensity. In earthquake 1A, the building endures 7.372 seconds but in earthquake 1B, it fails around time = 4.164 seconds. Possibly the distribution of high magnitude is not the same for both earthquakes. A contributing factor could be the features of main elements in the building, particularly shear walls on the critical story.

Shear responses caused by the shear wall's shear spring for earthquakes 2A and 2B with seismic intensity of 0.3 g differ from those responses for simulated earthquakes of 0.2 g. In the case of simulated earthquakes with maximum intensity of 0.3 g, acceleration is one and a half of times greater than that with maximum intensity of 0.2 g. More shear is thus taken by the shear wall's shear spring, particularly on the critical story, and the building could fail sooner. In this case, the building fails after 3.30 seconds for earthquake 2A and after 1.58 seconds for earthquake 2B. Similarly, the building fails very quickly for simulated earthquakes with seismic intensity of 0.4 g, after 2.718 and 0.936 seconds for earthquakes 3A and 3B, respectively. Shear response history indicates that the elastic response for earthquakes of 0.3 g is smaller than **that** for earthquakes of 0.2 g. Elastic response for earthquakes of 0.4 g may be even smaller.

c. <u>Responses of shear and rotational springs of shear walls on critical story</u>
Shear response history of shear walls was discussed previously (sections b.). Seismic duration significantly affects degree of elasticity, as shown in Figure 143(a) and (b). The
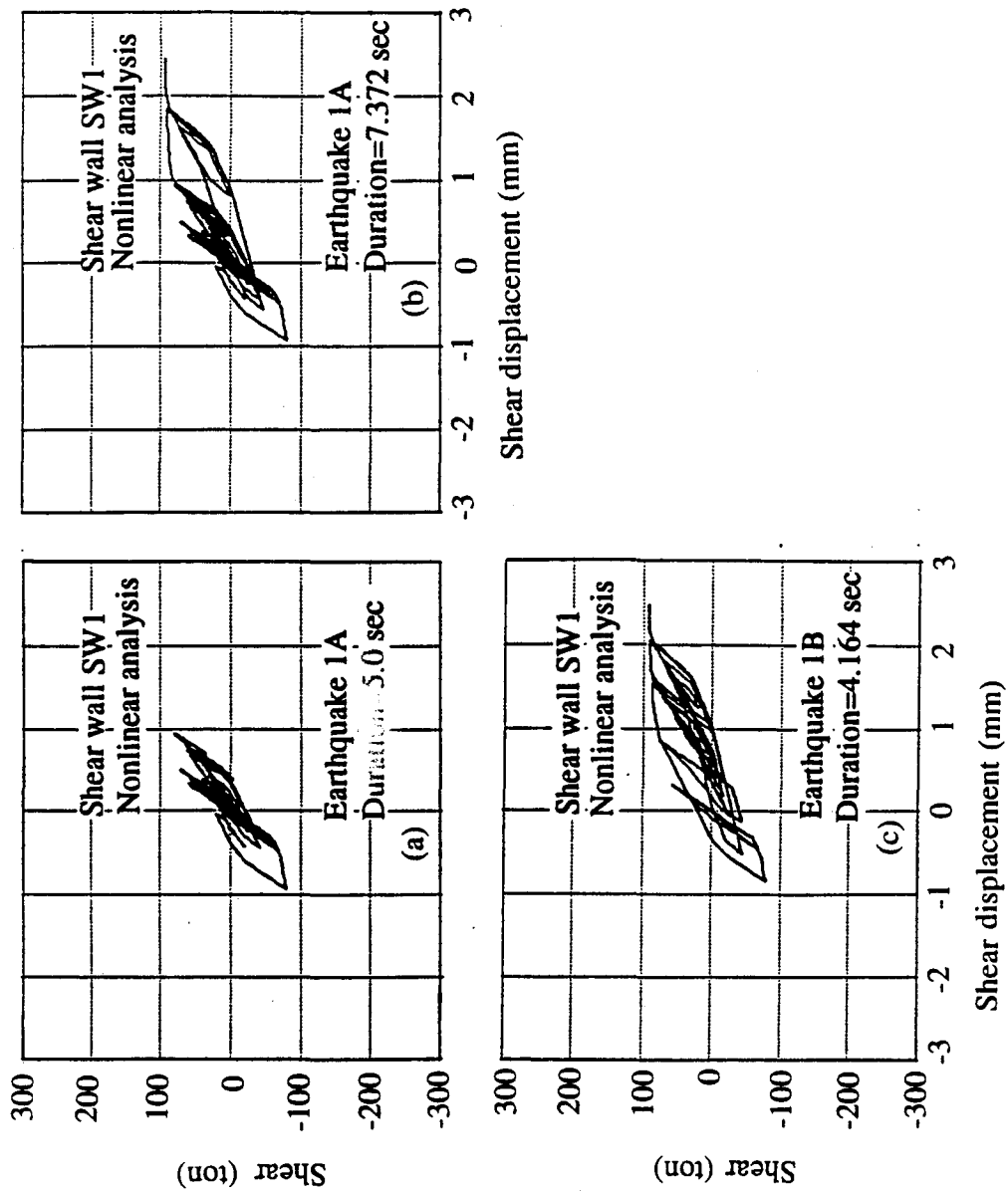
Figure 143   Shear vs. shear displacement by shear spring of shear wall SW1 for three-story building

293
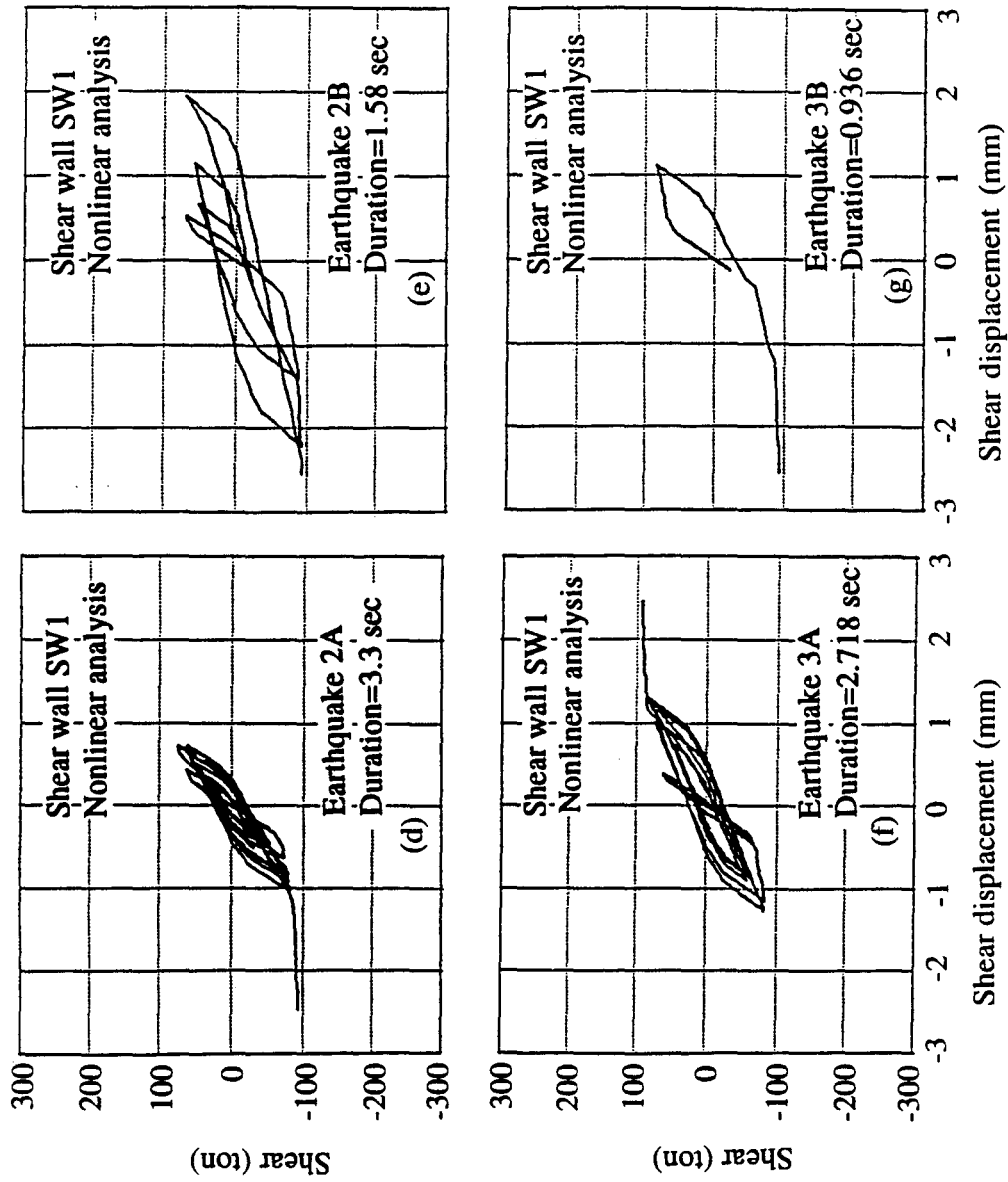
Figure 143 (continued) Shear vs. shear displacement by shear spring of shear wall SW1 for three-story building

294

latter shows more ductility and energy dissipation than the former. The difference between Figure 143(b) (subjected to earthquake 1A) and (c) (subjected to earthquake 1B) is mainly due to the earthquake's randomness even though 1A and 1B have a close maximum seismic intensity of 0.2 g. Similarly, earthquakes 2A and 2B have the similar maximum intensity of 0.3 g but shear wall response differs. Shear walls of the building subjected to earthquake 2A have numerous hysteretic cycles (see Figure 143(d)) but shear walls of the building subjected to earthquake 2 B have a limited hysteretic response (see Figure 143(e)).

When maximum seismic intensity increases to 0.4 g, as in earthquakes 3A and 3B, the situation is similar. Hysteretic response of the building's shear walls when subjected to earthquake 3A is intense (Figure 143(e)) but involves only one cycle when subjected to earthquake 3B (Figure 143(f)).

These cases indicate that the response of a predominantly shear wall building is affected by earthquake duration. The response of such a building may also vary depending on the shape of earthquakes even when magnitude is the same.

As mentioned in Section IX, a shear wall's rotational spring, taking limited shear throughout the monotonic static process, plays an insignificant role in resisting shear from an external load in these cases. This holds true for dynamic analysis as well. All the responses for a shear wall's rotational springs show that these springs are generally in the elastic range, although some exceed the cracking point of the backbone curve.

    d. Shear ratio by shear springs of shear walls on critical story Figure 144 shows the ratio of shear taken by shear walls on the critical story to total base shear for all cases. This ratio can be expressed as shear ratio by shear springs of shear walls

$$= \frac{\text{shear force taken by shear springs of shear walls in force direction}}{\text{base shear}} \times 100\% \qquad (297)$$

Point A in Figure 142(a) represents the shear wall as it enters the inelastic range from the cracking point of the backbone curve. At the corresponding point in Figure

295
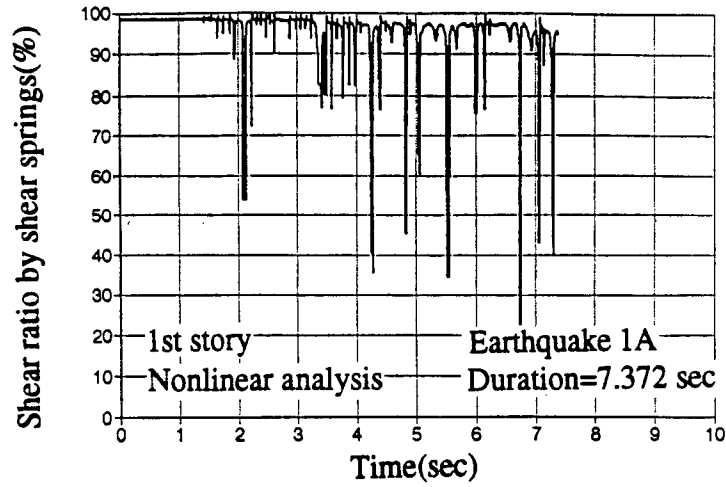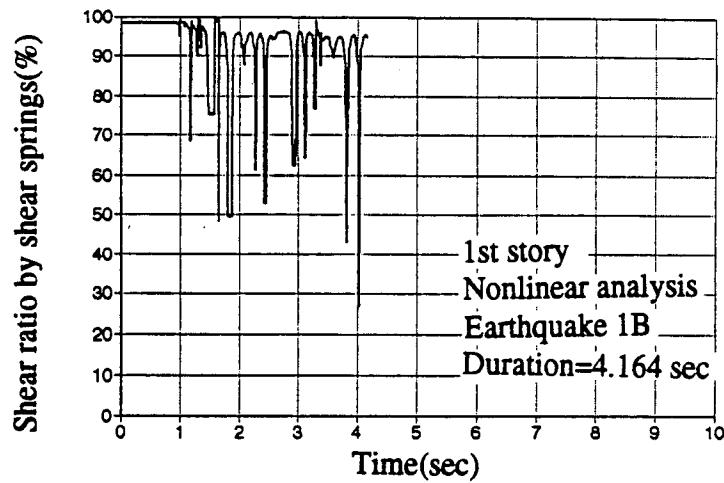
Figure 144 Shear ratio by shear springs of shear walls on critical story for three-story
building

144(a), the shear taken by all the shear walls on the critical story fluctuates and lowers the

ratio slightly. Before this point, shear ratio for all shear walls on the critical story is about

98%. Figure 145 illustrates how an abrupt jump occurs. Compare a time interval from 1

to 2 seconds for shear ratio by the shear wall's shear springs to the time relationship in the
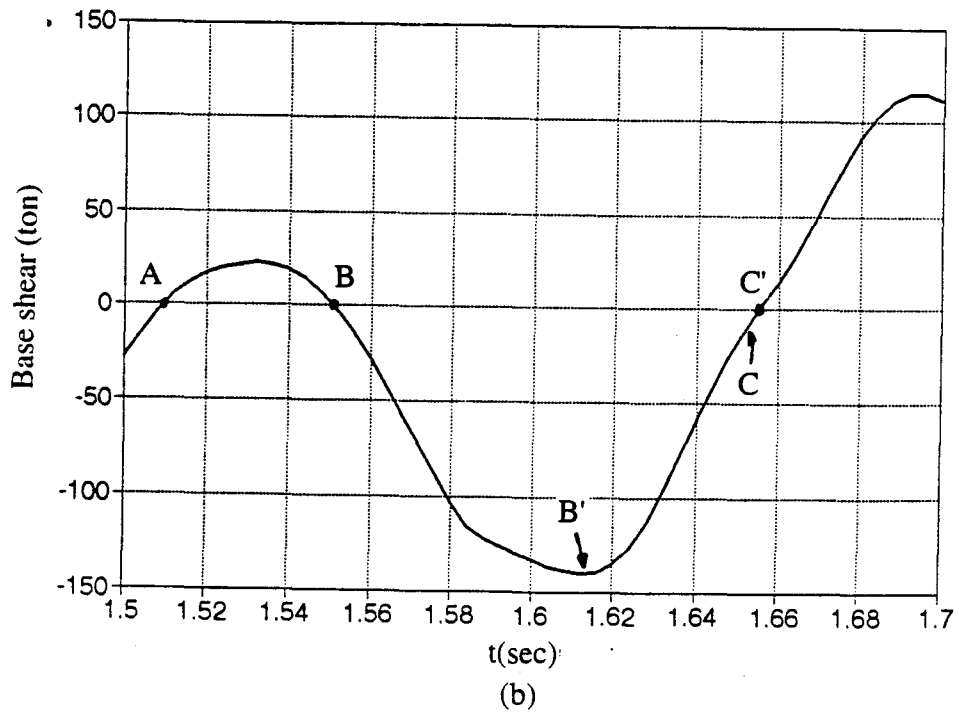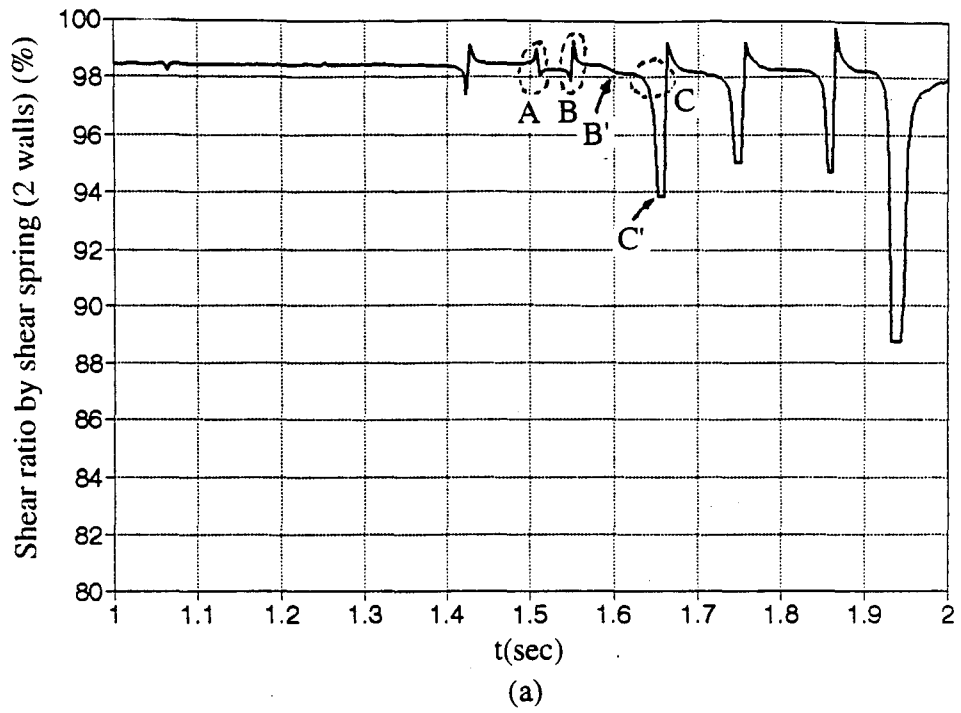
Figure 145 Shear ratio by shear springs of shear walls vs. time for time interval of 1 to 2 seconds and base shear vs. time for time interval of 1.5 to 1.7 seconds

case of an earthquake of 0.2 g. It can be seen that there are jumps at points A, B, B' and C of 1.5 to 1.7 seconds, as shown in Figure 145(a). The corresponding base shear vs. time plot shows points A, B, B',and C' in a time interval of 1.5 -1.7 seconds. Points A, B, B' and C' are located at zero base shear. When base shear approaches to zero, the ratio can be high or low, or even negative with a small denominator (i.e., base shear). This results in discontinuity of the curve. Except at these points, the curve shows stability for the characteristics of shear ratio. For the sake of analysis, ratios smaller than zero or greater than 100% are eliminated.

As noted in Section IX, three-story commercial building's configuration has two main elements, six RC shear walls and twenty-eight columns throughout the structure. Here a 2 % shear ratio could be taken by the columns. Since the shear wall's shear spring becomes highly plastic after a duration of 3.3 seconds, the ductility of the shear wall increases. This increase in ductility causes more lateral displacement of columns on the critical story, which adds slightly to the shear resistance taken by the columns. During the whole process, shear walls on the critical story of the building are the main resisters of seismic force. The shear ratio taken by columns is at most 3% even though shear walls on the critical story behave highly inelastically up to failure. Shear walls on the critical story thus take 97% of base shear upon entering into higher inelasticity and up to collapse.

When elastic analysis is applied to the building, the shear taken by shear walls on the critical story occupies 98% of base shear. Ductility characteristics of the shear wall cause its strength to deteriorate (i.e., the wall's load capacity declines). Other elements of the building then take more shear. In this situation, buildings fail more quickly due to yielding of main elements (i.e., shear walls).

In earthquake 1B (shown in Figure 144(b)), shear ratio of the shear walls on the critical story begins to drop at 1.1 seconds. At this, shear walls begin to crack and thereafter yield (see point A in Figure 142(b)). After the shear walls yield at 1.1 seconds, the range of shear ratio taken by all shear walls on the critical story is about 96~97%.

Similarly, shear walls take 97% of base shear for earthquake 2A and 94~96% for 2B with a maximum intensity of 0.3 g for both. For maximum seismic intensity of 0.4 g, shear ratios taken by shear walls on the critical story for earthquakes 3A and 3B are 96% and 93%, respectively.

e. Displacement ratio by shear springs of shear walls on critical story

Displacement ratio by shear springs of shear walls on the critical story is defined as

Displacement ratio by shear springs of shear walls =

$$\frac{\text{Lateral displacement caused by shear springs of shear walls in force direction}}{\text{Total lateral displacement of mass center}} \times 100\% \qquad (298)$$

where total lateral displacement here means critical story drift.

Figure 146 shows the displacement ratio by shear springs of shear walls on the critical story vs. time relationship for earthquake cases 1A and 1B. Many jumps appear so this phenomenon should be discussed first. The relationship of displacement ratio by shear springs of shear walls on the critical story vs. time is shown in Figure 147(a). This figure shows points A through L on the curve representing the locations of jumps for a time interval 1 to 2 seconds with a simulated earthquake of 0.2 g. Corresponding points A through L in Figure 147(b) are identical. This figure depicts the relationship of critical story drift vs. time; points A through L stand for critical story drift of zero displacement. When critical story drift is close to zero, the denominator of definition for shear ratio is small. Shear ratio thus could change, becoming high, low, smaller than zero or greater than 100%. These points cause unstable jumping in Figure 147(a). Analysis of the stable section can show displacement characteristics of the shear wall on the critical story. To analyze this, the ratio smaller than zero (i.e., the flat portion just before point L in Figure 147(a)) or greater than 100% (i.e., the flat portion just before points H and I) must be neglected. From Figure 147(a), the displacement ratio by shear springs of shear walls on the critical story is 40% or 50%.
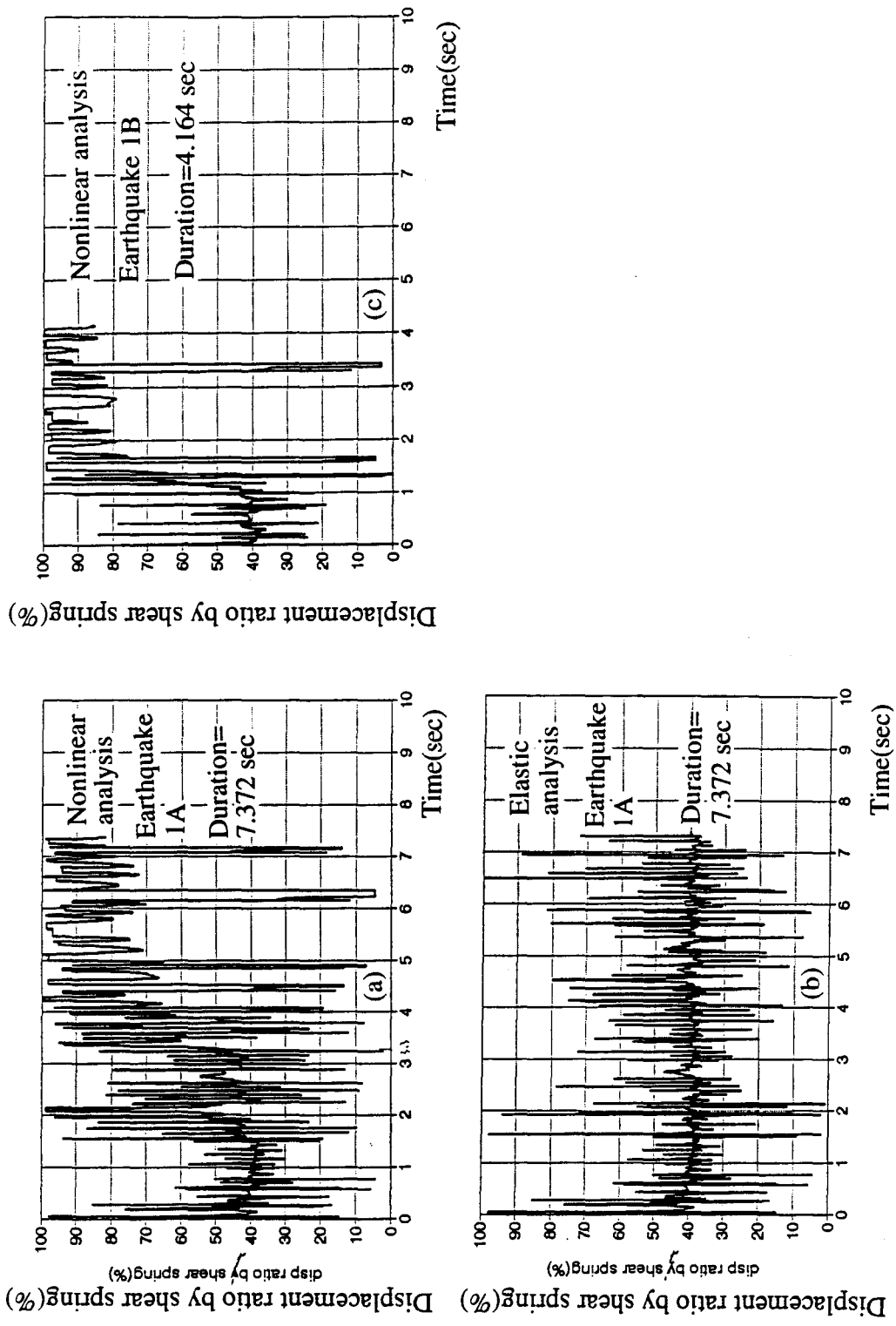
Figure 146 Displacement ratio by shear springs of shear walls on critical story of three-story building
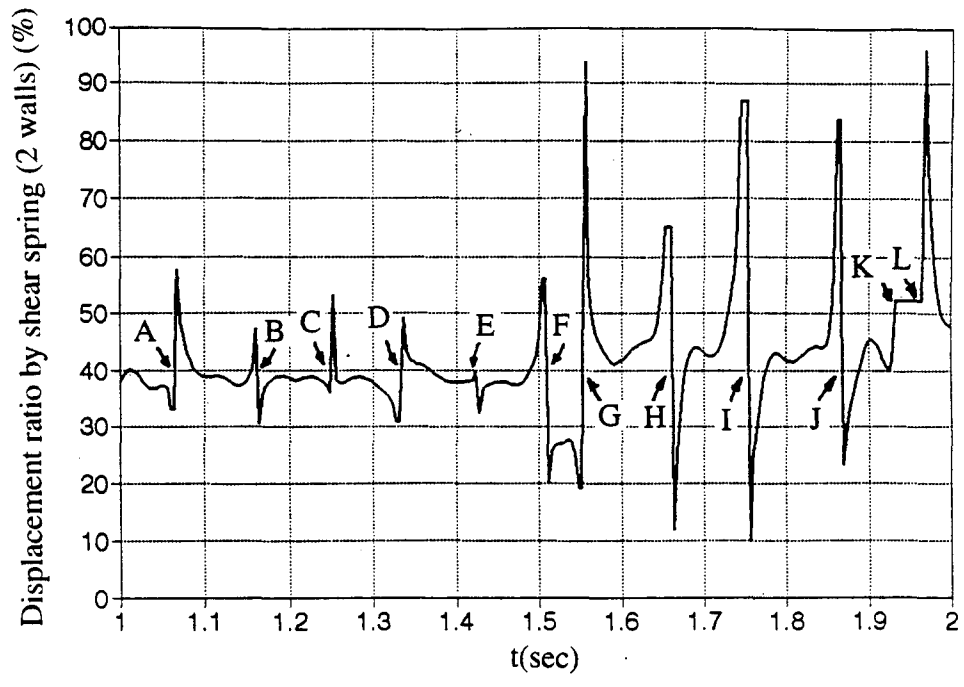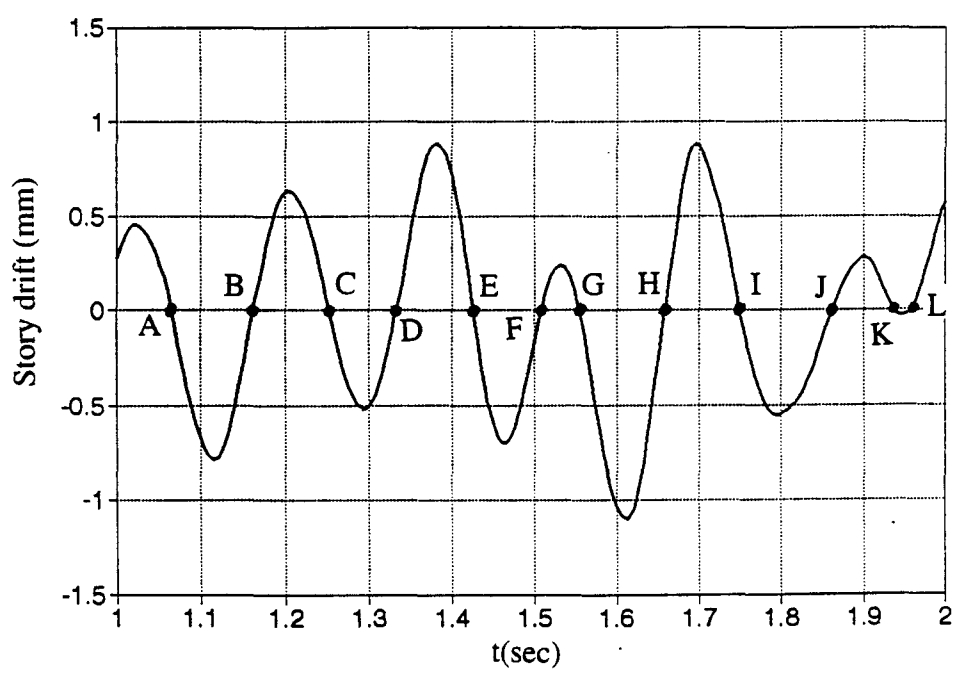
Figure 147 Displacement ratio by shear springs of shear walls on critical story vs. time for time interval of 1 to 2 seconds and critical story drift vs. time relationship

301

Figure 146(a) shows the ratio taken by shear springs of shear walls on the critical story is about 40% before 1.6 seconds. Displacement is caused by rotational springs of shear walls on the critical story. This displacement ratio range starts at 40% and goes up to 85%. At the final stage before the building fails, displacement induced by rotational springs of shear walls on the critical story is about 15% of total critical story drift.

Before cracking of shear walls at a time of 1.3 seconds, displacement caused by rotational springs of shear walls on the critical story generally occupies 60% of total critical story drift. These rotational springs have less stiffness than the shear wall's shear spring in the elastic range. When entering the highly inelastic range, shear springs of shear walls exhibit a high ductility range which increases displacement ratio by shear springs of shear walls on the critical story. A stable displacement ratio of 40%, which is the same as the period before 1.3 seconds for nonlinear analysis, can exist throughout elastic analysis. Other cases of earthquakes show that the same displacement ratio (i.e., 40%) due to shear springs of shear walls on the critical story.

Displacement ratio of 40% due to shear spring of shear walls on the critical story holds true for earthquake 1B before 1.1 seconds when the shear springs of shear walls enter the inelastic range. After 1.1 seconds, displacement ratio caused by shear springs of shear walls goes up drastically to more than 90%. For earthquakes 2A and 2B, displacement ratios caused by shear springs of shear walls increase from 40 to 60% and 40 to 80%, respectively. For maximum seismic intensity of 0.4 g, the displacement ratios go from 40 to 70% on average.

f. Investigation of design parameters Figure 148 shows the relationship of base shear vs. critical story drift for both nonlinear and elastic analysis of all the simulated earthquake cases 1A and 1B. This relationship is closely related to that of shear force and shear displacement by shear springs of shear walls on the critical story. Table XXXX summarizes all possible design parameters based on various earthquake duration for earthquake 1A. Earthquake duration is classified as 5, 10, 15 or 20 seconds, except the
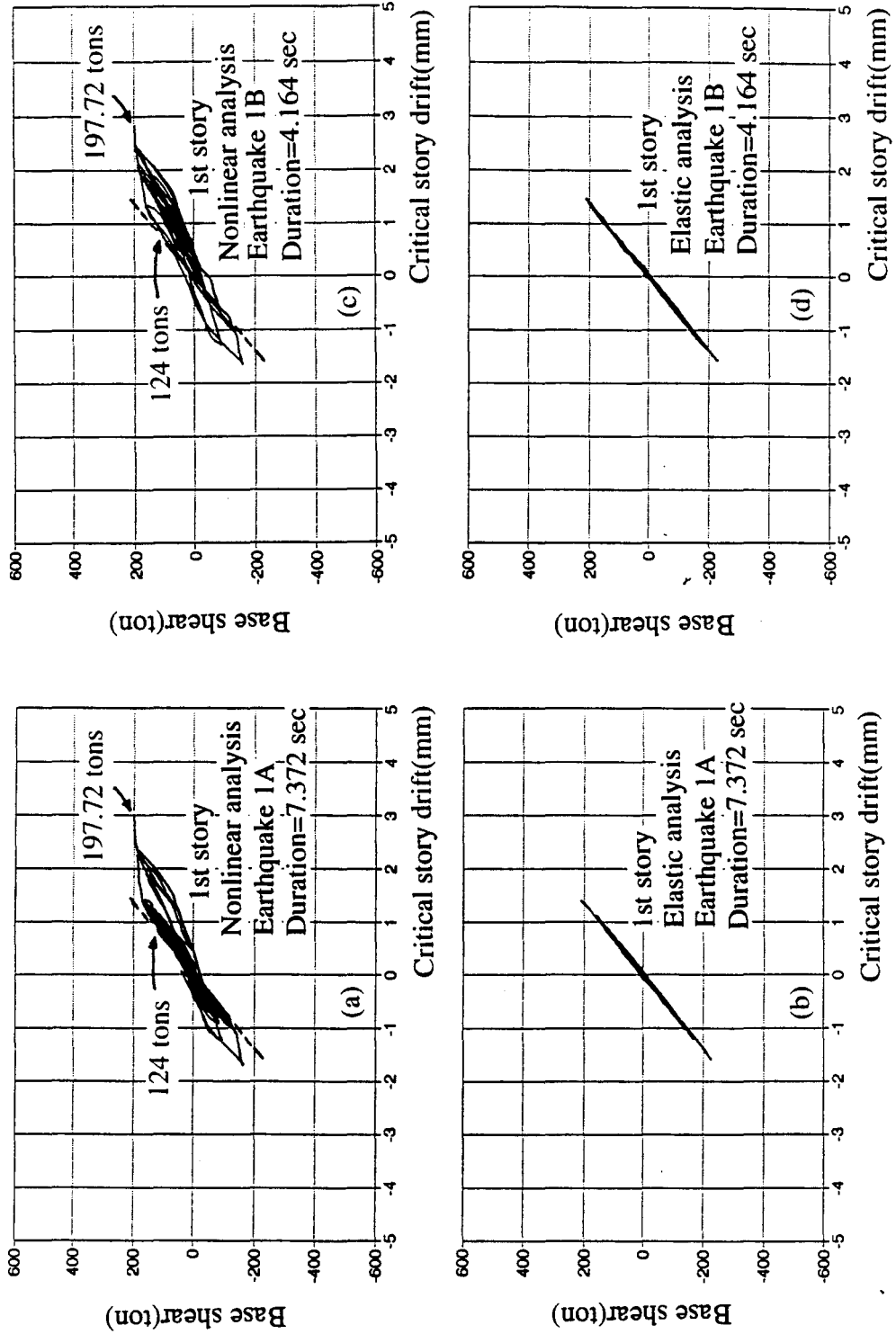
Figure 148 Relationship of base shear vs. critical story drift for both nonlinear and elastic analyses

303

duration of failure. Figure 148, which defines some variables, shows earthquake 1A with a duration of 5 seconds. Maximum displacement for nonlinear analysis is defined as Δ_{max}, similar to Figure 148(b) where elastic analysis is Δ_{eu}. The corresponding maximum base shears in Figure 148(a) and (b) are failure base shear and maximum elastic base shear, expressed as V_y and V_{eu}, respectively. Therefore, DAF/FRF is defined as the ratio of Δ_{max} to Δ_{eu} (see Ref. [77]). Ductility reduction factor R_μ is expressed as the ratio of maximum elastic base shear to failure base shear , i.e., V_{eu}/V_y. This procedure holds true for other cases. A summary of Table XXXX shows the results from Figure 148(a) and (b). In the table, $(time)_1$ expresses when the building reaches maximum (failure) base shear for nonlinear analysis; $(time)_2$ expresses when the building reaches the maximum base shear for elastic analysis. From this table, it can be found (with the exception of building failure) that maximum critical story drift Δ_{max}, maximum elastic story drift Δ_{eu} ,maximum failure base shear V_y and maximum elastic base shear increase with the duration of the earthquake. Table XXXXI shows the range of design parameters from all the cases. It can be seen that the ratio of displacement amplification factor to force reduction factor DAF/FRF is in the range of 1.0 to 1.9. Ductility reduction factor R_μ ranges from 1.1 to 2.3. System ductility factor μ_s is 2.1~2.4, an average of 2.3.

To explore further information on the relationship between ductility reduction factor and overstrength factor, the DAF/FRF ratio and overstrength factor, based on force reduction factor R_w (i.e., FRF), is of interest. Figures 149 and 150 are set up accordingly. Other research shows the DAF/FRF ratio for multistory steel and RC buildings is greater than 1.0. From Uang [77], the DAF/FRF ratio for a multistory steel frame structure is in the range of 1.2~2.5. In this section, the DAF/FRF ratio for a predominantly shear wall building is determined to be 1.0 to 1.9. If a minimum value of 1.0 for DAF/FRF is used in Figure 149, then overstrength factor Ω is in the range of 1.15 to 1.70, which is based on force reduction factor R_μ of 4.0 to 6.0. Using the second definition of design parameter (see Section IX) and overlapping Figure 148(b) onto (a), it can easily be found that

Table XXXX   Summary of some design parameters for simulated earthquake 1A

Earthquake duration	5.0	7.372*	10.0	15.0	20.0
δ_{max}	1.700	2.970	2.970	2.970	2.970
δ_{eu}	1.496	1.584	1.584	1.584	1.584
DAF/FRF	1.136	1.875	1.875	1.875	1.875
(time)$_1$	—	7.372	7.372	7.372	7.372
(time)$_2$	3.284	7.080	7.080	7.080	7.080
V_{eu}	215.38	225.53	225.53	225.53	225.53
$(V_i)_f$	163.50	197.72	197.72	197.72	197.72
R_μ	1.317	1.141	1.141	1.141	1.141

Unit: mm,ton
* = Failure state
DAF/FRF = δ_{max} / δ_{eu}
R_μ = V_{eu} / $(V_i)_f$
(time)$_1$=time when failure state occurs for nonlinear analysis

(time)$_2$=time when max. base shear occurs for elastic analysis

overstrength factor Ω is 1.6 ($\approx$ 197.72/124). An identical overstrength factor Ω is seen in Figure 148(c) and (d) where 1.6 fits the range of 1.15~1.70, based on the force reduction factor of 4.0~6.0. If an overstrength factor of 1.6 is used, the force reduction factor is assumed to be 6.0. By using the first definition of design parameters (see Section IX), the overstrength factor Ω is assumed to be 1.0. Force reduction factor R_ω can then be calculated as 3.22, assumed to be 3.5, with the formula $R_\mu=\mu_s\Omega Y$. Applying both overstrength factor of 1.15~1.6 and force reduction factor of 4.0~6.0 into Figure 150, the

305

minimum ductility reduction factor is 1.6. Combining this value with the observed range of 1.1~2.3 for the ductility reduction factor, a more reasonable range of 1.6~2.3 is obtained for the ductility reduction factor R_μ. Force reduction factor R_ω, 3.5,   based on the first definition of general response curve in Section IX, is kind of lower while a value of 6.0 is based on the second definition of the general response curve (see Section IX). The latter is the same as the UBC code design parameter. A force reduction factor of 6.0 obtained from dynamic analysis in this section is quite agreeable with the result from monotonic static analysis in Section IX. Therefore, the second definition could be recommended for use in the building with RC shear wall.

Table XXXXI   Summary of range of design parameters DAF/FRF, R_μ, and μ_s

Earthquake	1A	1B	2A	2B	3A	3B
DAF/FRF	1.875	1.807	1.421	1.375	0.962	1.044
R_μ	1.141	1.160	1.709	1.749	2.274	2.311
μ_s	2.1	2.1	2.4	2.4	2.2	2.4

C. MODIFIED THREE-STORY COMMERCIAL BUILDING SUBJECTED TO SIMULATED EARTHQUAKE

As modified, the three-story commercial building contains one more shear wall in the middle of both ground level and second floor (described as case 2g in Section IX). The middle shear wall (here called SW19) on the ground level has twice the load capacity but half the maximum displacement of shear wall SW1. Shear wall SW2 has one and a half times the load capacity but three-fourths the maximum displacement of shear wall SWA.

306

$$\frac{DAF}{FRF} = \left(\frac{\mu_s Y}{R_w}\right) \Omega \; ; \; \mu_s = 2.3$$
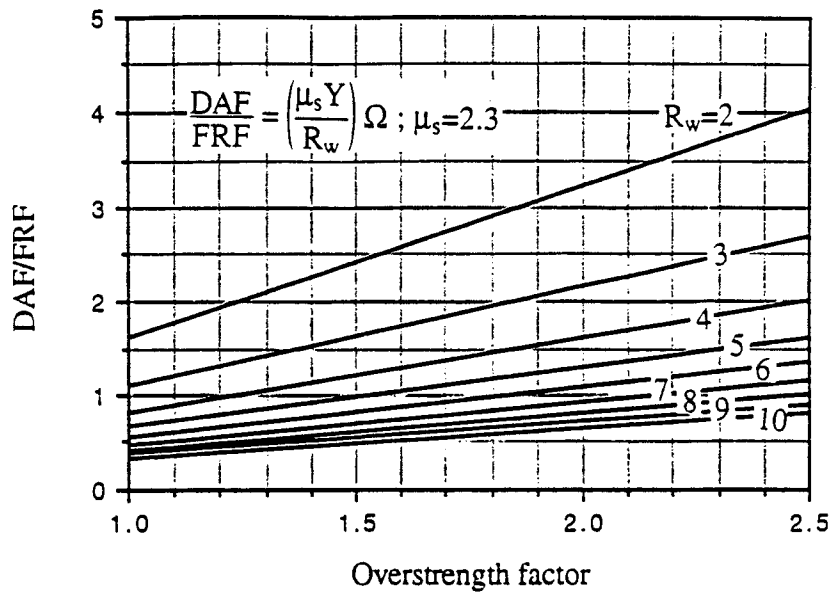
Figure 149 Relationship between DAF/FRF and overstrength factor

The second floor's middle shear wall (here called SW20) has the same properties as shear wall SW7. As stated, this modified three-story commercial building is subjected to the same simulated earthquakes. In general, the mass center is still close to the center of rigidity due to the building's symmetry.

1. Effect of Shear Springs of Shear Walls on Critical Story Figure 151(a) through (c) shows shear responses caused by shear springs of shear walls at ground level. In a simulated earthquake of 0.2 g, the building behaves elastically which is not shown in this figure. In a simulated earthquake with seismic intensity of 0.3 g, shear walls on the ground level (i.e., the first story) still dominate the whole behavior of the building. After 4 seconds or so, shear walls SW1, SW19 and SW2 on the ground level enter the fully inelastic range. Comparing all shear responses in Figure 151 and 152, the shear ratio of a shear wall's shear spring in the elastic range (4 seconds for earthquake 2A as shown in Figure 151 and 152) could be strongly related to the ratio of a shear wall's initial stiffness. After a period of elasticity, the shear walls soon behave highly inelastically. The shear ratio

307
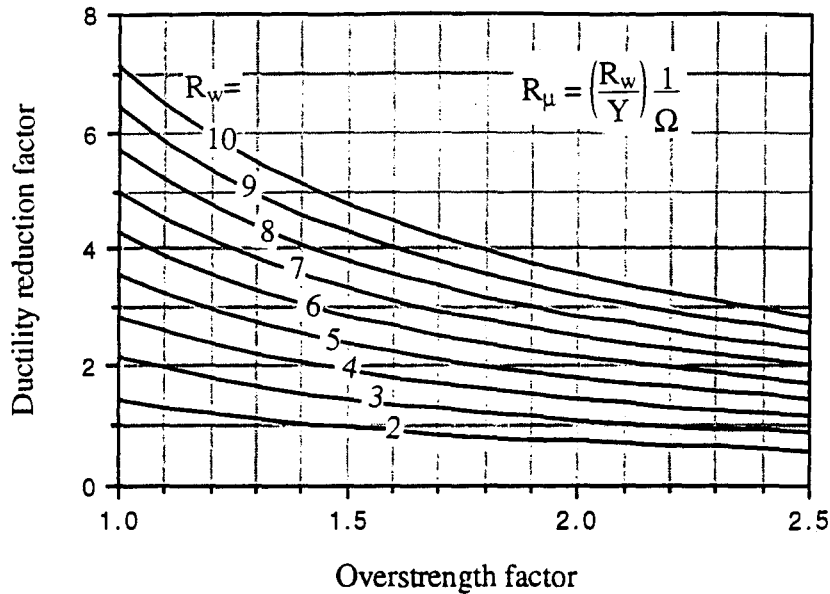
Figure 150 Relationship between ductility reduction factor and overstrength factor

of a shear wall's shear spring is about the same as the ratio of the shear ultimate strength of shear walls. During elastic response (see Figure 152), shear ratios taken by shear springs of shear walls SW1, SW19 and SW2 are 26%, 36% and 38%, respectively.

As noted, all possibilities except the shear wall's initial stiffness depend on the configuration of the building, mass center, and location of shear walls. When entering the phase of inelastic response, shear ratios of shear walls SW1, SW19, and SW2 are 22% (SW1), 28% and subsequently 25% (SW19), 47% and subsequently 49% (SW2), respectively. Since shear wall SW2 has much higher ultimate strength, it occupies about 50% of base shear.

Displacement ratios by shear springs of shear walls are shown in Figure 153. In terms of elastic response for shear walls SW1, SW19, and SW2 these ratios are 38%, 35% and 27%, respectively. Displacement ratios by rotational springs of shear walls SW1, SW19, and SW2 are 62%, 65%, and 73%, respectively. For these walls flexural lateral displacement is larger than shear lateral displacement. In terms of highly inelastic

308
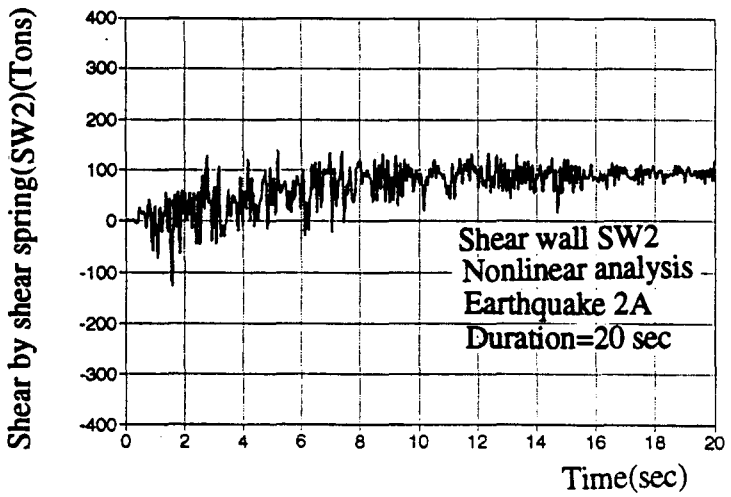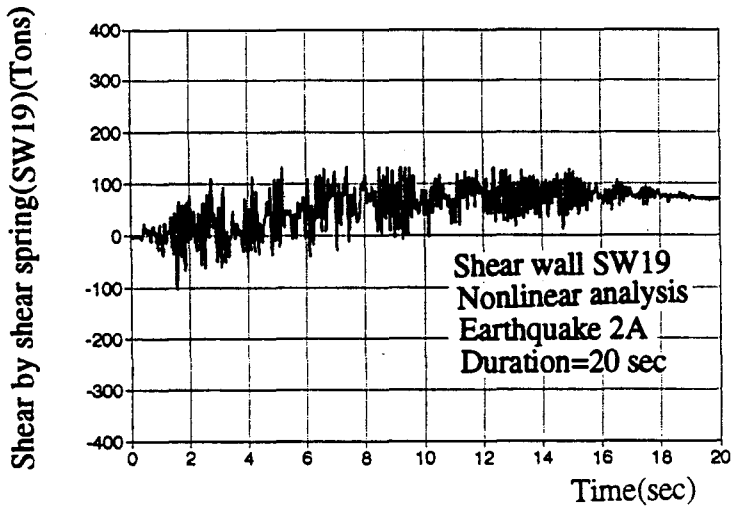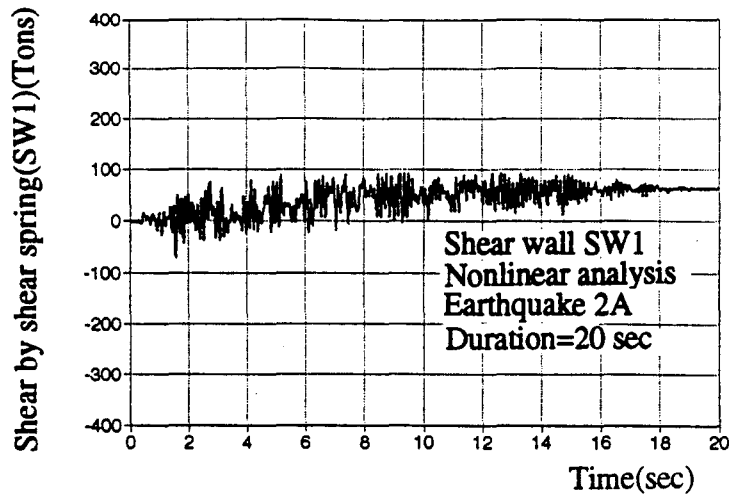
Figure 151   Shear by shear spring of shear wall vs. time on critical story of modified three-story building
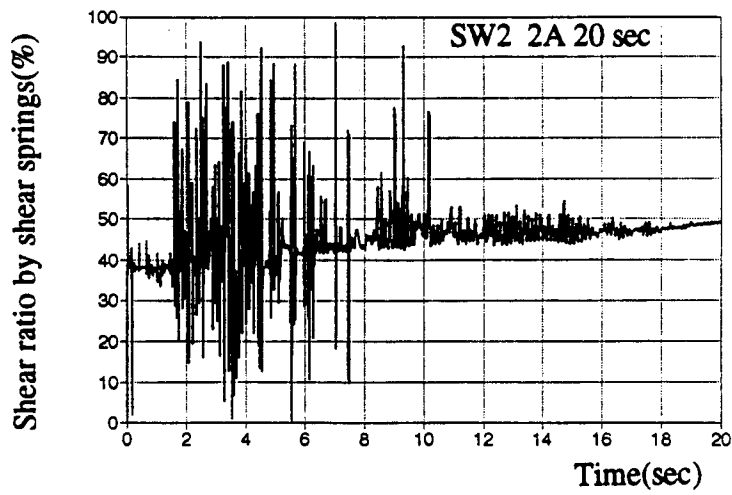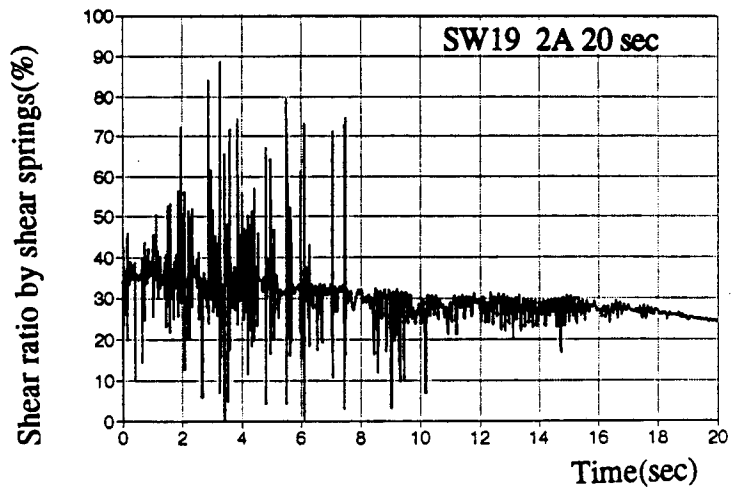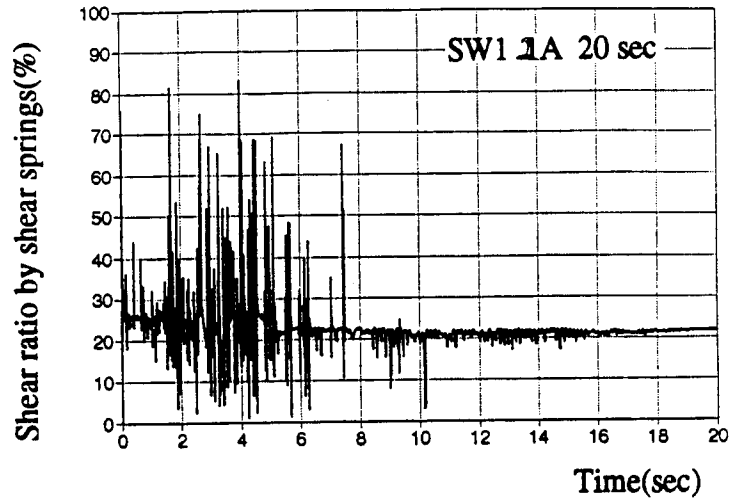
Figure 152   Shear ratio by shear springs of shear walls on critical story of modified three-story building

response, displacement ratios by shear springs of shear walls become 98%, 98% and 80%, respectively. Displacement ratios by rotational springs of shear walls SW1, SW19 and SW2 are 2%, 2% and 20%, respectively. The former ratios become 100% when shear springs of shear walls enter the range of high inelasticity and the latter ratios become zero.

Relationships between shear resistance and shear displacement by shear springs of shear walls on the critical story are shown in Figure 154. In these figures, shear walls for simulated earthquakes (2A and 2B) with a seismic intensity of 0.3 g have two quite different responses. More hysteretic cycles occur in shear walls on the critical story for earthquake 2A than for earthquake 2B. The former also has more energy dissipation than the latter. These results are similar to those for monotonic static analysis with columns taking very little shear.

2. Investigation of Design Parameters Figure 155 shows the relationship between base shear and critical story drift for both nonlinear and elastic analysis in the earthquake cases 2B and 3B. A key factor is the behavior of shear walls on the critical story, which can be seen in Figure 154. A summary is shown in Table XXXXII. Simulated earthquakes with a seismic intensity of 0.2 g have a DAF/FRF ratio of 1.0, a ductility reduction factor R_μ of 1.0, and a system ductility factor of 1.0. Generally, building response with seismic intensity of 0.2g involves elastic behavior. Later analysis concerns only simulated earthquakes of 0.3 g and 0.4 g.

In summary, the ratio of displacement amplification factor to force reduction factor DAF/FRF is in the range of 1.1~2.3. Compared with the previous building (case 1g), the DAF/FRF is 1.0~1.9, stable in these cases. For practical purposes, a conservative recommendation is 1.0 to 2.0. Ductility reduction factor R_μ ranges from 1.0 to 1.12. System ductility factor μ_s is of 1.15 to 2.2, an average of 1.82. Note the difference from the case of the previous building, having a range of 1.1~2.3 for R_μ and an average μ_s of
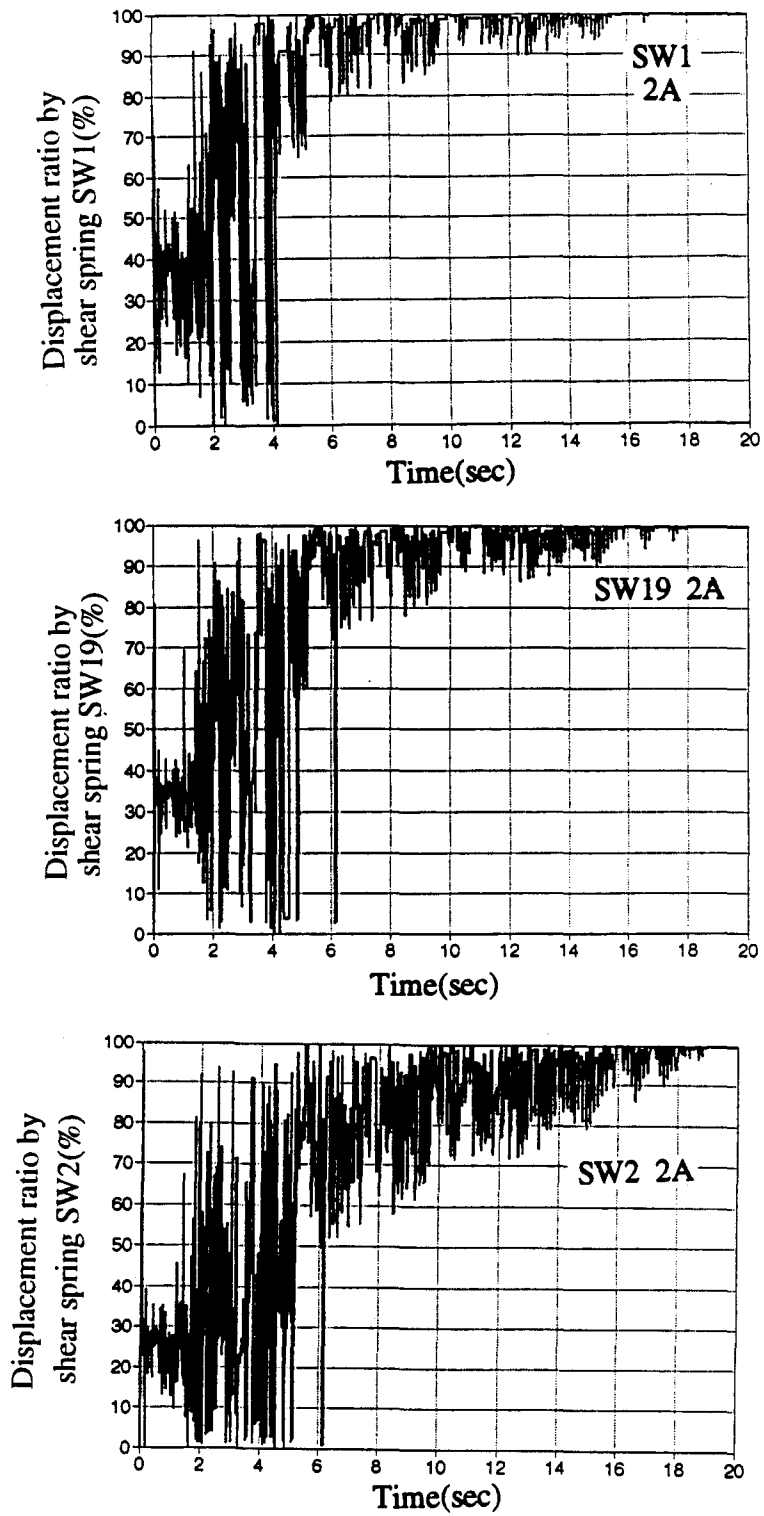
Figure 153 Displacement ratio by shear spring of shear wall on critical story of modified three-story building

312
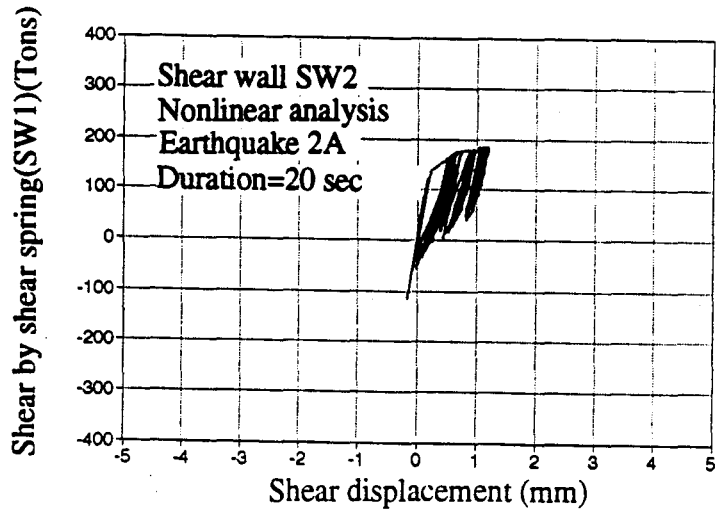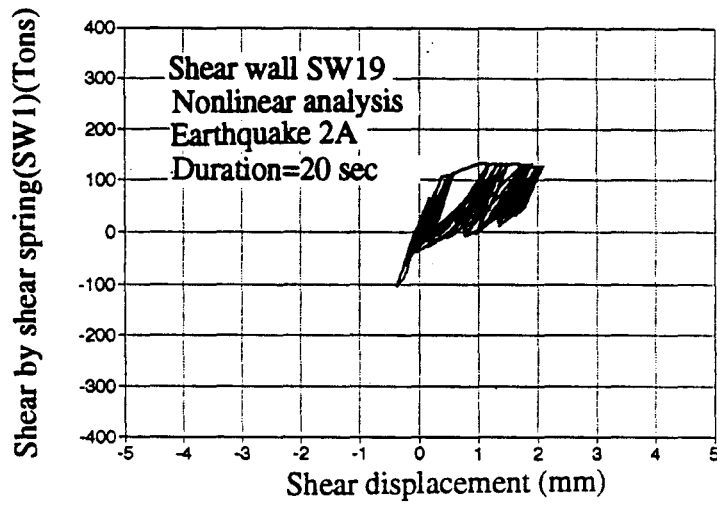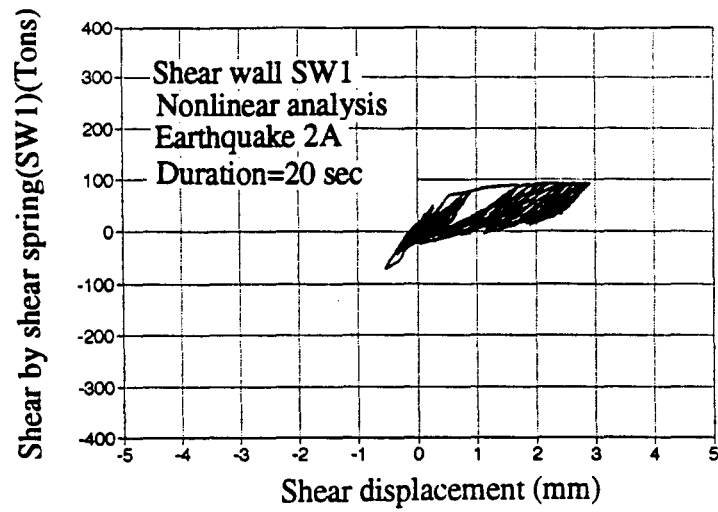
Figure 154 Shear vs. shear displacement relationship of shear wall on critical story of modified three-story building
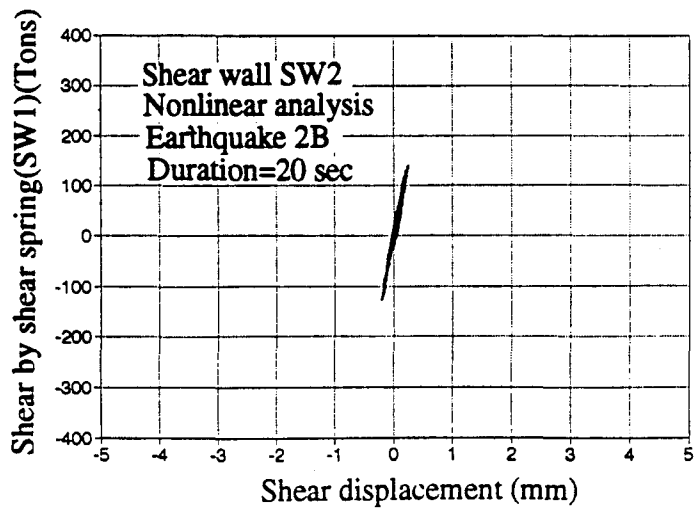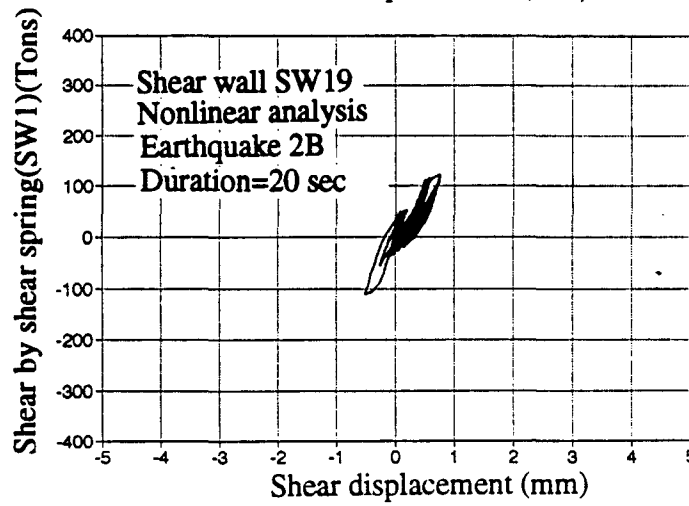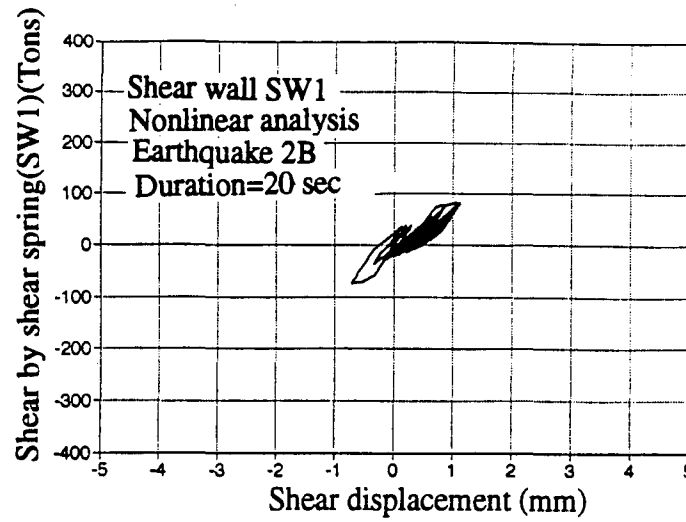
Figure 154 (continued) Shear vs. shear displacement relationship of shear wall on critical story of modified three-story building

314
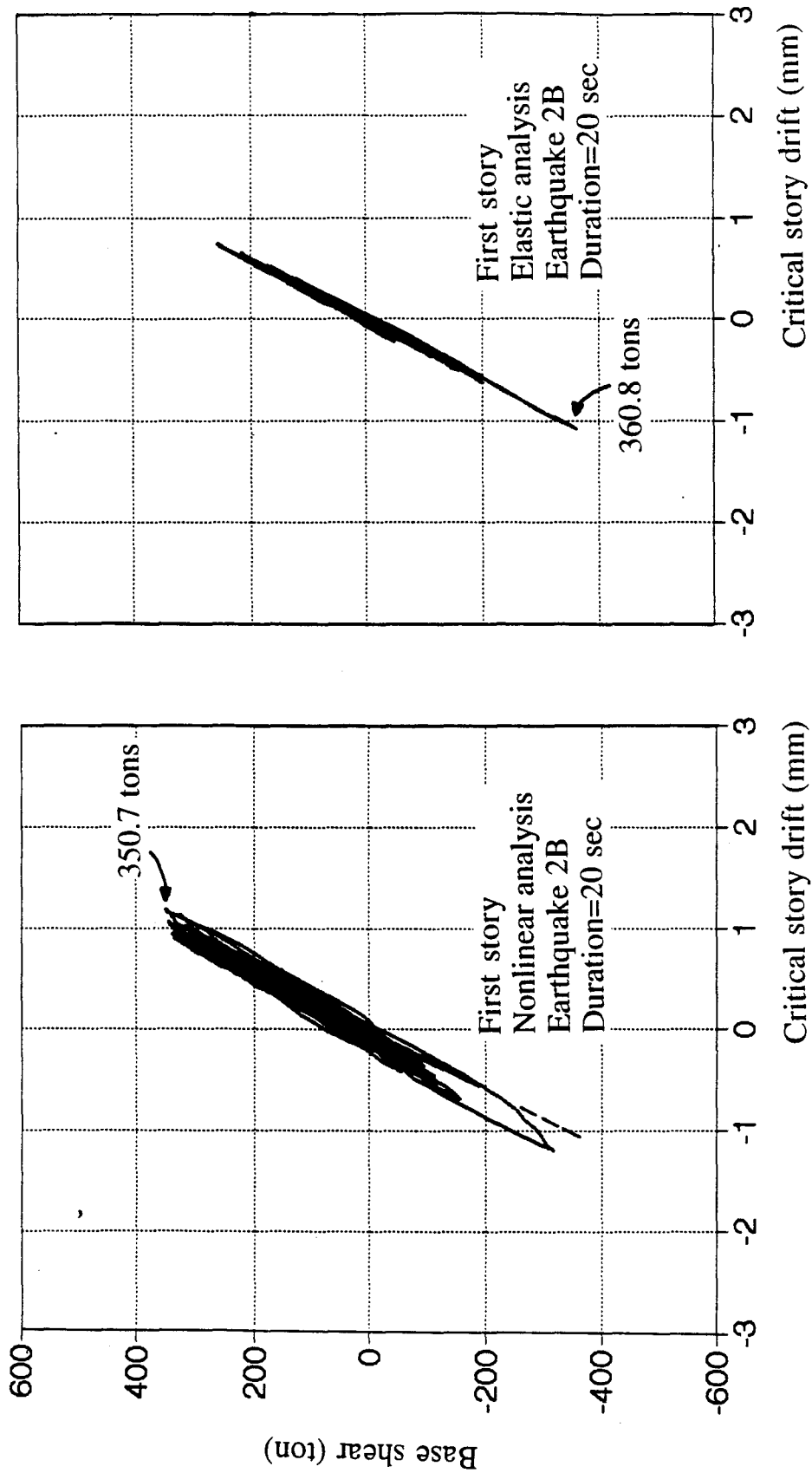
Figure 155 Base shear vs. story drift on critical story of modified three-story building
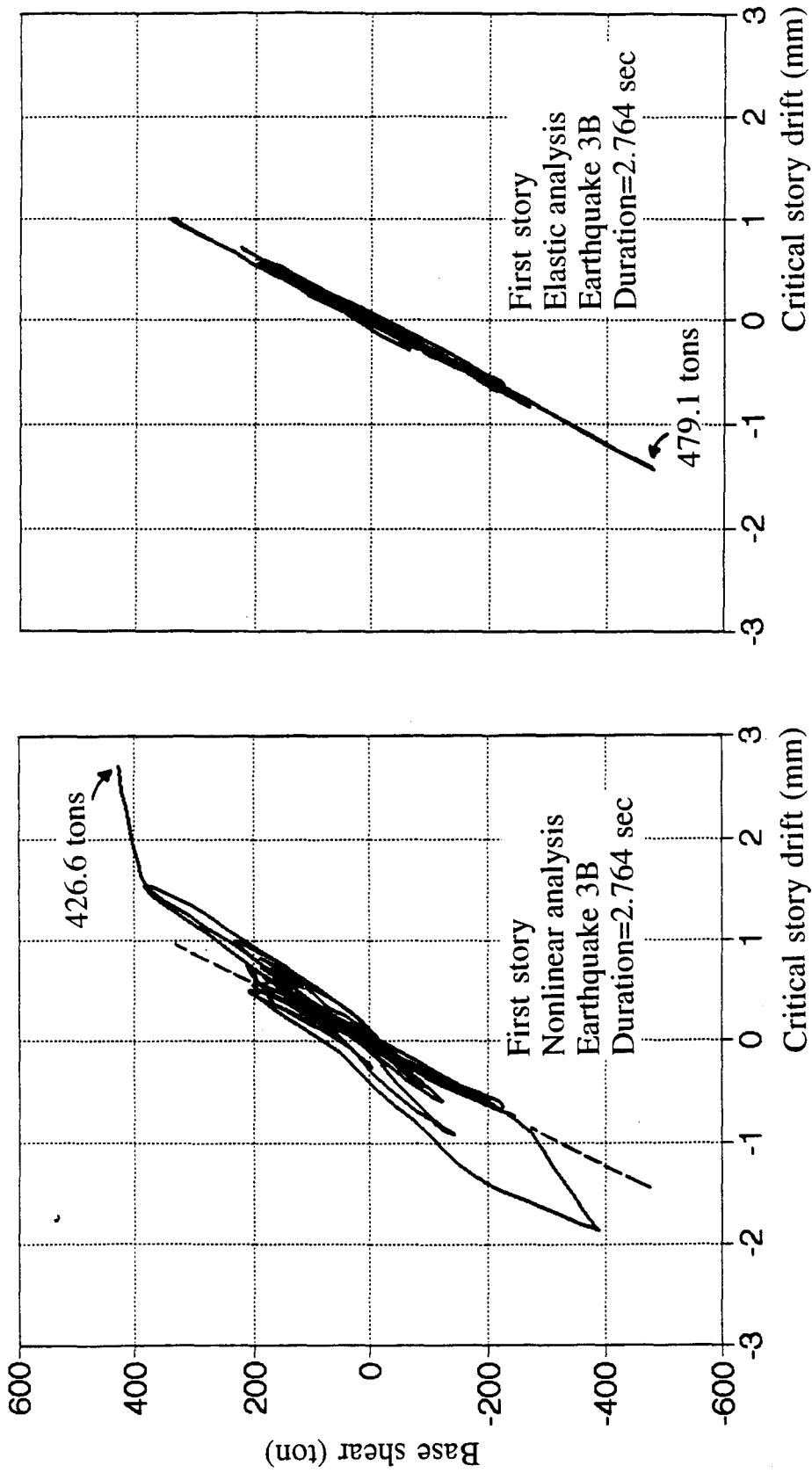
Figure 155 (continued) Base shear vs. story drift on critical story of modified three-story building

Table XXXXII Summary of range of design parameters DAF/FRF, R_μ, and μ_s for modified three-story building

Earthquake	1A	1B	2A	2B	3A	3B
DAF/FRF	1.000	1.000	2.311	1.116	2.220	1.900
R_μ	1.000	1.000	1.000	1.029	0.982	1.123
μ_s	1.000	1.000	1.806	1.148	2.180	2.130

2.3. System ductility seems stable for these two buildings and can be assumed to be 2.1 (=(1.82+2.3) / 2) on average. As to overstrength factor Ω (DAF/FRF=1.0 assumed), if it is 1.0 (based on the first definition in Section IX), force reduction factor R_w ($=\dfrac{\mu_s Y}{DAF/FRF}\Omega$, which is derived from Eq. (216)) is 1.61 (for μ_s =1.15) and 3.08 (for μ_s = 2.2). These force reduction factors R_w (based on the first definition of the general response curve) are quite low compared to UBC code design parameters. If DAF/FRF ratio equals 1.0 (presumed minimum), overstrength factor Ω ($=\dfrac{DAF/FRF}{\mu_s Y}R_w$, which is derived from Eq. (216)) is in the range of 2.48~3.73 (for μ_s =1.15 and R_w =4.0~6.0) and of 1.30~1.95 (μ_s =2.20 and R_w =4.0~6.0). As shown in Figure 155, overstrength factor can also be calculated as 1.40 (based on the second definition). It can be concluded that 1.15~1.70 (for the previous building) or 1.30~1.95 (for the current building) are stable ranges for the overstrength factor. Accordingly, force reduction factor R_w can be obtained in a more reasonable range of 4.0~6.0. As shown in Figures 148 and 155 (based on the second definition), a calculated overstrength factor of 1.60 (for the previous building) and 1.40 (for the current building) are in the range noted above. These values are in good

agreement either from base shear vs. critical story drift curve based on the second definition, or from formulation of design parameters based on the results of dynamic analysis.

XI. SUMMARY AND CONCLUSIONS

To study the possible response of an isolated shear wall and a building with shear walls subjected to external force, a joint research project was conducted by National Cheng Kung University (NCKU) and University of Missouri-Rolla (UMR). Theoretical analysis at UMR included (1) observations of NCKU experimental work; (2) establishment of backbone curve of perforated shear wall; (3) development of hysteresis rules for isolated shear walls; (4) calculation of equivalent viscous damping model and its associated damping range for perforated shear walls subjected to seismic loading; (5) illustration of parameters for design code with respect to overstrength factor; (6) formulation of element model of perforated shear wall; (7) evaluation of design parameter for shear-wall-dominating buildings under monotonic loading application; (8) assessment of design parameter of shear wall dominating building subjected to simulated earthquakes. A summary and conclusions are outlined in this section.

A. EXPERIMENTAL OBSERVATIONS AND MATERIAL MODEL OF ISOLATED SHEAR WALL

Experimental results Experimental results at NCKU come from two groups of shear walls. One group was subjected to monotonic static loading, the other to earthquake quasi-static loading. Twelve perforated shear walls as well as five solid shear walls were tested with a height/width ratio of 0.5 and 0.75 for each type of wall. Single slit, single window, and double windows were used for perforated shear walls.

Comparing solid shear walls and perforated shear walls based on experimental results, the yielding and ultimate load capacities for the former are almost twice that of the latter. Critical displacements are not stable at the cracking point for both solid and perforated shear walls. Average yielding displacement of the perforated shear wall is about 2.10~2.20 mm, two-thirds of the solid shear wall (whose average yielding displacement is

3.35 mm). Ultimate displacement of 3.79 mm for the perforated shear wall is about two-fifths that of the solid shear wall (whose average ultimate displacement is 9.62 mm). Openings thus play an important role in load capacity and maximum displacement of shear walls.

Curvature response differs for solid vs. perforated shear walls at locations throughout a given wall. Solid shear walls have a larger curvature capacity than perforated shear walls. Curvature illustrates the effect of bending behavior on a shear wall. With larger curvature capacity, more flexural response occurs when a wall is subjected to external load. This suggests more applied load can be resisted by shear wall. Comparing solid and perforated shear walls, the former has more load capacity and maximum displacement due to its flexural characteristics.

Note the relationship between bending, shear, and total displacement. It can be seen that shear displacement takes a higher percentage of the total than flexural displacement. If a shear wall is designed with more horizontal steel bars to improve its shear capacity, initial stiffness of shear wall's backbone curve is increased. This may result in less displacement. Then ductility characteristics are not obvious. Optimization between load capacity and maximum displacement becomes a crucial theme. An average failure ductility of 4.0 is recommended for the design of perforated shear walls.

Backbone curve of shear wall For perforated shear walls, the location of initial cracks is important due to possible stress concentration at the corner of openings. Observations from experiments illustrate this. An initial diagonal crack pushes the block above the opening segregated from the rest of the wall. Load capacity as well as maximum displacement are then decreased. Again perforated shear walls behave differently from solid shear walls. Vertical steel bars above the opening are not long enough to be considered in the calculation of load and displacement.

On shear walls the region subjected to the effect of combined shear and bending is the hinging region. It usually absorbs most of the input energy and thus deteriorates. For

a solid shear wall, the hinging region spreads over the entire wall. From observations of a perforated shear wall experimentally, the hinging region only covers both sides of the opening and extends slightly upward or downward. The limited size of the perforated shear wall's hinging region decreases the wall's potential load capacity and ductility characteristics.

Considerations in the development of backbone curve for perforated shear wall include location and size of openings. Generally, comparison between experimental results and calculated curve is favorable vis-a-vis NCKU perforated shear walls. Note that in semi-empirical equations for backbone curve, a segment with a negative slope shows the characteristics of stiffness deterioration after the ultimate state. For better curve-fitting, more experimental results are needed to calculate the coefficients of semi-empirical equations presented here.

Hysteresis rules for perforated shear walls An algorithm develops hysteresis rules pertaining to perforated shear walls. Prior to this, a dissipated envelope is established for a possible path based on hysteresis energy. This envelope is a reference curve which is a type of load-displacement curve with energy dissipation. The backbone curve for a shear wall is unique. But a reference curve may vary, depending on external load history. Three empirical equations define critical points in the reference curve.

After establishing this reference curve, hysteresis rules can be developed. Five groups of rules reflect different stages: loading process, unloading process, reversal loading process, reloading after unloading process, and unloading after reversal loading. Each group of rules defines the path by calculated stiffness. Agreement between expected hysteresis curves and experimental hysteresis results is good. All the shear walls display a pinching effect. This effect, as part of the hysteretic response, shows that RC perforated shear walls are strongly influenced by shear.

Equivalent viscous damping of RC perforated shear wall As noted in prior research, hysteretic damping can be observed in a given material. This damping comes

from internal friction and other complex mechanisms. For practical purposes, equivalent viscous damping is used to find the effect of hysteretic damping. From NCKU experimental work, irregular load-displacement cycles can be seen in perforated shear walls. The formulation herein is aimed to account for irregular skew hysteresis looping. For reinforced concrete shear walls, hysteretic damping might not be taken into account before the cracking stage. Damping ratio gradually increases with maximum ductility of shear walls. Calculated damping ratio based on experimental results may be as high as 15.7%. Initial damping ratio for hysteretic damping, however, ranges from 5 to 6 percent.

B. ELEMENT MODEL OF PERFORATED SHEAR WALL

A panel with four joints at corners serves as a model for the perforated RC shear wall. Ten degrees of freedom are assumed in ten directions: two in the horizontal direction; four in the axial direction on both sides of the rigid body; four out of plane to account for P-Δ effect. If the bottom of the wall is fixed and out-of-plane deformations do not pertain, then three springs are necessary to provide adequate resistant force for this shear wall. Nonlinear equivalent shear springs and nonlinear axial springs are applied to nonlinear total lateral displacement and nonlinear axial displacement.

From experimental results, lateral displacement caused by flexure is less than that caused by shear. Total displacement for perforated shear walls, as depicted by the equivalent shear spring, is a result of both flexure and shear. Deformation caused by flexure in the vertical direction is expressed by one pair of nonlinear springs. This model, with equivalent shear spring only, could be used for low-rise shear-wall buildings.

C. RESPONSE STUDY OF THREE-STORY AND FOUR-STORY BUILDINGS

There are two types of buildings used to study global behavior. First is an RC box-type four-story industrial building with all four shear walls forming an effective resistance system on each floor. Adjacent walls interconnect and bear a heavy dead load on each

floor. Shear capacity of the walls is high due to their large dimensions and strong reinforcement. **Second** is a three-story commercial building with curtain walls. Six solid shear walls on each floor comprise its resistance system. Comparatively, the four-story building has thicker walls than the three-story building. Wall dimensions in the three-story building are much smaller than the four-story building. Monotonic loading is applied to the four-story industrial building and then to the three-story commercial building. Other three-story buildings with modifications are also studied here with regard to perforated shear walls.

<u>Four-story industrial building</u> Shear walls have a higher initial stiffness for rotational springs than for shear springs in terms of load-displacement relationship. This allows the shear spring to deform further than the rotational spring. Walls with rotational springs thus fail earlier than those with shear springs. For all the shear walls, ultimate shear displacement is higher than ultimate flexural displacement. SW12 and SW16 at ground level have a larger ratio of bending displacement vs. shear displacement than the other shear walls. Bending and shear displacements of SW12 and SW16 at ground level are more sensitive to the building's global response.

Overall response of the building under monotonic static loading, with ductility of 4.0 for shear walls, shows that SW12 fails first in the flexural mode followed by SW16 in the same mode. Walls on the upper level of the building remain in the elastic range. Overall response is controled by shear walls on the first story.

Story response is strongly related to the load-displacement relationship of shear walls for each floor. Differences in story displacement from floor to floor depend on wall height as well as backbone curve of shear walls. The four-story industrial building fails at the first story. Characteristics of backbone curves here show that shear walls after the yielding point become partly inelastic and then fully inelastic. Even a slight increase in ductility hastens ultimate displacement of shear walls. Due to high plasticity, ultimate

lateral load does not change much. Critical story drift may thus vary for shear walls with different ductilities but maximum base shear remains stable despite ductility.

Note what generally happens if more load increments are applied to the building after the critical story fails in the flexural mode. Due to stress redistribution, the shear wall's shear spring takes extra shear from that wall's rotational spring. Failure of the building in the shear mode soon occurs. The situation is similar whether the building fails in the flexural mode or in both the flexural and shear mode.

Three-story commercial building As noted earlier, this structure contains RC columns. Under monotonic static loading, two shear walls along the force direction resist external load. Compared to shear walls in the four-story building above, shear walls in this building have quite different configuration and reinforcement. This difference is partly due to less wall thickness as well as greater height/width ratio in the three-story building. Overall backbone curve of shear walls in this building reveal their main features: more flexural lateral displacement than shear lateral displacement and stiffer shear initial stiffness. One of the shear walls, SW1, along the force direction fails first in the shear mode; almost simultaneously, another shear wall, SW2, fails at the next load step. At this time, critical state at the first story occurs due to failure of SW1 and SW2. Before shear walls at the critical story fail, flexural behavior caused by their rotational springs is still within elastic range. After shear walls at the critical story fail, columns located there gradually take over stress from these failed walls, due to shear redistribution, and from external force as well.

As mentioned earlier, some modified three-story buildings are considered in monotonic static analysis. Perforated shear walls, placed at different stories, might cause significant change in maximum base shear and maximum story drift. Clearly the configuration and material properties of solid and perforated shear walls are important factors in the design of buildings. Adequate story drift and sufficient shear capacity are major concerns. In some cases, perforated shear walls increase the capacity of structures to withstand external loads.

D. DYNAMIC RESPONSE OF RC SHEAR-WALL-DOMINATING BUILDINGS

RC shear wall buildings have three types of failure modes: shear, flexural, and both flexural and shear. For dynamic analysis here, an existing three-story commercial building is studied under Loma Prieta earthquake and six other simulated earthquakes. Maximum intensity of the Loma Prieta earthquake was 0.15g, imposed on the structure along the skew direction. The output of acceleration response, which shows that the results from nonlinear analysis and elastic analysis are the same, agrees with the seismic records. Thus, under the Loma Prieta earthquake, the existing structure displayed an elastic response.

Under six simulated earthquakes, the structure was tested with the same procedure. Seismic intensity is 0.2g for earthquakes 1A and 1B, 0.3g for earthquakes 2A and 2B, and 0.4g for earthquakes 3A and 3B. 1A and 1B have a different earthquake time history as do 2A and 2B as well as 3A and 3B. For earthquake 1A, the three-story building fails at 3.3 seconds, for earthquake 1B at 4.164 seconds, for earthquakes 2A and 2B at 3.3 and 1.58 seconds, respectively, and for earthquakes 3A and 3B at 2.718 and 0.936 seconds, respectively. A shear-wall-dominating building fails at different time intervals for earthquakes which have the same seismic intensity: it depends on the type of earthquake. Given the same type of earthquake, a building fails under stronger seismic excitation. In this case, for buildings with symmetric configuration, shear walls SW1 and SW2 take the same percentage of shear resistance. At the critical story, shear displacement by shear springs of shear walls is important. Shear taken by shear springs of shear walls is 98 percent of base shear while that taken by columns is 2 percent. The effect of rotational springs of shear walls can be neglected. At the critical story, displacement ratio by shear springs of shear walls is also important. Before cracking of shear walls, displacement caused by rotational springs of these walls is 60 percent of total critical story drift. Note that rotational springs of shear walls have less stiffness than shear springs of shear walls in the elastic range. When a structure behaves in a highly plastic manner, shear springs of

shear walls exhibit ductility characteristics. This increases the displacement ratio by shear springs of shear walls at the critical story.

A modified three-story building is used for dynamic analysis. This building has two additional shear walls: one in the middle of the first story and one in the middle of the second story. Two boundary columns are fixed at each side of these additional walls. Shear capacity ratio for shear walls SW1, SW19 and SW2 on the first story is 1:1.5:2 while their maximum displacement ratio is 1:0.75:0.5. SW1 has less initial stiffness and more maximum displacement. Thus it has a somewhat larger vibration than shear wall SW19, a much larger vibration than shear wall SW2. Its total lateral displacement is also larger.

Displacement ratios by shear springs of shear walls on the critical story indicate the following: 30 to 40 percent within the elastic range and 80 to 98 percent in the plastic range. It can be seen that shear springs of shear walls dominate the entire structure's response. Overall, the arrangement of shear walls and their load-displacement relationship, especially on the critical story, is vital for the building's survival during a severe earthquake.

E. DESIGN PARAMETERS FOR RC SHEAR-WALL-DOMINATING BUILDINGS

Table XXXXIII summarizes design parameters based on monotonic static analysis of a four-story industrial building and three groups of three-story buildings as well as dynamic analysis of the three-story building (case 1g of Group I) and a modified three-story building (case 2g of Group II).

It should be noted that the concept of the first plastic hinge provides a good definition of design parameters for frame structures. For frame structures, the first and second definition actually yield the same results.

Table XXXXIII   Summary of design parameters and relevant factors based on analytical results obtained from monotonic and dynamic tests

Case	R_μ	R_w	μ_s	DAF	Ω	DAF/FRF
Monotonic loading (4 story bld.)	1.7-1.8	3* 7.5**	1.0* 2.94-4.81**	1.40* 12.29-20.71**	1.0* 3.0**	0.6* 1.6-2.8**
Monotonic loading (3 story bld.)	2.3	4.0* 6.0**	1.0* 4.0-7.5**	1.40* 4.0-24.9**	1.0* 1.8-2.2**	0.4* 1.82-3.37**
Dynamic loading (3 story bld.)	1.1-2.3*** 1.0-1.12*****	—	2.3*** 1.82*****	—	1.15-1.70*** 1.30-1.95*****	1.0-1.9*** 1.1-2.3*****

* Based on first definition of global structural response at critical story
** Based on second definition of global structural response at critical story
*** Based on original three-story commercial building (case 1g)
**** Based on modified three-story commercial building

327

In a shear-wall-dominating building, shear wall doesn't have a plastic hinge. The first significant yield stage is where the first shear wall fails. From Table XXXXIII, (i) system ductility factor μ_s (1.0), (ii) overstrength factor Ω (1.0), and (iii) displacement amplification factor DAF (1.4) are the same for four-story and three-story buildings under static analysis based on the first definition. It is apparent that the structural system has much larger inelastic deformation than yielding deformation. From above results, it can be concluded that system ductility factor μ_s (1.0) and overstrength factor Ω (1.0) are not reasonable. Then DAF calculated as Y (i.e., $DAF = 1 \cdot 1 \cdot Y = Y$), which is based on the expression of $DAF = \mu_s \cdot \Omega \cdot Y$, is not reasonable. The first definition for design parameters is therefore not adequate for shear-wall-dominating buildings.

For the second definition, the first significant yield level is the point where the critical story response deviates from elastic range. Based on this definition, system ductility factor μ_s (2.9 ~7.5), overstrength factor Ω (1.8~2.2 and 3), force reduction factor R_w (7.5 and 6), DAF/FRF ratio (1.6~3.37), DAF (4~24.9), and ductility reduction factor R_μ (1.7~1.8 and 2.3) are obtained for both 3-story and 4-story buildings. These factors except factor DAF are reasonable physically. Thus, the second definition for design parameters is suitable for shear-wall-dominating buildings.

Results from dynamic analysis show that ductility reduction factor R_μ (1.0~2.3), system ductility factor μ_s (1.82 and 2.3), overstrength factor Ω (1.15~1.95), DAF/FRF ratio (1~2.3) are also reasonable. Force reduction factor R_w and displacement amplification factor DAF can then be obtained on the basis of the formulations $R_w = R_\mu \cdot \Omega \cdot Y$ and $DAF = \mu_s \cdot \Omega \cdot Y$.

In summary, force reduction factor R_w of 6 and 7.5 is for the two low-rise RC shear-wall-dominating buildings presented in this report. Compared with these values, R_w of 6 specified for bearing wall system with RC shear walls in the UBC design code is different. Actually UBC design code does not identify the influence of building

configurations and shear wall layout of a structure on R_w. Further research would benefit from studying more varieties of RC shear wall buildings.

Displacement amplification factor DAF has a wide range of values (4~24.9) for both static and dynamic analyses but DAF/FRF ratio has a narrow range of 1~3.37. This ratio can be used to predict adequate DAF. Furthermore, consideration of overstrength factor Ω, preventing structures from failure, in the UBC design code is urgently needed in UBC. For low-rise RC shear-wall-dominating buildings, overstrength factor of 1.2~2.2 is recommended.

APPENDIX A

SHEIKH'S MODEL

Sheikh proposed a general curve for the stress-strain relationship of confined concrete, in which three sections are to be defined. The curve is shown in Figure 156. The first section is a curve of second-degree parabola, denoted by OA, A being $(\varepsilon_{s1}, f_{cc})$. Term fcc, representing the relationship between the concrete strength and lateral confinement produced by rectilinear reinforcement, can be written as

$$f_{cc} = f_{cp} + f(\rho_s, \ s, \ f_s', \ \lambda, \ \eta) \tag{299}$$

in which fcp = strength of concrete in plain specimen; ρ_s = ratio of volume of total lateral reinforcement to volume of core; s= tie spacing in laterally reinforced specimen; f_s' = stress in lateral reinforcement; λ = factor that accounts for configuration of section and distribution of longitudinal bars around core parameter; η shows the effect of the size of the section.

In brief, the compressive strength of confined concrete in the specimen, fcc, can be expressed as follows

$$f_{cc} = K_s \cdot f_{cp} \tag{300}$$

in which

$$K_s = 1.0 + \frac{2.73B^2}{P_{occ}} \left[\left(1 - \frac{nC^2}{5.5B^2}\right)\left(1 - \frac{s}{2B}\right)^2 \right] \sqrt{\rho_s f_s'} \quad (f_s' \text{ is in kips/in}^2 \text{ and } P_{occ} \text{ in kips})$$
$$\tag{301}$$

or

$$K_s = 1.0 + \frac{B^2}{140P_{occ}} \left[\left(1 - \frac{nC^2}{5.5B^2}\right)\left(1 - \frac{s}{2B}\right)^2 \right] \sqrt{\rho_s f_s'} \quad (f_s' \text{ is in megapascals and } P_{occ} \text{ in}$$
$$\text{kilonewtons)} \tag{302}$$
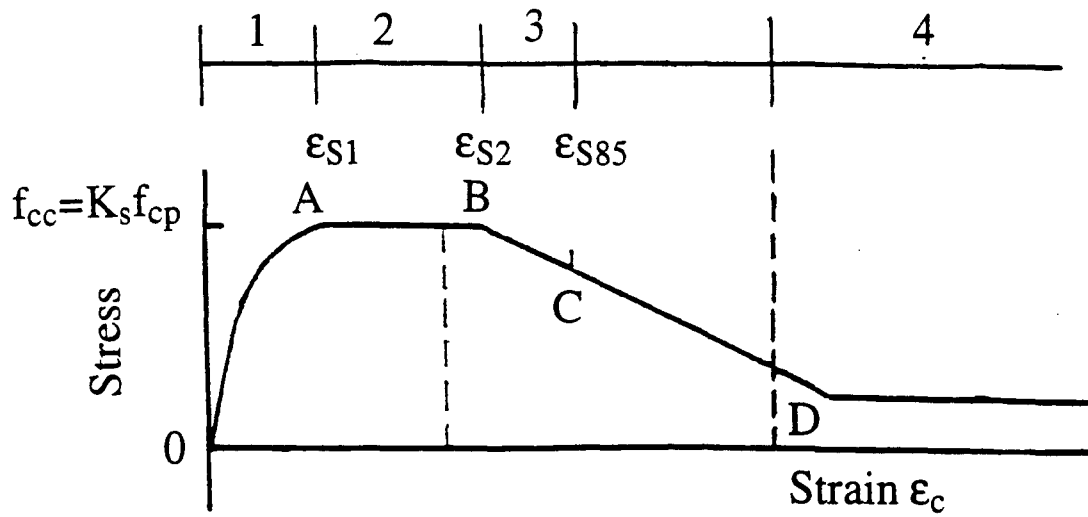
Figure 156   Sheikh's confined concrete model

Here B is center-to-center distance of perimeter tie of core; $P_{occ} = 0.85f'_c(A_{co}-A_s)$, theoretical capacity of column core concrete; f'_c = compressive strength of plain concrete as measured from standard cylinder [152 mm x 305 mm] test; As = area of longitudinal steel; Aco = area of core bounded by center-to-center of perimeter tie; n = number of arc along one side of perimeter tie; C = base of arc curve; ε_{s1} is minimum strain corresponding to maximum concrete stress, which can be expressed as

$$\varepsilon_{s1} = 0.55 \cdot K_s \cdot f'_c \times 10^{-6} \text{ (if } f'_c \text{ in pounds per square inch)} \tag{303}$$

or

$$\varepsilon_{s1} = 80 \cdot K_s \cdot f'_c \times 10^{-6} \text{ (if } f'_c \text{ in megapascals)} \tag{304}$$

Section AB and BC of the curve are straight lines. Strain ε_{s2} is the maximum strain value corresponding to the maximum stress and is written as

$$\frac{\varepsilon_{s2}}{\varepsilon_{oo}} = 1 + \frac{0.81}{C}\left(1 - 5.0\left(\frac{s}{B}\right)^2\right)\frac{\rho_s f_s'}{\sqrt{f_c'}} \quad \text{(C in inches; stress in pounds per square inch)}$$

(305)

or

$$\frac{\varepsilon_{s2}}{\varepsilon_{oo}} = 1 + \frac{248}{C}\left(1 - 5.0\left(\frac{s}{B}\right)^2\right)\frac{\rho_s f_s'}{\sqrt{f_c'}} \quad \text{(C in millimeters; stress in megapascals)} \quad (306)$$

in which ε_{oo} = strain corresponding to maximum stress in plain concrete(0.0022 in the case of present tests).

ε_{s85} is the strain corresponding to 85% of maximum stress on the unloading branch of the curve, which has the form of

$$\varepsilon_{s85} = 0.225\rho_s\sqrt{\frac{B}{s}} + \varepsilon_{s2}$$

(307)

Beyond point C, the curve drops down linearly until the stress is about 30% of maximum stress. Beyond point D, due to lack of experimenal data, the assumed horizontal load can not be confirmed.

Further details can be found in the study by Sheikh and Uzumeri [72].

APPENDIX B

AXIAL HYSTERESIS MODEL

Kabeyasawa et al. [78] developed the axial hysteresis model for shear walls and boundary columns as part of analytical studies for a full-scale 7-story test structure. This model concerns behavior before tensile yield and after tensile yield. A brief illustration is shown in the following.

Tensile Backbone Curve This curve is bilinear. Its initial tensile stiffness is

$$K_t = 0.90 \ E_c \ A_g \qquad (308)$$

where E_c is the concrete modulus of elasticity and A_g is the gross cross sectional area of the member. When the steel bar yields at (D_{yt}, F_y)

$$F_y = f_y \ A_s \qquad (309)$$

and

$$D_{yt} = F_y \ / \ K_t \qquad (310)$$

where f_y is the yield point of the steel bars and A_s is the area of the steel bars. Stiffness becomes

$$K_{t2} = 0.001 \ E_c \ A_g \qquad (311)$$

Compression Backbone Curve This curve is linear. Its compressive stiffness is expressed by

$$K_c = E_c \ A_g \qquad (312)$$

Compressive stresses usually remain below $0.50f'_c$.

335

Cyclic Loadings before Yielding A bilinear hysteresis loop is used for cyclic loading before the member has yielded, as shown in Figure 157. When a member is subjected to a tensile load within critical yielding point, stiffness as noted above is K_t. Say the member is subjected to a tensile load FB (point B in the figure), and unloads from point B. Unloading stiffness of the member is K_c, which is the same as compression initial stiffness. When unloading to point C, the member is on the compression side and the load between point B and point C is equal to F_y. If reloading from point D, the member follows the path with a stiffness of K_c.

Behavior when the member has yielded is shown in Figure 158 where point E is the maximum load beyond the yielding point on the tension side. The member unloads with stiffness defined as follows

$$K_r = K_c\left(\frac{D_{yt}}{D_{max}}\right)^\alpha \geq \left(\frac{F_{max} + F_y}{D_{max} - D_{yc}}\right) \qquad (313)$$

where $D_{yc} = -F_y / K_c$ and $\alpha = 0.90$. Unloading continues to point F where load and displacement of the member are given by

$$FF = F_{max} - F_y \qquad (314)$$

and

$$DF = D_{max} - \frac{F_y}{K_r} \qquad (315)$$

The path between points F and G has the stiffness of

$$K_s = \frac{FF + F_y}{DF - D_{yc}} \qquad (316)$$
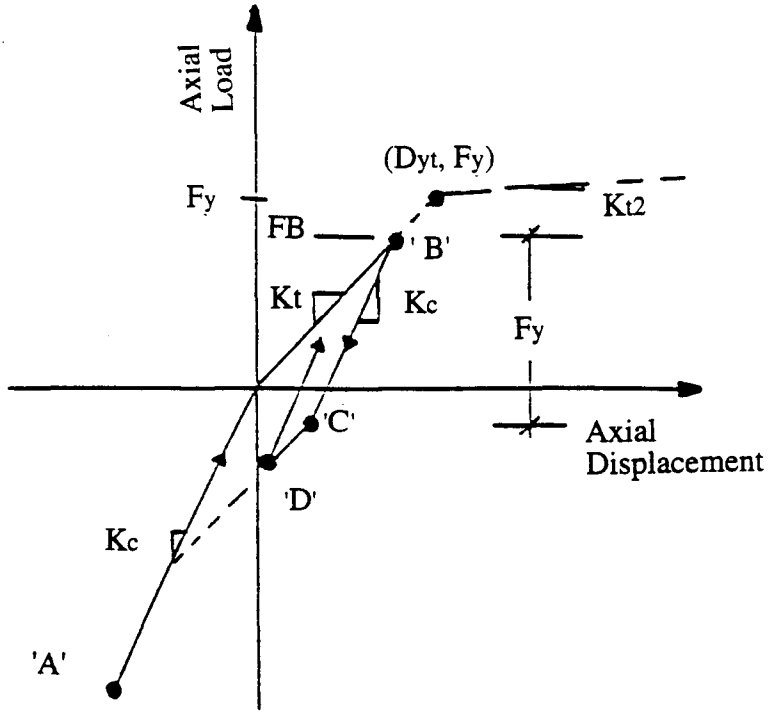
Figure 157 Axial hysteresis model before tensile yield
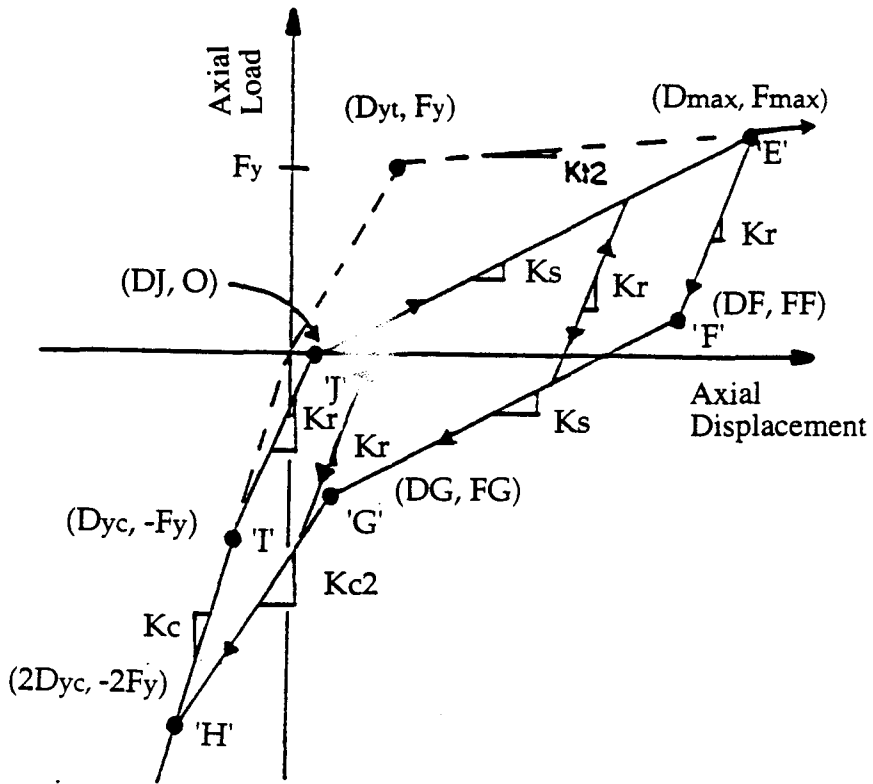
Figure 158 Axial hysteresis model after tensile yield

Load and displacement of the member at point G become

$$FG = FF + K_s (DG - DF) \tag{317}$$

and

$$DG = D_{yc} + 0.20 (DF - D_{yc}) \tag{318}$$

Beyond point G unloading continues on a transition curve that goes from point G to point H on the compression backbone curve. Stiffness is defined as

$$K_{c2} = \frac{FG + 2 \times F_y}{DG - 2 \times D_{yc}} \tag{319}$$

Further unloading and loading remain on the compression backbone curve except in the region beyond point I (D_{yc}, $-F_y$). Loading beyond point I has the same stiffness as unloading stiffness on the tension side, which is expressed by K_r. Loading and unloading on small amplitude loops inside the region E-F-G-H-I-J-E have a stiffness of K_r.

Summary The axial hysteresis model presented here was developed for reinforced boundary columns. Further research to study RC shear walls with axial loads experimentally and analytically is recommended.

BIBLIOGRAPHY

1. Hiraishi, H., S. Nakata, Y. Kitagawa, and T. Kaminosono, "Static Tests on Shear Walls and Beam-column Assemblies and Study on Correlation between Shaking Table Tests and Pseudo-dynamic Tests", Earthquake Effects on Reinforced Concrete Structures, U.S. -Japan Research Publication SP-84, American Concrete Institute (ACI), Detroit, pp. 11-48, 1985.

2. Hwang, T.-H., "Effects of Variation in Load History on Cyclic Response of Concrete Flexural Members", Thesis submitted in partial fulfillment of the requirement for the degree of Doctor of Philosophy, University of Illinois at Urbana-Champaign, 1982.

3. Aristizabal-Ochoa, J. D. and M. A. Sozen, "Behavior of Ten-story Reinforced Concrete Walls Subjected to Earthquake Motions", University of Illinois at Urbana-Champaign, October 1976.

4. Darwin, D. and D. A. Pecknold, "Analysis of RC Shear Panels under Cyclic Loading", Journal of the Structural Division, Proc. American Society of Civil Engineer (ASCE), Vol. 102, No. ST2, pp. 355-369, February 1976.

5. Bolander J. Jr. and J. K. Wright, "Finite Element Modeling of Shear-wall-dominant Buildings", Journal of Structural Engineering, ASCE, Vol. 117, No. 6, pp. 1719-1739, June 1991.

6. Yuzugullu, O. and W. C. Schnobrich, "A Numerical Procedure for the Determination of the Behavior of a Shear Wall Frame System", ACI Journal, No. 70-47, pp. 474-479, July 1973.

7. Mo, Y. L., "Effect of First-story Shearwalls on Earthquake-Resistant Buildings", Structural Engineering in Natural Hazards Mitigation, Vol. 1, Proc. ASCE Structures Congress '93, Irvine, California, pp. 283-294, April 1993.

8. Wallace, J. W., J. P. Moehle, and J. Martinez-Cruzado, "Implications for the Design of Shear Wall Building Using Data from Recent Earthquakes", Proceedings of Fourth U.S. National Conference on Earthquake Engineering, Palm Springs, Vol. 2, pp. 359-368, May 1990.

9. Cevallos-Canolau, P. J. and S. Roy, "A Simple Procedure for the Seismic Analysis of Low Rise Buildings", Proceedings of 3rd International Earthquake Microzonation Conference, Seattle, Vol. II, pp. 831-842, June 28-July 1, 1982.

10. Wallace, J. W. and J. P. Moehle, "Ductility and Detailing Requirements of Bearing Wall Buildings", Journal of Structural Engineering, ASCE, Vol. 118, No. 6, pp. 1625-1644, June 1992.

11. Watabe, M., R. Fukuzawa, O. Chiba, and T. Hatori, "Study on Load-Deflection Characteristics of Heavily Reinforced Concrete Shear Walls", Transactions of 10th International Conference on Structural Mechanics in Reactor Technology, Vol. H, pp. 209-214, 1989.

12. Coladant, C. and B. Foure, "Experimental Behavior of RC Shear Walls for NPP", Transactions of the 10th International Conference on Structural Mechanics in Reactor Technology, Vol. H, pp. 245-249, 1989.

13. Wang, F., F. Gantenbein, J. Dalbera, and C. Duretz, "Seismic Behavior of Reinforced Concrete Shear Walls", Transactions of 10th International Conference on Structural Mechanics in Reactor Technology, Vol. K1, pp. 473-478, 1989.

14. Anderson, C. A., J. G. Bennett and R. C. Dove, Seismic Category-I Structures Program: Current Status and Program Plan for FY84-FY85, Appendix A, Loa Alamos National Laboratory, 1984.

15. Dove, R. C. and J. G. Bennett, Scale Modeling of Reinforced Concrete Category-I Structures Subjected to Seismic Loads, Los Alamos National Laboratory Report, NUREG/CR-4474, 1986.

16. Dove, R. C., E. G. Endelbrock, W. E. Dunwoody, and J. G. Bennett, "Seismic Test on Models of Reinforced Concrete Category-I Buildings", Proceedings of 8th International Conference on Structural Mechanics in Reactor Technology, Brussels, 1985.

17. Endebrock, E. G., R. C. Dove and C. A. Anderson, "Seismic Category-I Structures Program", Proceedings of 12th Water Reactor Safety Research Information Meeting, National Bureau of Standard, Bethesda, Maryland, 1984.

18. Endebrock, E. G., R. C. Dove, and C. A. Anderson, "NRC Experimental/ Analytical Program for Investigating Margins to Failure of Category-I Reinforced Concrete Structures", Nuclear Engineering and Design, Vol. 69, pp. 169-178, 1982.

19. Endebrock, E. G. and R. C. Dove, "Nonlinear Seismic Response of Small-Scale Reinforced Concrete Shear Wall Structures", Proceedings of 7th International Conference on Structural Mechanics in Reactor Technology, Vol. K(a), pp. 259-266, 1983.

20. Farrar, C. R. and J. G. Bennett, "An Overview of an Experimental Program for Testing Large Reinforced Concrete Shear Walls", Transactions of 10th International Conference on Structural Mechanics in Reactor Technology, Vol. K1, pp. 461-466, 1989.

21. Sheu, M. S.,"Behavior of Low-rise RC Shear Walls Subjected to Reversed Cyclic Loading", Technical Report to the National Science Council, Architectural Engineering Department, National Cheng Kung University, 1988.

22. Yamada, M., H. Kawamura, and K. Katagihara, "Reinforced Concrete Shear Walls with Openings: Test and Analysis", Shear in Reinforced Concrete, Vol. 2, Publication SP-42, ACI, Detroit, pp. 559-578, 1974.

23. Chiba, O., R. Fukuzawa, T. Hatori, and K. Yagishita, "Experimental Study on Heavily Reinforced Concrete Shear Walls", Transactions of 8th SMiRT Conference, H4/1, pp. 131-136, 1985.

24. Fukuzawa, R., O. Chiba, T. Hatori, K. Yagishita, M. Watabe, and H. Yamanouchi, "Study on Load-deflection Characteristics of Heavily Reinforced Concrete Shear Walls", Proceedings of 9th International Conference on Structural Mechanics in Reactor Technology, Lausanne, Vol. H, pp. 537-542, 1987.

25. Sato, Y., A. Higashiura, K. Sato, H. Yamanouchi, and T. Kubo, "Load-deflection Characteristics of Shear Walls with Openings", Proceedings of 9th International Conference on Structural Mechanics in Reactor Technology, Lausanne, Vol. H, pp. 537-542, 1987.

26. Sotomura, K., Y. Murazumi, S. Yoshizaki, and T. Korenaga, "Ultimate Shear Strength of Shear Wall in Nuclear Power Plant", Transactions of 8th SMiRT Conference, H4/4, pp. 145-150, 1985.

27. ACI Committee 318R-166, "Building Code Requirements for Reinforced Concrete", Detriot, ACI, 1989.

28. Uang, C.-M., "Seismic Force Reduction and Displacement Amplification Factors", Proceedings of 10th World Conference on Earthquake Engineering, pp. 5875-5880, July 1992.

29. Cheng, F. Y. and G. E. Mertz, "Inelastic Seismic Response of Reinforced Concrete Low-rise Shear Walls and Building Structures", NSF Report, NTIS No. PB90-123217, U.S. Department of Commerce, Washington, D.C., 1989.

30. Cheng, F. Y. and J. A. Volker, "Response Behavior of Inelastic Box-Type Reinforced Concrete and Steel Structures Subjected to 3-Dimensional Ground Motions", NSF Final Report, University of Missouri-Rolla, June 1982.

31. Jeary, A. P.,"Damping in Tall Buildings-A Mechanism and a Predictor", Earthquake Engineering and Structural Dynamics, Vol. 14, pp. 733-750, 1986.

32. Malushte, S. R. and M. P. Singh, "A Study of Seismic Response Characteristics of Structures with Friction Damping", Earthquake Engineering and Structural Dynamics, Vol. 18, pp. 767-783, 1989.

33. Crandall, S. H., G. R. Khabbaz, and J. E. Manning, "Random Vibration of an Oscillator with Nonlinear Damping", Journal of the Acoustical Society of America, Vol. 36, No. 7, pp. 1330-1334, July 1964.

34. Jennings, P. C., "Equivalent Viscous Damping for Yielding Structures", Journal of the Engineering Mechanics Division, Proceedings, ASCE, No. EM1, pp. 103-116, February 1968.

35. Kwok, K. C. S., "Damping Increase in Building with Tuned Mass Damper", Journal of Engineering Mechanics, ASCE, Vol. 110, No. 11, pp. 1645-1649, November 1984.

36. Zhang, R.-H. and T. T. Soong, "Seismic Design of Viscoelastic Dampers for Structural Applications", Journal of Structural Engineering, ASCE, Vol. 118, No. 5, pp. 1375-1392, May 1992.

37. Aquirre, M. and A. R. Sanchez, "Structural Seismic Damper", Journal of Structural Engineering, ASCE, Vol. 118, No. 5, pp. 1158-1171, May 1992.

38. Iwan, W. D. and N. C. Gates, "The Effective Period and Damping of a Class of Hysteretic Structures", Earthquake Engineering and Structural Dynamics, Vol. 7, pp. 199-211, 1979.

39. Crandall, S. H., "The Hysteretic Damping Model in Vibration Theory", Proceedings, Institution of Mechanical Engineers, Vol. 205, pp. 23-28, 1991.

40. Bishop, R. E. D., "The Treatment of Damping Forces in Vibration Theory", Journal of the Royal Aeronautical Society, Vol. 59, pp. 738-742, November 1955.

41. Lancaster, P., "Free Vibration and Hysteretic Damping", Journal of the Royal Aeronautical Society, Vol. 63, pp. 229, June 1959.

42. Crandall, S. H., "The Role of Damping in Vibration Theory", Journal of Sound and Vibration, Vol. 11, No. 1, pp. 3-18, 1970.

43. Bert, C. W., "Material Damping: An Introductory Review of Mathematical Models, Measures and Experimental Techniques", Journal of Sound and Vibration, Vol. 29, pp. 129-153, 1973.

44. Mertz, G. E., "Nonlinear Analysis of Low-rise Reinforced Concrete Shear Wall Buildings subjected to Multicomponent Seismic Input", Dissertation presented to the Faculty of the Graduate School of the University of Missouri-Rolla in partial fulfillment of the requirements for the Ph. D. Degree, 1989.

45. Uang, C.-M. and V. V. Bertero, "Earthquake Simulation Tests and Associated Studies of a 0.3-Scale Model of a 6-story Concentrically Braced Steel Structure", Report No. UCB/EERC-86/10, EERC, University of California, Berkeley, 1986.

46. NEHRP Recommended Provisions for the Development of Seismic Regulations for New Building Seismic Safety Council, Washington, D.C., 1985.

47. Uniform Building Code (UBC), International Conference of Building Officials, Whittier, California, 1991.

48. Newmark, N. M. and W. J. Hall, Earthquake Spectra and Design, Earthquake Engineering Research Institute (EERC), El Cerrito, California, 1982.

49. Bertero, V. V., J. C. Anderson, H. Krawinkler, E. Miranda, and the CURE and the Kajima Research Teams, "Design Guidelines for Ductility and Drift Limits: Review of State-of-the-practice and State-of-the art in Ductility and Drift-based Earthquake-resistant Design of Buildings", Report No. UCB/EERC-91/15, EERC, University of California, Berkeley, July 1991.

50. Uang, C.-M., "Establishing R(or R_w) and C_d Factors for Building Seismic Provisions", Journal of Structural Engineering, ASCE, Vol. 117, No. 1, January 1991.

51. Whittaker, A. S., C.-M. Uang, and V. V. Bertero, "Experimental Behavior of a Dual Steel System", Journal of Structural Engineering, ASCE, Vol. 115, ST1, pp. 183-200, 1989.

52. Cheng, F. Y. and G. E. Mertz, INRESB-3D-SUP, User's Manual - A Computer Program for Inelastic Seismic Analysis of 3-Dimensional Reinforced Concrete and Steel Buildings, NSF Report, U.S. Department of Commerce, NTIS No. PB90-122225, (197 pages), 1989.

53. Cheng, F. Y., J. F. Ger, and G. E. Mertz, Manual for Computer Program INRESB-3D-SUPII, 1990.

54. Cheng, F. Y. and J. F. Ger, "Collapse Studies of Seismic Steel Tall Buildings", Forefronts, Vol. 5, No. 10, Cornell Theory Center, February 1990.

55. Cheng, F. Y. and J. F. Ger, "Hysteresis Studies Including Post Buckling of Angle Web-Member for Truss-Type Girders", Steel Structures, ASCE, pp. 627-636, 1989.

56. Cheng, F. Y. and J. F. Ger, "Post-Buckling and Hysteresis Rules of Truss-Type Girders", Proceedings, Structural Stability Research Council, Fritz Engineering Laboratory 13, Lehigh University, pp. 207-218, 1990.

57. Cheng, F. Y. and J. F. Ger, "Maximum Response of Buildings to Multi-Seismic Input", Dynamics of Structures, ASCE, pp. 397-410, 1987.

58. Cheng, F. Y. and J. F. Ger, "Translational-Torsional Spectral Method and Maximum Response for Six-component Seismic Input", Proceedings, Korea-Japan Joint Seminar on Engineering Technologies in Structural Engineering and Mechanics, pp. 334-345, 1988.

59. Ger, J. F., " Inelastic Response and Collapse Behavior of Steel Tall Buildings Subjected to 3-D Earthquake Excitations", Dissertation presented to the Faculty of the Graduate School of the University of Missouri-Rolla in partial fulfillment of the requirement for the Ph. D. Degree, 1990.

60. Cheng, F. Y., J. F. Ger, D. Li, and J. S. Yang, INRESB-3D-SUPII, General Purpose Program for Inelastic Analysis of Reinforced Concrete and Steel Building Systems for 3-D Ground Motions, NSF Report, Civil Engineering Structural Series 94-31, University of Missouri-Rolla, 1994.

61. CSMIP Strong-motion Records from the Santa Cruz Mountains (Loma Prieta), California, Earthquake of 17 October 1989, California Department of Conservation, Division of Mines and Geology, Office of Strong Motion Studies, Report OSMS 89-06, 1989.

62 Wang, C. K. and C. G. Salmon, Reinforced Concrete Design, 4th edition, 1985.

63. Park, R., M. J. N. Priestley, and W. D. Gill, "Ductility of Square-confined Concrete Columns", Journal of Structural Engineering, ASCE, Vol. 108, No. ST4, pp. 929-950, April 1982.

64. Ford, J. S., D. C. Chang, and J. E. Breen, "Behavior of Concrete Columns under Controlled Lateral Deformation", ACI Journal, Title No. 78-1, pp. 3-20, January-February 1981.

65. Sheikh, S. A. and C. C. Yeh, "Flexural Behavior of Confined Concrete Columns", ACI Journal, Title No. 83-39, pp. 389-404, May-June 1986.

66. Fafitis, A. and S. P. Shah, "Predictions of Ultimate Behavior of Confined Columns Subjected to Large Deformations", ACI Journal, Title No. 82-35, pp. 423-433, July-August 1985.

67. Burdette, E.G. and H. K. Hilsdorf, "Behavior of Laterally Reinforced Concrete Columns", Journal of the Structural Division, ASCE, Vol. 97, No. ST2, pp.587-602, February 1971.

68. Mander, J. B., M. J. N. Priestley, and R. Park, "Theoretical Stress-strain Model for Confined Concrete", Journal of Structural Engineering, ASCE, Vol. 114, No. 8, pp. 1804-1826, August 1988.

69. Mander, J. B., M. J. N. Priestley, and R. Park, "Observed Stress-strain Behavior of Confined Concrete", Journal of Structural Engineering, ASCE, Vol. 114, No. 8, pp. 1827-1849, August 1988.

70. Sheikh, S. A. and S. M. Uzumeri, "Strength and Ductility of Tied Concrete Columns", Journal of Structural Division, Proc. ASCE, Vol. 106, No. ST5, pp. 1079-1102, 1980.

71. Sheikh, S. A., "A Comparative Study of Confinement Models", ACI Journal, Vol. 79, No. 4, pp. 296-306, July-August 1982.

72. Sheikh, S. A. and S. M. Uzumeri, "Analytical Model for Concrete Confinement in Tied Columns", Journal of the Structural Division, ASCE, Vol. 108, ST12, pp. 2703-2722, December 1982.

73. Wallace, J., V. V. Bertero, and E. P. Popov, "Concrete Confined by Rectangular Hoops and subjected to Axial Loads", EERC, University of California, Berkeley, Report No. UCB/EERC-77/13, August 1977.

74. Bertero, V. V., "Implications of Recent Earthquakes and Research on Earthquake-resistant Design and Construction of Buildings", Report No. UCB/EERC-86/03, EERC, University of California, Berkeley, March 1986.

75. Blume, J. A., "Allowable Stresses and Earthquake Performance", Proc. Sixth World Conference on Earthquake Engineering, New Delhi, Vol. 1, pp. 165-174, 1977.

76. SIMQKE, A Program for Artificial Motion Generation, User's Manual and Documentation, Department of Civil Engineering, Massachusetts Institute of Technology, November 1976.

77. Uang, C.-M. and A. Maarouf, "Displacement Amplification Factor for Seismic Design Provisions", Structural Engineering in Natural Hazards Mitigation, Proc., ASCE Structures Congress, Irvine, California, Vol. 1, pp. 211-216, April 1993.

78. Kabeyasawa, H., H. Shioara, and S. Otani, " U.S.-Japan Cooperative Research on RC Full-scale Building Test-Part 5: Discussion of Dynamic Response System", Proceedings of 8th World Conference on Earthquake Engineering, Vol. 6, San Francisco, pp. 627-634, 1984.